ACHIEVEMENT OF HIGH FATIGUE RESISTANCE IN METALS AND ALLOYS

ASTM STP 467

AMERICAN SOCIETY FOR TESTING AND MATERIALS

ACHIEVEMENT OF HIGH FATIGUE RESISTANCE IN METALS AND ALLOYS

A symposium
presented at the
Seventy-second Annual Meeting
AMERICAN SOCIETY FOR
TESTING AND MATERIALS
Atlantic City, N. J., 22–27 June 1969

ASTM SPECIAL TECHNICAL PUBLICATION 467

List price $28.75

AMERICAN SOCIETY FOR TESTING AND MATERIALS
1916 Race Street, Philadelphia, Pa. 19103

Library of Congress Catalog Card Number: 74-101591
ISBN 0-8031-0062-1

NOTE

The Society is not responsible, as a body,
for the statements and opinions
advanced in this publication

Printed in Baltimore, Md.
September 1970

Foreword

The Symposium on Achievement of High Fatigue Resistance in Metals and Alloys was given at the Seventy-second Annual Meeting of ASTM held in Altantic City, N. J., 22–27 June 1969. ASTM Committee E-9 on Fatigue, Subcommittee I on Research sponsored the symposium, which was held in three sessions: Parameters Important to High Fatigue Resistance, H. F. Hardrath, National Aeronautics and Space Administration, chairman of Session I; Mechanisms for Achieving High Fatigue Resistance, J. C. Grosskreutz, chairman of Session II; and Processes for Achieving High Fatigue Resistance, C. E. Feltner, Ford Motor Co., chairman of Session III. J. C Grosskreutz and C. E. Feltner presided as symposium cochairmen.

Related ASTM Publications

Structural Fatigue in Aircraft, STP 404 (1966), $18.50

Plane Strain Crack Toughness Testing of High-Strength Metallic Materials, STP 410 (1967), $5.50

Electron Fractography, STP 436 (1968), $11.00

Fatigue at High Temperature, STP 459 (1969), $11.25

Contents

Introduction

This symposium recognizes that, while every design engineer strives to prevent fatigue failures, he must, at the same time try to achieve the highest possible fatigue resistance at a minimum cost and often at a minimum weight and space. Reaching this goal requires an acute knowledge of those phenomenological parameters which best characterize fatigue resistance and those processes by which the fatigue resistance of existing materials can be improved. Furthermore, his future choice of new and improved materials may be determined by the extent to which materials researchers are able to evolve and apply knowledge about those micromechanisms which control fatigue resistance.

It is, therefore, the purpose of this symposium to present up-to-date views on those parameters, mechanisms, and processes that are important in achieving high fatigue resistance in materials.

J. C. Grosskreutz
Midwest Research Institute,
Kansas City, Mo. 64110;

C. E. Feltner
Ford Motor Co.,
Dearborn, Mich. 48121;
symposium cochairmen.

R. W. Landgraf[1]

The Resistance of Metals to Cyclic Deformation

REFERENCE: Landgraf, R. W., "**The Resistance of Metals to Cyclic Deformation,**" *Achievement of High Fatigue Resistance in Metals and Alloys, ASTM STP 467*, American Society for Testing and Materials, 1970, pp. 3–36.

ABSTRACT: Fatigue behavior of metals is reviewed with particular emphasis on those properties and parameters which relate to cyclic deformation resistance. Representative data for aluminum-, titanium-, and nickel-base alloys and steels strengthened by various processes are presented to illustrate procedures for characterizing cycle-dependent deformation and fracture behavior.

The nature and extent of cyclically induced changes in deformation resistance are conveniently described in terms of a cyclic stress-strain curve. A metal's monotonic strain hardening behavior provides an indication of cyclic stability. Fracture behavior is characterized by simple relations in terms of stress resistance, plastic strain resistance, and total strain resistance. True monotonic fracture strength and ductility can be related to fatigue strength and ductility, thus providing useful approximations of life behavior. Indications of notched fatigue resistance can be gained from smooth specimen data through consideration of local stress-strain response. Finally, the utility of such material behavior considerations in arriving at the proper combination of properties to maximize the fatigue resistance of a metal under specified conditions is discussed.

KEY WORDS: fatigue (materials), cyclic loads, stresses, strains, hardening (materials), softening, notch strength, evaluation, aluminum alloys, titanium alloys, nickel alloys, steels, deformation

Recent fatigue research has emphasized the mechanical response of metals to repeated strains as well as to repeated stresses. As a result, strain cycling fatigue data have been generated for a wide range of engineering materials over the entire life range. In addition to fatigue fracture information, the changes in deformation resistance accompanying cyclic loading have been well documented, thus providing a mechanics description of the fatigue process. A number of relations have been proposed to characterize phenomenological cycle-dependent deformation and fracture behavior of metals in

[1] Scientific research staff, Ford Motor Co., Dearborn, Mich. 48121. Formerly research associate, Department of Theoretical and Applied Mechanics, University of Illinois, Urbana, Ill.

terms of strength, ductility, and strain hardening properties. Such characterization techniques are relevant, both to the materials engineer in materials evaluation and selection and to the metallurgist in designing and processing alloys with improved fatigue resistance.

In this paper I plan to review first the response of metals to repeated plastic strains. Representative axial push-pull data for aluminum-, titanium-, and nickel-base alloys and a variety of steels are presented to illustrate behavioral trends and the significant associated properties and parameters. A similar treatment is then given to fracture behavior in terms of stress resistance, plastic and total strain resistance, and notch resistance. Finally, the utility of such material behavior considerations in optimizing fatigue resistance under specified conditions is discussed.

Response of Metals to Repeated Plastic Strains

The flow properties of a metal may be greatly altered by repeated plastic strains. Depending on the initial state and the test conditions, a metal's deformation resistance may increase (cyclic hardening), decrease (cyclic softening), or remain essentially unchanged (cyclic stability).

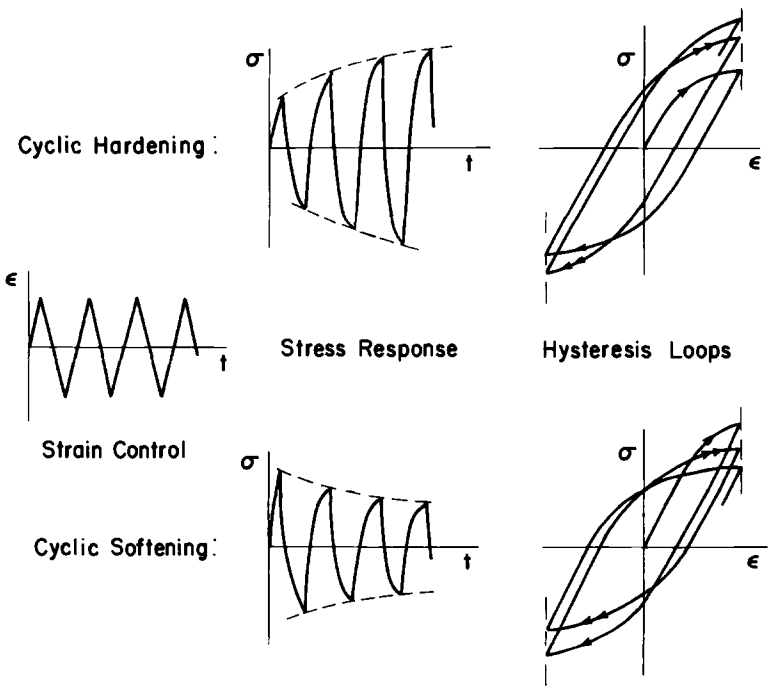

FIG. 1—*Schematic representation of the response of metals to reversed strains.*

Cyclic Hardening and Softening

Two types of response under completely reversed strain cycling are illustrated schematically in Fig. 1. In the first case the stress required to enforce the strain limit on successive reversals increases, indicating cyclic hardening. In contrast, the stress required to enforce the strain limit decreases with successive reversals in the second case, indicating cyclic softening.

Tuler and Morrow [*1*][2] have reviewed the pertinent literature on the cyclic stress-strain behavior of metals prior to 1963, and representative data have been reported by Morrow [*2*]. Smith et al [*3*] have reported cyclic stress-strain data for a variety of engineering metals. In general, annealed metals exhibit cyclic hardening and heavily cold-worked metals cyclic softening. The trends are not as clear for thermally strengthened and thermomechanically processed alloys.

Stress changes during reversed strain cycling of 2024-T4 aluminum and quenched and tempered SAE 4340 steel from Endo and Morrow [*4*] are shown in Fig. 2. The aluminum is observed to cyclically harden, while the steel exhibits cyclic softening. Note that the stress adjustments take place early in the life such that the stress amplitude is reasonably constant over most of the fatigue life.

Cyclic Stress-Strain Curve

The steady state cyclic deformation resistance of a metal is conveniently described by the cyclic stress-strain curve. As shown in Fig. 3, such a curve is obtained by connecting the tips of stable hysteresis loops for companion specimens tested at different strain amplitudes. By comparing the cyclic stress-strain curve with the monotonic curve, the nature and extent of cyclically induced changes are immediately apparent. The 4340 steel exhibits cyclic softening, since the cyclic curve is below the monotonic curve.

The relation between stress amplitude, σ_a, and plastic strain amplitude, $\Delta\epsilon_p/2$, can be expressed by a power function of the form used for the monotonic curve [*2*]:

$$\sigma_a = K'(\Delta\epsilon_p/2)^{n'} \quad \ldots\ldots\ldots\ldots\ldots\ldots\ldots\ldots\ldots\ldots (1)$$

where K' and n' are the cyclic strength coefficient and cyclic strain hardening exponent, respectively.

The monotonic and cyclic curves for the aluminum and steel from Fig. 2 are compared on logarithmic coordinates in Fig. 4*a*. Cyclic stress-plastic strain plots for several hardnesses of quenched and tempered SAE 1045 steel [*5*] are shown in Fig. 4*b*. The cyclic strain hardening exponents are found to fall in a range of 0.11 to 0.14, fitting the pattern that most metals are observed

[2] The italic numbers in brackets refer to the list of references at the end of this paper.

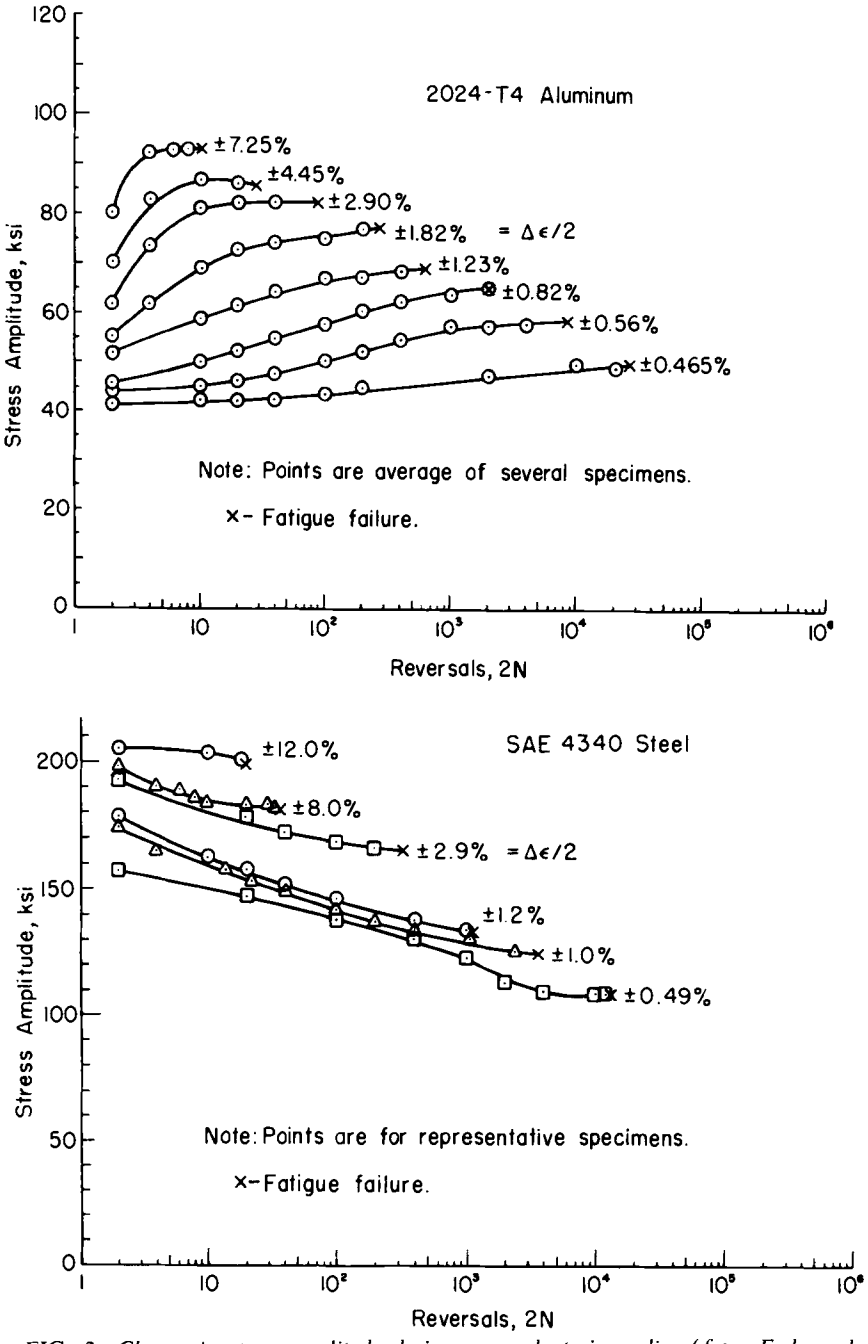

FIG. 2—*Change in stress amplitude during reversed strain cycling (from Endo and Morrow* [4]).

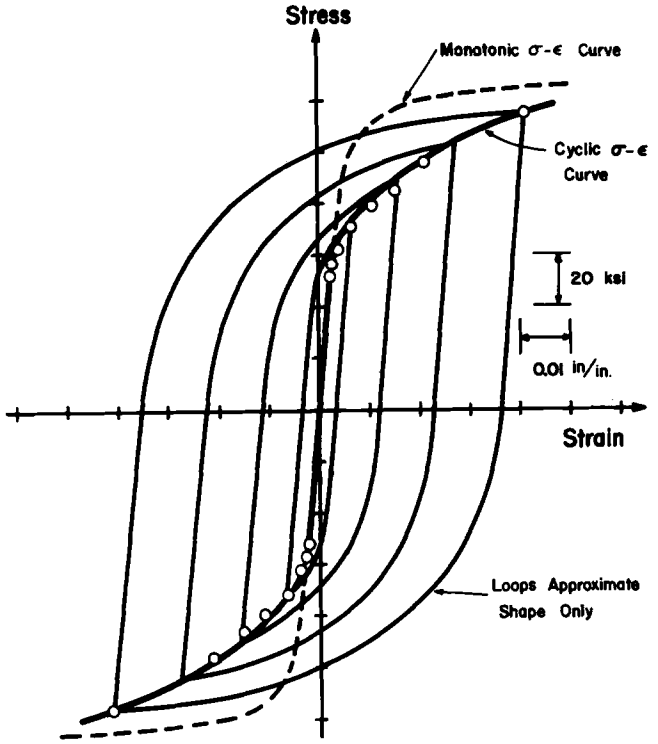

FIG. 3—*Monotonic and cyclic stress-strain curves for SAE 4340 steel. Points are tips of stable loops from companion specimens (data from Smith et al* [3]).

to have n' values between 0.1 and 0.2 [*2*]. Thus, metals with high monotonic strain hardening exponents can be expected to cyclically harden, while those with low monotonic exponents can be expected to soften.

The validity of this approach is shown in Fig. 5 where monotonic and cyclic exponents are compared for representative metals. All but two of the n' values fall between 0.1 and 0.2. Further, metals with monotonic exponents less than 0.1 are observed to soften, while those having values greater than 0.1 are either stable or cyclically harden. This is consistent with the observations of Smith et al [*3*], who found that metals with an ultimate strength to yield strength ratio greater than 1.4 (a high n) cyclically harden, while those with a ratio less than 1.2 (a low n) cyclically soften.

A number of alternate procedures for determining the cyclic stress-strain curve using a single specimen have been investigated [*6*]. The most promising technique appears to be the incremental step test in which a specimen is subjected to a program of continually increasing and then decreasing strain amplitudes such that a continuous plot of stress versus strain yields a series

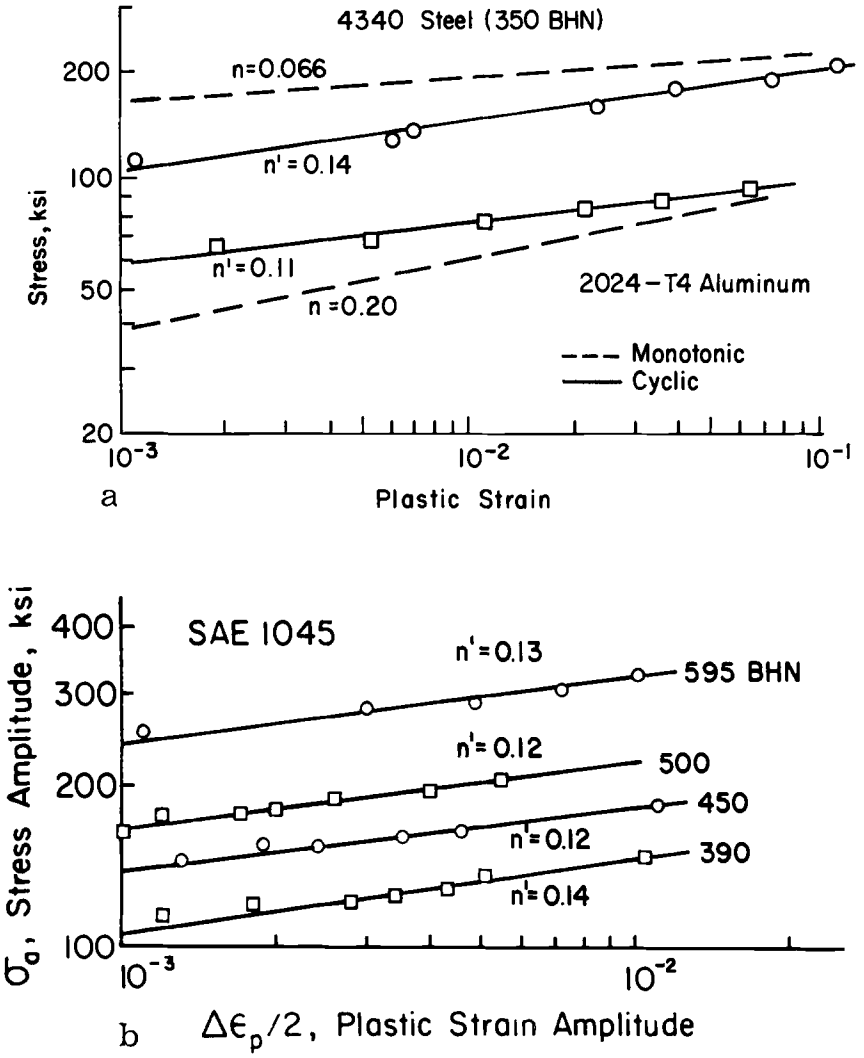

FIG. 4—*Representative monotonic and cyclic stress-strain behavior.*

of superimposed hysteresis loops, as shown in Fig. 6 for a maraging steel. After several of these blocks the metal cyclically stabilizes and the locus of loop tips describes the cyclic stress-strain curve.

In Fig. 7 monotonic and cyclic stress-strain curves for several engineering metals are compared. The aluminum alloys and the nickel-vase Waspaloy[3] exhibit cyclic hardening, while the quenched and tempered steel softens

[3] Wrought nickel-base superalloy; Pratt & Whitney Aircraft trademark.

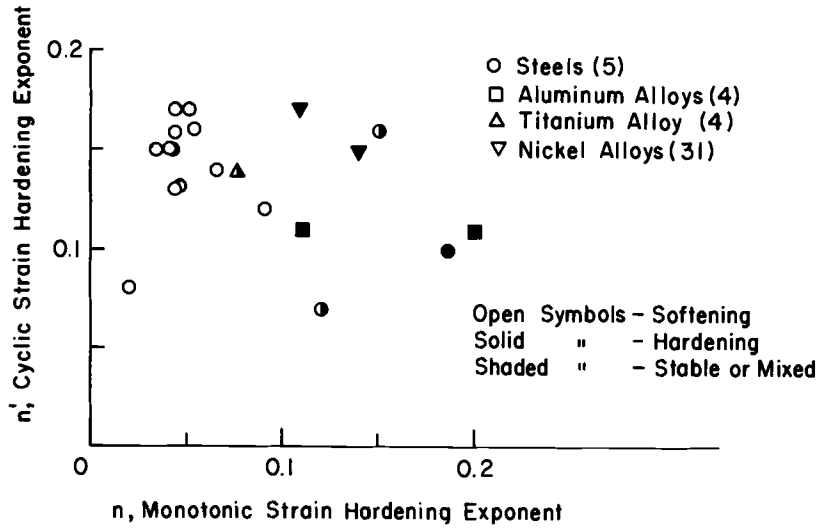

FIG. 5—*Comparison of monotonic and cyclic strain hardening exponents illustrating hardening and softening trends.*

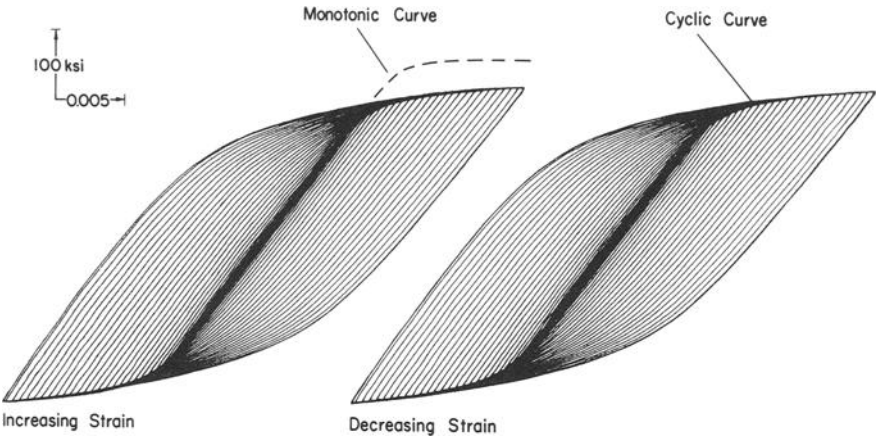

FIG. 6—*Stress-strain record of incremental step test on 18 percent nickel maraging steel* [5].

drastically. Man-ten[4] steel and the titanium alloy soften at small strains and harden at large strains. The cyclic curves determined by the incremental step test are observed to compare well with the companion specimen points.

Monotonic and cyclic stress-strain curves for several hardnesses of quenched and tempered SAE 4142 steel [5] are shown in Fig. 8. While the

[4] Manganese-copper steel in accordance with ASTM Specification for High-Strength Structural Steel (A 440-66); United States Steel Corp. trademark.

intermediate hardness steels exhibit cyclic softening as expected, at high hardnesses a slight hardening is noted. This behavior is explained by considering the change in the monotonic strain hardening exponent with hardness shown in Fig. 9. The value of n is found to be relatively high at both low and high hardnesses and goes through a minimum at an intermediate hardness. Thus, very hard and very soft steel would be expected to harden cyclically, with maximum softening occurring between 400 and 500 BHN.

Similar considerations for the other conditions of steel shown in Fig. 9 explain the behaviors displayed in Fig. 10, namely, quenched and deformed steel and maraging steel cyclically soften, while the ausformed steel hardens slightly. Additionally, note that these steels, due to their thermomechanical processing, display differences in monotonic tensile and compressive yield strengths and strain hardening exponents which may affect their cyclic response. Ausformed steel, for example, has a lower monotonic strain hardening exponent in compression than in tension. During strain cycling, the stress limit in compression exhibits little change, while the tensile limit increases resulting in a net hardening. This emphasizes the importance of determining both monotonic tensile and compressive properties before predicting deformation changes due to axial cycling of such materials. Finally, the incremental step test curves are again found to be in excellent agreement with the companion specimen points in Figs. 8 and 10.

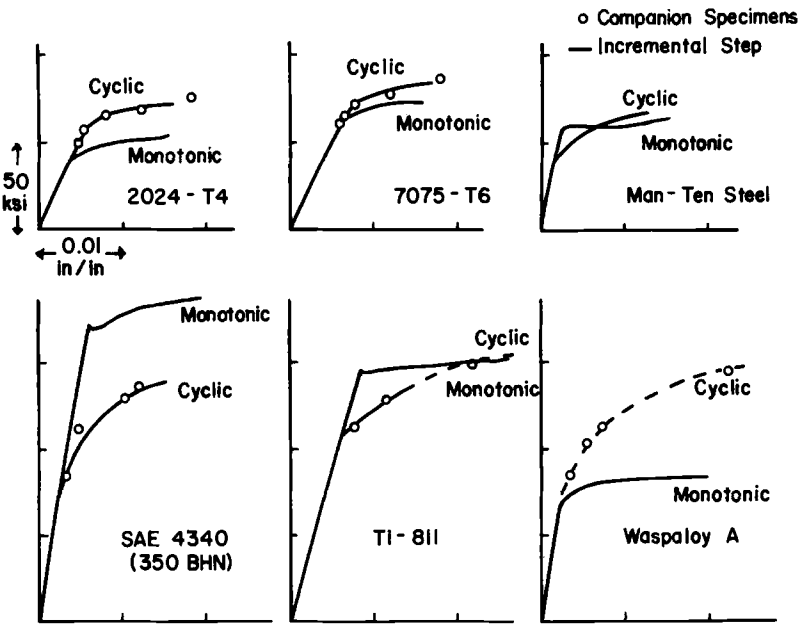

FIG. 7—*Monotonic and cyclic stress-strain curves for representative materials* [6].

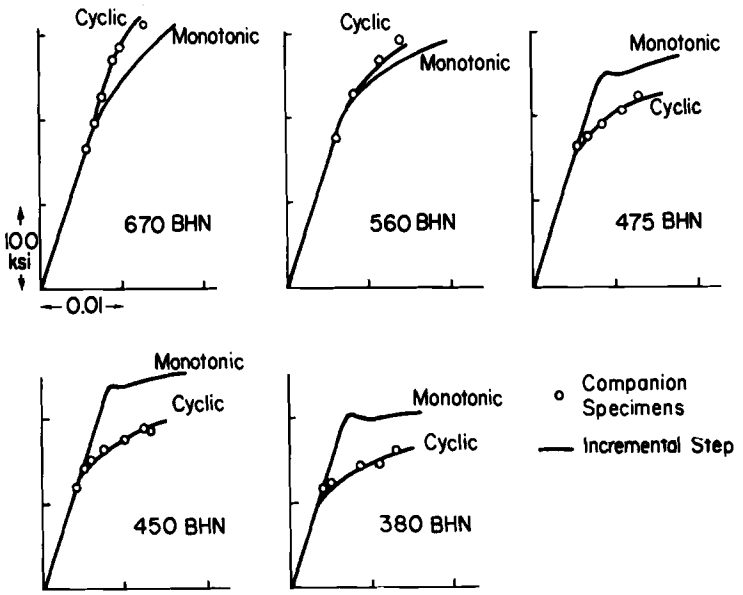

FIG. 8—*Monotonic and cyclic stress-strain curves for five hardnesses of quenched and tempered SAE 4142 steel* [5].

Cyclically Induced Instabilities

Cycle-dependent changes in deformation resistance can give rise to mechanical instabilities in metals, resulting in failure other than by fatigue [*7*, *8*, *9*]. For example, the response of an intermediate-hardness steel to reversed stressing is shown in Fig. 11. As a result of cyclic softening, the strain limits are seen to increase continually, causing a "runaway" process. Depending upon the specimen configuration, failure may occur by either necking in tension or buckling in compression. Such behavior can often be predicted by comparing the monotonic and cyclic stress-strain curves.

If a tensile mean stress is superimposed upon an alternating stress, cycle-dependent creep may result, as shown for 1045 steel in Fig. 12. The mean stress causes a large tensile mean strain to accumulate, eventually leading to a ductile tensile failure. A compressive mean stress would promote creep into compression, possibly causing a buckling failure.

While such effects generally result from biased loading, similar behavior is observed in certain alloys exhibiting a strength differential. The maraging steel shown in Fig. 13 has a higher monotonic yield strength in compression than in tension. When subjected to reversed strains (Fig. 13*a*), the stress limits adjust to a completely reversed condition. Under stress cycling, however, the inferior tensile properties may give rise to an initially high softening

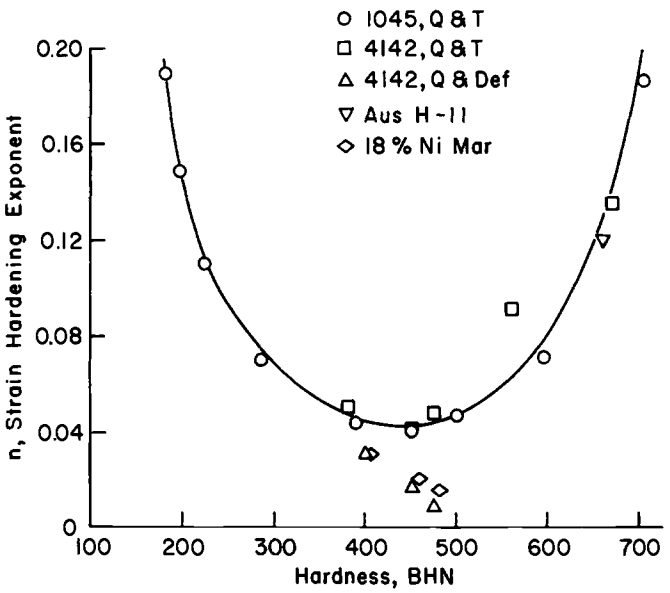

FIG. 9—*Monotonic strain hardening exponent as a function of hardness for various steels* [5].

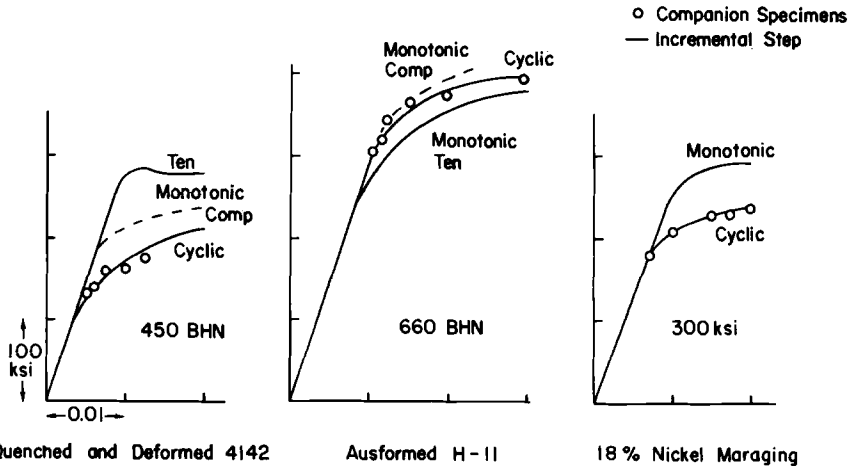

FIG. 10—*Monotonic and cyclic stress-strain curves for steels strengthened by different processes* [5].

rate in tension, which results in a ductile tensile failure (Fig. 13*b*). The quenched and deformed steel in Fig. 14 possesses a higher yield strength in tension than compression. Again, under strain cycling, the stress limits adjust as shown (Fig. 14*a*). When subjected to stress cycling a preferential softening in compression leads to a buckling failure (Fig. 14*b*).

Finally, the relaxation of mean stress under 0-max strain cycling is illustrated in Fig. 15. The tensile mean stress present on the first cycle is observed to relax to zero upon subsequent cycling. Morrow and Sinclair [*10*] have investigated this effect in steel, demonstrating how it accounts for the fading of residual stresses at high strain amplitudes.

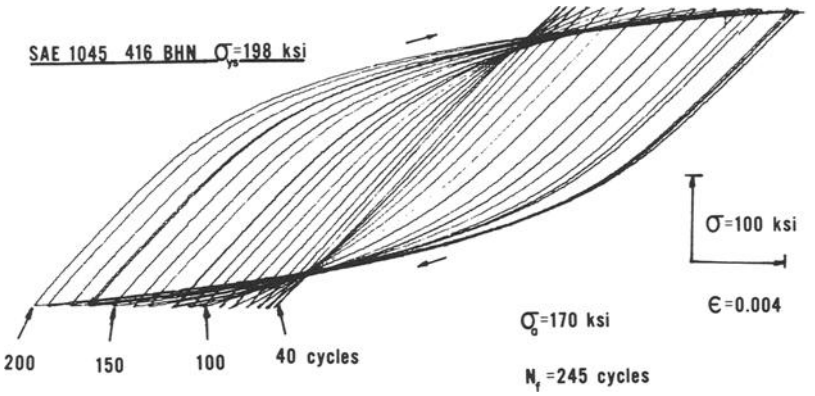

FIG. 11—*Cyclic softening of an intermediate hardness steel under stress cycling (from Morrow* [19]).

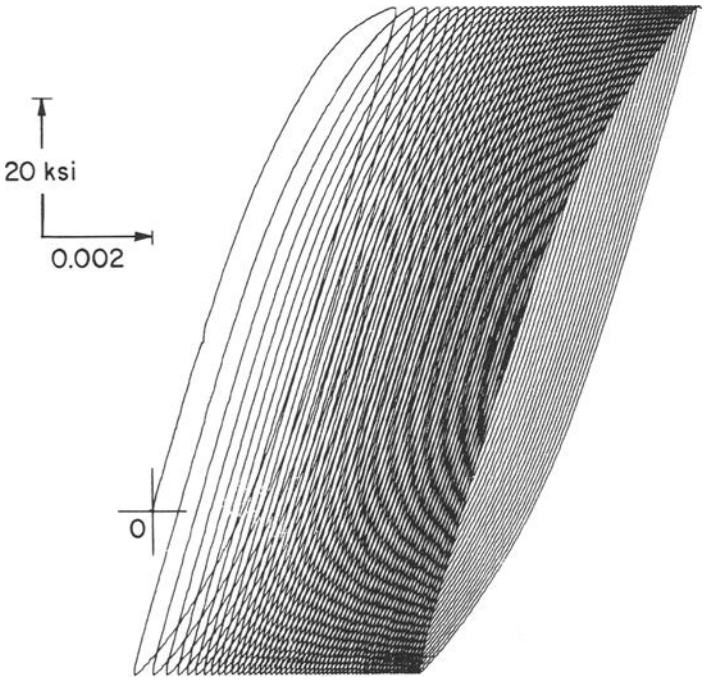

FIG. 12—*Cycle-dependent creep of SAE 1045 steel (20 HRc) under stress cycling with a tensile mean stress.*

Summary

In view of the large changes in deformation resistance which may result from mechanical cycling, a metal's cyclic behavior is best characterized by a cyclic stress-strain curve. Such a curve can be conveniently approximated from one specimen using the incremental step test.

An indication of a metal's cyclic response can be gained from its strain hardening behavior, the monotonic strain hardening exponent serving as an index of cyclic stability. A high strain hardening exponent is indicative of cyclic hardening, a low exponent of cyclic softening. A monotonic strain hardening exponent of about 0.1 appears to result in cyclically stable behavior. In predicting the response of alloys displaying a strength differential, both tensile and compressive flow properties should be considered.

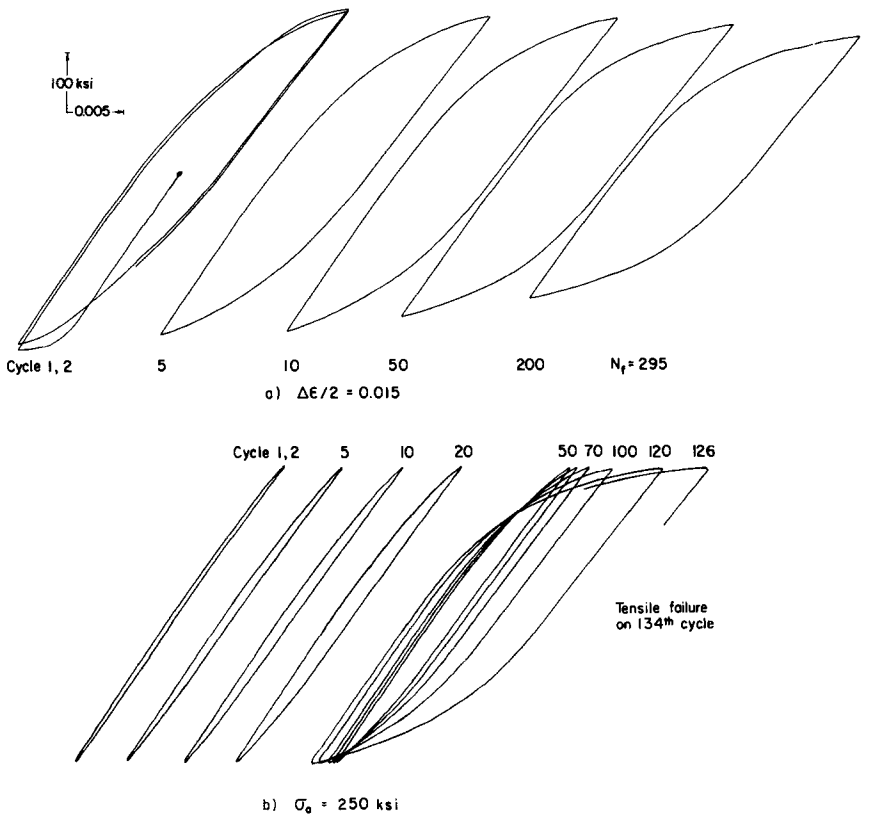

FIG. 13—*Stress-strain response of 18 percent nickel maraging steel during* (a) *strain and* (b) *stress cycling* [5].

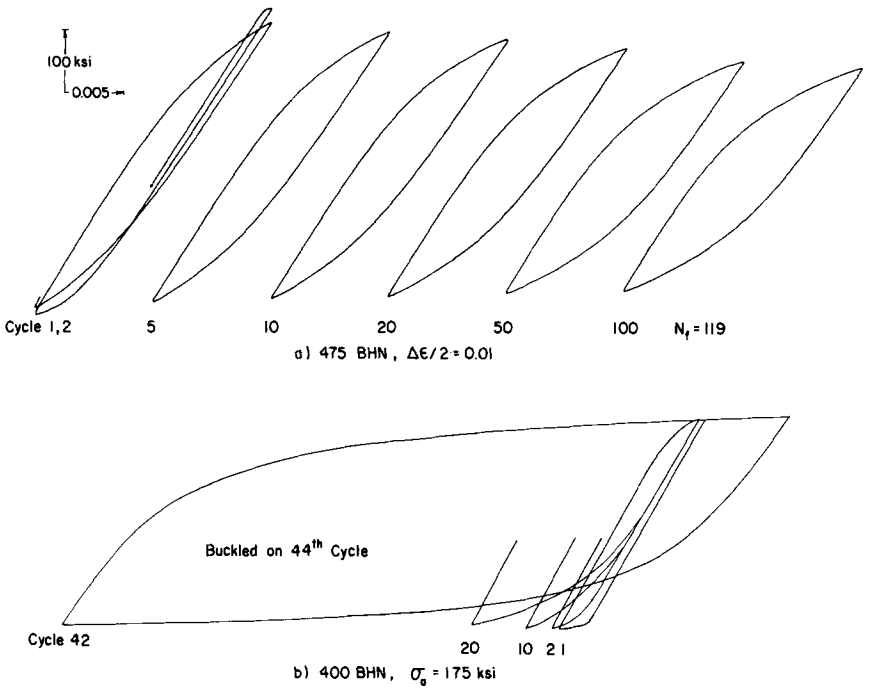

FIG. 14—*Stress-strain response of quenched and deformed SAE 4142 steel during* (a) *strain and* (b) *stress cycling* [5].

Depending on the type of loading and material, related mechanical responses such as cycle-dependent creep, relaxation, or buckling may occur. Such instabilities can often be anticipated by comparing the monotonic and cyclic stress-strain curves of a material.

Fatigue Resistance

As shown in the previous section, metals in general respond differently to strain cycling than to stress cycling when measurable plastic strains are present. That cyclic fracture behavior may show a similar dependence should not be unexpected. Thus, in assessing the fatigue resistance of metals it is necessary to distinguish between stress and strain resistance.

The various expressions proposed to characterize fatigue behavior [*11*, *12*, *2*] essentially involve log-log linear relations between elastic strain (stress)-fatigue life and plastic strain-fatigue life. In the following discussion the notation of Morrow [*2*] will be employed and the other approaches compared on this basis.

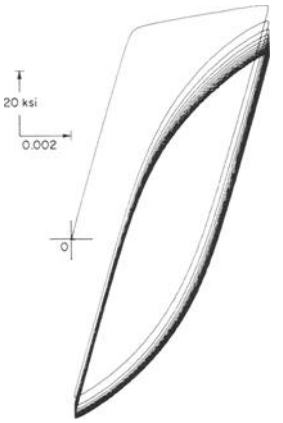

FIG. 15—*Cycle-dependent stress relaxation of SAE 1045 steel (20 HRc) under 0-max strain cycling.*

Stress Resistance

The relation between true stress amplitude, σ_a, and cycles to failure, N_f, is given by

$$\sigma_a = \sigma_f'(2N_f)^b \quad \ldots\ldots\ldots\ldots\ldots\ldots\ldots\ldots\ldots\ldots (2)$$

where σ_f', the fatigue strength coefficient, is the stress intercept at one reversal ($2N_f = 1$), and b, the fatigue strength exponent, is the slope of the logarithmic stress amplitude-life plot. A metal's stress cycling resistance is thus characterized by σ_f' and b, which may be considered *fatigue strength properties.*

The fatigue strength coefficient is related to the true monotonic fracture strength, σ_f, and may be approximated by setting $\sigma_f' = \sigma_f$ [*13*].[5] Life data for a number of high-strength steels [*5*] are compared in dimensionless form in Fig. 16. All data sets tend to converge toward a stress ratio of unity at one reversal, verifying the general validity of the monotonic fracture strength approximation. The observed scatter in life is largely the result of variations in b with material.

Alternate methods of approximating fatigue strength from the monotonic fracture strength are compared in Table 1 [*13–16*]. All correlations result in a similar correspondence between σ_f' and σ_f. In Fig. 17, data for several representative metals further substantiate the close agreement between the fatigue strength coefficient and the true fracture strength.

[5] The true fracture strength should be corrected for constraints due to necking.

TABLE 1—*Comparison of methods for predicting the fatigue strength coefficient,* σ_f'.

Investigator	Proposed Correlation	Value of σ_f' in Eq 2
Halford and Morrow [*13*]....	$\sigma_a = \sigma_f$ at $1/2$ cycle	$\sigma_f' = \sigma_f$
Manson [*14*].....	$2\sigma_a = 2\sigma_f$ at 1 cycle $b = -0.12$	$\sigma_f' = 1.09\ \sigma_f$
Manson [*15*].....	$2\sigma_a = 2\sigma_f$ at $1/4$ cycle	$\sigma_f' = 0.92\ \sigma_f$ $(b = -0.12)$
Manson and Hirschberg [*16*]..	$2\sigma_a = 2.5\sigma_f$ at $1/4$ cycle	$\sigma_f' = 1.15\sigma_f$ $(b = -0.12)$

Referring again to Fig. 16, it can be seen that variations in the slope, b, can cause large life variations in the high cycle region. Reported values of b range from about -0.05 for certain highly strengthened alloys to -0.15 for annealed metals [*3*, *4*, *5*, *17*]. Cold working decreases the absolute magnitude of b with little effect on σ_f', thus increasing long-life fatigue strength [*17*]. Transformation hardening of steels appears to have little effect on b, while in thermomechanically processed steels b tends to decrease in absolute value with increasing fracture strength [*5*].

Morrow [*2*] has shown through an energy argument that b is related to the cyclic strain hardening exponent, n', as follows:

$$b = -n'/(1 + 5n') \quad \ldots\ldots\ldots\ldots\ldots\ldots\ldots\ldots\ldots\ldots (3)$$

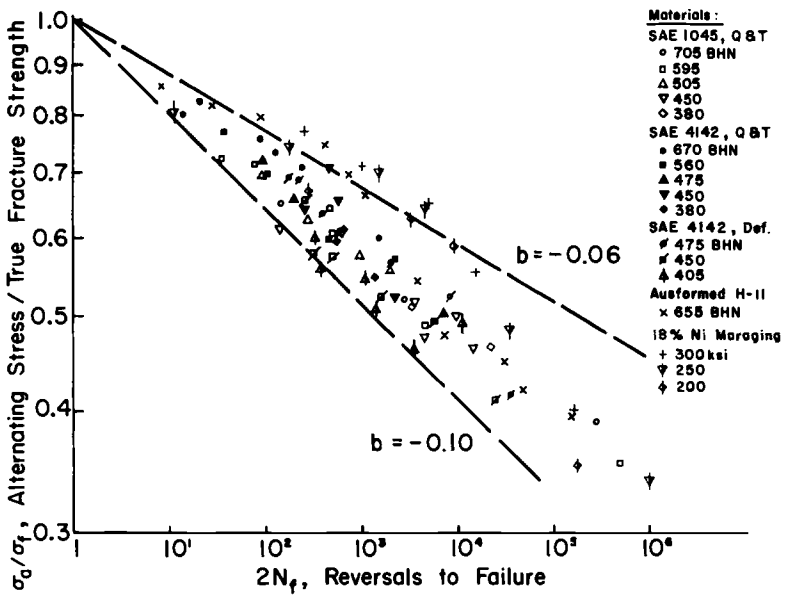

FIG. 16—*Stress amplitude-fatigue life behavior of hardened steels* [5].

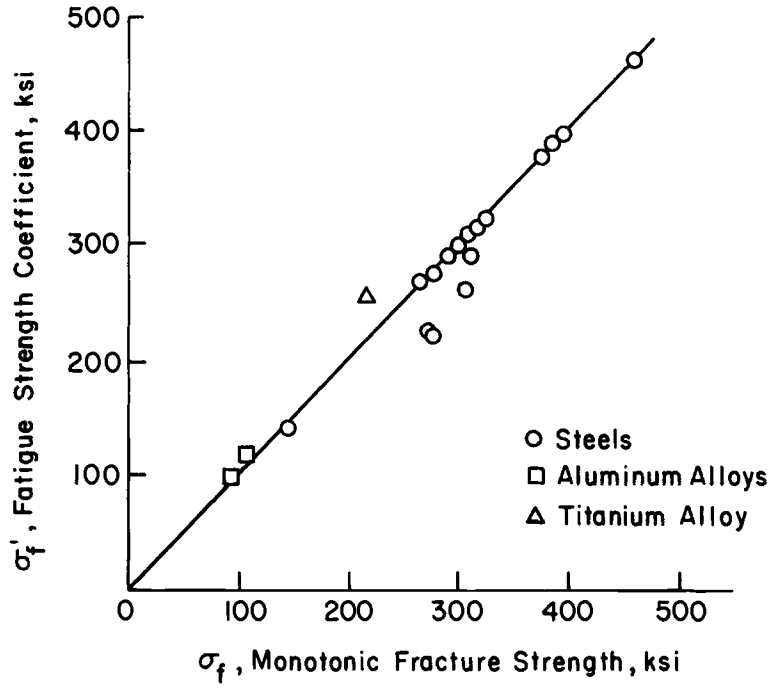

FIG. 17—*Correlation between the fatigue strength coefficient and monotonic fracture strength.*

This correlation is compared with representative data in Fig. 18 and is found to fit generally the experimental trends. Values of n' are easily determined from the incremental step test.

The presence of a fatigue limit in certain irons and steels may be accounted for by introducing a fatigue strength limit, S_f [*2*]. A small offset yield strength from the cyclic stress-strain curve may be used to approximate S_f. Nonferrous metals and most highly strengthened steels will not show a fatigue limit and the exponential relation (Eq 2) will describe behavior even at very long lives.

Mean stress effects can be accounted for in Eq 2 as follows [*17*]:

$$\sigma_a = (\sigma_f' - \sigma_0)(2N_f)^b \quad \ldots\ldots\ldots\ldots\ldots\ldots\ldots\ldots\ldots\ldots (4)$$

where σ_0 is the mean stress. A tensile mean stress can thus be considered as an effective reduction in the fatigue strength coefficient, a compressive mean stress an increase in the coefficient. Mean stress data for different hardnesses of 1045 steel [*18, 19*] are shown in dimensionless form in Fig. 19, indicating reasonably close agreement with the prediction based on Eq 4. High combinations of stress amplitude and mean stress may result in cycle-dependent

creep as shown in the previous section. The effect of residual stresses on fatigue behavior can also be predicted by Eq 4, assuming they do not relax out.

Plastic Strain Resistance

The Manson-Coffin equation relating the plastic strain amplitude, $\Delta\epsilon_p/2$, and cycles to failure, N_f, is of the form

$$\Delta\epsilon_p/2 = \epsilon_f'(2N_f)^c \quad (5)$$

where ϵ_f', the fatigue ductility coefficient, is the plastic strain intercept at one reversal ($2N_f = 1$), and c, the fatigue ductility exponent, is the slope of the logarithmic plastic strain amplitude-life plot. These latter two quantities may be considered *fatigue ductility properties* of a metal.

Several investigators have attempted to relate plastic strain resistance with monotonic fracture ductility, ϵ_f [*12, 13, 15, 16, 17, 20, 21, 22, 23*]. These proposed correlations along with the equivalent values of ϵ_f' are presented in Table 2. No general agreement is found between investigators with approximations of ϵ_f' ranging from 0.35 ϵ_f to ϵ_f. A comparison of the correlations with experimental data in Fig. 20 reveals that no one technique is adequate for all materials. For a majority of the materials shown, letting $\epsilon_f' = \epsilon_f$ is a reasonably good approximation; however, several steels fall far below this prediction.

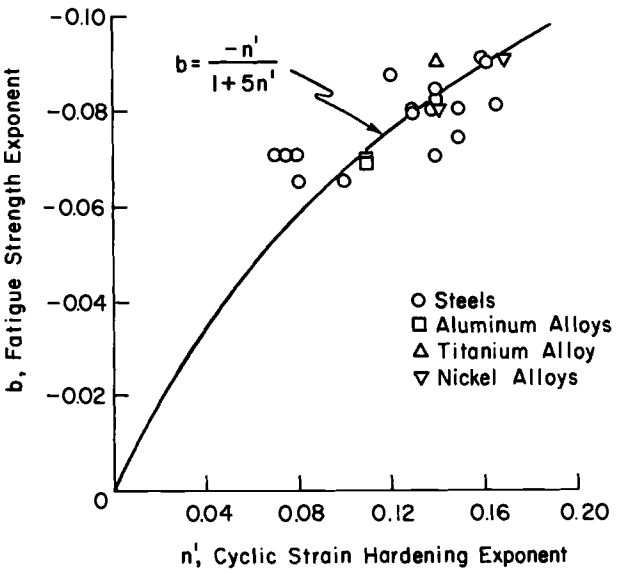

FIG. 18—*Correlation between Eq 3 and experimental data.*

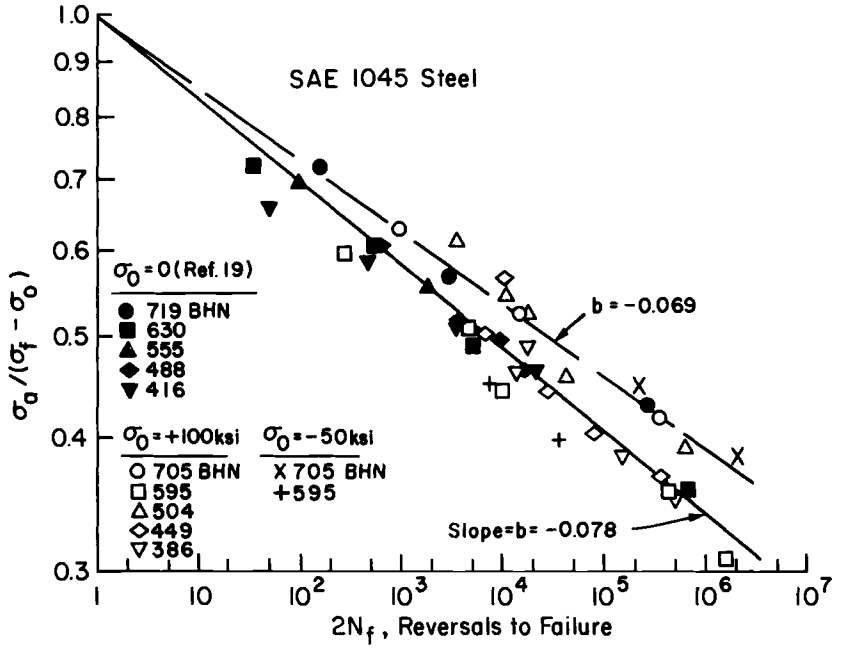

FIG. 19—*Mean stress data for SAE 1045 steel compared with prediction based on Eq 4* [18].

TABLE 2—*Comparison of methods for predicting the fatigue ductility coefficient,* ϵ_f'.

Investigator	Proposed Correlation	Value of ϵ_f' in Eq 5
Coffin [*20*] Tavernelli and Coffin [*21*]	$\Delta\epsilon_p = \epsilon_f$ at 1/4 cycle $c = -0.5$	$\epsilon_f' = 0.35\ \epsilon_f$
Manson [*15*]	$\Delta\epsilon_p = 1.5\ \epsilon_f$ at 1/4 cycle	$\epsilon_f' = 0.5\ \epsilon_f$ $(c = -0.6)$
Manson and Hirschberg [*16*]	$\Delta\epsilon_p = 0.25\ (\epsilon_f)^{0.75}$ at 10 cycles	$\epsilon_f' = 0.75\ (\epsilon_f)^{0.75}$ $(c = -0.6)$
Manson [*12*]	$\Delta\epsilon_p = \epsilon_f^{0.6}$ at 1 cycle	$\epsilon_f' = 0.76\ (\epsilon_f)^{0.6}$ $(c = -0.6)$
Martin [*22*] Halford and Morrow [*13*]	$\Delta\epsilon_p = \epsilon_f$ at 1/2 cycle	$\epsilon_f' = 0.50\ \epsilon_f$
Sessler and Weiss [*23*]	$\Delta\epsilon_p = \epsilon_f$ at 1 cycle $c = -0.5$	$\epsilon_f' = 0.71\ \epsilon_f$
Morrow [*17*]	$\Delta\epsilon_p/2 = \epsilon_f$ at 1/2 cycle	$\epsilon_f' = \epsilon_f$

An alternative procedure is to estimate ϵ_f' from the cyclic stress-strain curve [*5*]. Equation 1 can be rewritten in the form

$$\sigma_a = \sigma_f'(\Delta\epsilon_p/2\epsilon_f')^{1/n'} \quad (6)$$

Setting $\sigma_f' = \sigma_f$, introducing the cyclic 0.2 percent offset yield strength, σ_y', and rearranging terms, produces

$$\epsilon_f' = 0.002(\sigma_f/\sigma_y')^{1/n'} \quad (7)$$

Predicted and experimental values of ϵ_f' are compared in Fig. 21. Good agreement is found, particularly for those steels which fell far below the fracture ductility approximations in Fig. 20. Perhaps more importantly, Eq 7 tends to give conservative predictions for most materials. Plastic strain-life data for several steels, using intercept predictions from Eq 7, are shown in Fig. 22.

The value of c is variously reported as being essentially constant at -0.5 [*11*] or -0.6 [*12*], or to range from -0.5 to -0.7 [*2*]. Experimentally, c is observed to vary with material and condition, with values for the steels in Fig. 22 ranging from -0.6 to -0.8. In general, c tends to decrease in absolute magnitude with increasing ductility. Since both of these effects contribute to high plastic strain resistance, usually only fracture ductility need be considered in comparing the low-cycle fatigue resistance of various materials.

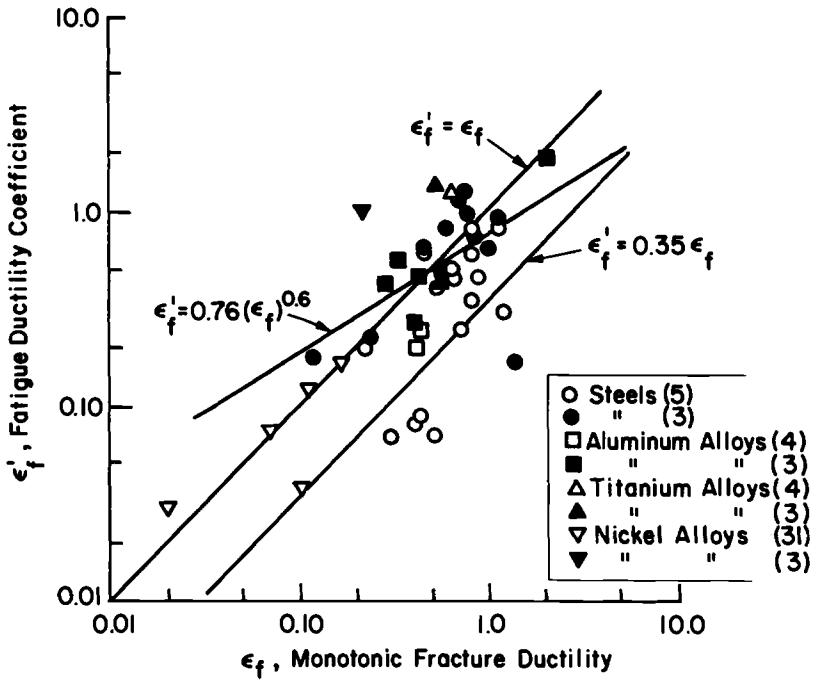

FIG. 20—*Correlation between the fatigue ductility coefficient and monotonic fracture ductility.*

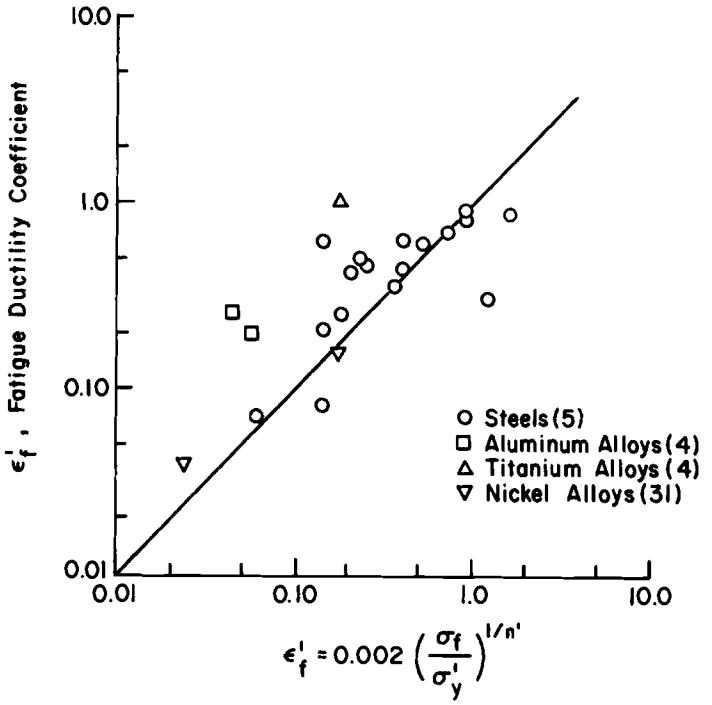

FIG. 21—*Comparison of experimental and calculated values of the fatigue ductility coefficient.*

Morrow [*2*] allows for the variability of c by relating it to the cyclic strain hardening exponent

$$c = -1/(1 + 5n') \quad (8)$$

Comparing Eq 3 and Eq 8, the following relation between the cyclic exponents results:

$$n' = b/c \quad (9)$$

Taking average values for b and c of -0.09 and -0.6, respectively, an n' value of 0.15 is obtained which is consistent with the results shown in the previous section.

Total Strain Resistance

Experimentally it is often most convenient to control the total strain amplitude, since stress or load cycling may lead to instabilities and plastic strain cycling requires rather sophisticated equipment. This circumstance is not without practical justification, since in many structural components the material at the critical location (a notch root, the surface of a bending

member) is subjected to essentially strain cycling conditions due to the constraint of surrounding elastic material.

Manson [*16*] has shown that a metal's resistance to total strain cycling can be considered as the summation of its elastic and plastic strain resistance, hence in Morrow's notation

$$(\Delta\epsilon/2) = (\Delta\epsilon_e/2) + (\Delta\epsilon_p/2) = (\sigma_f'/E)(2N_f)^b + \epsilon_f'(2N_f)^c \ldots\ldots (10)$$

A schematic representation of Eq 10 is shown in Fig. 23. It can be seen that at short lives the plastic strain component predominates, emphasizing the importance of ductility. At long lives the elastic component becomes predominant, emphasizing the role of strength. Life data for two high-strength steels are shown in this form in Fig. 24.

Insight into the relative roles of strength and ductility in resisting fatigue failure at various lives can be gained from the transition fatigue life, that is, the life where the total strain amplitude consists of equal elastic and plastic components. The change in transition fatigue life, $2N_t$, with hardness for a variety of steels is shown in Fig. 25. Values of $2N_t$ are seen to vary from about 10^5 reversals at low hardness to less than 10 reversals at the highest hardnesses. Thus, highly strengthened steels resist cyclic strains largely on

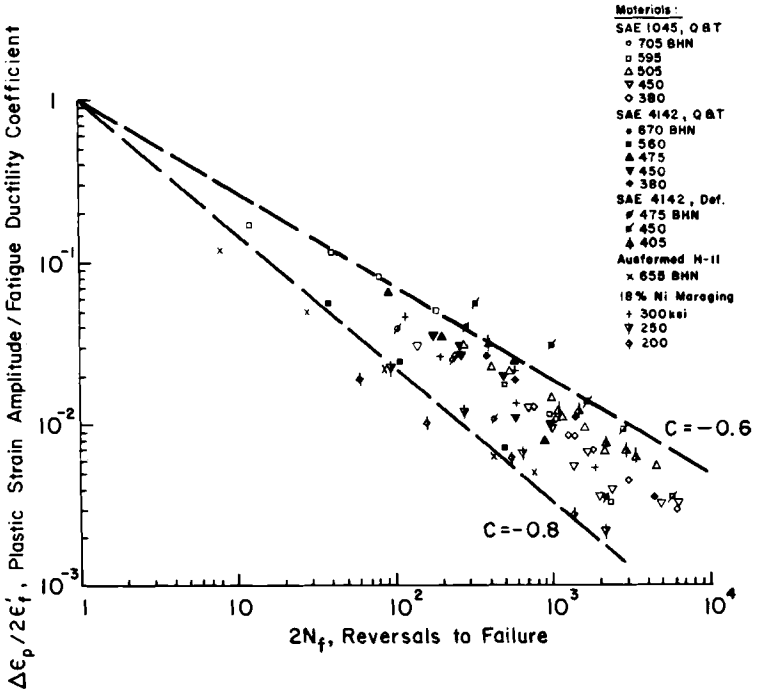

FIG. 22—*Plastic strain amplitude-fatigue life behavior of hardened steels* [5].

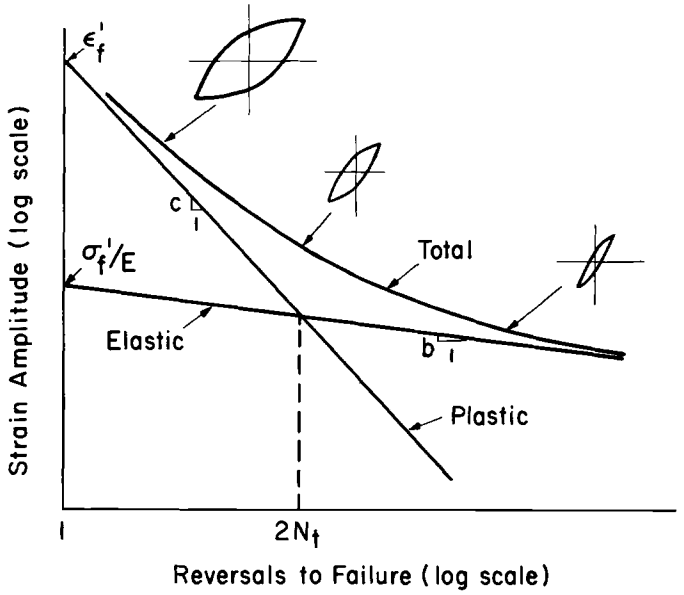

FIG. 23—*Representation of elastic, plastic, and total strain amplitude-fatigue life relations.*

the basis of strength over the entire life range. In contrast, normalized steel will display appreciable plastic strain even at very long lives.

The strain resistance of three idealized metals is illustrated schematically in Fig. 26*a*. Observe that relative material rankings will depend upon the life range of interest. Thus the "ductile" metal offers maximum strain resistance in the low-cycle region, while the "strong" metal is superior at high cyclic lives. Good overall strain resistance is displayed by the "tough" metal.

It is further noted that the curves cross at a common point, illustrating the "rule of thumb" that most metals when subjected to a strain amplitude of 0.01 will fail in approximately 2000 reversals [*24*, *25*]. Although similar lives are observed, as Morrow has shown [*17*], the manner in which a metal resists a strain amplitude of 0.01 may differ markedly. In Fig. 26*b* the stress-strain responses of the three metals at this strain amplitude are compared. A "strong" metal resists the imposed strain elastically on the basis of its strength, while a "ductile" metal resists the strain plastically on the basis of its ductility.

Departures from the log-log linear relations for elastic and plastic strain have been observed in certain alloys. Metallurgical instabilities induced by plastic straining have been shown to promote nonlinear behavior [*16*]. Also, the plastic strain line is sometimes observed to take on a steeper slope at small strains [*4*, *5*]. Adequate behavior descriptions can still be attained from the given relations in such instances by emphasizing plastic strain points at

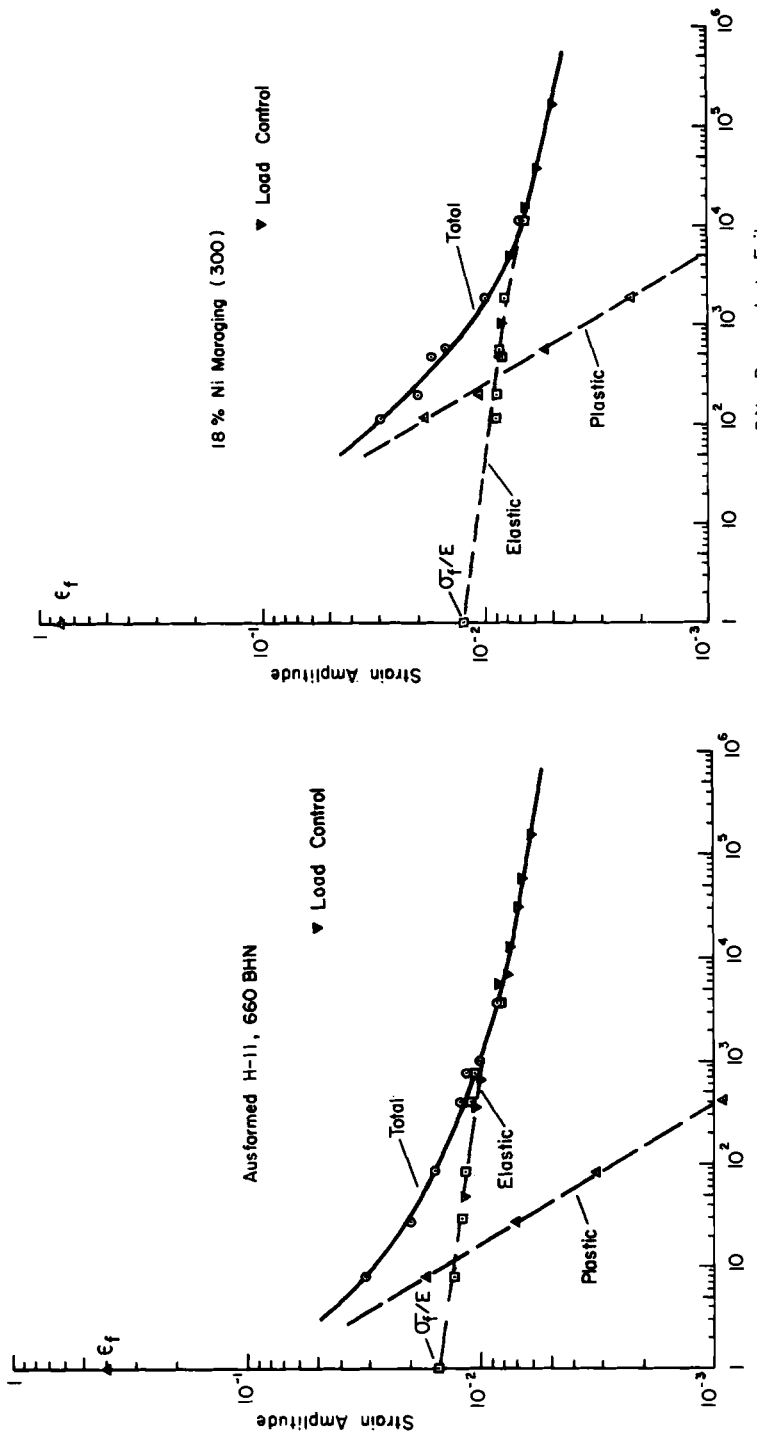

FIG. 24—*Elastic, plastic, and total strain amplitude-fatigue life behavior of two steels* [5].

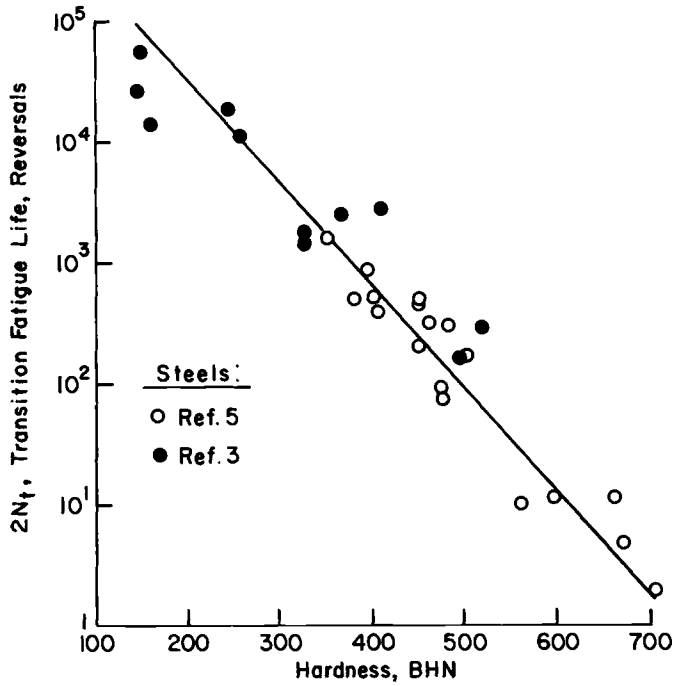

FIG. 25—*Transition fatigue life as a function of hardness for steel.*

lives less than the transition life, and elastic strain points at lives greater than the transition life.

Notch Resistance

Significant progress has been made in understanding notched fatigue behavior through consideration of local stress-strain response at a critical location [*24*, *26*, *27*]. Particularly promising is an analysis developed by Topper et al [*28*] from a rule proposed by Neuber [*29*]. It states that in a notched member the peak-to-peak changes in nominal stress, ΔS, and nominal strain, Δe, are related to the peak-to-peak changes in local stress, $\Delta\sigma$, and local strain, $\Delta\epsilon$, through the fatigue concentration factor, K_f,[6]

$$K_f(\Delta S \Delta e E)^{1/2} = (\Delta\sigma \Delta\epsilon E)^{1/2} \quad \ldots\ldots\ldots\ldots\ldots\ldots (11)$$

where E is the elastic modulus. Since nonlinear stress-strain behavior is accounted for, the analysis should apply equally well at short and long lives.

By relating nominal stress-strain behavior to the actual stress-strain response at the critical location, it is possible to simulate notch fatigue behavior with a smooth specimen [*30*]. Such a simulation is shown in Fig. 27

[6] The fatigue concentration factor is here considered a constant throughout the life range.

for a notched aluminum plate subjected to zero-to-tension loading. Due to yielding at the notch root the initial local mean stress relaxes out and the critical location experiences completely reversed stresses.

For notched members subjected to completely reversed, constant-amplitude loading, life predictions can be made from smooth specimen data [*28*]. This is accomplished by determining the parameter on the right side of Eq 11, $(\Delta\sigma\Delta\epsilon E)^{1/2}$, as a function of life from smooth specimen stress-life and strain-life curves. The resulting master life curve can be entered with the appropriate value of $K_f(\Delta S\Delta eE)^{1/2}$ to determine the life at which a detectable crack should be observed in the notched member. Noting the form of the smooth specimen parameter, it can be seen that notch resistance is dependent upon the product of stress and strain resistance.

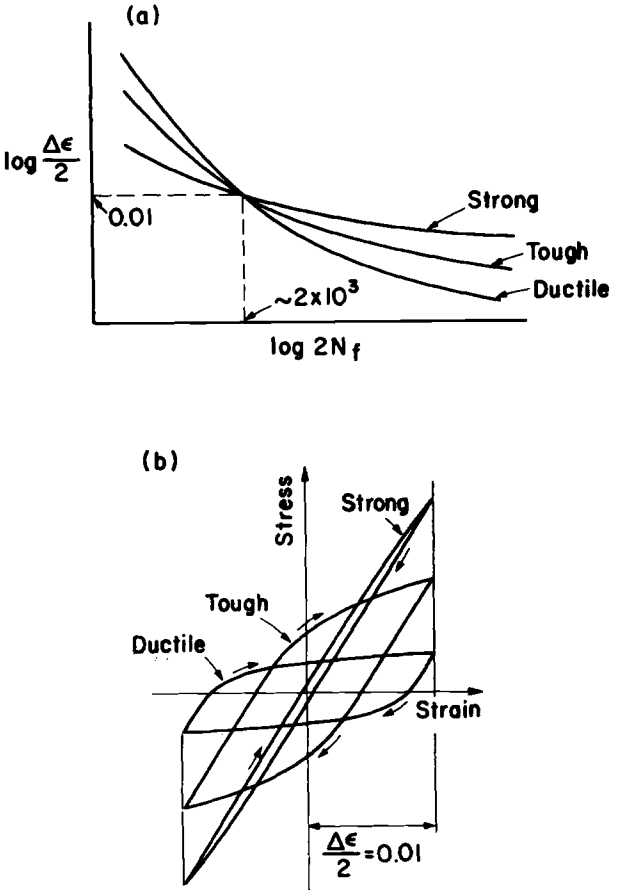

FIG. 26—*Schematic representation of the cyclic strain resistance of idealized metals.*

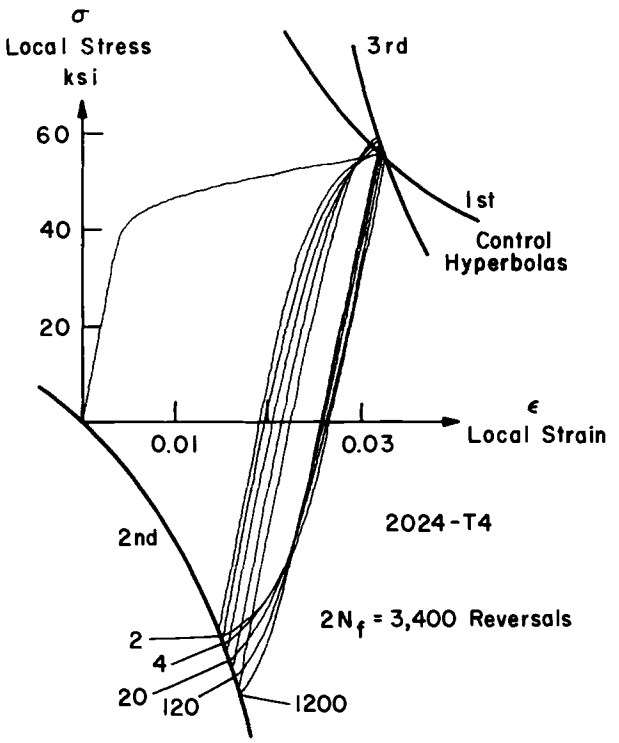

FIG. 27—*Smooth specimen simulation of the local stress-strain behavior of a notch in a plate subjected to 0-max loading (from Wetzel* [30]).

Summary

Since metals in general respond differently to repeated stresses than to repeated strains, their fatigue resistance will likewise depend on the imposed loading conditions. Cyclic stress resistance will be determined by a metal's strength, while plastic strain resistance is dependent on ductility. The resistance of a metal to total strain cycling can be considered as the summation of elastic strain resistance, or fatigue strength, and plastic strain resistance, or fatigue ductility. Notch fatigue resistance can be estimated from smooth specimen data and is found to depend on the product of stress and strain resistance.

Expressions resulting in linear log-log relations between elastic strain-fatigue life and plastic strain-fatigue life provide useful quantitative descriptions of fatigue behavior for a wide variety of materials. True monotonic fracture strength and ductility can be related to fatigue strength and ductility, thus providing a method of approximating the coefficients in the life relations. Further, the exponents in these relations, b and c, are related to the cyclic strain hardening exponent, n'.

Optimizing the Fatigue Resistance of Metals

Characterization of Cyclic Behavior

Cyclic deformation and fracture behavior of metals is observed to fit consistent patterns that can be described by simple power relations. Considering the constants in these relations, σ_f', ϵ_f', b, c, and n', as cyclic properties of a metal provides a quantitative basis for assessing cyclic behavior similar to that used so effectively in characterizing monotonic deformation and fracture behavior. Also, the utility of such relations in developing cumulative damage procedures and in adapting computer techniques to material behavior analysis should not be overlooked.

Correlating the cyclic properties with their monotonic counterparts, σ_f, ϵ_f, and n, greatly extends the usefulness of monotonic tension data in quantitatively predicting cyclic behavior in terms of the strength, ductility, and strain hardening properties of a metal. A monotonic tension curve in conjunction with a cyclic stress-strain curve determined by means of the incremental step test provide a great deal of information regarding the cyclic deformation and fracture behavior of a metal [*32*]. A cyclic curve is especially useful in determining a material's cyclic stability and hence the effectiveness of a particular strengthening technique in resisting cyclic deformation.

In light of the large changes in flow properties that may result from cycling, it should not be surprising that monotonic fracture properties are more indicative of a metal's fatigue resistance than either yield or ultimate strengths.[7] Another advantage of using monotonic fracture properties is that they are sensitive to many of the internal defects which are known to affect fatigue behavior. Thus anisotropic effects, such as inferior transverse fatigue properties in directionally worked plates or bars, would be predicted by σ_f and ϵ_f values measured from transverse tension specimens [*33*, *34*]. Often no difference would be observed in yield and ultimate strengths [*35*]. McClintock [*36*] has demonstrated that inclusions may greatly affect fracture ductility. Fracture strength would be similarly affected, thus accounting for the frequently observed high sensitivity of fatigue strength to inclusion content [*37*].

Such characterization techniques provide the materials engineer with a basis for materials evaluation and for determining the effect of variables on fatigue performance. For the metallurgist a criterion for designing and processing alloys to resist fatigue is established. In either case, information is available to guide selection of the proper combination of properties to optimize fatigue performance for a given set of conditions.

Because of the varying influence of strength and ductility on fatigue resistance, the optimum condition of a metal will depend upon the type of loading

[7] Halford and Morrow [*13*] have shown that such correlations between fracture properties and fatigue resistance are equally applicable to torsional cycling.

and the desired life. Thus the requirement for high stress cycling resistance will be a high σ_f, while high plastic strain resistance requires a high ϵ_f. Total strain cycling resistance will depend on a high ϵ_f at short lives, a high σ_f at long lives, and a combination of high strength and ductility at intermediate lives.

Such considerations are illustrated for various hardnesses of quenched and tempered 1045 steel in Fig. 28. In Fig. 28*a* the total strain-life curves for three conditions of steel illustrate that material rankings often reverse themselves when proceeding from long-life to short-life regions because of the reciprocal strength-ductility relationship. Figure 28*b* illustrates the shift in optimum hardness for steel under strain cycling conditions. At long lives where behavior is nominally elastic, the hardest condition displays the highest strain

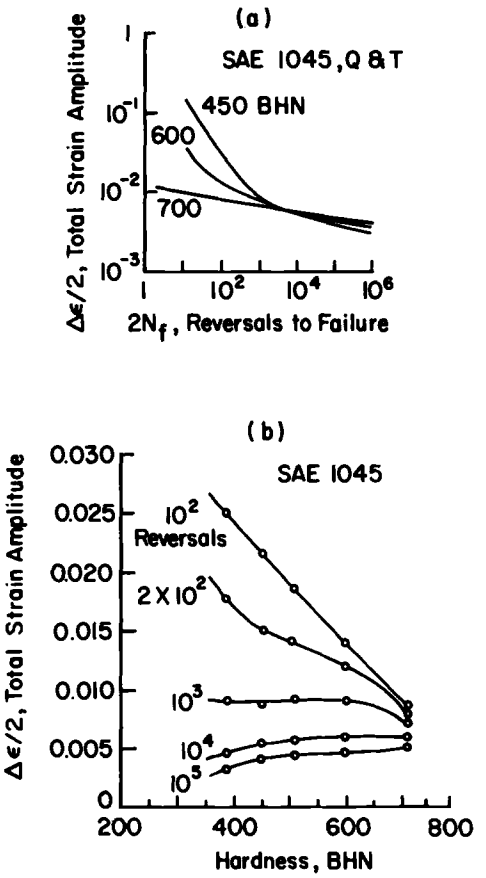

FIG. 28—*Strain cycling resistance of SAE 1045 steel illustrating the shift in optimum hardness* [5].

resistance. At shorter lives where plastic strain becomes a factor, the softer, more ductile conditions offer the highest strain cycling resistance. Note that at 10^3 reversals all conditions show about the same resistance. Thus optimum hardness for maximum fatigue resistance decreases with decreasing life or increasing strain amplitude.

Combined strength-ductility considerations are particularly relevant in determining notch fatigue resistance. The Neuber parameter, $(\Delta\sigma\Delta\epsilon E)^{1/2}$, which provides an indication of relative notch resistance, is dependent upon both stress and strain resistance.

Material Processing Considerations

A cyclic properties approach can be a valuable aid in determining effective processing techniques for achieving high fatigue resistance. Alloy strengthening processes are traditionally evaluated on the basis of their effect on tensile yield and ultimate strengths. A number of thermomechanical treatments [*38*] are presently available which result in significant increases in yield strength while often having little effect on fracture strength. Thus the strain hardening exponent will be substantially reduced, as evidenced by a low uniform elongation, and pronounced cyclic softening can be anticipated. Further, if the fracture properties are not increased, little change in fatigue resistance can be expected.

If the "ideal" fatigue-resistant material for structural applications could be achieved, it might have the following characteristics: (1) a strain hardening exponent of about 0.1 to insure cyclic stability, (2) a high fracture strength to resist the imposed loads, and (3) a high fracture ductility to accommodate large plastic strains at critical locations (notches, inclusions, voids, etc.).

Presently attainable combinations of fracture strength and ductility for various alloy classes are illustrated in Fig. 29.[8] From a mechanics of materials viewpoint, improvements in fatigue resistance can be associated with increasing the upper bounds of the various banded regions. That progress along these lines is being made is evident in the case of steel. Ausforming is observed to impart uncommonly high strength coupled with moderate ductility, while maraging steels exhibit good strength with high ductility.

The fatigue resistances of an ausformed H-11 steel and an 18 percent nickel maraging steel are compared with two conditions of conventionally quenched and tempered steel in Fig. 30. The ausformed steel gives maximum long-life resistance on the basis of its strength, while the maraging steel shows good overall performance because of its high combination of strength and ductility.

[8] Density and temperature considerations are obviously ignored in this mechanics comparison.

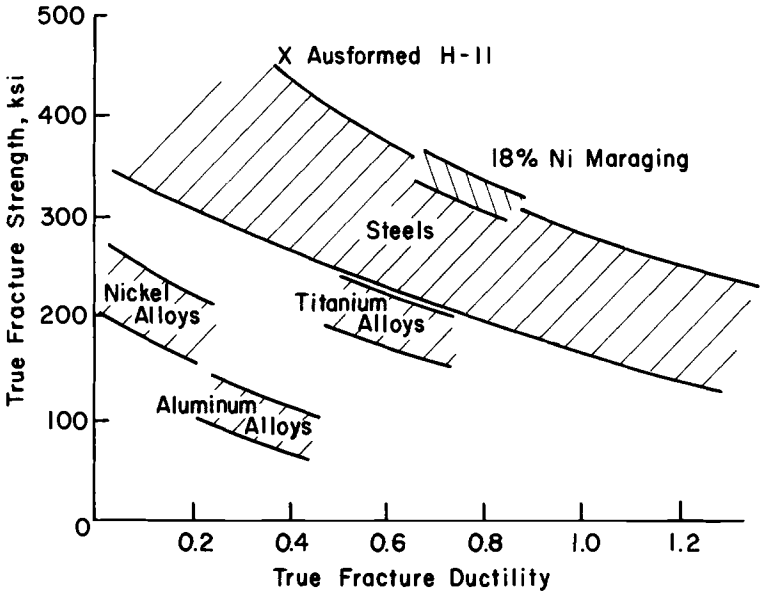

FIG. 29—*Monotonic fracture strength-ductility combinations presently attainable in various alloy classes.*

Often bending, torsion, and notched structural members are subjected to surface treatments in an effort to improve fatigue resistance. The foregoing discussion suggests some guidelines for these approaches, for instance, surface hardening techniques such as induction hardening, carburizing, and nitriding have the effect of increasing the strength and decreasing the ductility of the surface material.[9] Thus, from Fig. 28, it can be concluded that such treatments will be effective at low strains and long lives but may be detrimental to fatigue performance at high strain amplitudes. Increased strength is not necessarily synonymous with increased fatigue resistance!

Techniques such as shot peening, which impart high compressive residual stresses at the surface, will likewise be most effective at long lives, since at high cyclic strains relaxation of such stresses due to inelastic action may occur. As shown in Ref *39*, residual stresses will be stable as long as the sum of the residual stress and the imposed stress amplitude does not exceed the yield strength of the material. Thus a material with a high yield strength which is cyclically stable would benefit most from such treatments. A stable residual stress can be treated as a mean stress and its effect on fatigue life assessed from Eq 4. Knowledge of the monotonic and cyclic stress-strain

[9] Residual stress effects associated with these techniques are discussed in the next paragraph.

curves for a material allows estimation of the strain amplitudes over which a residual stress will remain stable.

In short, valuable insight into the cyclic response of components or structures can be gained through characterization techniques by viewing a smooth specimen as a filament of material which could be located at any critical location in the structure.

Concluding Remarks

Our ability to describe cyclic behavior in terms of simple relations using cyclic properties is quite good. Likewise, a number of useful correlations exist with monotonic behavior allowing interpretation of cyclic phenomena in terms of familiar material properties. It should be emphasized that the significant monotonic properties, σ_f, ϵ_f, and n, result from a true stress-strain analysis of monotonic tension data as opposed to the conventional engineering analysis. Also, the cyclic stress-strain curve is rapidly gaining acceptance as a useful input into fatigue studies and analyses. The ease of obtaining such a curve using the incremental step test recommends it as a promising standard materials test.

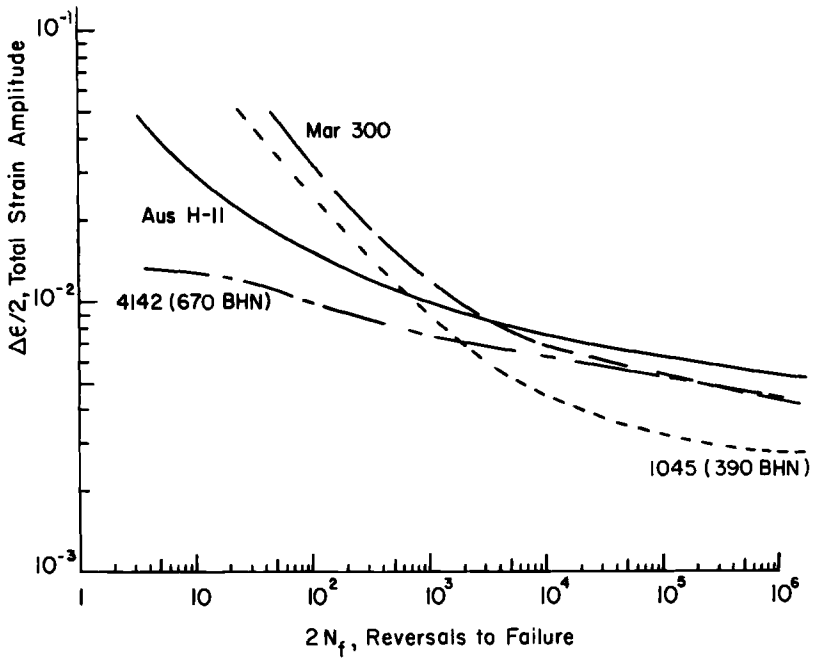

FIG. 30—*Cyclic strain resistance of representative hardened steels* [5].

Consideration of local stress-strain response suggests that in many engineering structures the material at the critical location experiences essentially reversed strain cycling, thus emphasizing the importance of strain-based fatigue data. Further, since strain gage readings are frequently used in service history studies, development of reliable strain-based cumulative damage procedures remains a fruitful research area.

The analysis of notched fatigue behavior by relating nominal and local cyclic stress-strain response is presently being extended to a wider range of notch geometries and more complicated loading spectra. If successful, the utility of material characterization techniques will be further enhanced. The demonstrated success of this approach suggests that similar considerations may prove conceptually and analytically useful in crack propagation studies [*40*].

Acknowledgments

Many of the approaches in this paper reflect a philosophy developed over the past several years in the H. F. Moore Fracture Research Laboratory of the Department of Theoretical and Applied Mechanics, University of Illinois. I particularly wish to acknowledge Professor JoDean Morrow's motivating influence on this activity.

References

[*1*] Tuler, F. R. and Morrow, JoDean, "Cycle-Dependent Stress-Strain Behavior of Metals," Report No. 239, Department of Theoretical and Applied Mechanics, University of Illinois, Urbana, Ill., March 1963.

[*2*] Morrow, JoDean in *Internal Friction, Damping, and Cyclic Plasticity, ASTM STP 378*, American Society for Testing and Materials, 1965, pp. 45–84.

[*3*] Smith, R. W., Hirschberg, M. H., and Manson, S. S., "Fatigue Behavior of Materials Under Strain Cycling in Low and Intermediate Life Range," NASA TN D-1574, National Aeronautics and Space Administration, April 1963.

[*4*] Endo, T. and Morrow, JoDean, *Journal of Materials*, JMLSA, Vol. 4, No. 1, March 1969, pp. 159–175.

[*5*] Landgraf, R. W., "Cyclic Deformation and Fatigue Behavior of Hardened Steels," Report No. 320, Department of Theoretical and Applied Mechanics, University of Illinois, Urbana, Ill., Nov. 1968.

[*6*] Landgraf, R. W., Morrow, JoDean, and Endo, T., *Journal of Materials*, JMLSA, Vol. 4, No. 1, March 1969, pp. 176–188.

[*7*] Benham, P. P. and Ford, H., *Journal of Mechanical Engineering Science*, JMESA, Vol. 3, No. 2, 1961, p. 119.

[*8*] Dolan, T. J., "Nonlinear Response Under Cyclic Loading," *Proceedings*, Ninth Midwestern Mechanics Conference, Madison, Wis., 1965.

[*9*] Coffin, L. F., Jr., *Transactions of the American Society for Metals*, TASEA, Vol. 60, No. 2, 1967, p. 160.

[*10*] Morrow, JoDean and Sinclair, G. M. in *Symposium on Basic Mechanisms of Fatigue, ASTM STP 237*, American Society for Testing Materials, 1958, pp. 83–101.

[11] Tavernelli, J. F. and Coffin, L. F., Jr., *Journal of Basic Engineering, Transactions of the American Society of Mechanical Engineers*, TASMA, Vol. 84, Series D, 1962, p. 533.
[12] Manson, S. S., *Experimental Mechanics*, EXMCA, Vol. 5, No. 7, 1965, p. 193.
[13] Halford, G. R. and Morrow, JoDean, *Proceedings*, American Society for Testing and Materials, ASTEA, Vol. 62, 1962, pp. 695–707.
[14] Manson, S. S., *Machine Design*, MADEA, June 23, 1960, p. 153.
[15] Manson, S. S., *Machine Design*, MADEA, Nov. 23, 1961, p. 165.
[16] Manson, S. S. and Hirschberg, M. H. in *Fatigue An Interdisciplinary Approach*, Syracuse University Press, Syracuse, N. Y., 1964, p. 133.
[17] Morrow, JoDean, "Fatigue Properties of Metals," paper submitted to Fatigue Design Committee of Society of Automotive Engineers Iron and Steel Technical Committee Division 4, April 1964; see also *Fatigue Design Handbook*, Society of Automotive Engineers, New York, 1968, Chapter 3.2.
[18] Landgraf, R. W., "Effect of Mean Stress on the Fatigue Behavior of a Hard Steel," Report No. 277, Department of Theoretical and Applied Mechanics, University of Illinois, Urbana, Ill., Jan. 1966.
[19] Morrow, JoDean, "Low Cycle Fatigue Behavior of Quenched and Tempered SAE 1045 Steel," Report No. 277, Department of Theoretical and Applied Mechanics, University of Illinois, Urbana, Ill., April 1965.
[20] Coffin, L. F., Jr., *Transactions of the American Society of Mechanical Engineers*, TASMA, Vol. 76, 1954, p. 931.
[21] Tavernelli, J. F. and Coffin, L. F., Jr., *Transactions*, American Society for Metals, TASEA, Vol. 51, 1959, p. 438.
[22] Martin, D. E., *Journal of Basic Engineering, Transactions of the American Society of Mechanical Engineers*, TASMA, Vol. 83, Series D, 1961, p. 565.
[23] Sessler, J. G. and Weiss, V., "Low Cycle Fatigue Damage in Pressure Vessel Materials," Paper No. 62-WA-233, *American Society of Mechanical Engineers*, 1963.
[24] Peterson, R. E., *Materials Research & Standards*, MTRSA, Vol. 3, No. 2, Feb. 1963, pp. 122–139.
[25] Morrow, JoDean and Johnson, T. A., *Materials Research & Standards*, MTRSA, Vol. 5, No. 1, Jan. 1965, pp. 30–32.
[26] Crews, J. H., Jr., and Hardrath, H. F., *Experimental Mechanics*, EXMCA, Vol. 6, No. 6, 1966, p. 313.
[27] Wetzel, R. M., Morrow, JoDean, and Topper, T. H., "Fatigue of Notched Parts with Emphasis on Local Stresses and Strains," Naval Air Development Center Report No. NADC-ST-6818, Johnsville, Warminster, Pa., Sept. 1968.
[28] Topper, T. H., Wetzel, R. M., and Morrow, JoDean, *Journal of Materials*, JMLSA, Vol. 4, No. 1, Mar. 1969, pp. 200–209.
[29] Neuber, H., *Journal of Applied Mechanics*, American Society of Mechanical Engineers, Vol. 28, 1961, pp. 544–550.
[30] Wetzel, R. M., *Journal of Materials*, JMLSA, Vol. 3, No. 3, Sept. 1968, pp. 646–657.
[31] Morrow, JoDean and Tuler, F. R., *Journal of Basic Engineering, Transactions of the American Society of Mechanical Engineers*, TASMA, Vol. 87, Series D, 1965, p. 275.
[32] Feltner, C. E. and Landgraf, R. W., "Selecting Materials to Resist Low Cycle Fatigue," Paper No. 69-DE-59, American Society of Mechanical Engineers, 1969.
[33] English, A. T., *Journal of Metals*, American Institute of Mining, Metallurgical, and Petroleum Engineers, April 1965, p. 395.
[34] Toth, R. G. and Polakowski, N. H., *Transactions Quarterly*, American Society for Metals, ASMQA, Vol. 55, 1962, p. 420.
[35] Bush, R. H., McEvily, A. J., Jr., and Justusson, W. M., *Transactions*, American Society for Metals, TASEA, Vol. 57, 1964, p. 991.
[36] McClintock, F. A. in *Ductility*, American Society for Metals, Metals Park, Ohio, 1968, p. 255.

[37] Stulen, F. B., Cummings, H. N., and Schulte, W. C., "Relation of Inclusions to the Fatigue Properties of High-Strength Steels," International Conference on Fatigue of Metals, Institution of Mechanical Engineers, 1956, p. 439.

[38] Kula, E. B. in *Strengthening Mechanisms, Metals and Ceramics*, Syracuse University Press, Syracuse, N. Y., 1966, p. 83.

[39] "Influence of Residual Stress on Fatigue of Steel," SAE Handbook Supplement TR-198, JoDean Morrow and J. F. Millan, Eds., Society of Automotive Engineers, New York, 1961.

[40] Feltner, C. E. and Beardmore, P. in *Achievement of High Fatigue Resistance in Metals and Alloys, ASTM STP 467*, American Society for Testing and Materials, 1970, pp. 77–112.

J. H. Crews, Jr.[1]

Crack Initiation at Stress Concentrations as Influenced by Prior Local Plasticity

REFERENCE: Crews, J. H., Jr., **"Crack Initiation at Stress Concentrations as Influenced by Prior Local Plasticity,"** *Achievement of High Fatigue Resistance in Metals and Alloys, ASTM STP 467*, American Society for Testing and Materials, 1970, pp. 37–52.

ABSTRACT: The effects of high loads on crack initiation lives of notched specimens were quantitatively assessed from an analysis of local behavior at the stress concentration. Local cyclic stresses were determined by a simulation technique involving unnotched specimens and agreed well with experimental local stresses. Unnotched specimens were fatigue tested under stress sequences equal to the local stresses in notched specimens, and test results were used as estimates of crack initiation lives for the notched specimens. These estimates reflected the general effects of prior local plasticity on crack initiation behavior at a stress concentration but were consistently shorter than experimentally determined crack initiation lives. This discrepancy was attributed to the large difference in volume of highly stressed material for the notched and unnotched specimens.

KEY WORDS: fatigue (materials), notch strength, crack initiation, loads (forces), stresses, residual stress, plastic properties, simulation, stress concentration

A few cycles of high loading on a structure can have a significant effect on fatigue life. The major portion of this effect has been attributed to residual stresses at stress concentration sites. Residual stresses develop as a result of plastic deformation due to high loads. A high tensile load causes compressive residual stresses that increase fatigue life for subsequent lower load levels. Conversely, a high compressive load causes tensile residual stresses that decrease fatigue life for subsequent lower load levels. These residual stresses are effective primarily during the crack initiation life of a structure and have diminishing influence on fatigue life as cracks grow away from the stress concentration.

Quantitative analyses of the effects of high loads on crack initiation life have not been possible because of difficulties in assessing the cyclic plastic stress-strain behavior at a stress concentration site. Recently, however, a

[1] Aerospace technologist, Fatigue Branch, Structures Research Div., National Aeronautics and Space Administration, Langley Research Center, Hampton, Va. 23365.

useful technique has been developed [*1*, *2*][2] which accounts for plastic deformation in calculating the stresses at a stress concentration (herein denoted as local stresses). The technique is based on the simulation of local stress-strain conditions with unnotched specimens.

In the present study the effects of prior high loads on crack initiation lives of notched specimens were assessed from an analysis of local behavior at the stress concentration. The local cyclic stress-strain conditions were determined by the simulation technique and were compared with experimental results. Unnotched specimens were fatigue tested under stress sequences equal to the local stresses in the notched specimens, and test results were used as estimates of crack initiation lives for the notched specimens. The estimates were compared with experimentally determined crack initiation lives of notched specimens.

Nomenclature

E	Young's modulus, ksi (MN/m^2)
K_f	Fatigue notch factor
K_T	Theoretical elastic stress concentration factor
K_ϵ	Strain concentration factor
K_σ	Stress concentration factor
N	Number of cycles
N_{cp}	Crack propagation life, cycles
N_f	Total fatigue life, cycles
N_o	Crack initiation life, cycles
R	Ratio of minimum to maximum stress
S	Nominal net section stress, ksi (MN/m^2)
$S_{\max}$	Maximum nominal net section stress, ksi (MN/m^2)
ΔS_i	Range of nominal stress for ith monotonic load excursion, ksi (MN/m^2)
ϵ	Local strain
$\Delta\epsilon_i$	Range of local strain corresponding to ΔS_i
σ	Local stress, ksi (MN/m^2)
$\Delta\sigma_i$	Range of local stress corresponding to ΔS_i, ksi (MN/m^2)

Observed Behavior of Notched Specimens with Prior Loading

In the present study, fatigue tests were conducted on sheet specimens (2024-T3 aluminum alloy) with a circular hole (K_T = 2.57 [*3*]). The specimens were subjected to one of two loading sequences, shown schematically in Fig. 1. Both sequences consisted of a few cycles of high loading followed by cyclic loading at a lower level. The initial high loading was selected to produce reversed local plasticity at the stress concentration. It was repeated for

[2] Italic numbers in brackets refer to the list of references at the end of this paper.

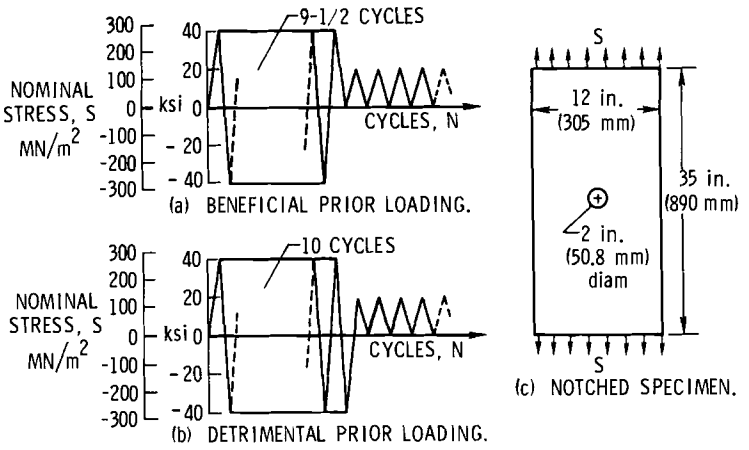

FIG. 1—*Prior loading sequences and notched specimen configuration.*

approximately 10 cycles to stabilize local strain hardening [*2*]. The subsequent low loading was selected to produce only elastic cyclic behavior at the stress concentration. The essential difference between the two sequences in Fig. 1 is the manner in which the high loading ends. High loading in Fig. 1*a*, "beneficial prior loading," ends after a tension half cycle, producing a compressive residual stress. High loading in Fig. 1*b*, "detrimental prior loading," ends after a compression half cycle, producing a tensile residual stress. Fatigue tests were also conducted at the lower loading level (S_{max} = 20 ksi [318 MN/m²], R = 0) without high prior loading.

Fatigue cracks were detected by observing the edge of the hole with a microscope while tests were in progress. Crack initiation life, N_o, was defined as the number of cycles required to produce a 0.03-in. (0.76-mm) crack. In many tests, however, cracks extended beyond this length before they were detected, and for these N_o was found by subtracting crack propagation life, N_{cp}, from the total life, N_f. N_{cp} was assumed to be constant for each loading sequence and was determined from tests in which 0.03-in. (0.76-mm) cracks were detected. The N_{cp} values were: 4000 cycles for the case of no prior loading, 34,000 cycles for beneficial prior loading, and 3000 cycles for detrimental prior loading. Errors in crack initiation life resulting from this procedure were believed to be small because the crack propagation lives were less than 10 percent of the total fatigue life for all test conditions.

Test results given in Table 1 and also presented in Fig. 2 display the anticipated effects of prior loading. Beneficial prior loading increased lives and detrimental prior loading decreased lives, compared to tests with no prior loading. The geometric mean life for beneficial prior loading was approximately 4 times the life for no prior loading, and the geometric mean life for

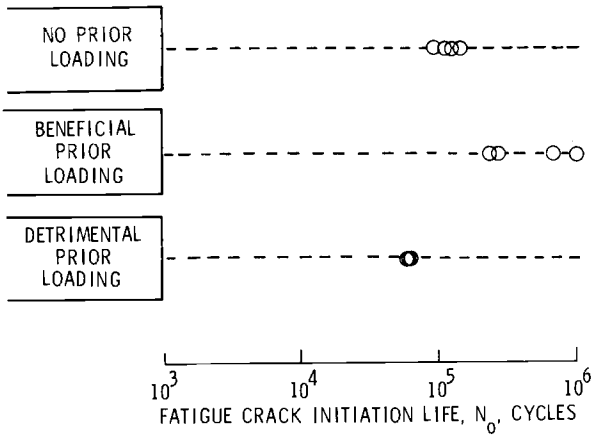

FIG. 2—*Experimentally determined fatigue crack initiation lives for notched specimens.*

detrimental prior loading was approximately 0.5 times that for no prior loading (Table 1). In the following sections of this paper these prior loading effects are interpreted in terms of local cyclic stress conditions that led to crack initiation at the stress concentration site.

TABLE 1—*Experimentally determined crack initiation lives for notched specimens; 2024-T3 aluminum alloy,* $K_T = 2.57$.

Test Condition	Crack Initiation Lives, N_o, cycles	Geometric Mean of Crack Initiation Lives, cycles
No prior loading[a]	90 700	115 600
	113 600	
	123 100	
	140 800	
Beneficial prior loading (Fig. 1*a*)	233 000	458 900
	269 100	
	696 400	
	1 016 200	
Detrimental prior loading (Fig. 1*b*)	61 800	62 900
	62 000	
	62 800	
	65 400	

[a] S_{max} = 20 ksi (138 MN/m²), and $R = 0$.

Local Stress-Strain Behavior

To assess quantitatively the influence of prior loading, an analysis of detailed stress conditions at the stress concentration site is required. Such an analysis was not possible but the simulation procedure given in Refs *1* and *2* provides a reasonable estimate (see the Appendix for description). Maximum and minimum local stress-strain conditions were calculated for each load cycle. An unnotched specimen was cycled between these maximum and minimum stress-strain conditions to establish the local stress-strain history for the notched specimen.

Cycle-by-cycle application of the procedure produced the dashed curves in Figs. 3 and 4, which represent the maximum and minimum local stresses for 50 loading cycles. The dash-dot curves shown for the first 10 cycles represent residual stresses corresponding to half-cycle and full-cycle loadings on the notched specimens. For comparison, the maximum, minimum, and residual local stresses were also determined experimentally. Local strains were measured with small strain gages during each load cycle and were reproduced in unnotched specimens to find the corresponding local stresses. Experimental stresses are shown in Figs. 3 and 4 by symbols. As indicated in the figures, stresses from the simulation procedure agree well with the experimentally determined stresses.

Figure 3 shows the effect of beneficial prior loading. After the 10 cycles of prior loading, local stresses cycle between approximately −30 ksi (207

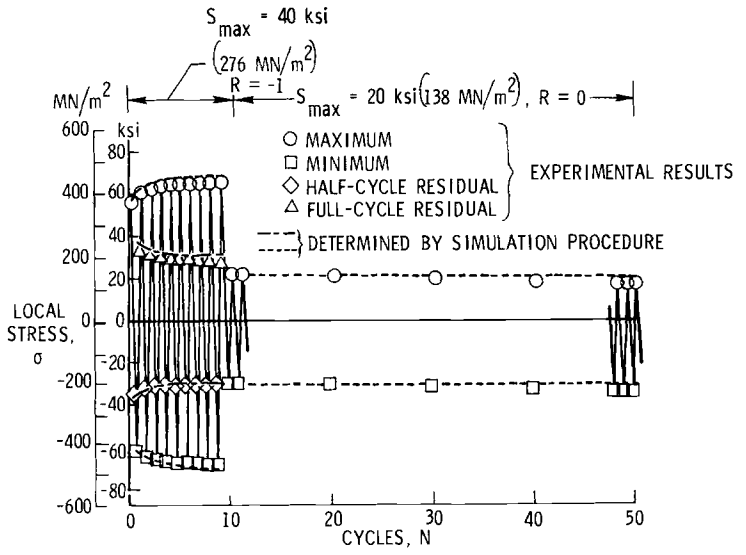

FIG. 3—*Local stress sequence for beneficial prior loading.*

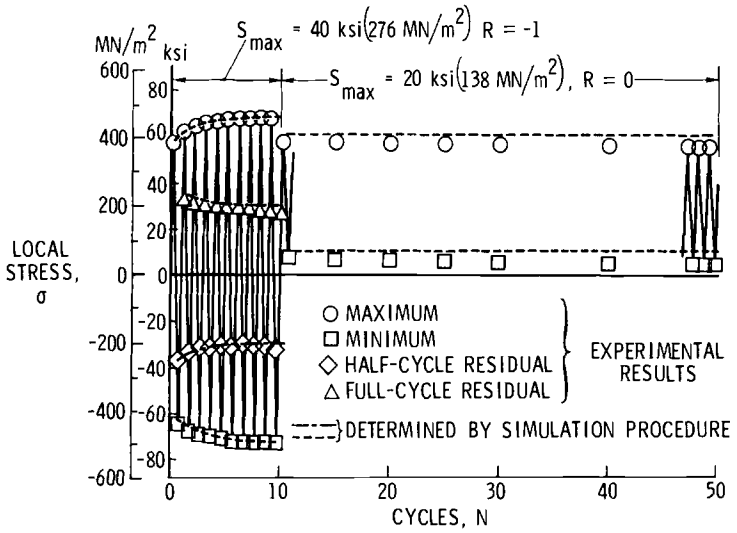

FIG. 4—*Local stress sequence for detrimental prior loading.*

MN/m²) and 20 ksi (138 MN/m²). For comparison consider the case of no prior loading, in which local conditions would be elastic and local stress would cycle between 0 and 51.4 ksi (354 MN/m²). It is evident that beneficial prior loading had the effect of algebraically reducing subsequent local stresses by approximately 30 ksi (207 MN/m²), a reduction which caused the increase in crack initiation life shown in Fig. 2.

The effect of detrimental prior loading is shown in Fig. 4. A tensile residual stress of approximately 30 ksi (207 MN/m²) remained at the end of the 10 prior loading cycles. However, the first 20-ksi (138-MN/m²) load cycle produced local yielding in tension and therefore altered the residual stress. A residual stress of approximately 10 ksi (69 MN/m²) remained at the end of this 20-ksi (138-MN/m²) load cycle, so after 10 cycles local stresses cycled between approximately 60 ksi (413 MN/m²) and 10 ksi (69 MN/m²). Comparison again with the elastic range of 0 to 51.4 ksi (354 MN/m²) for the case of no prior loading shows that detrimental prior loading increased local stresses by only 10 ksi (69 MN/m²), an increase which caused a small reduction in crack initiation life as shown in Fig. 2.

Analysis of Crack Initiation Behavior

Prediction of Crack Initiation Lives for Notched Specimens

Unnotched specimens cycled to stress levels corresponding to those at a stress concentration site should accumulate fatigue damage in approximately

the same manner as the material at the stress concentration; therefore, fatigue tests with unnotched specimens could provide predictions for crack initiation lives of notched specimens. To investigate this possibility, unnotched specimens (made with the same material and fabrication procedures as used for the notched specimens) were cycled to appropriate stress levels until failure occurred. These unnotched specimens usually failed before fatigue cracks grew to an appreciable length; thus, these fatigue lives were used as estimates of the number of cycles to initiate the 0.03-in. (0.76-mm) crack in the notched specimens.

TABLE 2—*Estimated crack initiation lives from simulation tests with unnotched specimens.*

Simulated Test Conditions	Estimated Crack Initiation Lives, cycles	Geometric Mean of Estimated Lives, cycles
No prior loading	19 200	35 100
	22 700	
	43 500	
	48 100	
	58 400	
Beneficial prior loading	140 000	190 600
	181 000	
	273 300	
Detrimental prior loading	17 300	22 600
	23 100	
	28 800	

Estimated crack initiation lives are given in Table 2 and are also presented in Fig. 5 for comparison with the experimentally determined crack initiation lives for the notched specimens. The symbols represent geometric mean lives for Tables 1 and 2, and the brackets indicate scatterbands. The geometric mean of estimated lives for beneficial prior loading was approximately 5 times the estimated life for no prior loading. For the experimentally determined crack initiation lives this ratio was approximately 4. The geometric mean of the estimated lives for detrimental prior loading was 0.6 (60 percent), as long as the estimated life for no prior loading, compared to a factor of approximately 0.5 for the experimental crack initiation lives. The estimated lives, therefore, reflect the general effects of prior loading on notched specimens.

In all cases the estimated mean lives are only approximately 0.4 times as long as the corresponding experimentally determined lives. This trend was believed to be in part related to the volume of material subjected to high stresses. A much larger volume was highly stressed in the unnotched specimens than in the notched specimens (test section for unnotched specimens

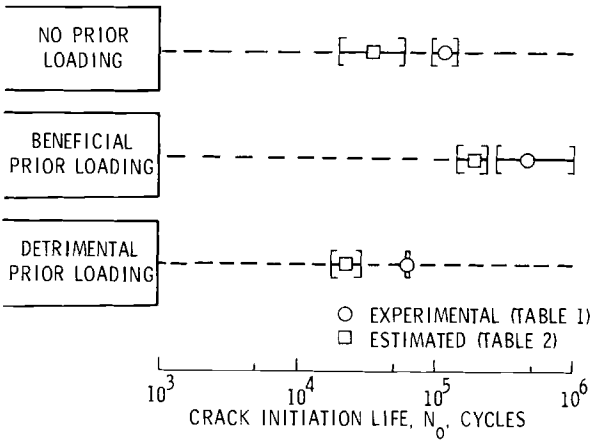

FIG. 5—*Estimated and experimentally determined crack initiation lives.*

was 1.00 in. (25.4 mm) long and 0.800 in. (20.3 mm) wide). Since inherent microscopic flaws of various sizes are distributed throughout the specimen material, it is reasonable to expect the unnotched specimen to contain a larger initial flaw than the highly stressed material in the notched specimen. For the same applied cyclic stresses, this larger flaw would grow faster than its counterpart in the notched specimen, and, as a result, the unnotched specimen would develop a macroscopic fatigue crack in fewer cycles than the notched specimen. Thus, the life to crack initiation predicted from an unnotched specimen cycled under local stresses may be expected to be consistently shorter than the life to initiate cracks in the corresponding notched specimen.

In an effort to account for this "size effect," Wetzel [*1*] replaced K_t by K_f in Eq 2 (found in the Appendix), which resulted in smaller calculated local stresses and, consequently, larger estimates for crack initiation lives. In the present study, however, K_f was nearly equal to K_t; therefore, this approach would not have significantly improved estimates for crack initiation. Further study of this "size effect" correction is required for other test conditions.

Influence of Residual Stresses

To investigate the effects of residual stresses produced by prior loading on the notched specimens, additional tests were conducted with unnotched specimens. For these tests the 10 cycles of high stress in Figs. 3 and 4 were omitted and the unnotched specimens were cycled to failure under the local stresses shown beyond the tenth cycle (Table 3). These tests simulated only the residual stress effects of prior loading. Results are presented in Table 3 and are also plotted in Fig. 6. For beneficial prior loading, the geometric mean life from these tests (Table 3) was nearly 9 times the estimated life for

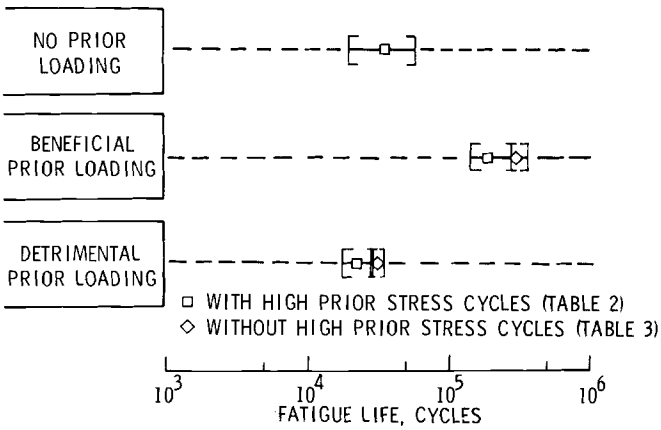

FIG. 6—*Fatigue lives for unnotched specimens with and without high local stress cycles.*

no prior loading (Table 2), and the life for detrimental prior loading was approximately 0.9 as long. These ratios are significantly larger than the corresponding values of 4 and 0.5 determined from crack initiation tests with notched specimens (Table 1), a discrepancy that indicates the influence of high loads on notched specimens cannot be predicted solely from residual stress effects.

TABLE 3—*Fatigue lives from constant amplitude tests with unnotched specimens.*

Maximum Stress, ksi (MN/m²)	Minimum Stress, ksi (MN/m²)	Fatigue Lives, cycles	Geometric Mean of Fatigue Lives, cycles
21.3.....	−30.1	270 900	300 500
(147)	(−208)	276 900	
		361 700	
61.5.....	10.1	28 300	31 700
(424)	(69.6)	32 400	
		34 600	

Damaging Effect of High Local Stress Cycles

In addition to the effects of residual stress on crack initiation lives, high prior loading may produce a second effect. Topper and Sandor [*4*] found that high prior stress cycles had a damaging influence on fatigue lives of unnotched specimens, larger than predicted by the linear damage rule. Because the local stress sequences in Figs. 3 and 4 are similar to those used by Topper and Sandor, the 10 cycles of high local stress probably had a damaging effect on

the crack initiation lives in the present study. The high stress cycles could have initiated microscopic cracks which would grow under subsequent lower stress cycles to produce this damaging effect, as suggested by Dolan and Corten [5].

The procedure used in the present study to estimate crack initiation lives inherently accounted for both the damaging influence of high local stress cycles and the effects of residual stresses. The estimated crack initiation lives from Table 2 are plotted in Fig. 6 for comparison with the lives simulating only the residual stress effects. Differences between them were attributed to the effects of the 10 cycles of high local stress on subsequent fatigue behavior. (The 10 cycles of high stress represented a negligibly small percentage of fatigue life based on the linear damage rule.) In beneficial prior loading, Fig. 6, the residual stress effect increased the geometric mean life from 35,100 to 300,500 cycles, but the damaging effect of high local stress cycles reduced the estimated life to 190,600 cycles. For detrimental prior loading, fatigue lives are within the scatterband of the reference case of no prior loading; however, comparison of geometric mean lives shows a very small life reduction due to residual stresses and a larger reduction caused by the 10 cycles of high local stress. The 10 cycles of high local stress appear to have been the the primary cause for life reduction in the case of detrimental prior loading in Fig. 2. In general, the results in Fig. 6 illustrate the importance of considering both residual stress effects and the damaging effects of high local stress cycles for analyses of crack initiation behavior at stress concentrations.

Conclusions

Fatigue tests of notched specimens demonstrated that prior loads which produced compressive residual stresses caused longer crack initiation lives than were observed in tests without high prior loading. Conversely, high prior loads that produced tensile residual stresses caused shorter crack initiation lives. In addition to producing the effects of residual stresses, a few cycles of high local stress had a damaging effect on life. This effect was attributed to microcracks, produced by the high local stress cycles, that grew readily under subsequent low stress cycles. The observed effects of prior loading on notched specimens were interpreted as the combined result of residual stresses and the damaging effect of high local stress cycles.

The procedure used to simulate local conditions at a stress concentration produced accurate local stresses. Unnotched specimens were cycled to stress levels corresponding to those at the stress concentration site to obtain estimates of crack initiation lives for the notched specimens. These estimates reflected the general effects of prior local plasticity on crack initiation behavior at a stress concentration but were consistently shorter than experimentally determined crack initiation lives for notched specimens. This trend was attributed to the large difference in volume of highly stressed material for the notched and unnotched specimens.

APPENDIX

Simulation of Local Stress-Strain Behavior

In Refs *1* and *2* local stress and strain at a stress concentration were simulated using unnotched specimens. The basis of this simulation is illustrated schematically in Fig. 7 for the case of a sheet containing a circular hole. When loaded as shown in Figure 7*a*, the fatigue critical points lie on the boundary of the hole at Points *C*. In a thin sheet a state of uniaxial stress exists at these symmetrically located points, and the local stress there is shown schematically as σ, acting on a small element of material. An identical stress state can be produced in an unnotched specimen under an applied stress of σ, as shown in Fig. 7*b*; therefore an unnotched specimen can be used to represent the cyclic stress-strain behavior at points *C* by cycling the unnotched specimen between limiting conditions for stresses and strains that occur at points *C*. For this investigation, limiting conditions for stress and strain at point *C* were calculated by the Neuber equation [*6*]

$$K_T^2 = K_\sigma K_\epsilon \quad \ldots\ldots\ldots\ldots\ldots\ldots\ldots\ldots\ldots\ldots (1)$$

which relates stress and strain concentration factors to the elastic stress concentration factor. This equation was rewritten as

$$\Delta\sigma_i = (K_T \Delta S_i)^2 / E\Delta\epsilon_i \quad \ldots\ldots\ldots\ldots\ldots\ldots\ldots\ldots\ldots\ldots (2)$$

where $\Delta\sigma_i$ and $\Delta\epsilon_i$ are the changes in local stress and strain corresponding to the ith monotonic excursion of nominal stress, ΔS_i. Substituting into Eq 2 values of K_T and E for a given configuration and material and a value of ΔS_i for a given load cycle results in a hyperbolic relationship between $\Delta\sigma_i$ and $\Delta\epsilon_i$. A particular solution for this relationship can be determined by plotting Eq 2 together with a uniaxial stress-strain curve for the material. The intersection of the stress-strain curve and the hyperbola from Eq 2 provides values of $\Delta\sigma_i$ and $\Delta\epsilon_i$ that satisfy Eq 2 and are also consistent with the stress-strain behavior of the material.

The cycle-by-cycle application of this procedure can be explained with Fig. 8, which shows a typical first cycle of nominal stress for which local behavior is sought.

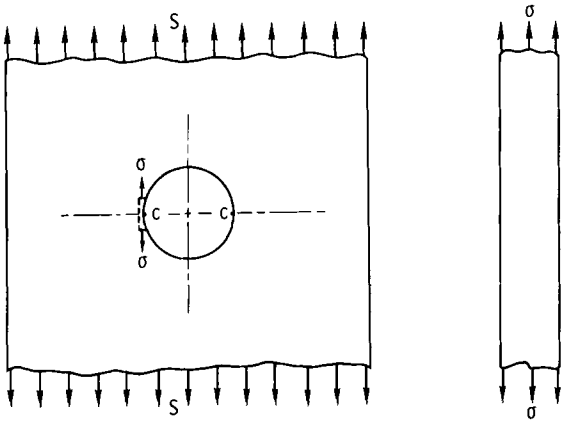

(a) SPECIMEN WITH STRESS CONCENTRATION. (b) UNNOTCHED SPECIMEN.

FIG. 7—*Simulation of local stress with an unnotched specimen.*

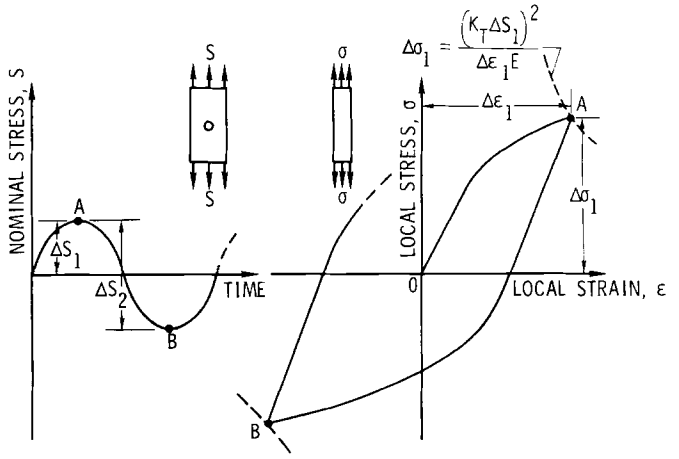

(a) NOMINAL STRESS CYCLE. (b) SIMULATED LOCAL STRESS-STRAIN CURVE.

FIG. 8—*Nominal stress cycle and corresponding local stress-strain curve.*

The cycle has been divided into monotonic excursions of nominal stress and each excursion has been labeled. To illustrate, Eq 2 has been evaluated for a given K_T and E and plotted in the first quadrant of Fig. 8*b* for ΔS_1. This hyperbola represents the locus of maximum values of local stress and strain corresponding to ΔS_1. An *unnotched* specimen was loaded in uniaxial tension to obtain the stress-strain curve, *OA*. Point *A* corresponds to the intersection of the curves and therefore represents the only combination of $\Delta\sigma_1$ and $\Delta\epsilon_1$ that satisfies Eq 2 and is also consistent with the stress-strain curve, *OA*. Thus point *A* represents the estimated maximum values of local stress and strain during the first quarter cycle. For the second excursion of nominal stress, ΔS_2, point *A* was taken as the initial state. Accordingly, Eq 2 was plotted relative to point *A* for ΔS_2, as shown in the third quadrant. The unnotched specimen was unloaded from point *A* and loaded into compression until the resulting stress-strain curve intersected this limiting curve corresponding to ΔS_2. The intersection, point *B*, represents the estimate for the minimum values of local stress and strain for this cycle of nominal stress. The local stress-strain curves for cycling beyond the first cycle were determined by repeatedly applying this procedure to find the extreme points for each cycle.

Similarly, half-cycle residual stresses and strains were found for the nominal stress cycle in Fig. 8*a* by plotting Eq 2 relative to point *A* with $\Delta S_i = \Delta S_1$. The intersection of this curve for Eq 2 with the curve *AB* established the half-cycle residual stresses and strains for the unloading excursion, ΔS_1. Subsequent residual conditions were determined by repeating this procedure for each unloading excursion.

References

[*1*] Wetzel, R. M., *Journal of Materials*, JMLSA, Vol. C, No. 3, Sept. 1968, pp. 646–657.

[*2*] Crews, J. H., "Elasto-Plastic Stress-Strain Behavior at Notch Roots in Sheet specimens Under Constant-Amplitude Loading," NASA TN D-5253, National Aeronautics and Space Administration, 1969.

[*3*] Howland, R. C. J., *Transactions of the Royal Society*, London, TRSOA, Vol. A229, 1929-1930, pp. 49–86.

[4] Topper, T. H. and Sandor, B. I., "Effects of Mean Stress and Prestrain on Fatigue Damage Summation," Report No. 318, Theoretical and Applied Mechanics Laboratory, University of Illinois, Urbana, Ill., Aug. 1968.
[5] Dolan, T. J. and Corten, H. T., "Progressive Damage Due to Repeated Loading," Wright Air Development Center Symposium on Fatigue of Aircraft Structures, WADC TR59-507, 1959, pp. 598–625.
[6] Neuber, H., *Journal of Applied Mechanics, ASME Transactions, Series E*, JAMCA, American Society of Mechanical Engineers, Vol. 28, No. 4, 1961, pp. 544–550.

DISCUSSION

R. M. Wetzel[1] *(written discussion)*—We have learned a great deal from Dr. Crews and his colleagues at the NASA Langley Research Center. With this in mind I should like to ask him to comment on the following.

Notches are frequently less severe in fatigue than indicated by K_T, the theoretical elastic stress concentration factor. For this reason K_f, a "fatigue strength reduction factor" or "fatigue concentration constant," is frequently defined for a given notched specimen as [*1*][2]

$$K_f = \frac{\text{fatigue strength, unnotched specimen at a given life}}{\text{fatigue strength, notched specimen at the same life}} \quad \ldots\ldots (1)$$

K_f factors so defined are constant at long lives but tend to decrease toward 1.0 at shorter lives because of inelastic deformation. Several authors (for example, Refs *2–4*) have derived empirical expressions for determining the value of K_f at long lives; however, it has been my experience that these expressions are unreliable particularly when applied to specimens of a different material or geometry than originally used to derive the relationships. Therefore, whenever possible, I think it advisable to determine, or at least verify, K_f values using Eq 1 and experimental data for the specimen in question.

With this introduction I should like to question Dr. Crews' statement that K_f was nearly equal to K_T for the specimens he used. The unnotched specimens used to simulate the fatigue behavior of notched plates lasted 0.4 as long as the notched plates. This was explained as being the result, in part, of a size effect, since a larger volume of metal was highly stressed in the unnotched specimens than in the notched specimens. The observation, as well as Dr. Crews' explanation, supports the alternate view that K_f as defined by Eq 1 would be significantly less than K_T. Use of this K_f in place of K_T in Neuber's equation (Eqs 1 and 2) would improve the agreement between the unnotched specimen lives and the notched specimen lives.

In general, I believe that the "fatigue concentration constant," K_f, determined from long-life data and Eq 1, should be substituted for K_T when Neuber's equation is applied to fatigue problems. This conclusion is verified in Refs *5–8*.

[1] Scientific research staff, Ford Motor Co., Dearborn, Mich.

[2] Italic numbers in brackets refer to the list of references at the end of the Discussion.

It is gratifying that Dr. Crews' results agree with a similar investigation which also studied the effect of prior plasticity and utilized Neuber's equation and the technique of simulating notch behavior with unnotched specimens. This work was done at the University of Illinois. It is reported in detail in Ref *8* and is summarized in Refs *6* and *7*.

J. H. Crews, Jr. (author's closure)—The size effect present in the fatigue behavior of notched specimens can be interpreted as the combined result of two effects, both related to the size of the highly stressed region at the notch. In small notched specimens or in specimens with high K_T values, the highly stressed region may be small compared to the microstructure of the material. For such cases, the local stress gradient may be attenuated by material inhomogeneity, and, as a result, local stress may be less than predicted by K_T. The second factor that produces a size effect is related to the initial size of the critical flaw that eventually develops into a fatigue crack. As previously discussed in this paper, the critical flaw at the notch is smaller than its counterpart in the unnotched specimen. As a result of this difference in initial flaw size, a notch may be less severe than predicted from the fatigue behavior of unnotched specimens.

In large specimens with mild stress concentrations, as in the present study, elastic local stresses are in agreement with K_T. Observed long-life size effects for such cases are usually small (K_f nearly equal to K_T) and are attributed to the initial flaw size effect.

In the present study measured elastic local stresses (strains) were in agreement with K_T, as expected. Therefore, K_T was used in Neuber's equation for the calculation of local cyclic stresses. The substitution of K_f for K_T in Neuber's equation, as suggested by Dr. Wetzel, would have decreased these calculated local stresses and would have increased the life estimates. However, since the size effect was attributed to the initial flaw size effect, it would have been inappropriate to correct for this effect by deliberately altering the calculated local stresses.

In my view, since the notched specimens in the present study were large, K_T was appropriately used in Neuber's equation. The question of using K_T or K_f for smaller specimens was beyond the scope of this study.

References

[*1*] Grover, H. J., *Fatigue of Aircraft Structures*, NAVAIR 01-1A-13, U. S. Government Printing Office, 1966, p. 70.

[*2*] Peterson, R. E. in *Metal Fatigue*, Sines and Waisman, Eds., McGraw-Hill, 1959, pp. 293–306.

[*3*] Neuber, H., *Theory of Notch Stresses: Principles for Exact Stress Calculations*, J. W. Edwards, Ann Arbor, Mich., 1946.

[*4*] Kuguel, R., *Proceedings*, American Society for Testing and Materials, ASTEA, Vol. 61, 1961, pp. 732–748.

[5] Topper, T. H., Wetzel, R. M., and Morrow, JoDean, *Journal of Materials*, JMLSA, Vol. 4, No. 1, March 1969, pp. 200–209.

[6] Wetzel, R. M., Morrow, JoDean, and Topper, T. H., "Fatigue of Notched Parts With Emphasis on Local Stresses and Strains," Report No. NADC-ST-6818, Naval Air Development Center, Sept. 1968.

[7] Morrow, JoDean, Wetzel, R. M., and Topper, T. H. in *Effects of Environment and Complex Load History of Fatigue Life*, *ASTM STP 462*, American Society for Testing and Materials, 1970, pp. 74–91.

[8] Stadnick, S. J., "Simulation of Overload Effects in Fatigue, Based on Neuber's Analysis," Report No. 325, Theoretical and Applied Mechanics Laboratory, University of Illinois, Urbana, Ill.

L. F. Coffin, Jr.[1]

The Deformation and Fracture of a Ductile Metal Under Superimposed Cyclic and Monotonic Strain

REFERENCE: Coffin, L. F., Jr., **"The Deformation and Fracture of a Ductile Metal Under Superimposed Cyclic and Monotonic Strain,"** *Achievement of High Fatigue Resistance in Metals and Alloys, ASTM STP 467*, American Society for Testing and Materials, 1970, pp. 53–76.

ABSTRACT: This paper describes an investigation on annealed Nickel A to explore the effects of simultaneously applied cyclic and monotonic strains. The results are presented in terms of the true stress-strain envelope of the end points of individual hysteresis loops. During mixed straining, early increased hardening, and later softening with progressive mean strain, occurs in comparison to simple tension. In the limit, the stress level required for deformation is controlled by the stress amplitude of the stabilized hysteresis loop associated with cyclic strain component, and monotonic hardening effects are absent. For tensile monotonic strains, superimposed cyclic strains lead to early necking, until, in the limit, necking occurs with zero mean strain and provides a mechanism for low-cycle fatigue crack nucleation. A failure criterion which fits the results is developed. Here $\epsilon_f/\epsilon_{f_0} = 1 - (N_f/N_{f_0})^{0.563}$ where ϵ_{f_0} is the tensile ductility, N_{f_0} the fatigue life for the cyclic strain component alone, ϵ_f and N_f the fracture strain and fatigue life, respectively, for the mixed mode of deformation.

KEY WORDS: deformation, fracturing, strains, fatigue (materials), ductility, nickel, hardening (materials), evaluation

It is the purpose of this paper to investigate the deformation and fracture of a ductile metal subjected to superimposed cyclic and monotonic strain. While much has been written on the flow and fracture of these processes considered separately, very little has been said about the concurrent effects of cyclic and monotonic strain. Reflection on the actual state of affairs in plastic flow suggests that these combined deformations can occur more frequently than is commonly accepted. Some of the more obvious examples include (1) deformation instabilities in local regions of a body subjected to controlled cyclic displacements at remote locations in the body, (2) bodies

[1] Metallurgy and Ceramics Laboratory, Research and Development Center, General Electric Co., Schenectady, N. Y. 12301.

subjected to constant externally applied loads and simultaneously subjected to cyclic plastic strains arising from some different loading system, (3) metalworking processes where the flow process is nonhomogeneous, and (4) flow processes where the deformation is the consequence of steady stress and intense ultrasonic vibrations. Each of these situations is considered in more detail below.

It is a common experience to observe plastic instabilities in controlled displacement experiments in low-cycle fatigue exploration. For example, a uniaxially loaded hourglass-shaped specimen subjected to controlled amplitude displacement at each end of the specimen will undergo a shape change with repeated cyclic plastic strain in which the minimum diameter decreases and the diameters at adjacent sections increase. If the cyclic strain at the minimum diameter is controlled, the adjacent sections will increase in diameter even more and the specimen will shorten. These effects and others, including similar shape changes in uniform cross section bars, have been reported earlier [*1*][2] and a mechanism for the behavior was given. More generally, shape instability can be expected to occur in bodies subjected to nonuniform cyclic plastic strain, the extent of which depends on the magnitude of the strain and on the cyclic strain hardening characteristics of the material. Thus, most fatigue failures fall into this category, since the strain at the precise location in the body where failure develops is never so carefully controlled that a mean strain component cannot occur. Indeed this mechanism has been proposed by McClintock [*2*] as the basis for fatigue crack nucleation. It is clear then that the process of simultaneous actions of cyclic and monotonic strain is vital to the fatigue question.

Bars subjected to steady uniaxial loads and cyclic plastic torsion or bending are examples of (2) above. Other loading combinations can be imagined. Under such circumstances the bar can undergo progressive length change, an effect referred to as "cyclic-strain-induced creep," "racheting," etc. Numerous references now exist reporting information on this subject [*3–5*], but an understanding of the process sufficient to allow prediction of results is lacking.

Many metalworking processes involve the simultaneous action of cyclic and monotonic strain. Swaging and forging are obvious examples. However, in many other processes, notably rolling and drawing, the flow is nonhomogeneous and involves extension accompanied by a reversed shear [*6*]. Little information exists as to how one accounts for this behavior by some metalworking theory.

Of particular interest to the present investigation is the reported influence of intense ultrasonic vibration on reducing the flow stress of metals during plastic flow [*7*]. While this effect has been described in terms of an acoustic

[2] Italic numbers in brackets refer to the list of references at the end of this paper.

energy mechanism, it may also be shown to be merely a special case of a broad behavior involving cyclic-monotonic strain interaction, in which the cyclic strain controls the deformation rate. It is this broader view to which this paper is addressed.

Some preliminary attention should be given to the complexities of the strain hardening and softening effects involved in the interaction of cyclic and monotonic strain. The concern here is with annealed, unalloyed metals where hardening or softening effects may be quite pronounced. In monotonic deformation, strain hardening alone will occur; while, under cyclic strain, hardening or softening results depending on the degree of prior cold work. Thus in the annealed state, imposition of cyclic strain produces cyclic hardening, the degree of which depends on the plastic strain range imposed. When the material has received prior cold work, subsequent cyclic strain may either harden the material further or soften it, depending on the amount of prior cold work and the imposed plastic strain range [*8*, *9*]. When the deformation is a combination of both monotonic and cyclic strains, the consequence is a more rapid hardening in the early stages of strain than for monotonic deformation alone, since the cyclic hardening effects of the two processes are additive. After some state of hardening is reached, however, softening can occur from the cyclic strain so that in the later stages of deformation the combined strain hardening effects are less than for monotonic deformation alone.

In an earlier paper [*1*] experiments were carried out on several materials in which simultaneous cyclic and monotonic strains were imposed. The interest was primarily directed toward the difference in material response rather than the specific effects of combining monotonic and cyclic strain. In the present paper a single metal is considered and attention is given to the straining history. Of principal interest is the load and stress response of the material and the eventual fracture of the material as a result of some mixed cyclic and monotonic strain. Although not all of the possible problem areas identified above will be fully resolved from this work, it is hoped that a clearer insight into the complexities of superimposed cyclic and monotonic straining can be achieved.

Material and Test Procedure

Test specimens for the planned experiments were prepared from $\frac{5}{8}$-in.-diameter bar stock of Nickel A, the nominal composition of which was 0.2 percent manganese, 0.15 percent iron, 0.1 percent copper, 0.1 percent carbon, 0.05 percent silicon, 0.005 percent sulfur, and the balance nickel. The test method involved uniaxial push-pull loading, requiring the use of hourglass-shaped specimens. These were prepared with a minimum diameter of 0.150 in. and a specimen radius of curvature of 0.5 in. Following careful surface

preparation ending with longitudinal polish to remove all circumferential scratches, the specimens were annealed in dry hydrogen for 1 h at 750 C.

Testing was performed in a 20,000-lb-capacity, reverse loading Instron machine. In all tests the machine crosshead rate was maintained constant during straining. Changes in diameter were measured and recorded and served as a basis for strain control. Loads were also continuously recorded against time, and by means of an X-Y recorder, plots of load versus diameter change were obtained.

The unique feature of this investigation was the strain program, which involved the superposition of cyclic and monotonic strain as described in Fig. 1. Because strains large enough to cause localized necking could be expected, the diametral strain was selected for measurement and control. To meet the

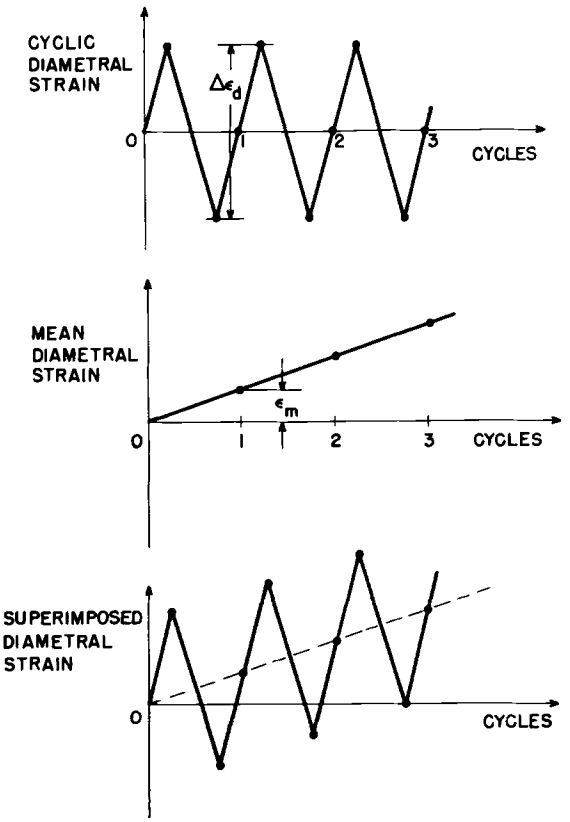

FIG. 1—*Cyclic tension straining pattern.*

requirements of the program depicted in Fig. 1, the diametral strain limits were defined as

$$\epsilon_{d_1} = -K_1 - K_2(N + \tfrac{1}{4}) \quad (1)$$

and

$$\epsilon_{d_2} = K_1 - K_2(N + \tfrac{3}{4}) \quad (2)$$

where K_1 is the diametral strain amplitude established for a specific test and K_2 is the mean diametral strain per cycle. A positive value for K_1 and K_2 corresponds to a decrease in diameter and specimen elongation. Also, N is the number of cycles and ϵ_{d_1} and ϵ_{d_2} the diametral strain limits at the peak tensile and compressive loads, respectively. Converting Eqs 1 and 2 into diameter limits gives

$$d_1 = d_0 e^{-K_1 - K_2(N + 0.25)} \quad (3)$$

$$d_2 = d_0 e^{K_1 - K_2(N + 0.75)} \quad (4)$$

where d_0, d_1 and d_2 are the initial diameter and the diameter limits corresponding to the peak tensile and compressive loads, respectively. Further, the longitudinal strain limits are considered to be twice the diametral strain limits given in Eqs 1 and 2. This assumes Poisson's ratio to be 0.5, an assumption which is in error only in the very early part of the program.

It is apparent from Eqs 3 and 4 that d_1 and d_2 are not linear with N and, as a result, that the diameter-cycle program is not simply controlled. As a consequence, a strain programmer was developed to establish the appropriate diameter limit on the diameter change recorder as the test proceeded (see Ref *10*). Figure 2 shows the test facility used, including the programmer, while Fig. 3 illustrates some typical outputs from an experiment, including force-time, total diameter change-time, and force-total diameter change records. Loads obtained from these records, together with the diameters predicted from Eqs 3 and 4, formed the basis of a computer program to calculate the tensile and compressive true stress amplitudes, the true strain limits, and other desired information.

The test program conducted in this investigation is outlined in Table 1. Note that most of the experiments involved specimen extension (positive K_2) although a few mean compression experiments were conducted. Tests were run until failure, except for those involving a value of $K_1 = 0.0004$.

Test Results

Monotonic Behavior

Room temperature true stress-strain data were obtained from a uniaxial tension test and are shown in Fig. 4. Here the flow stress is plotted versus the

TABLE 1—*Test program.*

Diametral Strain Amplitude, K_1	Mean Diametral Strain per Cycle, K_2
0.0004	0.0001
	0.00002
	0.000004
	−0.00002
0.002	0.0005
	0.0001
	0.00002
	0.000004
	0
	−0.0001
	−0.0005
0.005	0.01
	0.0025
	0.00125
	0.000625
	0.0001
	0
	−0.0001
	−0.000625
	−0.0025
0.01125	0.0225
	0.015
	0.0075
	0.0050
	0.0025
	0.00125
	0.000625
	0.0001
	0

longitudinal plastic strain (defined as $\log_e (A_0/A)$, A and A_0 being the instantaneous and initial areas, respectively). The measured true fracture strain was found to be 1.59.

Effect of Prior Monotonic Strain

A few experiments were undertaken to define the cyclic hardening or softening characteristics of Nickel A for different amounts of prestrain when subjected to controlled diametral cyclic strain. Typical test results are shown in Fig. 5. The behavior indicated is characteristic of many unalloyed metals reported in the literature [*8*, *9*]. Pertinent features include (1) early hardening and eventual saturation of the initially annealed material, with the rate of early hardening and the level of saturation increasing monotonically with the

FIG. 2—*Testing facility, including cyclic-monotonic strain programmer.*

strain range; (2) cyclic softening in the prestrained state, the initial hardness level being determined by the degree of prestrain and the rate of softening[3] increasing with decreasing strain range; and (3) the tendency of the metal to reach the same stress amplitude with continued cycling, independent of the initial state, that is the approach to a stabilized hysteresis loop. These statements presume that the imposed cyclic strain is sufficiently large that some plastic deformation is present.

The criterion for cyclic hardening or softening would appear to relate to the hardness in the prestrained state and the magnitude of the imposed cyclic strain range. A basis for determining what will happen can be found approximately with the aid of Fig. 4. Here the stabilized hysteresis loop data obtained from Fig. 5 have been added, after converting to the stress amplitude and longitudinal plastic strain amplitude. For a given prestrain, the monotonic flow stress is found from curve *A*. Assuming this value to be the stress amplitude of a stabilized hysteresis loop, the nonhardening or softening plastic

[3] The rate of hardening or softening is defined here as the change in stress range per cycle for a constant total strain range.

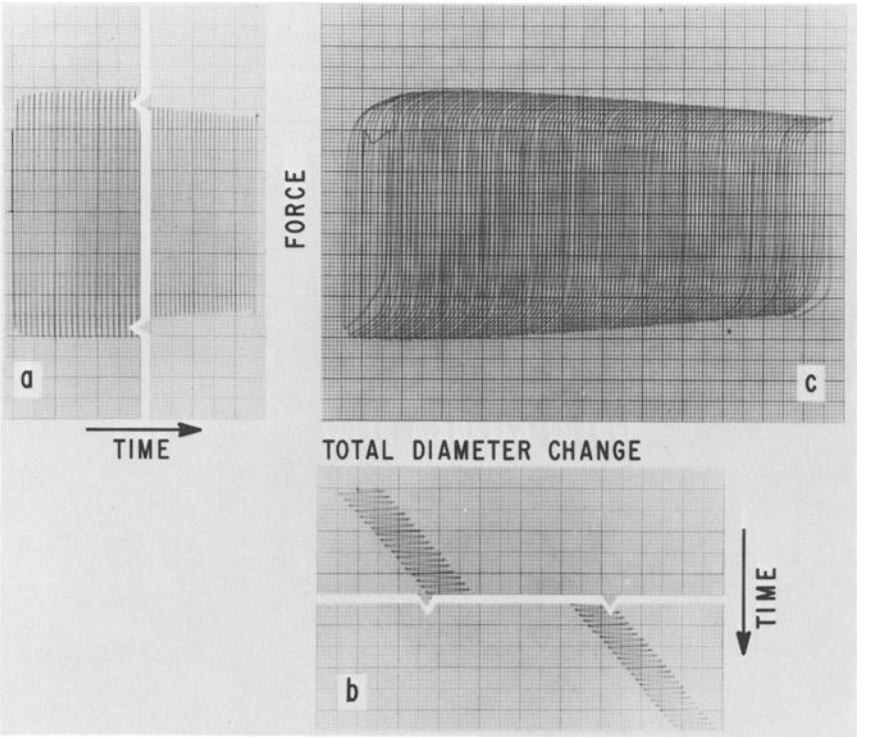

FIG. 3—*Typical cyclic tension data:* (a) *force versus time;* (b) *total diameter change versus time;* (c) *force versus total diameter change.*

strain amplitude is determined from curve *B*. If the applied plastic strain amplitude is less than this value, the prestrained metal will soften; for an applied plastic strain amplitude larger than this the metal will harden. Thus, for example, for a prestrain of 10 percent an imposed plastic strain amplitude of 0.004 or less causes cyclic softening, while a strain amplitude of 0.004 or greater leads to cyclic hardening.

The concept of the stabilized hysteresis loop is found to apply for several unalloyed metals, although such behavior cannot be generalized to all metals. Feltner and Laird [9] describe the tendency for stabilized loop formation in terms of the slip character of the metal involved; those exhibiting wavy slip (aluminum, copper) and having high stacking fault energies develop a prior strain-independent hysteresis loop. Materials with low stacking fault energies deform by planar slip, as, for example, Cu-7.5Al, and do not develop a single-valued stress level with cyclic straining. It is clear, however, that for Nickel A, where the stacking fault energy is high, there is a strong tendency to develop a unique hysteresis loop. This has an important bearing on the work that follows.

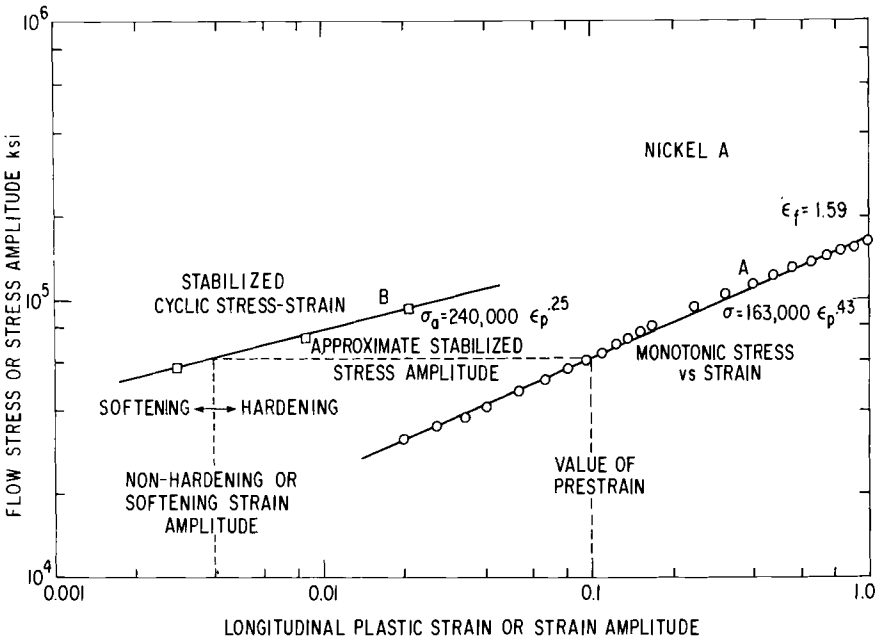

FIG. 4—*True stress-strain tension and stabilized cyclic stress-strain test results and method for determining cyclic hardening or softening.*

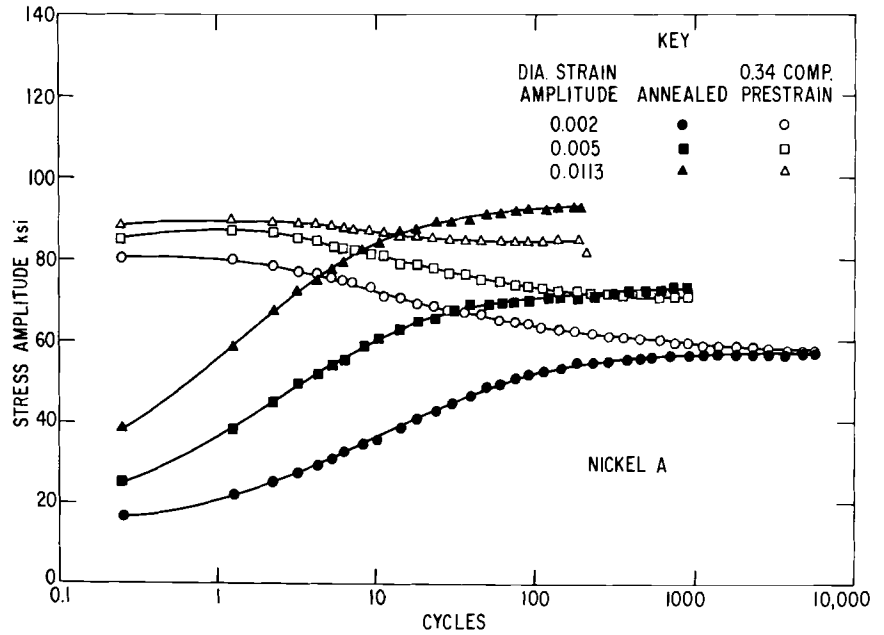

FIG. 5—*Cyclic hardening and softening characteristics of Nickel A.*

Cyclic Tension and Compression Experiments

There are several ways in which the results of the test program outlined in Table 1 can be represented, depending on whether a particular test is regarded primarily as monotonic or cyclic. First, however, there is one important point to be noted, namely that, save for the smallest value of K_1, all tests involve a fully reversed stress. This is seen in Table 2 where the numerically largest value of the mean stress in any one test is tabulated against the stress range obtained for that mean stress. Save for $K_1 = 0.0004$, the mean stress is very small in relation to the stress range. For this low value of K_1, the mean stresses are about one half of the stress range, indicating the absence of appreciable stress reversal.

Considering the tests from the viewpoint of controlled cyclic strain, the representation of data relating stress range and cycles of strain, as shown in Fig. 5, can be used. Figures 6 and 7 are included for two cases, namely, for $K_1 = 0.002$ and $K_2 = 0.005$. For all values of K_2 cyclic hardening occurs, and

TABLE 2—*Mean stresses produced by simultaneous cyclic and monotonic strains.*

Diametral Strain Amplitude, K_1	Mean Diametral Strain Amplitude, K_2	Largest Mean Stress, ksi	Corresponding Stress Range, ksi
0.01125.....	0.0225	4.7	256
	0.015	4.5	307
	0.0075	1.0	271
	0.005	3.8	251
	0.0025	1.0	245
	0.00125	1.1	220
	0.000625	0.7	205
	0.0001	0.2	190
0.005.....	0.01	6.5	226
	0.0025	2.9	257
	0.00125	2.0	245
	0.000625	0.5	188
	0.0001	1.3	158
0.002.....	0.0005	1.5	149
	0.0001	1.6	154
	0.00002	1.2	135
	0.000004	0.9	116
	−0.0001	2.7	125
	−0.0005	5.5	140
0.0004.....	0.0001	62.7	138
	0.00002	54.9	134
	0.000004	32.7	97.4
	−0.00002	55.7	90.7

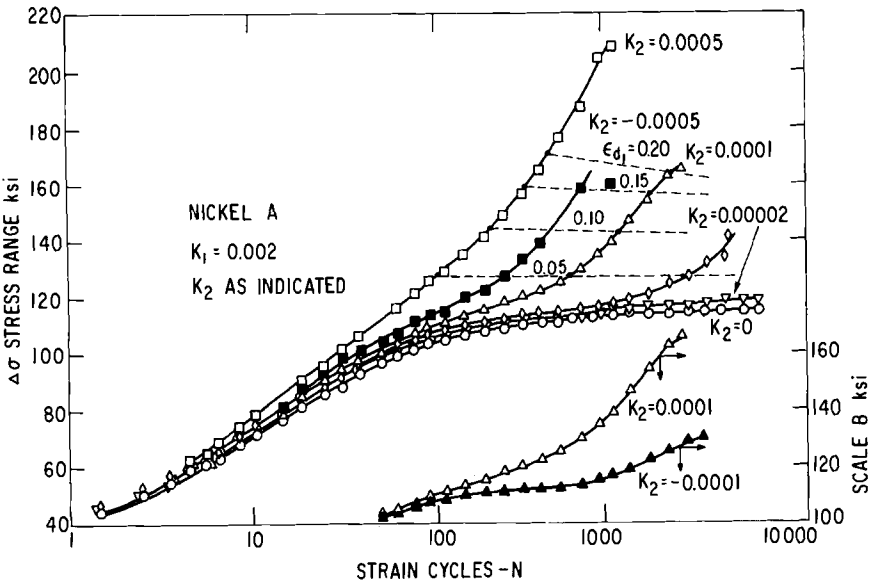

FIG. 6—*Stress range versus cycles of strain for various values of* K_2 *and mean diametral strain,* $K_1 = 0.002$.

the degree of hardening increases as K_2, the mean strain advance per cycle, increases. This is not surprising, since for any given number of strain cycles the mean strain increases with K_2.

These curves reflect the tendency of the material to develop a stabilized hysteresis loop for a specific value of K_1, the diametral strain amplitude, with mean strain accumulation, as determined by the product of K_2 and the number of cycles. To show directly how the accumulated mean strain interacts with the cyclic strain to affect the stress range, dashed lines of constant mean strain are included in Figs. 6 and 7. Note that the lower strain amplitude produces the same accumulated mean strain with a lower stress range. For example, 200 cycles with a $K_1 = 0.002$ and $K_2 = 0.0005$ produce a mean strain of 0.10 at a stress range of 140,000 psi. On the other hand, 40 cycles and a $K_1 = 0.005$ and a $K_2 = 0.0025$ produce the same mean strain but at a stress range of 170,000 psi. Thus, the same mean strain accumulation can be accomplished at lower strain and stress ranges, but more cycles are required.

Additionally, in Fig. 6 comparisons are made of the hardenening which develops in cases where the values of K_2 are the same in magnitude but opposite in sign. Note that a lower stress range is required to produce the same mean strain ($K_2 \times N$) when K_2 is negative. Arguments to justify this will be given later.

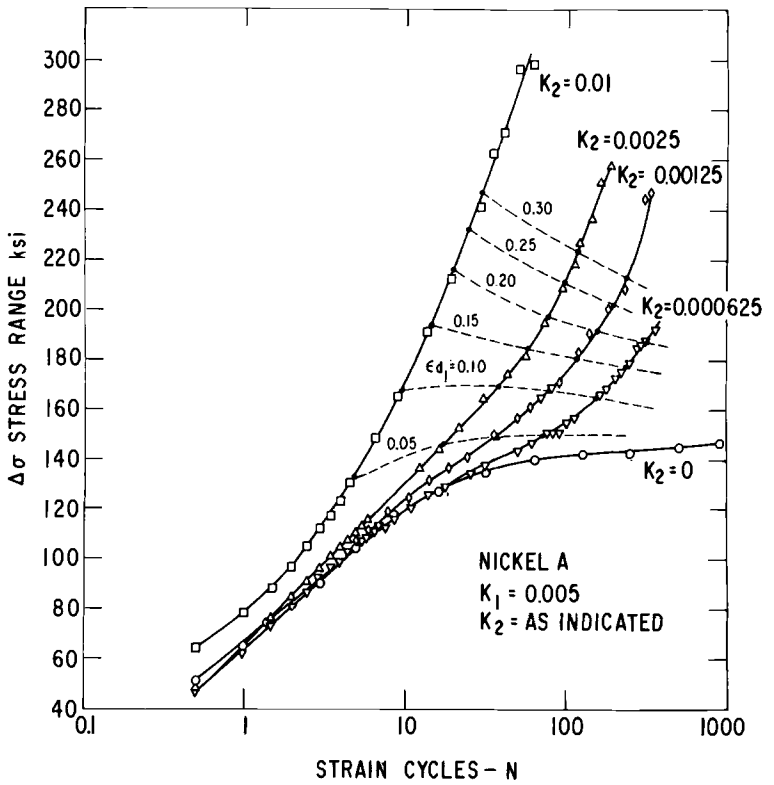

FIG. 7—*Stress range versus cycles of strain for various values of* K_2 *and mean diametral strain,* $K_1 = 0.005$.

A more interesting way to look at the results of the mixed cyclic and monotonic testing program is to consider them as one does a uniaxial monotonic tension or compression experiment. Considering first the cyclic tension tests, and plotting the ordinary stress found at each tensile limit versus the corresponding ordinary strain, defined as A_0/A, the ratio of areas (Figs. 8, 9, and 10) are obtained. Here for each K_1 the corresponding K_2 values become parameters. The ordinary monotonic tensile data ($K_1 = 0$) are included for comparison. Because of the early cyclic hardening in conjunction with the mean strain advance, in each case the ordinary stress values rise more rapidly than for tension without cycling: the hardening increases with the increasing value of K_2. The rate of hardening is then observed to decrease as the mean strain accumulates and the stress level rises. Just as in the simple tension test, a stress maximum is reached, followed by a gradually developing decrease in stress. Since the ordinary stress is being considered here, these curves are actually a reflection of the peak tensile load with each cycle. The behavior

of these peak stresses on loads then indicates the same type of necking instability that is characteristic of the simple tension test, but with certain notable differences. First, it will be observed that with increasing values of K_2, the ordinary strain required for necking decreases—most spectacularly seen in Fig. 8 when this mean strain decreases from 0.31 in simple tension to 0.06 for $K_2 = 0.000625$. In some instances, when K_2 is very low and the number of cycles very large, the effect disappears, probably because a fatigue crack has developed to cause local constraints.

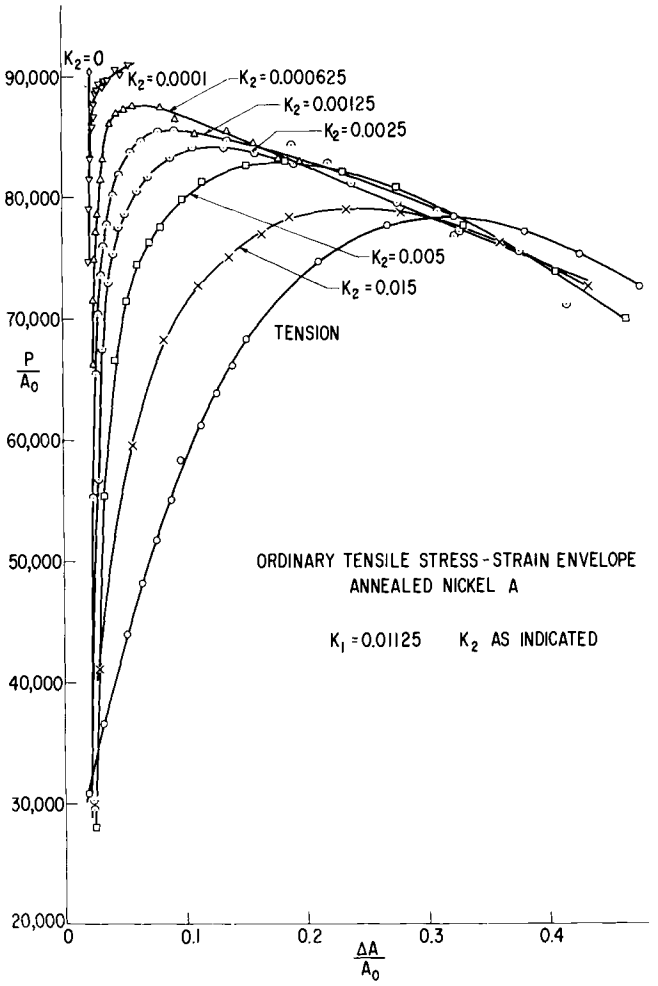

FIG. 8—*Ordinary stress-strain envelopes for various values of* K_2, $K_1 = 0.01125$.

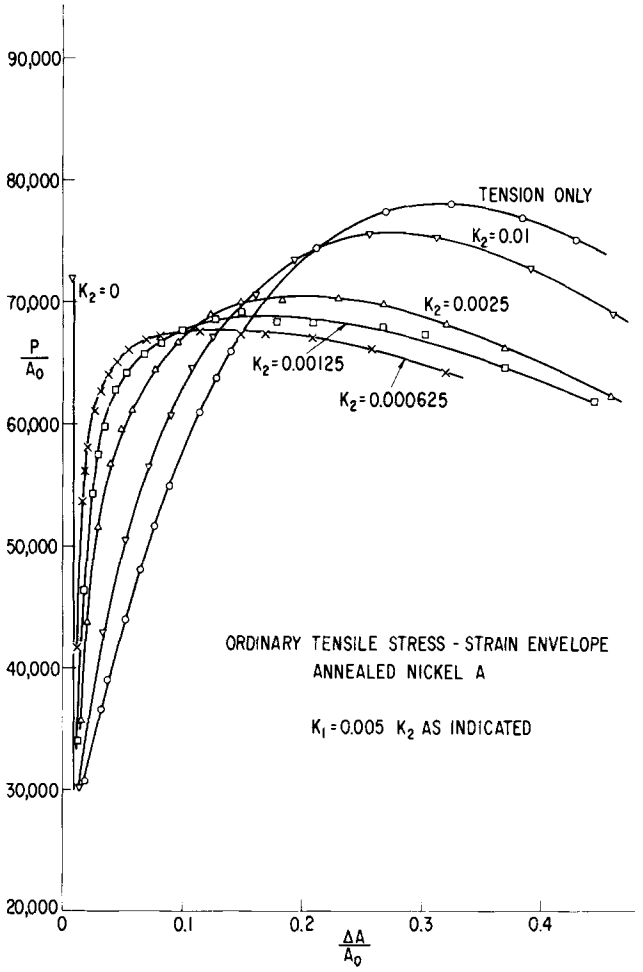

FIG. 9—*Ordinary stress-strain envelopes for various values of* K_2, $K_1 = 0.005$.

A second important observation is the change in the maximum in the ordinary stress envelope curve with increasing K_2. The change is found to depend on the value of K_1. In Fig. 8, where K_1 is 0.01125, the individual maximum stress increases with increasing K_2; while, in Figs. 9 and 10 where the K_1 value is lower, the individual maximum values decrease with increasing mean stress. The effect appears to depend on the stabilized hysteresis loop stress amplitude associated with the particular K_1 chosen. The values are indicated in the figures for $K_2 = 0$. When the stabilized stress amplitude is greater than the ordinary stress maximum in simple tension (the alternate tensile strength), the maximum stresses for decreasing values of K_2 rise; when

the stabilized stress amplitude is less than ultimate strength, the maximum decreases with decreasing K_2. In the limit, and in the absence of an intervening fatigue crack, it would appear that the stabilized stress amplitude and the maximum in the ordinary stress envelope are synonymous. This raises an interesting question regarding stability, a point which will be discussed later.

These same data may also be represented in terms of true stresses and strains, where curves can be constructed of the envelope of individual true stress and strain values obtained at the peak of each hysteresis loop. The curves are shown in Figs. 11–15 for the values of K_1 and K_2 outlined in Table 1. They reflect the observations described for Figs. 8–10, namely, the more rapid hardening in the early stages of mean strain deformation in comparison to the simple tensile behavior. Representation of the data in this manner,

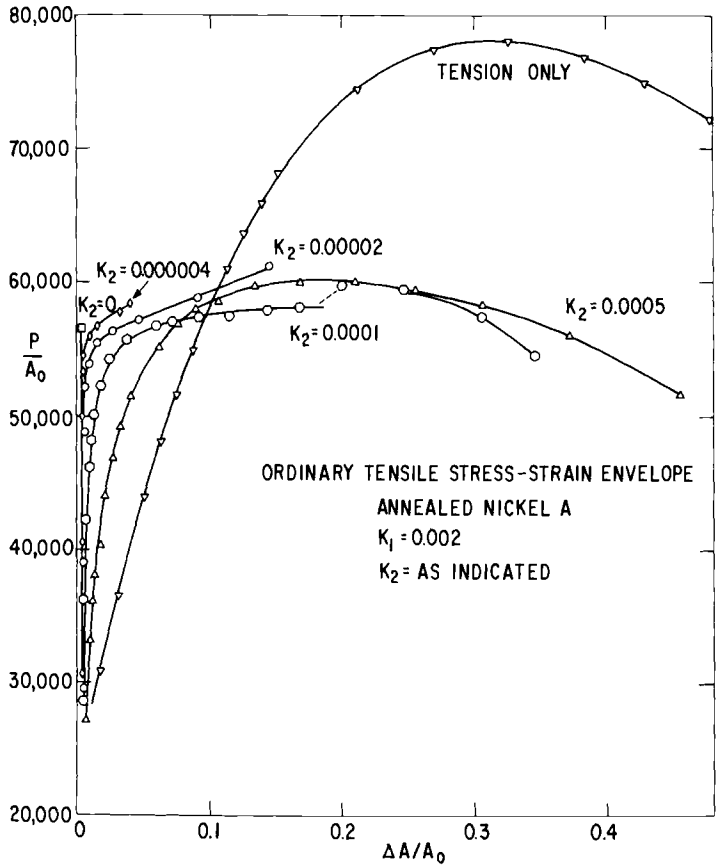

FIG. 10—*Ordinary stress-strain envelopes for various values of* K_2, $K_1 = 0.002$.

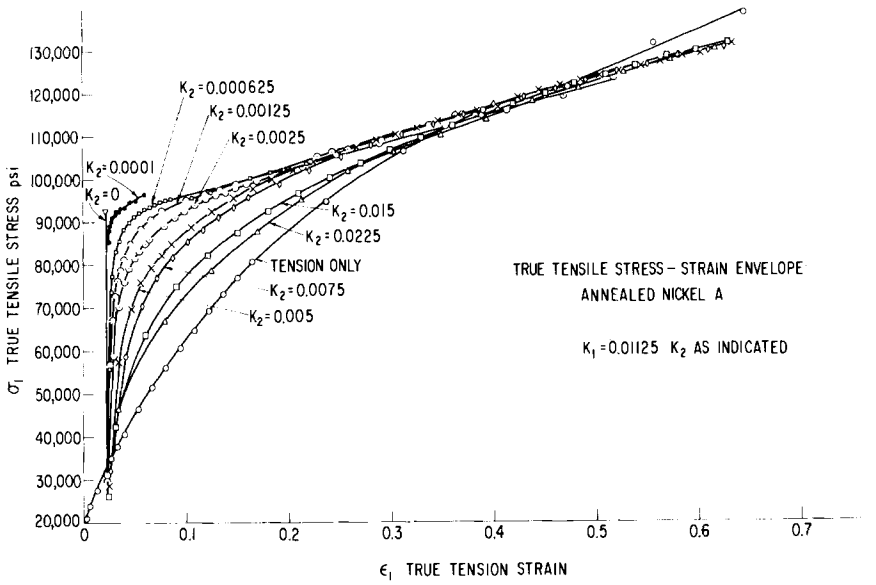

FIG. 11—*True tensile stress-strain envelopes for various values of* K_2, K_1 = 0.01125.

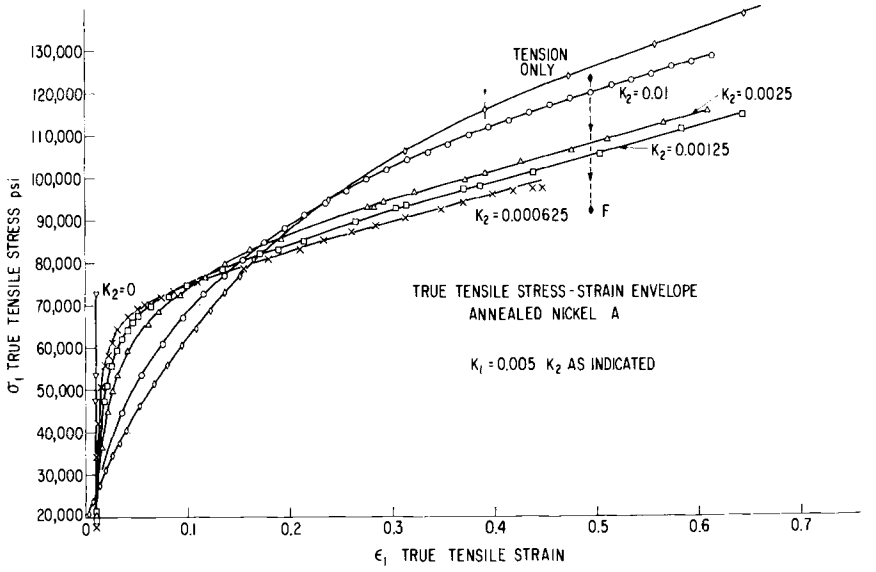

FIG. 12—*True tensile stress-strain envelopes for various values of* K_2, K_1 = 0.005.

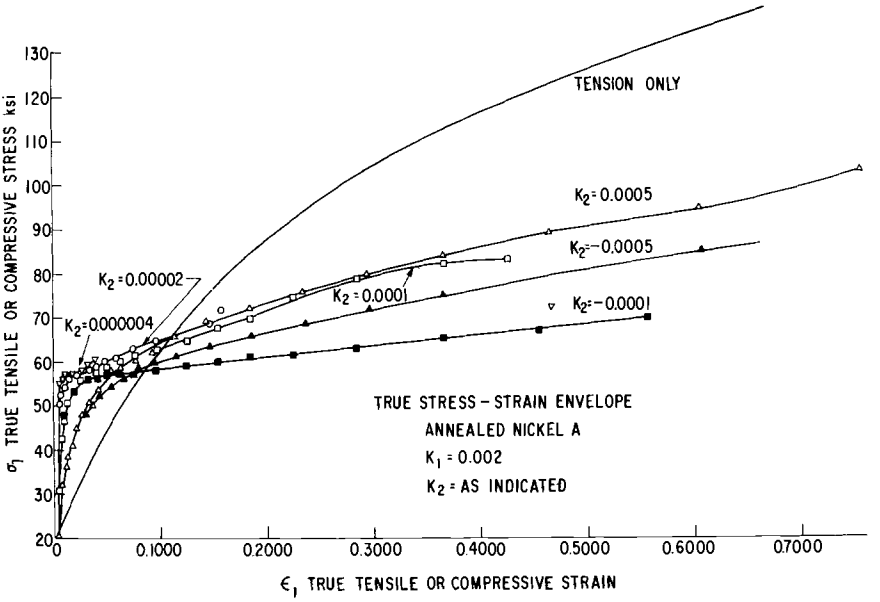

FIG. 13—*True tensile or compressive stress-strain envelopes for various values of* K_2, $K_1 = 0.002$.

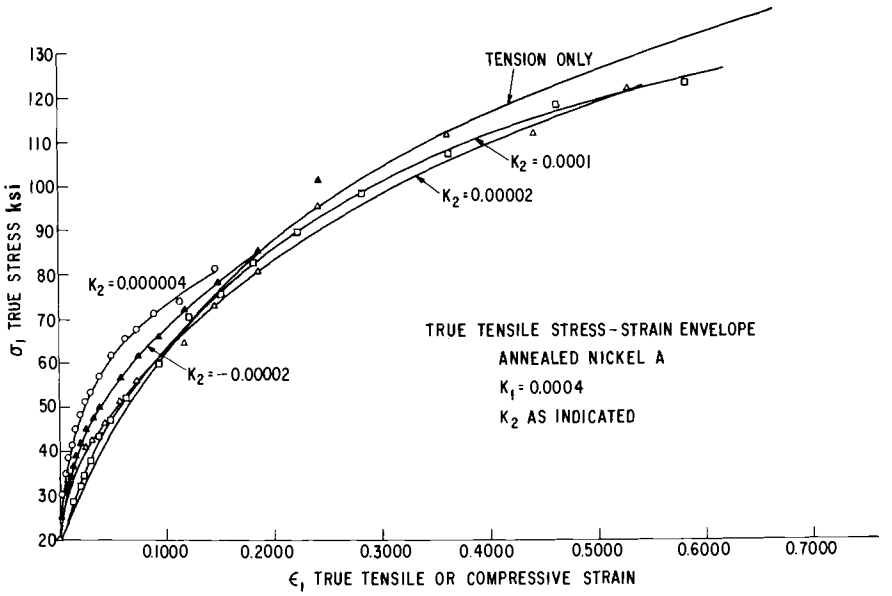

FIG. 14—*True tensile or compressive stress-strain envelopes for various values of* K_2, $K_1 = 0.0004$.

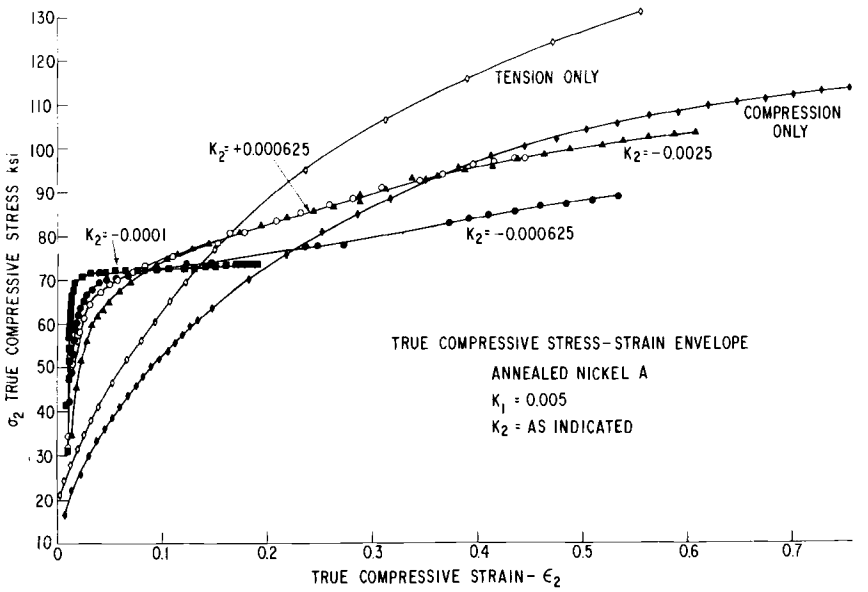

FIG. 15—*True compressive stress-strain envelopes for various values of* K_2, $K_1 = 0.005$.

however, describes more appropriately the behavior of the material after necking. As was shown above, necking occurs earlier with increasing K_2 and hence these curves have added meaning. Particularly note the increase in softening with decreasing values of K_2 at high mean strains (Fig. 12). In contrast to the early increased hardening, the later increased softening of the mixed strain mode of deformation reflects the influence of the cyclic softening phenomenon characteristic of cold-worked structures and shown in Fig. 5. It would also appear that the minimum slopes of the several curves in Figs. 11–13, after large accumulated mean strains have developed, are roughly the same, independent of K_1 or K_2. The average value of this slope is 65,800 psi—an interesting fact to be discussed later.

The behavior of early increased hardening and later increased softening depending on K_2 requires some crossover point or region, as shown for Figs. 11–13 where it is found to occur at lower mean strains as K_1 is reduced in magnitude. Further, it would appear that, for each K_1, the family of curves described by the parameter K_2 is bounded between the curve for simple tension and a straight line drawn from the point representing the stabilized stress amplitude, where K_2 is zero, with the minimum slope of 65,800 psi.

From the trends indicated in Figs. 11–13 it would appear that by lowering K_1 to reduce the stabilized stress amplitude, the true stress-strain envelope is correspondingly lowered, particularly when the ratio of K_2 to K_1 is small;

however, when K_2 is decreased to 0.0004 (Fig. 14) a different behavior is observed, in which the high mean strain cyclic softening no longer develops. Early hardening is evident, but following this the envelope closely follows the simple tension curve. This behavior is a matter for further discussion.

Experiments have also been conducted with negative values of K_2, and their true stress-strain envelopes are shown in Fig. 15 for $K_1 = 0.005$ and Fig. 13 for $K_1 = 0.002$. The same general trends are observed in the low mean strain regions for negative values of K_2 as for positive values. A significant difference is to be noted, however, at the higher mean strains, where the negative K_2 experiments reveal much less hardening. This is seen most dramatically in Fig. 15 for $K_2 = -0.0001$, where, after a very rapid hardening, the subsequent strain hardening is essentially zero. Similarly, in Fig. 13, also with $K_2 = -0.0001$, a mean strain is reached at a stress of 70,000 psi as compared to a stress of 107,000 psi in a simple compression test.

Fracture

Except for the lowest strain amplitude employed, $K_1 = 0.0004$, all tests were carried to failure, which occurred either by a sudden separation in the case where failure was by ductile fracture or by rapid decrease in load capacity with continued cycling when the failure was by fatigue. At failure the cyclic life and the mean strain were determined, and for each test the ratio $(\epsilon_f/\epsilon_{f_0})$ and (N_f/N_{f_0}) were computed. Here ϵ_f is the mean strain at fracture, ϵ_{f_0} the tensile ductility in simple tension, N_f the fatigue life, and N_{f_0} the fatigue life for the same K_1 when $K_2 = 0$.

The following procedure was used to represent the fracture results of this investigation. From the test results for $K_2 = 0$, that is for cyclic strain only, a plot of the plastic strain range, $\Delta\epsilon_p$, versus N_{f_0} gave, as a best fit, the relation

$$N_{f_0}{}^{0.563}\Delta\epsilon_p = 0.729 \quad \ldots\ldots (5)$$

Here, for simple tension, $N_{f_0} = \frac{1}{4}$ cycles, and $\Delta\epsilon_p = \epsilon_{f_0}$, the fracture ductility, or

$$N_{f_0}{}^{0.563}\Delta\epsilon_p = (\tfrac{1}{4})^{0.563}\epsilon_{f_0} \quad \ldots\ldots (6)$$

For a mixed failure, that is for positive values of both K_1 and K_2, it can be assumed that the actual ductility is reduced by the amount of mean strain ϵ_f. Thus the fatigue failure criterion, Eq 6, becomes

$$N_f{}^{0.563}\Delta\epsilon_p = (\tfrac{1}{4})^{0.563}(\epsilon_{f_0} - \epsilon_f) \quad \ldots\ldots (7)$$

Dividing Eq 7 by Eq 6

$$(N_f/N_{f_0})^{0.563} = 1 - (\epsilon_f/\epsilon_{f_0}) \quad \ldots\ldots (8)$$

The test data and Eq 8 are shown in Fig. 16.

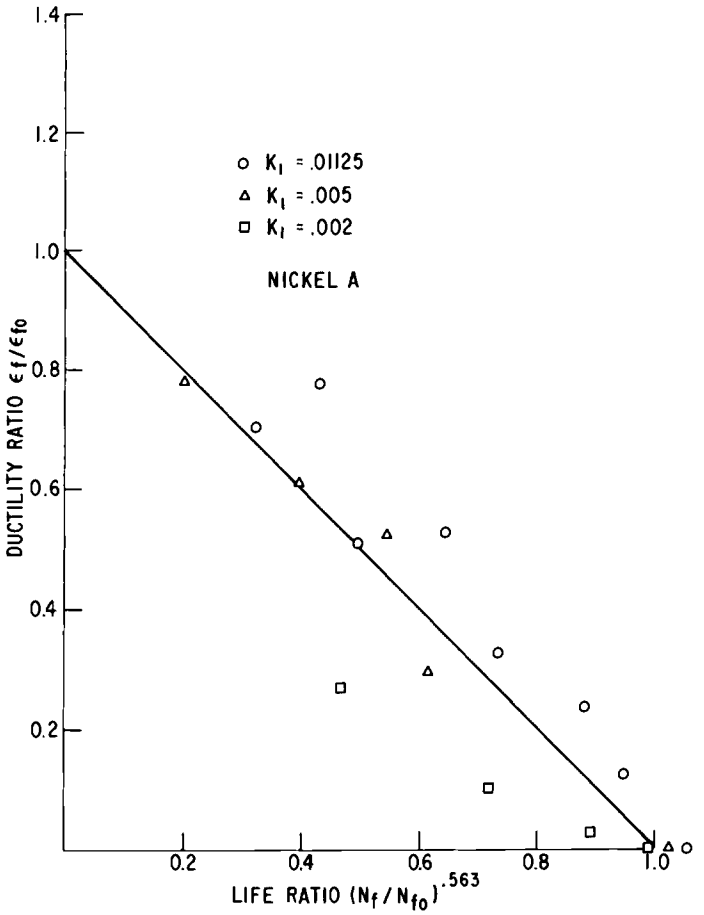

FIG. 16—*Representation of fracture for mixed cyclic and monotonic straining.*

Discussion

The effect of superimposed cyclic strain on monotonic deformation is shown to consist of early rapid hardening due to the additive effects of both monotonic and cyclic strain hardening. As the mean strain develops so does the cyclic strain softening, and the net strain hardening is then determined by the combination of monotonic hardening and cyclic softening. The limit in this process is perhaps best typified in the case of $K_1 = 0.005$, $K_2 = -0.0001$ (Fig. 15), where hardening to the stabilized hysteresis loop stress amplitude is developed after very little mean strain and the subsequent deformation occurs with no further hardening, the monotonic strain hardening being fully removed by the cyclic strain.

The behavior exhibited in compressive deformation (negative K_2) does not have a counterpart in tensile deformation. Here, even for the smallest value of K_2/K_1 where the greatest softening effect would be anticipated for a specific value of K_1, a finite value for monotonic strain hardening still exists. The explanation for this behavior most probably can be traced to the localized nature of the deformation process in cyclic tension tests, that is, to necking. As seen in Figs. 8–10, the superposition of cyclic strain decreases the mean strain required for necking, and a larger fraction of the total deformation is necking strain. Under such conditions, the developing notch geometry leads to constraints to flow, and the stresses generated are higher than those required to produce flow in the absence of the neck. Evidence for the constraint effect can be seen in Fig. 6, where the stress range required for specific values of K_1 and K_2 is higher when K_2 is positive than when K_2 is negative. It is also present in simple uniaxial loading, as seen by comparing the tension and compression curves in Fig. 15. At least part of the difference in flow stress here can be accounted for by the difference in geometry as deformation proceeds.

A quantitative measure of the effect of necking on the indicated hardening was not undertaken. The Bridgman correction [*11*] could have been applied, in which case the radius of curvature of the neck as well as the neck diameter would have to be determined throughout the test.

Evidence in support of the necking constraint view was obtained in a single test. A specimen with an initial diameter of 0.25 in. was pulled in tension to a prestrain of 0.495, a value sufficient to produce necking. The specimen was then remachined to a diameter of 0.172 in. to remove the neck and subjected to a $K_1 = 0.005$ and $K_2 = 0$. The specimen softened so as to produce a true stress envelope value of 92,000 psi after 155 cycles. This point, *F*, is shown on Fig. 12, where it is found to fall well below the various true stress-strain envelopes. Failure took place before complete softening had occurred, however, and it remains in doubt at the moment whether the necking constraint completely explains the observed hardening as $K_2 \rightarrow 0$.

The early necking for mixed cyclic and monotonic deformation is of interest and would appear to be a direct consequence of the requirement for necking in monotonic loading, that is, when $d\sigma/d\epsilon = \sigma$. Here cyclic strain hardening raises the early mean strain flow stress to shift the point of necking to lower mean strains. In the limit, when $K_2 \rightarrow 0$, this could occur at zero mean strain, which suggests the possibility that a necking instability may initiate a fatigue crack. In the absence of any mean strain, when cycling has proceeded to the point that the hysteresis loop has become fully stabilized, mean strain can be accommodated by the initiation of a neck and a corresponding decrease in load. Further localization of strain then occurs in the notch root formed by the neck, the root radius decreases further, and finally

a crack is formed. Because of the accompanying load decrease, it may in fact be difficult to prevent the instability from occurring, since less work is done by this process. A requirement for the initiation of the instability is a strain range sufficiently large to induce cyclic plastic strain over the entire cross section; hence, the argument would appear to be applicable for low-cycle fatigue only.

The ability to deform nickel monotonically at stress levels determined largely or entirely by the cyclic strain component requires a knowledge of the appropriate values of K_1 and K_2. In the present program; for the several values of K_1, ratios for K_2 to K_1 as low as 0.01 were employed. For K_1 = 0.0004, it would appear that even lower values of K_2/K_1 are required to effect softening at large mean strains. This becomes quite laborious even with the approach used, since 10^6 cycles or greater are required to produce mean strains of 0.01. It would appear from the present results that mean strains could be produced at low stress amplitudes, provided means could be found for introducing the high number of cycles required. This suggests the use of high-frequency vibration, such as ultrasonics. Unfortunately, fatigue failure serves as a limit to the total deformation, and with decreasing values of K_1 this becomes an increasingly important limitation.

In this regard the failure criterion shown as Eq 7 and experimentally supported in Fig. 16 can be rewritten as

$$\Delta\epsilon_p/\epsilon_{f_0} = (1/4)^{\alpha}[N_f^{-\alpha} - (2N_fK_2/\epsilon_{f_0})] \quad (9)$$

where $\epsilon_f = 2N_fK_2$. Plotting $\Delta\epsilon_p$ versus N_f for various values of K_2 and $\alpha = 0.563$, the effect of K_2 on life is shown in Fig. 17. This curve gives an indication of what might be expected when mean strain develops during cyclic strain, either by purpose or for lack of appropriate control.

The behavior of Nickel A as discussed above is felt to be typical of those metals which can exhibit a stabilized hysteresis loop that is independent of prior history. These metals are generally characterized as exhibiting wavy slip and have high stacking fault energies [9]. Although cyclic hardening and softening are characteristics of most metals, many show a history dependence (characterized by planar slip [9]) such that the stabilized hysteresis loop is not unique to the level of cyclic strain alone. Under such circumstances the cyclic and monotonic strain interactions are more complex than are represented here.

Conclusions

Based on the experimental results presented here, the following conclusions are drawn:

1. The simultaneous action of cyclic and monotonic strains on annealed Nickel A results in a monotonic deformation whose developed true stress-

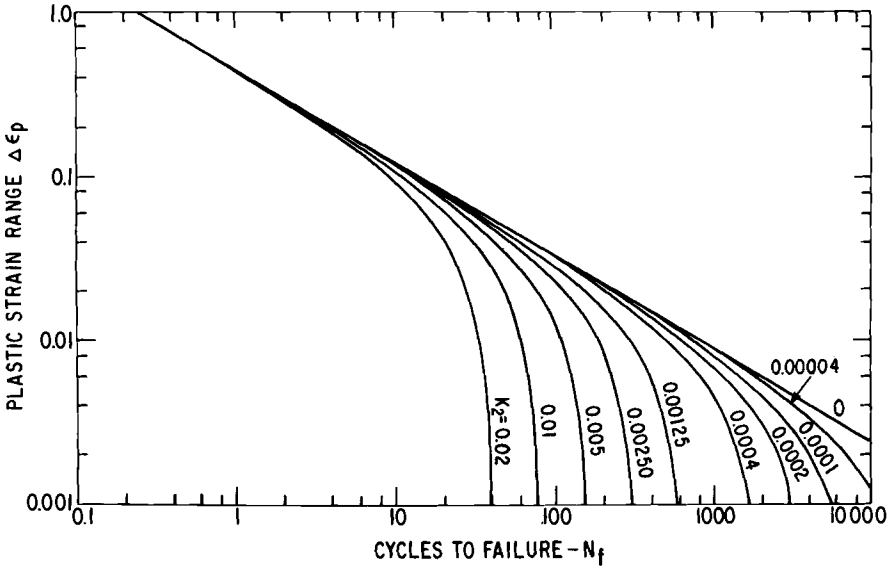

FIG. 17—*Life prediction for mixed cyclic and monotonic straining,* $\epsilon_{f_0} = 1.0$.

strain envelope shows an earlier hardening and a later softening in comparison to the simple tensile true stress-strain relationship. This behavior is traceable to the cyclic strain hardening characteristic of metals in the annealed state and cyclic strain softening for metals in the cold-worked state.

2. For a given value of K_1, as $K_2 \rightarrow 0$, the true stress-strain envelope hardens with little mean strain to the stabilized stress amplitude associated with K_1. If K_2 is negative, there is no further hardening with additional mean strain; while, if K_2 is positive, hardening continues with mean strain. The hardening in the latter case is attributed only to the constraint to flow due to localized necking.

3. When K_2 is positive for a given K_1, necking occurs at progressively lower mean strains with decreasing values of K_2, until for $K_2 \rightarrow 0$ necking occurs at zero mean strain. Under the action of pure cyclic strain, when the stabilized hysteresis loop stress amplitude is attained, the metal is unstable to any mean tensile strain. A fatigue crack is then initiated at the developing neck and failure proceeds in this more localized mode of deformation.

4. As K_1 becomes small the ratio K_2/K_1 becomes very low in order to produce the above effects. This requires a very large number of cycles to produce any significant mean strain, and premature fatigue failure occurs.

5. A relationship $\epsilon_f/\epsilon_{f_0} = 1 - (N_f/N_{f_0})^{0.563}$ describes failure for this mixed mode of straining.

Acknowledgments

During the course of this investigation a number of my associates have made significant contributions to the work. Early tests were conducted by J. Muscara; refinements in the method and experimental technique were provided by D. C. Lord; G. Jernakoff designed the punched tape programmer; and D. W. Lillie has provided continued support and encouragement. I would like to acknowledge their support with sincere gratitude.

References

[1] Coffin, L. F., Jr., *Transactions, Journal of Basic Engineering, Series D*, American Society of Mechanical Engineers, JBAEA, Vol. 82D, 1960, pp. 671–682.

[2] McClintock, F., *Fracture of Solids*, Interscience Publishers, New York, 1963, pp. 65–102.

[3] Coffin, L. F., Jr., *Transactions, Journal of Basic Engineering, Series D*, American Society of Mechanical Engineers, JBAEA, Vol. 86D, 1964, pp. 673–680.

[4] Moyar, G. J. and Sinclair, G. M., "Cyclic Strain Accumulation Under Complex Multiaxial Loading," *Proceedings*, Joint International Conference on Creep, Vol. 1, 1963, pp. 2-47 to 2-57.

[5] Ronay, M., "On Second Order Strain Accumulation in Aluminum in Reversed Cyclic Torsion at Elevated Temperatures," Report NONR 266(91)-No. 22, Columbia University, N. Y. June 1965.

[6] Hundy, B. B. and Singer, A. R. E., *Journal of the Institute of Metals*, JIMEA, Vol. 83, 1954–55, pp. 401–407.

[7] "The Application of Ultrasonic Energy in the Deformation of Metals," DMIC Report 187, Defense Metals Information Center, Aug. 16, 1963.

[8] Coffin, L. F., Jr., and Tavernelli, J. F., *Transactions of the American Institute of Mining and Metallurgical Engineers*, TAMMA, Vol. 215, 1959, pp. 794–807.

[9] Feltner, C. E. and Laird, C., *Acta Metallurgica*, AMETA, Vol. 15, 1967, pp. 1621–1653.

[10] Lord, D. C., "New Uniaxial Cyclic Strain Test Equipment," General Electric Research and Development Center Report 67-C-195, May 1967.

[11] Bridgman, P. W., *Transactions*, American Society for Metals, TASEA, Vol. 32, 1944, pp. 553–574.

C. E. Feltner[1] *and P. Beardmore*[1]

Strengthening Mechanisms in Fatigue

REFERENCE: Feltner, C. E. and Beardmore, P., **"Strengthening Mechanisms in Fatigue,"** *Achievement of High Fatigue Resistance in Metals and Alloys, ASTM STP 467*, American Society for Testing and Materials, 1970, pp. 77–112

ABSTRACT: The present state of knowledge of the role of metallurgical structure in the achievement of high fatigue resistance is critically examined and the application of such knowledge is discussed. At the present time resistance to fatigue is best characterized in terms of phenomenological parameters such as the cyclic strain hardening exponent. The effect of changes in metallurgical structure on these parameters is then the best index of the microstructural effects. The importance of distinguishing between resistance to repeated stresses as opposed to resistance to repeated plastic strains is emphasized, since the metallurgical means of achieving the required resistance can be radically different. The fatigue process is discussed in terms of plastic deformation, crack initiation, and crack propagation mechanisms, and the techniques by which these processes can be modified are detailed and related to the phenomenological parameters. Finally, a set of basic guidelines for achievement of high fatigue resistance by metallurgical means is outlined.

KEY WORDS: crack initiation, crack propagation, fatigue (materials), metallographic structures, microstructure, plastic deformation, strains, stresses

Nomenclature

σ	Stress
ϵ	Strain
σ_0	Stress amplitude
$\Delta\epsilon_t$	Total strain range
$\Delta\epsilon_p$	Plastic strain range
$\Delta\epsilon_e$	Elastic strain range
σ_i	Microcyclic yield stress = intrinsic fatigue strength limit
$\Delta\epsilon_i$	$2\sigma_i/E$
E	Young's modulus
N_f	Cycles to failure
n'	Cyclic strain hardening exponent
σ'_f	Fatigue strength coefficient

[1] Scientific Research Staff, Ford Motor Co., Dearborn, Mich. 48121. Dr. Feltner is a personal member of ASTM.

σ_f Monotonic true fracture strength
ϵ'_f Fatigue ductility coefficient
ϵ_f Monotonic fracture ductility

As yet, a commercial alloy has not been developed specifically for the purpose of resisting fatigue even though it is the most common mode of fracture occurring in practice today. In this paper we address ourselves to the problem of how to achieve high fatigue resistance in materials by metallurgical means. In seeking resolution of this problem, one must clearly know (1) the phenomenological parameters which provide the best indexes of high fatigue resistance, (2) the metallurgical factors important to the operation of those mechanisms which control fatigue fracture, and (3) the interrelation between these phenomenological and metallurgical factors. Finally, to be useful, this knowledge must be restated in a form which will serve as a set of guidelines for achieving high fatigue resistance by metallurgical means.

Although this paper is concerned primarily with micromechanisms in fatigue, it is not our intention to attempt a complete review of the literature on fatigue mechanisms. Several extremely good reviews treating mechanisms of fatigue hardening and softening and crack initiation and growth have appeared in recent years [*1–5*].[2] We shall attempt to correlate and synthesize this information into a form useful[3] to the metallurgist who seeks to develop new materials or optimize existent ones for best fatigue resistance.

Indexes of High Fatigue Resistance

Morrow [*6*] first set forth and discussed a set of fatigue properties analogous to those used to characterize the static strength of materials. These properties and other factors pertinent to the resistance of metals to cyclic deformation are reviewed in this symposium by Landgraf [*7*]. Our discussion is therefore concerned with those aspects of fatigue properties whose association with fatigue mechanisms can be identified.

One must first decide whether repeated stresses or repeated strains are to be resisted, since different applications may call for a material which is strain resistant, for example, rather than stress resistant. Typical of applications of strain-resistant materials are those involving thermal fatigue: that is, turbine blades, nuclear fuel element cans, spacecraft hardware subject to extreme temperature changes such as in a lunar environment, etc. Although many components may have to resist large loads, geometry and constraint factors may result in the critical location largely undergoing strain cycling and therefore locally requiring a strain-resistant material. Some applications, such

[2] Italic numbers in brackets refer to the list of references at the end of this paper.

[3] The understanding derived from basic studies on fatigue mechanisms has proved intrinsically useful in that the "mystery" of the fatigue process has been largely removed (as developed in a private discussion between J. C. Grosskreutz and C. E. Feltner in 1968).

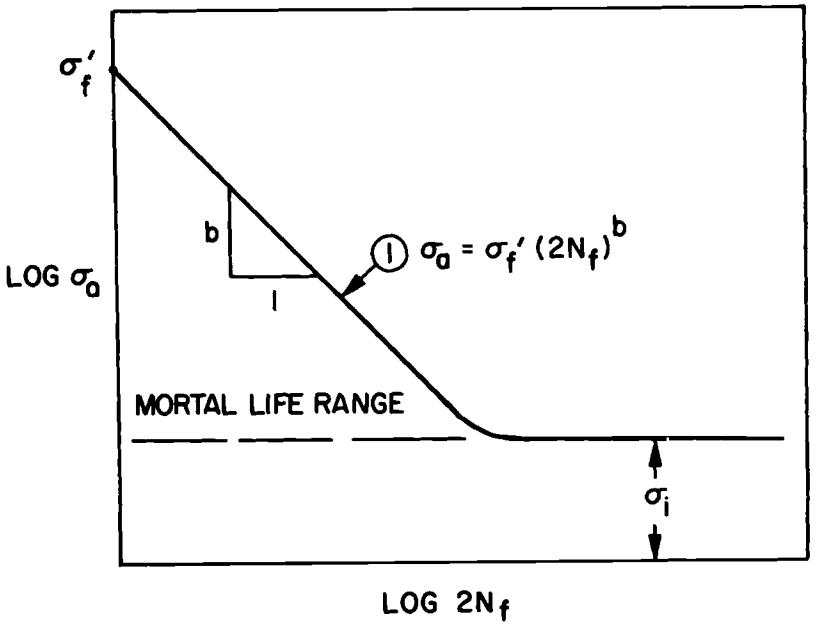

FIG. 1—*Schematic stress-life curve.*

as hot forging dies, may require a material which has both good strain resistance (thermal fatigue) and good stress resistance (impact fatigue).

The stress and strain resistance of materials is commonly characterized by stress-life and strain-life plots such as those shown schematically in Figs. 1 and 2. Inspection of Fig. 1 shows that for the mortal life range a high stress-resistant material should have a stress-life curve with a high intercept, σ'_f, and shallow slope, b. For the infinite life range a high value of σ_i is desired. Examination of Fig. 2 shows that in the long-life range good strain resistance is determined by the same parameters indicative of good stress resistance. For short lives, where plastic strain dominates, a large intercept, ϵ'_f, and shallow slope, c, are desirable.

It has been shown [*6–8*] that all of these slopes and intercepts are related at least empirically to monotonic and cyclic stress-strain properties, namely,

$$\sigma'_f \cong \sigma_f \quad \text{(1a)}$$

$$\epsilon'_f \cong \epsilon_f \quad \text{(1b)}$$

$$b \cong -n'/(1 + 5n') \quad \text{(1c)}$$

$$c \cong -1/(1 + 5n') \quad \text{(1d)}$$

where n' is the cyclic strain hardening exponent, σ_f is the monotonic true fracture strength, and ϵ_f is the monotonic fracture ductility (see Fig. 3).

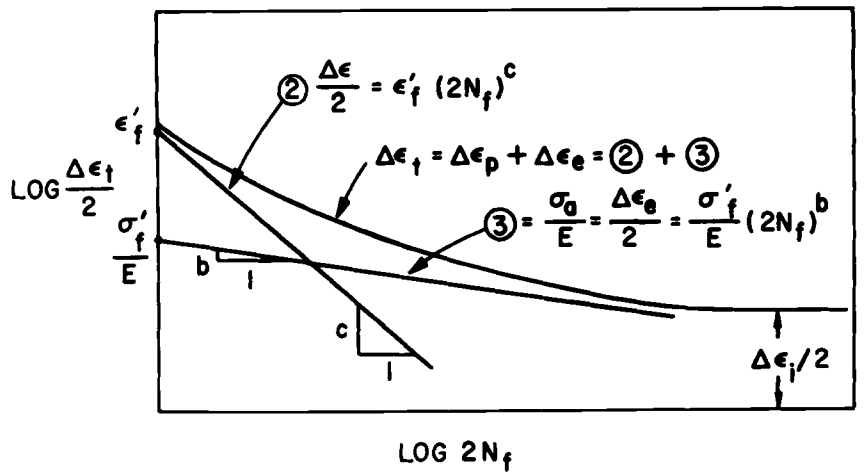

FIG. 2—*Schematic strain-life curve.*

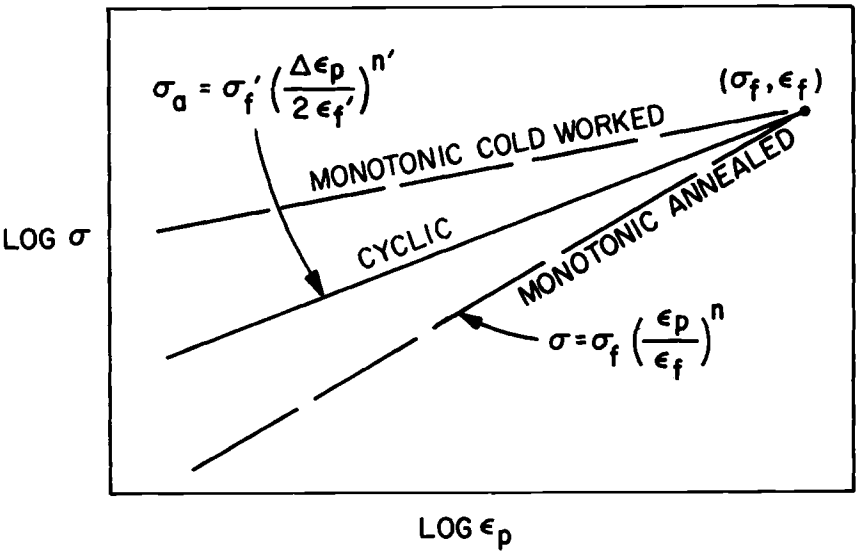

FIG. 3—*Schematic monotonic and cyclic stress-strain curves.*

Approximations (1*a*) and (1*b*) result in the monotonic and cyclic stress-strain curves going through the same point as shown in Fig. 3. The variation of b and c with n' is shown in Fig. 4. Changes in n' by metallurgical means to bring about desirable changes in b and c may not necessarily lead to increased fatigue resistance, since undesirable changes in σ_f and ϵ_f may result. Analysis of a large amount of data used and cited in Ref *8* has shown that σ_f and ϵ_f are empirically related to n' in the general manner shown schematically in Fig. 5. Thus, probably the best single index of the change in finite life fatigue

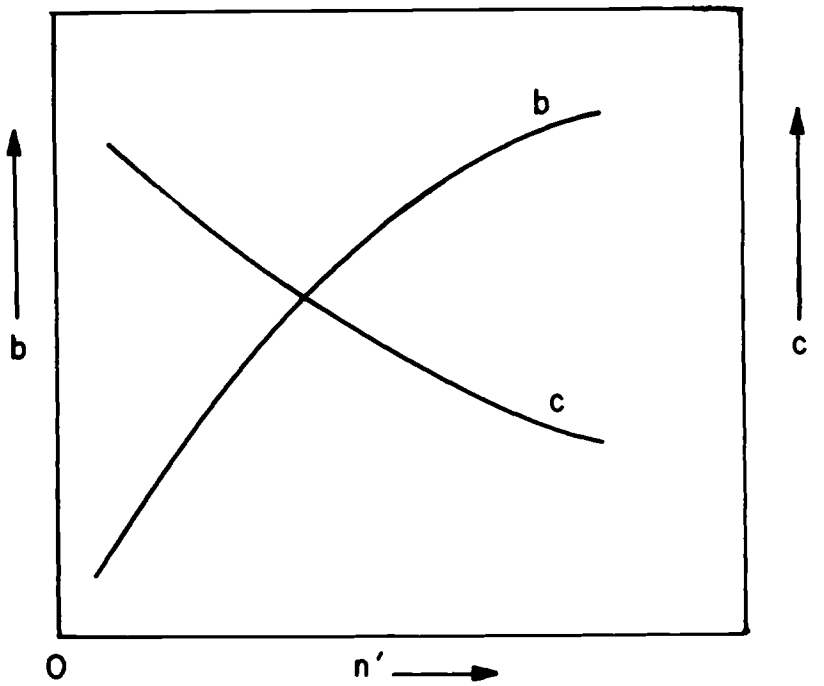

FIG. 4—*Schematic variation of fatigue strength and ductility exponents,* b *and* c, *with* n'.

resistance induced by alloying is the cyclic strain hardening exponent, n'. Using the symbols ↑ = increases and ↓ = decreases, we note from Figs. 1–5 that for increased *stress* resistance it is desirable to decrease n', since,

$$\text{as } n' \downarrow, \sigma_f \uparrow \text{ and } b \downarrow \quad \ldots\ldots\ldots\ldots\ldots\ldots\ldots\ldots (2)$$

both of which are desirable changes, while for increased plastic strain resistance it is best to increase[4] n', since,

$$\text{as } n' \uparrow, \epsilon_f \uparrow \text{ and } c \downarrow \quad \ldots\ldots\ldots\ldots\ldots\ldots\ldots\ldots (3)$$

Throughout the discussion of fatigue mechanisms we shall therefore attempt to delineate the interrelation of the cyclic strain hardening exponent, n', and metallurgical factors that determine fatigue mechanisms.[5]

[4] Note that both high plastic strain resistance and high stress resistance are not compatible, since opposite changes in n' are required. Stated another way, stress resistance requires good monotonic strength (σ_f) while strain resistance depends on good ductility (ϵ_f). Thus, the age-old problem in alloy development of balancing strength and ductility also occurs in the achievement of high fatigue resistance.

[5] Although we recognize that fatigue mechanisms may be influenced by elevated temperatures [*9–11*] and corrosive environments [*12, 13*], the following discussions are limited largely to room temperature and air environment.

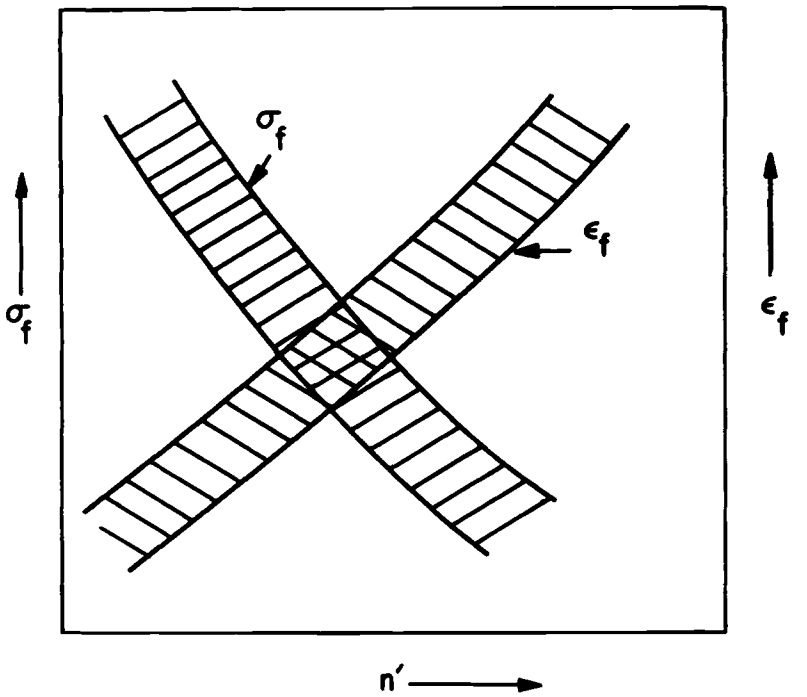

FIG. 5—*Schematic variation of* σ_f *and* ϵ_f *with* n'.

The Role of Metallurgical Structure in Mechanisms of Fatigue

Let us now examine the metallurgical factors important to the operation of those mechanisms that control fatigue fracture. To do so we will concentrate our attention on three particular aspects of plastic deformation: (1) the onset of plastic strain, (2) the distribution of plastic strain, and (3) strain hardening. That these factors are of primary concern can be justified on the following basis:

1. The results of many investigators show that the onset of plastic strain is essential to the fatigue process. Indeed, Mason [*14*, *15*] has shown that in germanium, a material in which dislocations will not move at room temperature, fatigue fracture is nonexistent.

2. Based on a large number of studies, crack initiation is known to occur in regions where the strain is concentrated or localized [*16*, *17*].

3. Microscopic observations of the manner in which fatigue cracks grow lead one to the conclusion that the factor controlling the rate of crack propagation is the strain hardening behavior of the material at the crack tip [*18–20*].

Thus, to control fatigue fracture we are forced to look for metallurgical means of controlling these three basic aspects of plastic deformation as they occur during fatigue.

Crack Initiation

A variety of specific dislocation models have been developed to describe the nucleation of fatigue cracks (for a review see Refs *17* and *21*). However, virtually all of these models inherently rely on the onset and localization of plastic deformation by slip, leading to crystallographic notching of the metal surface. Consequently, our discussion will center on this "descriptive" model rather than specific dislocation models. Although modes of deformation other than slip (for example, twinning) may be important in a few metals [*22–24*], they are not considered herein.

Ideal Behavior: The Case of the Copper Single Crystal—Before discussing crack initiation mechanisms in commercial alloys it is instructive to consider the nucleation of cracks in an "ideal" case such as in copper single crystals. In the low amplitude-long life region (10^5 to 10^7 cycles), a crystal oriented for single slip will form uniform fine slipbands on the surface[6] and appreciable cyclic strain hardening occurs [*25*, *26*] after only a few cycles. The matrix structure associated with this hardening consists of dislocation debris, dipole mats, etc. [*3*, *27*]. After some small percentage of the life (say less than 1 percent) the slip begins to concentrate in bands (see *A* in Fig. 6) 10 to 50 μm wide, termed persistent slipbands (PSB), in which cracks are eventually nucleated [*28*].

Extensive studies [*29–31*] have shown that the dislocation structure in these bands is a cell structure and thus characteristic of the high amplitude fatigue-matrix structure [*32*]. Flow stress [*25*], hardness [*33*], and hysteresis loop [*34*] measurements all indicate that PSB's are "softer" than the matrix, that is, they have both a lower flow stress and a lower strain hardening rate. Watt et al [*35*] have shown that there is a high degree of reversibility of slip in any one PSB (see Fig. 6). For example, in Fig. 6 the persistent slipbands in *A* formed after 4500 cycles were removed by electropolishing and the crystal was then pulled one-half cycle to the peak tensile stroke (*B* in Fig. 6), whereupon faint slip lines reappeared. However, at the peak compression stroke these slip lines virtually disappeared completely, *C*. Continuing the cycle, the bands reappeared at the peak of the second tensile stroke. This reversibility is also shown at 10½ and 11 cycles, *E* and *F*, and 100½ and 101 cycles, *G* and *H*. At the 100-cycle level, however, permanent nonreversible offsets are present, indicating incomplete reversibility, that is, slip racheting. After 2500 additional cycles, *I*, the persistent slipband pattern was nearly identical to that before electropolishing, *A*. Two conclusions can be drawn from these observations: (1) in support of indirect observation [*25*, *33*, *34*] the flow stress and degree of strain hardening are lower in the bands than in the matrix and (2) the high degree of slip reversibility in the bands indicates

[6] In the absence of internal defects and surface compressive residual stresses, cracks always nucleate at the surface because of the lack of constraint to plastic deformation.

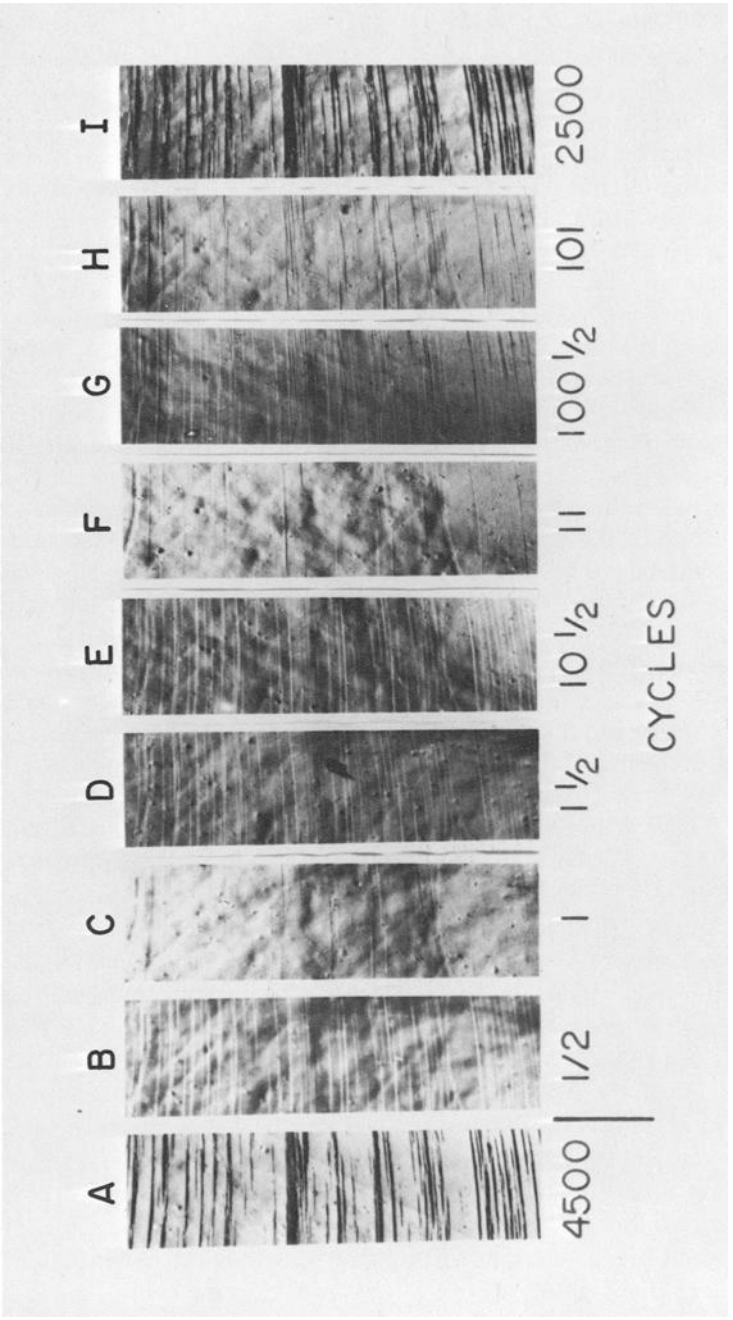

FIG. 6—*Persistent slipbands in a copper single crystal (after Watt et al [35]).*

that the bands themselves strain harden slowly once they are formed. Both of these effects are related to the cyclic strain hardening exponent, n'. The reason that persistent slipbands form is still unclear. However, the following description seems consistent: Initially the crystal hardens uniformly by a debris-hardening mechanism [*27*]. Once the crystal fills with debris the local stress becomes large enough to cause local softening, that is, there is a stress level above which the debris structure is locally unstable. This localized cyclic strain softening, by definition, results in concentration of plastic strain.

Slip racheting in bands results in a crystallographic notching (notch-peak topography) of the crystal surface as shown in Fig. 7. Crevices formed by slip racheting are embryonic cracks from which a fatal crack may grow by other mechanisms to be discussed subsequently.

Several variables can alter this picture, notably, strain amplitude, temperature, and slip character. As the amplitude is increased the entire surface is covered with PSB's [*31*] with a tendency in polycrystals to intergranular rather than transgranular initiation [*36*, *37*]. The influence of slip character seems less clear. Wells [*38*], for example, has suggested that planar slip will be heterogeneous, presumably resulting in more severe notching. Conversely, McEvily and Johnston [*39*] concluded that planar slip was beneficial in dispersing slip and thereby reducing the severity of notch-peak topography. Equally important is the reversibility of slip in a band, for unless racheting occurs a notch-peak topography will not develop. Laird and Feltner [*36*] have shown that a greater degree of slip reversibility in copper-aluminum alloy (Cu-7.5Al) than in copper leads to less racheting and therefore increased life. Thus both slip homogeneity and reversibility play a role in crack initiation, the worst combination being heterogeneous, nonreversible slip. In general, the weight of the evidence indicates that in single-phase materials alloying with substitutional atoms to achieve a more planar slip character will produce a more homogeneous slip distribution. Moreover, the tendency to "reversible" strain hardening is increased [*38*]. As will be shown, this conclusion is not usually applicable to multiphase materials (see next section). Finally, lower temperatures generally lead to more homogeneous, reversible slip [*36*] and therefore longer lives.

Crack Initiation and the Fatigue Strength Limit—Thus far our discussion has dealt with cases where cracks are actually formed, the implicit assumption being the stress is high enough to cause the onset of plastic strain. There is presumably some stress amplitude below which plastic strain is negligible. We conclude that an intrinsic fatigue strength limit exists in all materials below which fatigue can never occur. This limit has been labeled as σ_i in Fig. 1 ($\Delta\epsilon_i/2$ in Fig. 2 equals σ_i/E), and it marks the point ("knee") at which the stress-life curve becomes horizontal. Evidence that such a microyield stress exists in fatigued materials has been published by Feltner and Morrow

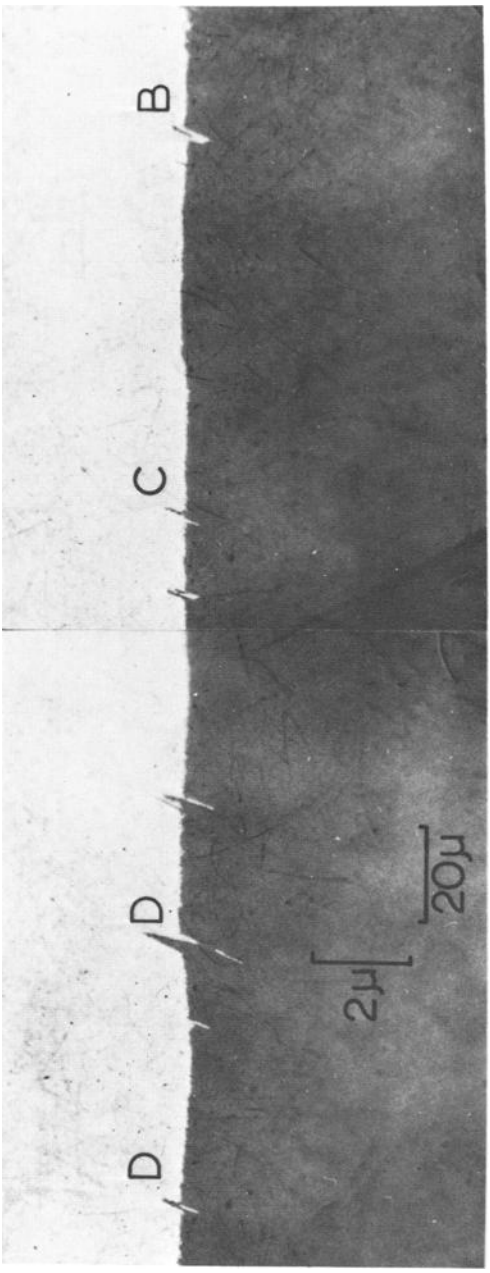

FIG. 7—*Taper section view showing crystallographic notching of the crystal surface by slip ratcheting in persistent slipbands (after Laufer and Roberts* [29]).

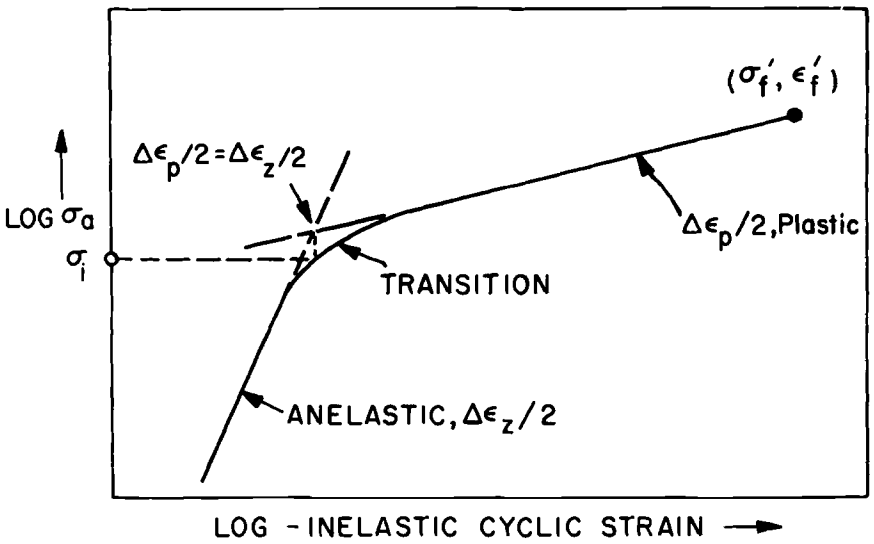

FIG. 8—*Variation of inelastic cyclic strain with stress amplitude.*

[*40*], whose results are shown schematically in Fig. 8. Note that at some small inelastic strain (say 10^{-5}), the anelastic strain [*41*] (which is nondamaging) equals the plastic strain. We arbitrarily define the stress at this point, σ_i, as the microcyclic yield stress. This stress is closely related to the "cyclic stress sensitivity limit" discussed by Lazan [*42*]. Examination of the results of Ref *40* shows that σ_i is nearly identical to the fatigue strength limit and thus serves as an indicator of the stress below which fatigue will not occur.

In the case of copper single crystals, both Helgeland [*33*] and Roberts [*31*] have shown that there is a stress (about 3 kg/mm^2) below which persistent slipbands will not form. Presumably fatigue failure will not occur below this level, although this point has not been "proven" by tests to very long lives (say 10^9 to 10^{10} cycles). The existence in copper crystals of a stress-inelastic strain behavior like that shown in Fig. 8 can be deduced from Helgeland's [*33*] work and the stress, σ_i, corresponds to the stress below which persistent slipbands will not form.

The intrinsic fatigue strength limit in germanium is equal to the fracture strength [*14*, *15*], undoubtedly because of the inherent high Peierls stress in covalent bond-diamond-type lattices [*43*]. Similarly, the intrinsic fatigue strength limit in body centered cubic (bcc) metals should be higher than in other structures such as face centered cubic (fcc) or hexagonal close packed (hcp), again because of a higher Peierls stress (or lattice friction stress) [*44*]. This may be hard to demonstrate, however, because of the difficulty of separating out the effects of interstitial impurities. We conclude from this dis-

cussion that, contrary to some beliefs, the concept of an intrinsic fatigue strength limit is valid for all materials. In many metals, such as aluminum alloys, the position of the knee may not be in the "visible" life range (say less than 10^9 cycles). Steels and some other metals, on the other hand, often show a knee in the 10^6 to 10^7 life range, which is easily observed at conventional testing machine frequencies. The exploitation of the intrinsic fatigue strength limit to achieve higher fatigue resistance will be discussed in subsequent sections.

Crack Initiation Resulting from the Instability of Metallurgical Structures Under Cyclic Strain—In a previous section it was noted for copper crystals that cracks may nucleate in regions of strain concentration that develop when the matrix structure, initially hardened by cyclic straining, becomes unstable and locally undergoes cyclic strain softening. Similar behavior occurs in metals that are initially strengthened by various metallurgical means. As in the case of copper crystals, persistent slipbands in commercial alloys undergoing low-amplitude fatigue must behave like bulk material undergoing large cyclic strains; accordingly, the analogy may be used that the cyclic stress-strain response of structures under large strain is representative of what occurs locally at small strains and long life.

Although commercial alloys are often strengthened by cold work, the dislocation substructures introduced are generally unstable and soften by appreciable amounts. The cyclic stress-strain behavior and changes in dislocation structures in cold-worked materials have been studied by several investigators [*45–49*]. The existence of both a unique cyclic stress-strain curve [*48*] and a unique saturation dislocation structure [*49*], irrespective of prior history in wavy slip-mode materials, explains why cold work has virtually no effect on life behavior at high amplitudes [*36, 47*]. Even in planar slip-mode materials, softening is so marked that little effect of cold work on life is observed [*36*]. On the contrary, macroscopic softening at long lives is small [*48, 50*] and cannot account for the only small improvement in fatigue strength relative to tensile strength [*51*]. Steels, for example, cold-worked by drawing or rolling, show improved fatigue strength but not to the same extent as the tensile strength [*52, 53*].

Recent studies of the dislocation structures in cold-worked pure metals after low-amplitude fatigue [*50*] allow an interpretation of the above problem. Copper specimens, cold-worked by 30 percent reduction in thickness, showed a uniformly dense dislocation cell structure of about $\frac{1}{2}$-μm diameter (Region *A*, Fig. 9). After fatigue at various percentages of life, large dislocation free regions about 10 μm in extent (Region *B*, Fig. 9) were observed. These locally softened regions had little or no effect on bulk softening measurements; nevertheless, they represent regions of low intrinsic flow stress surrounded by a highly strengthened matrix. Strain localization and resultant crack

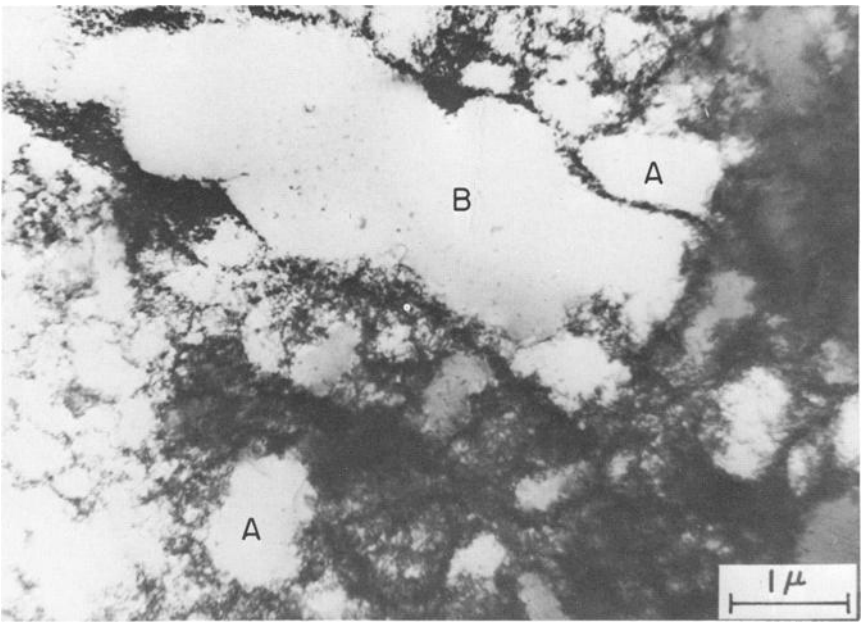

FIG. 9—*Dislocation structure in cold-worked copper after low-amplitude cyclic straining.*

nucleation should naturally occur in these regions. Since these soft regions develop early in the life [*50*], it is not surprising that cold work does not produce as significant an increase in long-life fatigue resistance as might be expected [*51*].

Dislocation substructures introduced during martensitic transformation, for example, in quenched and tempered steels, behave in a manner similar to substructures produced by cold working. Beardmore and Feltner [*54*] have demonstrated this effect in a low-carbon alloy steel.

Precipitation-hardened alloys often exhibit instability under cyclic strain as shown by the behavior of the γ'-strengthened nickel-base superalloys in Fig. 10. (See also the work of Wells and Sullivan [*55*].) After initial hardening these alloys undergo a subsequent softening. Similar observations have been made on aluminum alloys [*56*] and quench-aged iron-carbon alloys [*57*]. The subsequent softening effect is attributed to the shearing of precipitate particles by dislocations and their subsequent resolution in the matrix [*58–61*] leaving precipitate-free channels. These precipitate-free regions are then local soft spots of low flow stress in which strain concentrates and promotes crack initiation.

Instabilities are also observed in alloys strengthened by long-range order. Figure 11, for example, shows hardening and subsequent softening of an

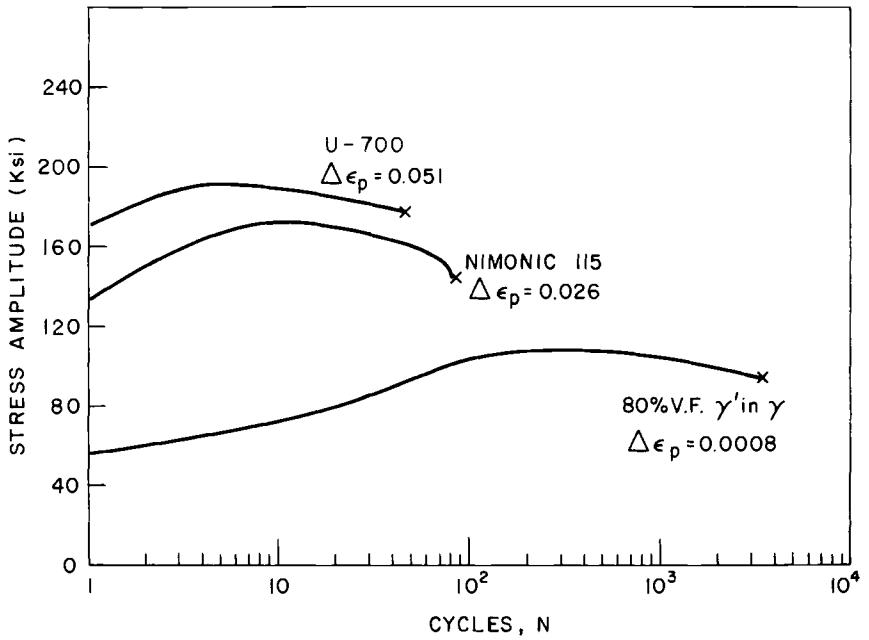

FIG. 10—*Hardening and subsequent softening of γ'-strengthened nickel-base superalloys.*

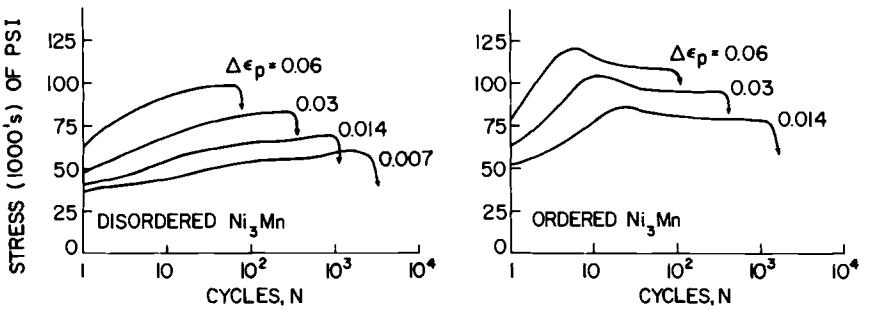

FIG. 11—*Cyclic stress response of disordered and ordered Ni_3Mn alloy subjected to cyclic straining.*

ordered NI_3Mn alloy [*62*]. This effect is interpreted as the breakdown of the long-range ordered structure. However, in this case the life is not decreased, because ordering results in a more planar slip character and a resultant homogenization of slip, which apparently outweighs any effects of strain concentration due to local softening. Long-range order has also been found to increase the long-life fatigue strength in single-phase materials [*63*].

A number of high-strength steels are strengthened by various combinations of precipitation (or dispersion) and dislocation substructure hardening, notably quenched and tempered steels, ausformed steels, maraging steels, etc. Appreciable cyclic strain softening is observed in several of these steels [7]. Although the cyclic stress-strain behavior of these materials has been investigated [7, *64*, *65*] in addition to their general fatigue resistance (see Refs *65* and *66* for a review), little is known concerning the details of crack initiation processes that may be related to the stability of the microstructures.

Mechanistically, instabilities often produce severe local strain concentrations, leading to early crack nucleation which is most detrimental at long lives. Phenomenologically, instabilities always produce softening, which means n' increases (see Fig. 3) either nominally or locally. Based on Eq 2, metallurgical structures which are unstable under cyclic straining will generally result in decreased fatigue strength resistance, the largest effect being observed at long lives, as the change in b is more severe than that in σ_f. On the other hand, Eq 3 shows that softening will give increased resistance to cyclic plastic strains.

As pointed out by Ham [5], metallurgical structures stable in fatigue, such as impenetrable particles (ThO_2 in nickel, that is, TD nickel [*67*, *68*]) and spinodally decomposed solid solutions (copper-nickel-iron) [*69*], may lead to higher fatigue strength resistance since the full-strength potential of the material is realized. Yet, their plastic strain resistance and notch fatigue resistance may be impaired because of their inability to soften. These effects are not completely related to crack initiation processes, the crack growth processes being significant, particularly at short lives. However, the above discussion does serve to point out that extreme care should be exercised in deciding whether an application requires a stress-resistant or plastic strain-resistant material.

The Relation of Aging Effects to Crack Initiation—Aging effects in fatigue arise from the interaction of point defects—primarily interstitial and substitutional solute atoms—with dislocations. These interactions inhibit plastic flow and therefore may play a role in both crack initiation and growth. The evidence indicates, however, that their major effect is upon crack nucleation. Consider, for example, that materials subject to aging effects always show significantly lower long-life fatigue strength and the absence of a distinct fatigue limit when specimens with "artificial cracks" (notches) are tested.

Aging reactions may influence fatigue resistance in three ways: (1) by raising the intrinsic fatigue strength limit by some amount, $\Delta\sigma_i$ (Fig. 12), (2) by decreasing (the absolute value of) the slope of the crack initiation line (from Line A to B in Fig. 12), and (3) by altering the crack growth rate. The resultant effect shown by Line D in Fig. 12 is to move the position of the

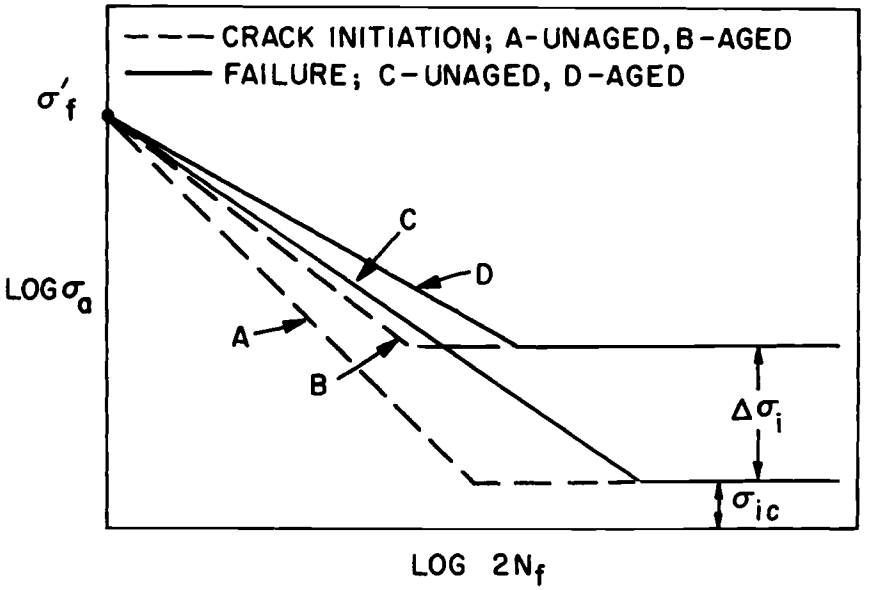

FIG. 12—*Schematic influence of aging reaction on stress-life behavior.*

knee to shorter lives and to increase the stress resistance in the mortal life range. The influence of aging reactions on σ_f is assumed to be small, although there are exceptions to this rule.

As discussed by Adair and Lipsitt [*70*], two types of aging phenomena occur which lead to increased fatigue resistance: (1) those due to strong dislocation-solute interactions prior to testing, such as that characterized by the distinct yield point exhibited by mild steel in a tension test, and (2) those due to dislocation-solute interactions during fatigue, such as that characterized by the Portevin-LeChatelier effect, that is the occurrence of jerky flow during tension testing.

In the mortal life range, mild steels with distinct yield points [*71–73*] and pure bcc metals like molybdenum [*74*] and iron [*75*] exhibit a net softening at low strain amplitudes and a net hardening at high amplitudes. At low strain amplitudes first softening and then hardening occurs [*73*]. These results have established that the dislocation locking is broken down and the yield point disappears [*71–74*]. A typical example of this behavior is shown in Fig. 13. The fatigue strength limit is clearly that cyclic stress which is just sufficient to cause significant cumulative plastic strain to bring about gradual dislocation unpinning. At low amplitudes this softening is localized and persistent slipbands are formed in which cracks are nucleated. The key to achieving the highest fatigue resistance in these materials is to raise the

microyield stress, σ_i, by employing a locking solute which has the highest possible solute-dislocation binding energy.

Strain aging during fatigue, on the other hand, is exceptionally complex and depends on a number of variables [*58*, *76–78*], not the least of which is the size of specimen employed [*79*]. Dynamic strain aging varies according to how long is required for the reaction to begin to be effective. However, the more rapid reactions apparently depend on the initial solute concentration, while reactions occurring over longer time periods may be related to the resolution of iron carbide particles [*78*]. For dynamic strain aging to be a potentially useful fatigue-strengthening mechanism two conditions are essential: (1) a solute migration energy that is sufficient to permit the solute to keep up with the mobile dislocation and (2) a high solute-dislocation binding energy. As pointed out by Ham [*5*], several variables may influence these two factors. We must conclude that more work on the kinetics of strain aging during fatigue is required before this process can be extensively employed as a fatigue-strengthening mechanism.

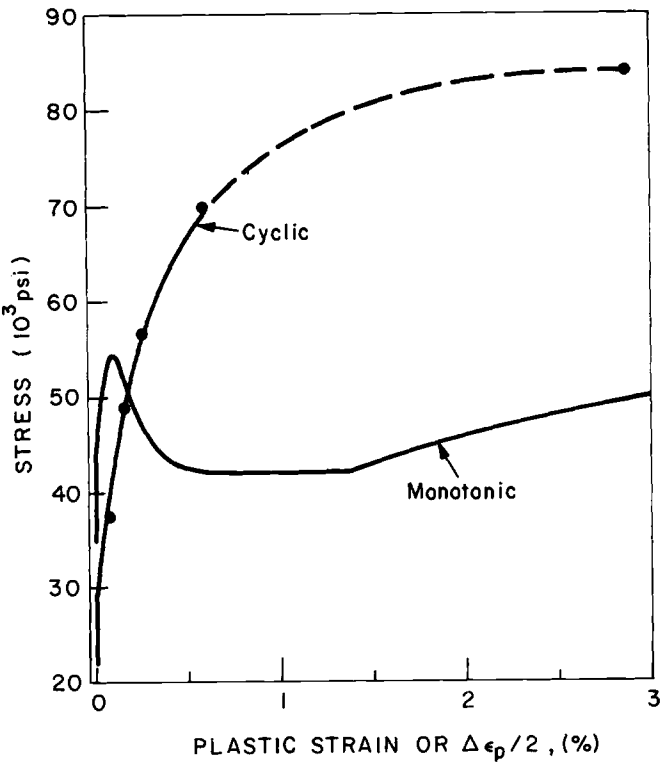

FIG. 13—*Monotonic and cyclic stress-strain curves for molybdenum* (*Ref* 74).

Grain Size and Boundary Effects—The influence of grain size on fatigue has recently been reviewed by Pelloux [*80*]. One can conclude from this review that grain size influences (1) only crack initiation in wavy slip-mode materials and (2) both crack initiation and propagation in planar slip-mode materials.

The influence of grain size on the low cycle fatigue of copper [*81*] and aluminum [*37*] is shown in Fig. 14. It is clear from this data that decreasing the grain size by a factor of 20 to 50 produces only about a factor-of-2 increase in life. Similarly, copper [*82*] shows only slight increases in long-life fatigue resistance for substantial changes in grain size. Forrest and Tate [*83*] concluded that in 70-30 brass, grain size influences the long-life fatigue strength primarily through its effect on crack propagation.

The mechanism of intergranular crack initiation at high amplitudes ($\Delta\epsilon_p = 0.015$) in a disordered iron-cobalt-vanadium alloy is shown in Fig. 15. Early in the life (Fig. 15*a*) slipbands impinge upon a grain boundary and the offset shear in the band results in a high stress across the boundary. Continued cycling causes the stress to increase as slipband racheting creates continually

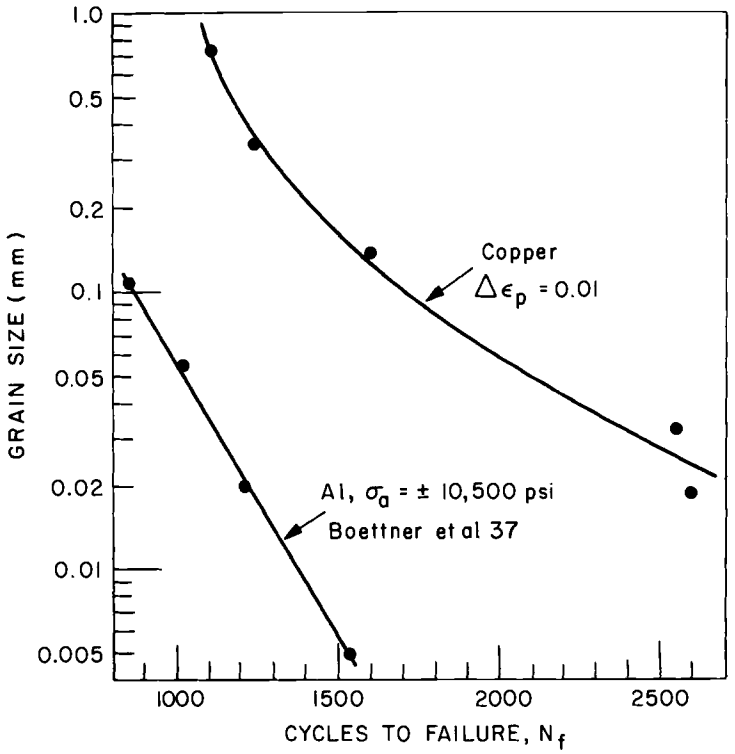

FIG. 14—*Influence of grain size on the low cycle fatigue of copper and aluminum.*

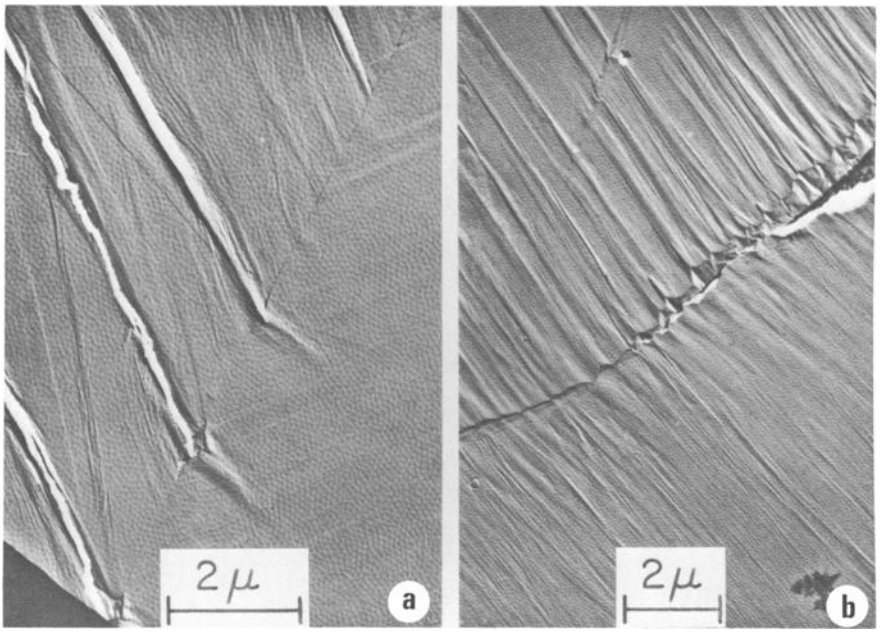

FIG. 15—*Mechanism of intergranular crack initiation in low cycle fatigue of disordered iron-cobalt-vanadium alloy.*

increasing offsets. Eventually the stress builds up to a value which exceeds the cohesive strength of the boundary and it pops open, as shown in Fig. 15*b*. Obviously, slip homogenization and "reversible" strain hardening will reduce the stresses on boundaries and lead to increased life. Such effects have been demonstrated by Laird and Feltner [*36*].

For the same cumulative plastic strain, small grain materials, on the average, will develop smaller offsets than will large grain materials. The reason for this is simply that, if $\Delta\epsilon_p = \Delta l/l$ is the same in each grain, and if l is taken as proportional to the grain size, then large grain materials will develop larger values of Δl at the boundary and therefore higher stresses causing shorter crack initiation periods. However, it appears that the benefits in life achieved by suppression of crack initiation are minimal for the very large changes in grain size that are required. Another approach would be to seek ways of increasing the cohesive strength of the boundary. Usage of small grain sizes as a fatigue-strengthening mechanism appears to have the greatest potential in suppressing crack growth in planar slip-mode materials. In multiphase alloys exhibiting more complex behavior, synergistic effects may arise because of the influence of grain boundary area on precipitation and aging reactions.

Microstructural Defects and Their Role in Crack Initiation—A variety of microstructural defects may be present in commercial alloys as a result of processing. These defects act as strain concentration centers which greatly speed up the crack nucleation period and lead to lower fatigue resistance.

Inclusions constitute one of the most common microstructural defects. A typical example of a fatigue crack nucleating from an inclusion is shown in Fig. 16. Factors affecting the degree to which inclusions influence the fatigue strength of materials include (1) size and shape, (2) location relative to the surface, (3) orientation to the tensile stress, (4) deformability of the inclusion, and (5) the deformation and strength characteristics of the matrix. Inclusions in steels have been extensively investigated [*84*, *85*], while some work has been done on commercial aluminum alloys [*86*].

Another major type of defect is the local "soft spot" in a high-strength microstructure resulting from improper heat treatment. Examples of such soft spots include aging inhomogeneities in aluminum alloys [*87*], proeutectoid ferrite in quenched and tempered steels [*66*], retained austenite in quenched and tempered steels [*88*], and mixtures of these structures [*89*]. The magnitude of the effect of incomplete heat treatment on the fatigue strength limit of two steels is shown in Fig. 17. Note that fatigue strength losses may be as large as 10 to 12 percent.

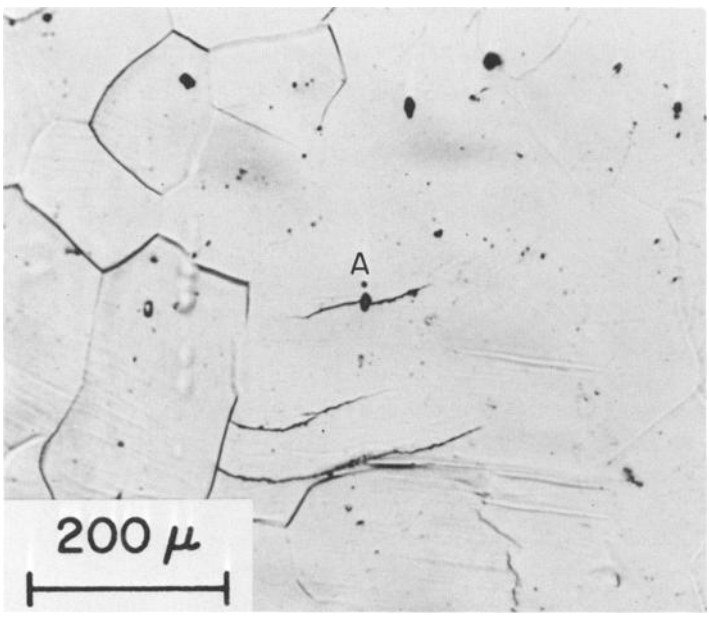

FIG. 16—*Crack initiation at an inclusion*, A, *in an ordered iron-cobalt-vanadium alloy.*

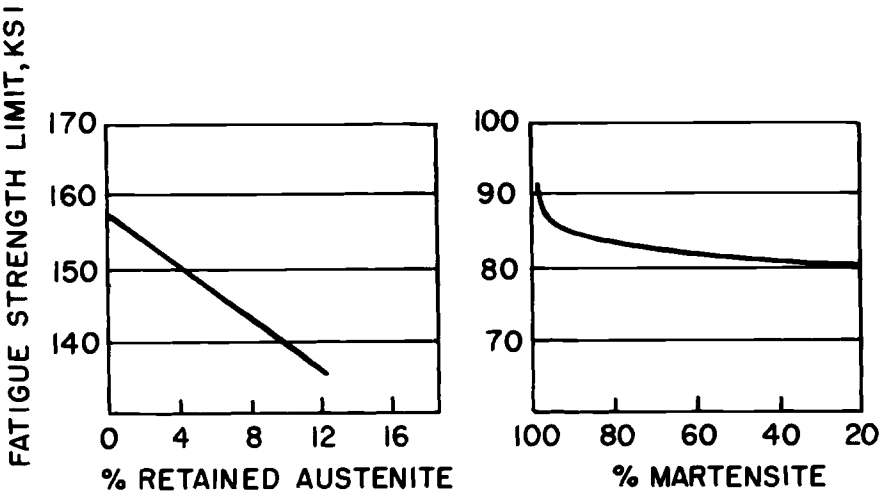

FIG. 17—*Influence of incomplete heat treatment on the fatigue strength limit of quenched and tempered* (left) *SAE 4340 steel* [88] *and* (right) *SAE 5140 steel* [89].

Pores due to gas evolution or shrinkage in cast metals may also be preferred sites for crack initiation. An example is shown in Fig. 18 for a cast nickel-base superalloy.[7] Coherent annealing twins also act as preferred crack nucleation sites both in single-phase [*21*, *90*] and multiphase materials [*91*].

There is no evidence to indicate that the crack initiation mechanism is altered by any of these metallurgical defects. It appears that they simply speed up the kinetics by virtue of their strain concentration effect. Fatigue strength improvements will always be obtained, primarily at long lives, by removal or minimization of these defects by standard metallurgical processing techniques, the discussion of which is beyond the scope of this article.

Crack Propagation

Metallurgy of Fatigue Crack Propagation—One of the major questions concerning fatigue mechanisms as yet unanswered is "When does nucleation end and propagation begin?" Schijve [*92*], for example, has developed the schematic picture shown in Fig. 19, which shows the average length of cracks (starting in different ways) as a function of percentage of life. Note that the values of crack length may vary by a factor of 10^8! Yet it is virtually impossible to decide at what length a crack may actually be considered a crack. Grosskreutz [*93*] has analyzed 19 sets of observations of crack nucleation and concluded that a crack has been nucleated whenever it gets large

[7] Feltner, C. E. and Wetzel, R. M., "The Influence of the Volume Fraction of γ' on the Cyclic Deformation and Fracture of Cast Nickel-Base Superalloys," unpublished research.

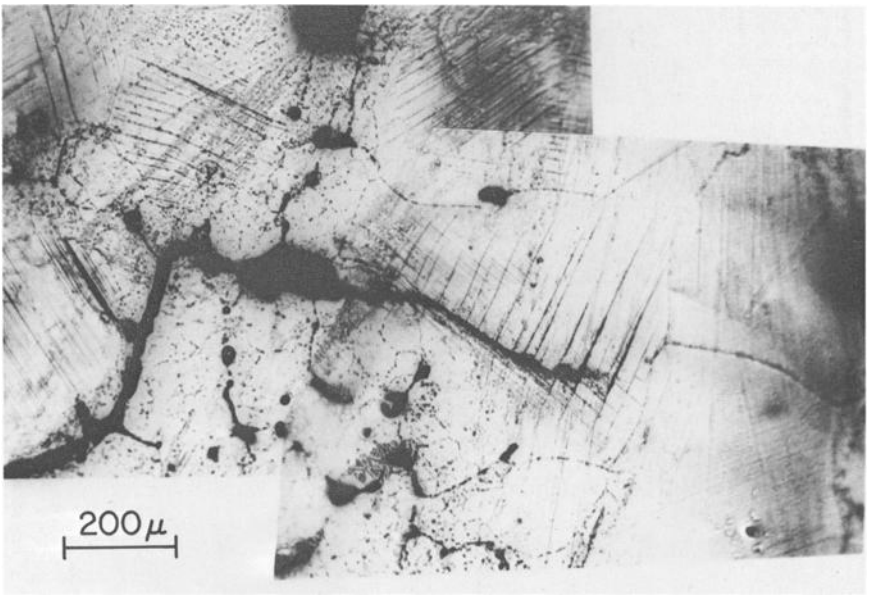

FIG. 18—*Fatigue crack initiation at a gas pore in a cast nickel-base superalloy.*

enough for an observer to see it, by whatever observational technique he is using. Analysis of the 19 cases recorded by Grosskreutz shows that the median nucleated crack is 0.003 in. long and requires 25 percent of the life ($N_f = 5 \times 10^4$) to reach this size. In the face of this unresolved problem, those interested in developing engineering cumulative damage theories have been forced to arbitrarily define an "engineering size" crack [*94*].

Nevertheless, considerable progress has been achieved in understanding and characterizing the growth of fatigue cracks, as evidenced by several symposia which have emphasized this subject [*95*, *96*]. Mechanistically, the picture has not significantly changed since the 1966 ASTM Symposium on Crack Propagation [*96*]. Thus in this section we will only briefly review the situation as it existed in 1966 and then consider that work done in the intervening three years which has added new insight.

Two different stages of crack growth have been defined [*18*], as illustrated in Fig. 20. Stage I (crystallographic or microcracking) cracks grow from slip-generated nuclei along planes of maximum shear stress (slip planes) until a critical depth[8] is reached. At this point the crack grows in a Stage II mode (noncrystallographic) along planes perpendicular to the maximum tensile

[8] The critical depth is undefined but it increases with increasing life.

stress. Figure 21 shows that Stage II cracking dominates the life at high amplitudes but plays only a minor role in the long-life regime. It is generally agreed that plastic deformation phenomena at the crack tip, particularly strain hardening, control the rate of crack growth. Observations of crack sections [*4*] and appreciable fractographic evidence [*97–99*] have provided the necessary information to construct [*4*, *100*] a description of Stage II crack growth shown in Fig. 22. During the tensile stroke, plastic strain occurs at the crack tip and results in a blunted crack which has an increased surface area. Upon reversal of the load, the crack faces close together without complete reversal of the plastic flow, and thus the crack advances some amount proportional to the difference of new surface created in the tensile stroke and that regained in compression. Full compression resharpens the crack, preparing it for the next cycle. The plastic blunting-collapse process is re-

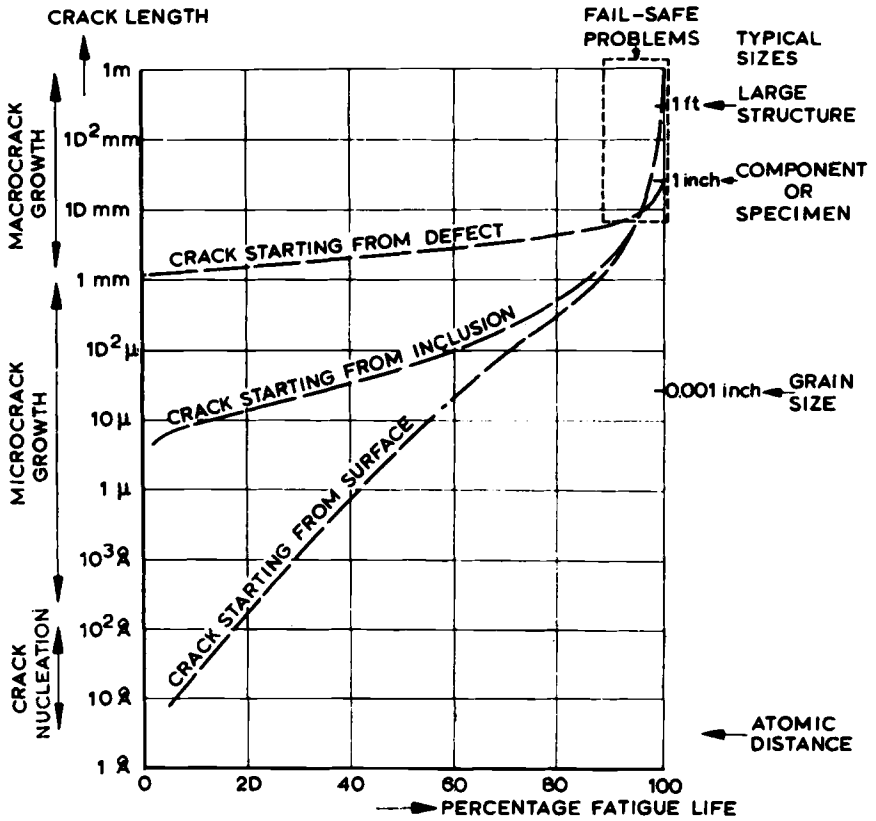

FIG. 19—*Schematic picture of crack growth curves, indicating the range of values for the crack length (after Schijve* [92]).

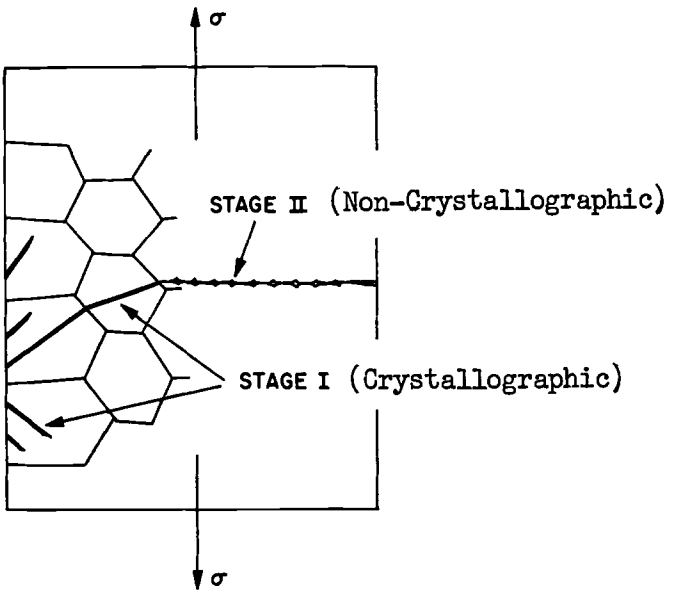

FIG. 20—*Different stages of crack growth (after Laird* [4]).

sponsible for the formation of ripples or striations on the fracture surface which have been shown to correspond to individual cycles [*101*].[9]

Laird [*4*, *104*] has suggested that there is no fundamental difference between the mechanisms of Stage I and Stage II crack growth, although a Stage I crack tends to be confined to a persistent slipband and is thus more constrained. Direct observations [*105*, *106*] of the dislocation structures at Stage I and Stage II crack tips in copper single crystals appear to support this idea.

From a strengthening mechanism point of view it is desirable to delineate those microstructures which will retard crack propagation. In the high-amplitude range, Laird [*4*] states that differences in microstructure have a minimal effect on crack growth rate. At low amplitudes it appears that the effects of only a few microstructural variables are understood [*4*]. The work of McEvily and Boettner [*107*] and Miller et al [*108*] show that increasing the planarity of slip (by substitutional alloying) generally decreases the growth rate.[10] Recent results by Karashima et al [*110*] appear to support this conclusion. They found for a given crack length that the plastic zone size

[9] Broek [*102*] has shown that if ripples are not observed on replicas in an electron microscope, it may be a consequence of viewing angle and replica flattening. Environment may also play a key role in whether ripples are observed on a fracture surface [*103*].

[10] In certain cases [*109*], substitutional alloying may induce a frequency effect, that is reduced growth rates at high frequencies, as a result of a solute pinning effect.

increased as the stacking fault energy of several fcc metals increased (that is, a more wavy slip character). Since crack growth rate is proportional to plastic zone size [*111*], one can conclude that planar slip tends to retard crack growth.

Although cold work increases long-life fatigue resistance (as discussed under crack initiation) the small amount of data available indicates that it has little influence on crack growth rate [*112*]. High strains at Stage II crack tips undoubtedly cause appreciable softening, thereby minimizing the benefit of cold working.

The role of grain size is unclear. Hoeppner [*82*] and Boettner et al [*37*] show for copper, a wavy slip-mode material, that grain size has little effect on Stage II growth rate, while for 70-30 brass, a planar slip-mode material, grain boundaries appear to suppress the growth of cracks from Stage I to Stage II [*83*]. In Cu-7.5 Al alloy decreasing grain size may suppress Stage II crack growth rate [*107*]. Based on these few results we conclude that grain size has virtually no effect on fatigue crack growth rate in wavy slip-mode materials and only a slightly greater effect for planar slip-mode materials.

Results obtained by Broek [*113*] show that inclusions increase crack growth rates at high stresses. At low stresses they are not particularly detrimental, which may explain differing results previously reported [*114*, *115*].

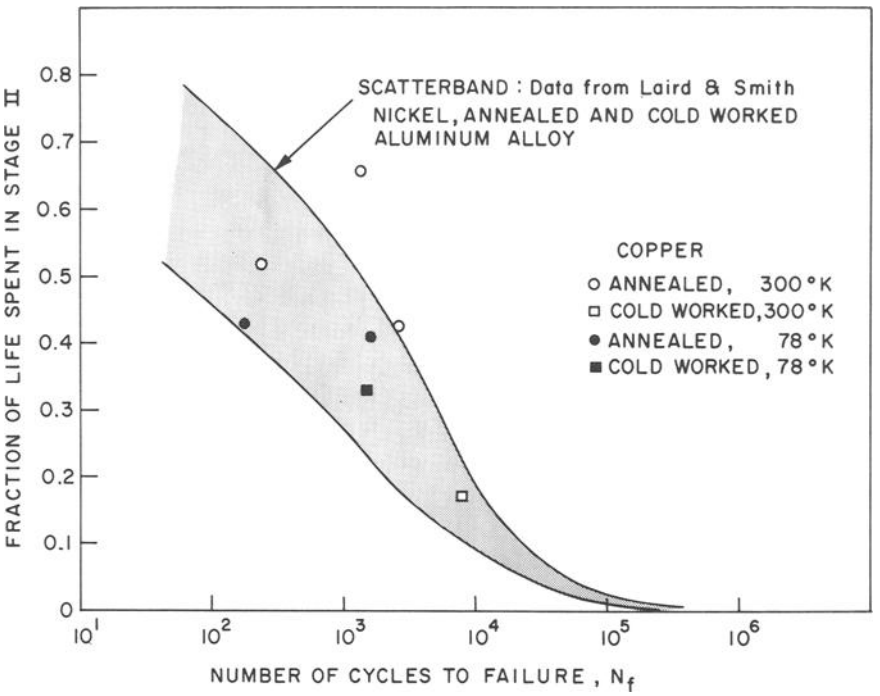

FIG. 21—*Fraction of life spent in Stage II crack growth mode (after Laird and Feltner* [36]).

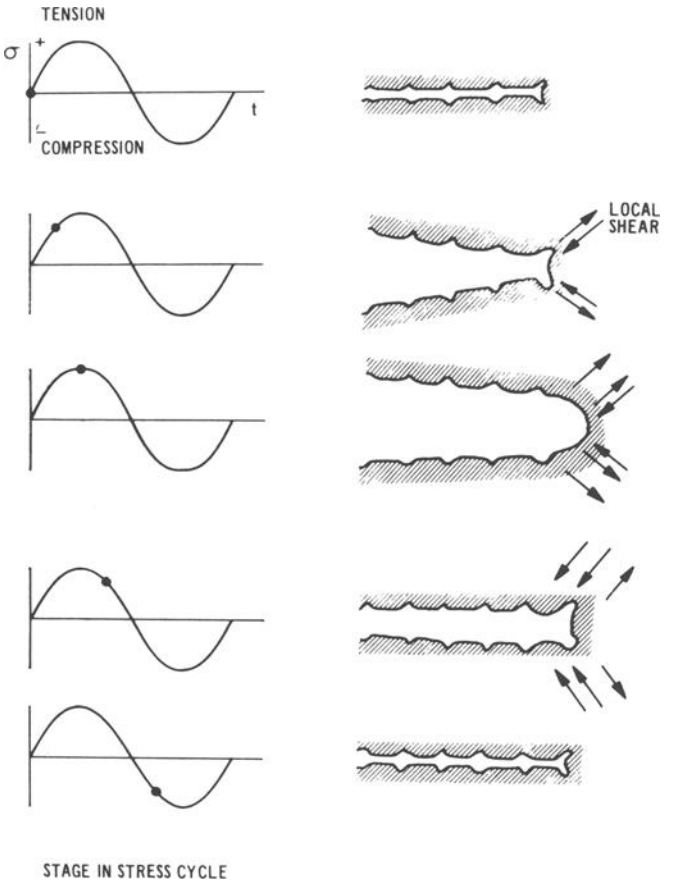

FIG. 22—*Mechanism of Stage II crack propagation (after Laird* [4] *as depicted by Broom* [9]).

We shall not comment on the effect of precipitation hardening or dispersion strengthening on fatigue crack propagation rates since as yet no clear picture has developed. Generally, we would conclude that the influence of various microstructures on the kinetics of crack growth is poorly understood. More systematic investigations on the effect of metallurgical structure are needed before a clear set of guidelines can be developed for achieving high fatigue resistance by suppressing crack propagation through metallurgical means. In the absence of such information, a more fruitful approach is to consider the mechanics of fatigue crack propagation and attempt to deduce what simple material properties provide the best indexes of high resistance to fatigue crack propagation. With this information, the effort expended in cut-and-try alloy development procedures may be greatly reduced.

Mechanics of Fatigue Crack Propagation—Considerable effort has been spent experimentally determining crack growth laws and in developing associated theories. These efforts have been reviewed by several authors [*5*, *92*, *93*, *111*]. The net result is that the fatigue crack propagation rate, dl/dn, is generally believed to obey the following law:

$$dl/dn = \Delta\sigma^m l^p / M \quad \ldots\ldots\ldots\ldots\ldots\ldots\ldots\ldots\ldots\ldots (4)$$

where $\Delta\sigma$ is the applied stress range, l the crack length, and m, p, and M parameters which may (or may not) depend on material properties. Several investigators have developed relations for m, p, and M [*2*, *8*, *116*, *117*] and in some instances these factors have been experimentally evaluated [*118–121*]. A typical set of results that demonstrates variations in these parameters for several materials is shown in Fig. 23.

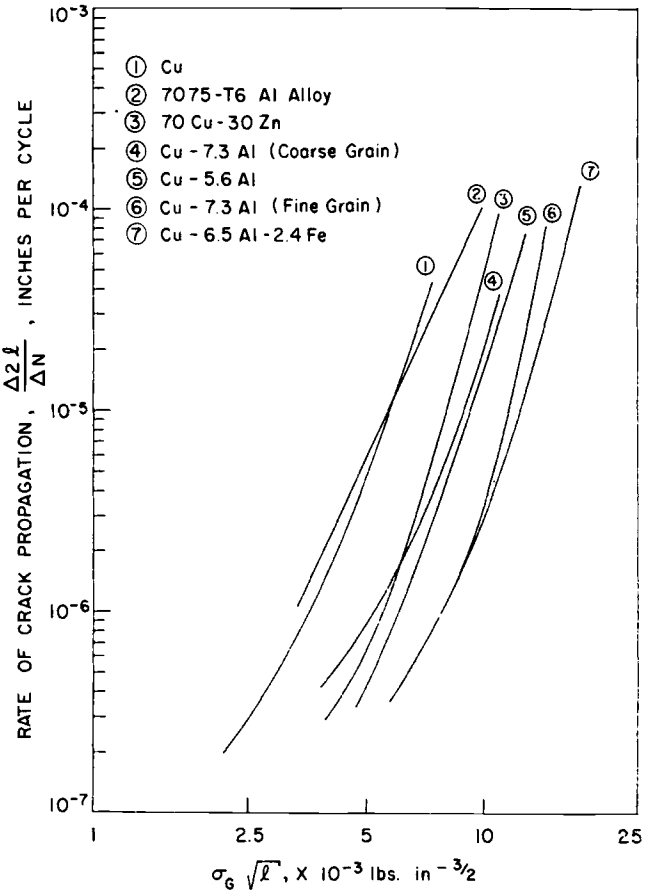

FIG. 23—*Crack growth results showing variations in* m, p, *and* M *for several materials (after McEvily and Boettner* [116]).

Based on the wealth of crack growth data and the direct observations of crack growth processes, a rash of theories of fatigue crack propagation have appeared very recently [*122–129*].[11] The fundamental problems in developing these theories have been (1) to determine the displacements in the vicinity of the crack tip and relate them to the nominal stress or strain, (2) to employ a realistic criterion for crack advance, and (3) to incorporate a realistic stress-strain law. In solving problem 1, loading and geometry (that is, the mechanics) are accounted for, while 2 and 3 introduce appropriate materials properties. Problem 1 has been particularly difficult and several approaches have been employed, including (a) usage of the Bilby-Cottrell-Swinden (BCS) theory of continuously distributed dislocations [*130*], (b) elastic-plastic analyses, and (c) elastic-plastic measurements.

A significant advance in elastic-plastic analysis has been made recently by Rice and Rosengren [*131*] and Hutchinson [*132, 133*], who have obtained the solution for the stress distribution for the case of an elastic-plastic crack using a deformation theory of plasticity and a power hardening law. These results have formed the basis of the crack propagation theory of Yokobori and Ichikawa [*127*]. The model of Frost and Dixon [*122*], on the other hand, uses the elastic solution of an elliptic crack and then corrects the displacements for local plasticity at the crack tip by means of the experimentally determined relation [*134, 135*]:

$$\epsilon = (E/E_s)^{1/2}\epsilon_e \quad \ldots\ldots\ldots\ldots\ldots\ldots\ldots\ldots\ldots\ldots (5)$$

where ϵ is the total (crack tip) strain, ϵ_e is the crack tip strain from elastic analysis, E is Young's modulus and E_s is the secant modulus corresponding to ϵ. It is interesting to note that Eq 5 is an experimentally determined version of Neuber's rule [*136*][12] which has been found extremely useful in describing notch fatigue behavior (Stage II crack propagation) [*137, 138*]. Finally, Tomkins [*126*] has used the BCS analysis, a power hardening law (the cyclic stress-strain curve), and a plastic decohesion crack advance criterion. Many of these crack growth theories result in m and p being constants (which does not agree with experiment) and M being the only parameter dependent on

[11] Grosskreutz, J. C., "A Theory of Stage II Fatigue Crack Propagation," 1966, unpublished research.

[12] Wetzel (private communication, 1969) has shown that Eq 5 is equivalent to Neuber's rule. Thus, substituting $E = S/e$, $E_s = \sigma/\epsilon$, and $\epsilon_e = K_t e$ (where S and e are nominal [elastic] values of stress and strain, σ and ϵ are local [crack tip] values of stress and strain, and K_t is the Hookean stress concentration factor), we obtain after rearrangement

$$K_t = (\sigma/s \times \epsilon/e)^{1/2}$$

Introducing the relation for stress and strain concentration factors (for any stress-strain law)

$$K_\sigma = \sigma/S,\ K_\epsilon = \epsilon/e$$

gives after substitution in the above

$$K_t = (K_\sigma \times K_t)^{1/2} \quad \ldots\ldots\ldots\ldots\ldots\ldots \text{(Neuber's rule)}$$

materials properties, generally due to unrealistic choices of stress-strain law and crack advance criterion.

From a fatigue-strengthening mechanism or alloy development viewpoint the resultant equations of Tomkins [*126*] contain the best combination of realism and usefulness. Tomkins' equations are

$$\frac{dl}{dN} = \left[\frac{\pi}{32}\frac{{\sigma_f}^2}{({\epsilon_f}^{n'}{\sigma'}_y)^2}\right]{\Delta\epsilon_p}^{(2n'+1)} \times l \quad \ldots\ldots\ldots\ldots\ldots\ldots (6)$$

for high amplitude, plastic strain cycling and

$$\frac{dl}{dN} = \left[\frac{\pi}{32}\frac{\epsilon_f}{{\sigma_f}^{1/n'}({\sigma'}_y)^2}\right]{\Delta\sigma}^{(2n'+1/n)} \times l \quad \ldots\ldots\ldots\ldots\ldots\ldots (7)$$

for stress cycling, where ${\sigma'}_y$ is a cyclic flow stress. Few results are available for plastic strain cycling, but those of Boettner et al [*37*] for copper are replotted in Fig. 24 according to Eq 6, with $n' = 0.15$ [*48*]. It can be seen that the agreement is excellent. Tomkins has shown that the integrated form of Eq 6 fits strain-life data well. Furthermore, his comparison of Eq 7 with several sets of stress-cycling crack growth data results in very good correlations. These equations are particularly useful in that they result in fairly simple indexes of crack propagation resistance, namely n', σ_f, and ϵ_f. We note

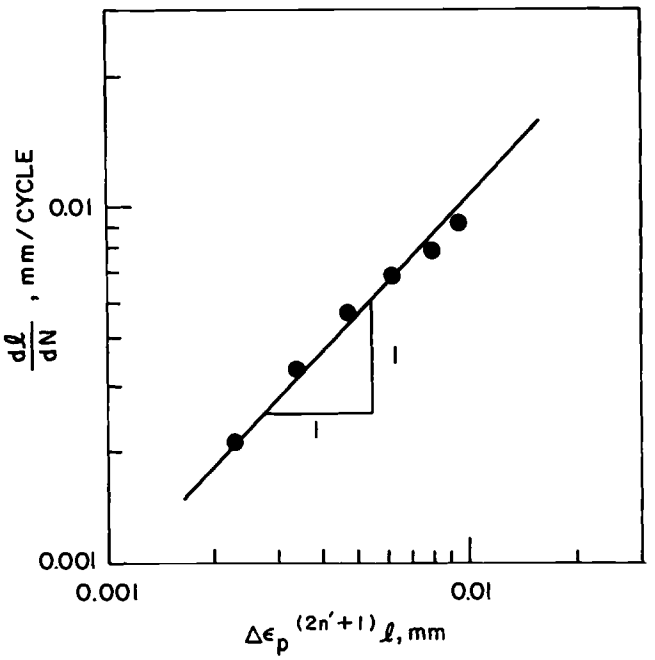

FIG. 24—*Crack propagation behavior of copper (with* n' = *0.15).*

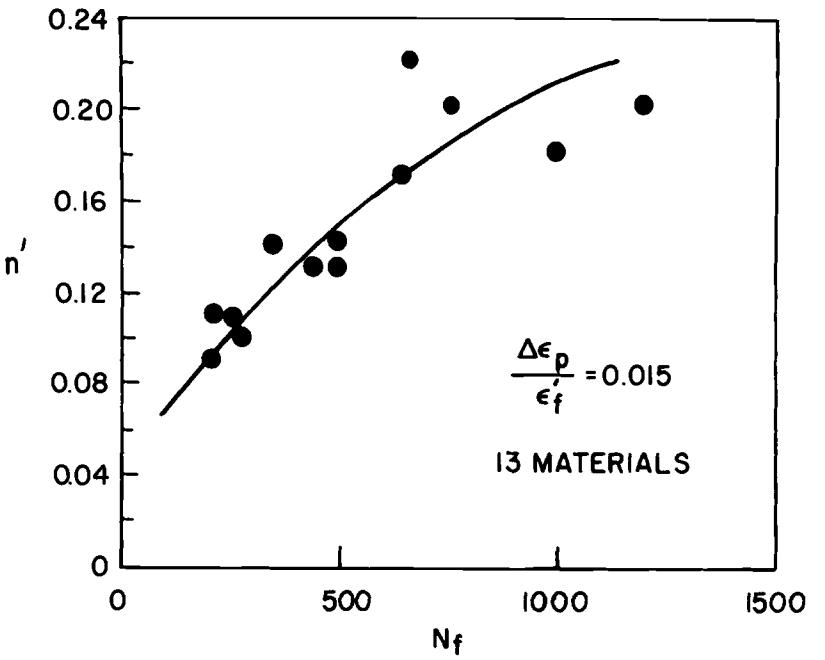

FIG. 25—*Variation of life with* n′ *of several steels, aluminum alloys, copper alloys, and pure metals.*

in Eq 6 as n' increases that the crack growth rate decreases, which correlates with the effect described earlier in Eq 3. This influence of n' is shown in Fig. 25 for the short-life region (that is, where the life is virtually all crack propagation) for several alloys. Similarly, one can show that the crack growth rate under stress-cycling will decrease as n' decreases, which agrees with the stress-life effect given by Eq 2.

The great value in these equations is that they allow us to circumvent the problem of the paucity of data, clearly showing the effects of microstructure on crack propagation behavior. Until further work is done in this area, one must generally rely on these parameters and their usage in mechanical crack growth theories to minimize the cut-and-try procedures so prevalent in alloy development work.

Guidelines for Achieving High Fatigue Resistance by Metallurgical Means—A Summary

We have attempted in this paper to synthesize the extant literature on the role of metallurgical structure in the achievement of high fatigue resistance. In so doing, we have been compelled to present our summary of those phenomenological parameters which provide the best index of high fatigue

resistance, as the alloy developer must have simple yardsticks by which to measure the results of his efforts. The cyclic strain hardening exponent n' is, in our opinion, the best single index; increased values give good plastic strain resistance and decreased values give good stress resistance. In certain cases the relation of n' to mechanisms of crack initiation and propagation in alloys of diverse microstructure can be shown. Ways in which crack initiation may be suppressed are summarized as follows:

1. Raise the microcyclic yield stress, σ_i, to stop plastic strain.
   a. Alloy, by case carburizing, etc.
   b. Introduce compressive residual stresses by mechanical/metallurgical methods.
   c. Alloy for strain aging and dislocation pinning.
2. Homogenize surface slip.
   a. Alloy in surface layer for planar slip character.
   b. Alloy for stable precipitates.
   c. Alloy to stabilize cold work or transformation substructures.
3. Eliminate metallurgical strain concentrations.
   a. Eliminate inclusions in hard steels and strong aluminum alloys.
   b. Eliminate "soft spots" with low intrinsic yield stresses—aging inhomogeneities in aluminum alloys, free ferrite, retained austenite, etc.
   c. Minimize casting defects.

Processes such as those in 1*a* and 1*b* are fully discussed in other contributions to this book. A similar summary for crack propagation is virtually impossible to draw up until further research is done.

The ideal material should have a planar slip character, "reversible" strain hardening, a small grain size, a stable precipitate structure or dislocation substructure, no "metallurgical" strain concentrations or "soft spots," effective dislocation pinning elements, and a crystal structure with a high Peierls stress. Undoubtedly no single material may have all these characteristics. Certain ones may in fact exclude others. Yet, some steels [*139*, *140*], composites [*141–143*], and dispersion-strengthened metals [*67*] combine several of these microstructural characteristics to give improved fatigue resistance. A better understanding of the interaction between strengthening mechanisms and fatigue crack initiation and propagation processes will no doubt in the future lead us to the achievement of yet higher fatigue resistance in the development of new commercial alloys.

Acknowledgments

The authors are grateful to T. L. Johnston, R. W. Landgraf, R. M. Wetzel, and M. R. Mitchell for helpful comments on the manuscript.

References

[1] Thompson, N. and Wadsworth, W., *Advances in Physics*, ADPHA, Vol. 7, 1958, pp. 72–169.

[2] Grosskreutz, J. C. in *Fatigue: An Interdisciplinary Approach*, J. Burke, N. Reed, and V. Weiss, Eds., Syracuse University Press, Syracuse, N. Y., 1964, pp. 27–62.

[3] Segall, R. L., "Fatigue Hardening in Face Centered Cubic Metals," *Advances in Materials Research*, Vol. 3, 1968 (in press).

[4] Laird, C. in *Fatigue Crack Propagation*, *ASTM STP 415*, American Society for Testing Materials, 1967, pp. 131–180.

[5] Ham, R. K. in *Thermal and High Strain Fatigue*, The Metals and Metallurgy Trust, London, 1967, pp. 55–79.

[6] Morrow, J. in *Internal Friction, Damping, and Cyclic Plasticity*, *ASTM STP 378*, American Society for Testing and Materials, 1965, pp. 45–87.

[7] Landgraf, R. W. in *Achievement of High Fatigue Resistance in Metals and Alloys*, *ASTM STP 467*, American Society for Testing and Materials, 1970, pp. 3–36.

[8] Feltner, C. E. and Landgraf, R. W., "Selecting Materials to Resist Low Cycle Fatigue," ASME Paper No. 69-DE-59, American Society of Mechanical Engineers, 1969.

[9] Broom, T., *Contemporary Physics*, CTPHA, Vol. 8, 1967, pp. 213–233.

[10] Glenny, E., *Metallurgical Reviews*, MREVA, Vol. 6, 1961, pp. 387–465.

[11] Broom, T., *Materials Science and Engineering*, MSCEA, Vol. 3, 1968, pp. 138–144.

[12] Gilbert, P. T., *Metallurgical Reviews*, MREVA, Vol. 1, 1956, pp. 379–417.

[13] Achter, M. R. in *Fatigue Crack Propagation*, *ASTM STP 415*, American Society for Testing and Materials, 1967, pp. 181–202.

[14] Mason, W. P., *Journal of the Acoustical Society of America*, JASMA, Vol. 28, 1956, pp. 1207–1218.

[15] Mason, W. P. in *Symposium on Basic Mechanisms of Fatigue*, *ASTM STP 237*, American Society for Testing and Materials, 1958, pp. 36–50.

[16] Wood W. A. in *Symposium on Basic Mechanics of Fatigue*, *ASTM STP 237*, American Society for Testing and Materials, 1958, pp. 110–119.

[17] Avery, D. H. and Backofen, W. A. in *Fracture of Solids*, D. C. Drucker and J. J. Gilman, Eds., Interscience Publishers, New York, 1963, pp. 339–382.

[18] Forsyth, P. J. E., "A Two-Stage Process of Fatigue Crack Growth," *Proceedings*, Crack Propagation Symposium, Cranfield, 1961, Vol. I, pp. 76–94.

[19] Laird, C. and Smith, G. C., *Philosophical Magazine*, PHMAA, Vol. 7, 1962, pp. 847–857.

[20] McEvily, A. J. and Boettner, R. C., *Acta Metallurgica*, AMETA, Vol. 11, 1963, pp. 725–743.

[21] Thompson, N. in *Fracture*, B. L. Averbach et al, Eds., Wiley, New York, 1959, pp. 354–375.

[22] Partridge, P. G., *Philosophical Magazine*, PHMAA, Vol. 12, 1965, pp. 1043–1054.

[23] Beevers, C. J. and Halliday, M. D., *Metals Science Journal*, Vol. 3, 1969, pp. 74–79.

[24] Beevers, C. J. and Robinson, J. L., *Journal of the Less Common Metals*, JCOMA, Vol. 17, 1969, pp. 345–352.

[25] Broom, T. and Ham, R. K., *Proceedings of the Royal Society*, PRSLA, Vol. A251, 1959, pp. 186–199.

[26] Kemsley, D. S. and Paterson, M. S., *Acta Metallurgica*, AMETA, Vol. 8, 1960, pp. 453–467.

[27] Feltner, C. E., *Philosophical Magazine*, PHMAA, Vol. 12, 1965, pp. 1229–1248.

[28] Thompson, N., Wadsworth, N. J., and Louat, N., *Philosophical Magazine*, PHMAA, Vol. 1, 1956, pp. 113–126.

[29] Laufer, E. E. and Roberts, W. N., *Philosophical Magazine*, PHMAA, Vol. 14, 1966, pp. 65–78.

[30] Lukas, P., Klesnil, M., and Krejci, J., *Physica Status Solidi*, PHSSA, Vol. 27, 1968, pp. 545–558.

[31] Roberts, W. N., "Persistent Slipbands in Fatigued Copper," Report PM-M-68-19, Bureau of Mines, Ottawa, Canada, 1968.
[32] Feltner, C. E. and Laird, C., *Transactions of the Metallurgical Society of AIME*, TMSAA, Vol. 242, 1968, pp. 1253–1257.
[33] Helgeland, O., *Journal of the Institute of Metals*, JIMEA, Vol. 93, 1965, pp. 570–575.
[34] Watt, D. F. and Ham, R. K., *Nature*, NATUA, Vol. 211, 1966, pp. 734–735.
[35] Watt, D. F., Embury, J. D., and Ham, R. K., *Philosophical Magazine*, PHMAA, Vol. 17, 1968, pp. 199–203.
[36] Laird, C. and Feltner, C. E., *Transactions of the Metallurgical Society of AIME*, TMSAA, Vol. 239, 1967, pp. 1074–1083.
[37] Boettner, R. C., Laird, C., and McEvily, A. J., *Transactions of the Metallurgical Society of AIME*, TMSAA, Vol. 233, 1965, pp. 379–387.
[38] Wells, C. H., *Acta Metallurgica*, AMETA, Vol. 17, 1969, pp. 443–449.
[39] McEvily, A. J. and Johnston, T. L., "The Role of Cross-Slip in Brittle Fracture and Fatigue," *Proceedings of the First International Conference on Fracture*, Sendai, Japan, Vol. 2, 1965, pp. 515–546.
[40] Feltner, C. E. and Morrow, J., *Journal of Basic Engineering, Transactions of ASME*, JBAEA, Vol. 83, 1961, pp. 15–22.
[41] Zener, C., *Elasticity and Anelasticity of Metals*, University of Chicago Press, Chicago, Ill. ,1948, p. 41.
[42] Lazan, B. J. in *Mechanical Behavior of Materials at Elevated Temperatures*, J. E. Dorn, Ed., McGraw-Hill, New York, 1961, pp. 477–515.
[43] Friedel, J., *Dislocations*, Pergamon Press, New York, 1964, pp. 54–55.
[44] Ferro, A., Mazzetti, P., and Montalenti, G., *Philosophical Magazine*, PHMAA, Vol. 12, 1965, pp. 867–874.
[45] Polakowski, N. and Palchoudhuri, A., *Proceedings*, American Society for Testing Materials, ASTEA, Vol. 54, 1954, pp. 701–716.
[46] Ham, R. and Broom, T., *Philosophical Magazine*, PHMAA, vol. 7, 1962, pp. 95–103.
[47] Coffin, L. F. and Read, J. H., "A Study of the Strain Cycling and Fatigue Behavior of a Cold-Worked Metal," International Conference on Fatigue of Metals, London, 1956, pp. 415–424.
[48] Feltner, C. E. and Laird, C., *Acta Metallurgica*, AMETA, Vol. 15, 1967, pp. 1621–1632.
[49] Feltner, C. E. and Laird, C., *Acta Metallurgica*, AMETA, Vol. 15, 1967, pp. 1633–1653.
[50] Feltner, C. E., "Dislocation Structures After Fatigue in Cold-Worked Materials," *Transactions of the Metallurgical Society of AIME* (to be published).
[51] Burghoff, H. L. and Blank, A. I., *Proceedings*, American Society for Testing Materials, ASTEA, Vol. 48, 1948, pp. 709–736.
[52] Gill, E. T. and Goodacre, R., *Journal of the Iron and Steel Institute*, JISIA, Vol. 130, 1934, p. 293; and Vol. 132, 1935, pp. 143–177.
[53] Cina, B., *Journal of the Iron and Steel Institute*, JISTA, Vol. 190, 1958, pp. 144–157.
[54] Beardmore, P. and Feltner, C. E., "Cyclic Deformation and Fracture Characteristics of a Low Carbon Martensitic Steel," *Fracture 1969*, Proceedings of the 2nd International Conference on Fracture, Brighton, England, April 1969.
[55] Wells, C. H. and Sullivan, C. P., *Transactions*, American Society for Metals, TASEA, Vol. 57, 1964, pp. 841–855.
[56] Abel, A. and Ham, R. K., *Acta Metallurgica*, AMETA, Vol. 14, 1966, pp. 1495–1503.
[57] McGrath, J. T. and Bratina, W. J., *Czechoslovak Journal of Physics*, CZYPA, Vol. B19, 1969, pp. 284–293.
[58] Broom, T., Mazza, J., and Whittaker, V., *Journal of the Institute of Metals*, JIMEA, Vol. 86, 1957, pp. 17–23.
[59] Clark, J. B. and McEvily, A. J., *Acta Metallurgica*, AMETA, Vol. 12, 1964, pp. 1359–1372.
[60] Stubbington, C. A. and Forsyth, P. J. E., *Acta Metallurgica*, AMETA, Vol. 14, 1966, pp. 5–12.

[61] McGrath, J. T. and Bratina, W. J., *Acta Metallurgica*, AMETA, Vol. 15, 1967, pp. 329–339.
[62] Feltner, C. E., "Cyclic Deformation and Fracture of Alloys Strengthened by Long Range Order," *Transactions of the Metallurgical Society of AIME* (to be published).
[63] Boettner, R. C., Stoloff, N. S., and Davies, R. G., *Transactions of the Metallurgical Society of AIME*, TMSAA, Vol. 236, 1966, pp. 131–133.
[64] Morrow, J., Halford, G. R., and Millan, J., "Optimum Hardness for Maximum Fatigue Strength of Steels," *Proceedings of International Conference on Fracture*, Sendai, Japan, Vol. 3, 1965, pp. 1611–1636.
[65] Landgraf, R., "Cyclic Deformation and Fatigue Behavior of Hardened Steels," PhD thesis, University of Illinois, Urbana, Ill., 1969; also TAM Report No. 320, Department of Theoretical and Applied Mechanics, University of Illinois, Urbana, Ill., Nov. 1968.
[66] Sinclair, G. M. and Dolan, T. J., *Proceedings*, American Society for Testing Materials, ASTEA, Vol. 50, 1950, pp. 587–616.
[67] Ham, R. K. and Wayman, M. L., *Transactions of the Metallurgical Society of AIME*, TMSAA, Vol. 239, 1967, pp. 721–725.
[68] Leverant, G. R., *Transactions of the Metallurgical Society of AIME*, TMSAA, Vol. 239, 1967, pp. 1992–1993.
[69] Ham, R. K., Kirkdaldy, J. S., and Plewes, J. T., *Acta Metallurgica*, AMETA, Vol. 15, 1967, pp. 861–869.
[70] Adair, A. M. and Lipsitt, H. A., *Transactions of the Metallurgical Society of AIME*, TMSAA, Vol. 236, 1966, pp. 1235–1237.
[71] Mackenzie, C. T. and Benham, P. P., *Proceedings of the Institution of Mechanical Engineers*, London, PIMLA, Vol. 180, 1965, pp. 709–725.
[72] Oates, G. and Wilson, D. V., *Acta Metallurgica*, AMETA, Vol. 12, 1964, pp. 21–23.
[73] Klesnil, M. and Lukas, P., *Journal of the Iron and Steel Institute*, JISIA, Vol. 205, 1967, pp. 746–749.
[74] Beardmore, P. and Thornton, P. H., "Fatigue Behavior of Polycrystalline Molybdenum," *Transactions of the Metallurgical Society of AIME* (to be published).
[75] Feltner, C. E. and Laird, C., *Transactions of the Metallurgical Society of AIME*, TMSAA, Vol. 245, 1969, pp. 1372–1373.
[76] Stubbington, C. A., *Metallurgia*, Manchester, England, METLA, Vol. 58, 1958, pp. 165–171.
[77] Forrest, P. G., *Journal of the Iron and Steel Institute*, JISIA, Vol. 200, 962, pp. 452–457.
[78] Mintz, B. and Wilson, D. V., *Acta Metallurgica*, AMETA, Vol. 13, 1965, pp. 947–956.
[79] Phillips, W. L. and Armstrong, R. W., *Journal of the Mechanics and Physics of Solids*, JMPSA, Vol. 17, 1969, pp. 1–6.
[80] Pelloux, R. M., "Influence of Grain Size on Fatigue," *Ultrafine Grain Size Metals*, Proceedings of the Sixteenth Sagamore Conference, Sagamore, N. Y., Aug. 1969.
[81] Feltner, C. E., "The Influence of Grain Size on the Low Cycle Fatigue Behavior of Copper and Copper-7.5% Aluminum" (to be published).
[82] Hoeppner, D. W. in *Fatigue Crack Propagation, ASTM STP 415*, American Society for Testing and Materials, 1967, pp. 486–504.
[83] Forrest, P. G. and Tate, A. E., *Journal of the Institute of Metals*, London, JIMEA, Vol. 93, 1965, pp. 438–444.
[84] Forrest, P. G. in *Fatigue of Metals*, Pergamon Press, New York, 1962, pp. 62–65.
[85] Duckworth, W. E., *Metallurgia*, Manchester, England, METLA, Vol. 9, 1964, pp. 53–55.
[86] Grosskreutz, J. C. and Shaw, G. G., "Critical Mechanisms in the Development of Fatigue Cracks in 2024-T4 Aluminum," *Fracture 1969*, Proceedings of the Second International Conference on Fracture, Brighton, England, April 1969.
[87] Laird, C. and Thomas, G., *International Journal on Fracture Mechanics*, IJFMA, Vol. 3, 1967, pp. 81–97.
[88] Frankel, H. E., Bennett, J. A., and Pennington, W. A., *Transactions*, American Society for Metals, TASEA, Vol. 52, 1960, pp. 257–276.

[89] Borik, F., Chapman, R. D., and Jominy, W. E., *Transactions*, American Society for Metals, TASEA, Vol. 50, 1958, pp. 242–257.
[90] Boettner, R. C., McEvily, A. J., and Liu, Y. C., *Philosophical Magazine*, PHMAA, Vol. 10, 1964, pp. 95–106.
[91] Wells, C. H. and Sullivan, C. P., *Transactions*, American Society for Metals, TASEA, Vol. 60, 1967, pp. 217–222.
[92] Schijve, J. in *Fatigue Crack Propagation, ASTM STP 415*, American Society for Testing and Materials, 1967, pp. 415–457.
[93] Grosskreutz, J. C., "Fatigue Mechanisms in the Sub-Creep Range," (to be published).
[94] Manson, S. S. and Hirscherg, M. H., "Crack Initiation and Propagation in Notched Fatigue Specimens," Proceedings of the First International Conference on Fracture, Vol. 1, Sendai, Japan, 1965, pp. 479–499.
[95] Proceedings of the Crack Propagation Symposium, Canfield, England, 1961.
[96] *Fatigue Crack Propagation, ASTM STP 415*, American Society for Testing and Materials, 1967.
[97] Pelloux, R., *Transactions*, American Society for Metals, TASEA, Vol. 60, Nov. 1967, pp. 26–37.
[98] Jacoby, G., "Application of Microfractography to the Study of Crack Propagation Under Fatigue Stresses," Defense Documentation Center Report AD 653 918, 1966.
[99] Hertzberg, R., in *Fatigue Crack Propagation, ASTM STP 415*, American Society for Testing and Materials, 1967, pp. 205–224.
[100] McEvily, A. J., Boettner, R. C., and Johnston, T. L. in *Fatigue: An Interdisciplinary Approach;* J. Burke et al, Eds., Syracuse University Press, Syracuse, N. Y., 1964, pp. 95–103.
[101] Forsyth, P. J. E. and Ryder, D. A., *Metallurgia*, Manchester, England, METLA, Vol. 13, 1961, pp. 117–124.
[102] Broek, D., "A Critical Note on Electron Fractography," *Engineering Fracture Mechanics* (to be published).
[103] Pelloux, R., "Corrosion Fatigue Crack Propagation," *Fracture 1969*, Proceedings of the Second International Conference on Fracture, Brighton, England, April 1969.
[104] Laird, C. and Kaplan, H., *Transactions of the Metallurgical Society of AIME*, TMSAA, Vol. 239, 1967, pp. 1017–1025.
[105] Klesnil, M. and Lukas, P., "Dislocation Substructure Associated with Propagating Fatigue Crack," *Fracture 1969*, Proceedings of the Second International Conference on Fracture, Brighton, England, April 1969.
[106] Lukas, P., Klesnil, M., and Fiedler, R., "Plastic Zone Around the Propagating Fatigue Crack," *Czechoslovak Academy of Sciences*, Brno, June, 1969.
[107] McEvily, A. J. and Boettner, R. C., *Acta Metallurgica*, AMETA, Vol. 11, 1963, pp. 725–743.
[108] Miller, G. A., Avery, D. H., and Backofen, W. A., *Transactions of the Metallurgical Society of AIME*, TMSAA, Vol. 236, 1966, pp. 1667–1673.
[109] Archer, M. J. and Martin, J. W., *Journal of the Institute of Metals*, JIMEA, Vol. 96, 1968, pp. 167–171.
[110] Karashima, S., Orkawa, H., and Agura, T., *Transactions of the Japan Institute of Metals*, TJIMA, Vol. 9, 1968, pp. 205–213.
[111] Rice, J. R. in *Fatigue Crack Propagation, ASTM STP 415*, American Society for Testing and Materials, 1967, pp. 247–309.
[112] McEvily, A. J., Boettner, R. C., and Bond, A. P., *Journal of the Institute of Metals*, JIMEA, Vol. 93, 1965, pp. 481–482.
[113] Broek, D., "The Effect of Intermetallic Particles on Fatigue Crack Propagation in Aluminum Alloys," *Fracture 1969*, Proceedings of the Second International Conference on Fracture, Brighton, England, April 1969.
[114] Pelloux, R., *Transactions*, American Society for Metals, TASEA, Vol. 57, 1964, pp. 511–518.
[115] Glassman, L. H. and McEvily, A. J., "Effect of Constituent Particles on the Notch Sensitivity and Fatigue Crack Propagation Characteristics of Aluminum-Zinc-Magnesium Alloy," NASA Report TD D-328, National Aeronautics and Space Administration, April 1962.

[116] Kraft, J. M., *Transactions*, American Society for Metals, TASEA, Vol. 58, 1965, pp. 691–695.
[117] McClintock, F. A. in *Fracture of Solids*, D. C. Drucker and J. J. Gilman, Eds., Interscience Publishers, New York, 1963, pp. 65–102.
[118] Paris, P. C. and Erdogan, F., *Journal of Basic Engineering, ASME Transactions*, JBAEA, Vol. 85, 1963, pp. 528–534.
[119] Pearson, S., *Nature*, NATUA, Vol. 211, 1966, pp. 1077–1078.
[120] Frost, N. E. and Dixon, J. R., *Nature*, NATUA, Vol. 212, 1966, pp. 1569–1570.
[121] Miller, G. A., *Transactions*, American Society for Metals, TASEA, Vol. 61, 1968, pp. 442–448.
[122] Frost, N. E. and Dixon, J. R., *International Journal of Fracture Mechanics*, IJFMA, Vol. 3, 1967, pp. 301–316.
[123] Gallina, V., Galotto, C., and Omini, M., *International Journal of Fracture Mechanics*, IJFMA, Vol. 3, 1967, pp. 37–44.
[124] Lardner, R. W., *Philosophical Magazine*, PHMAA, Vol. 17, 1968, pp. 71–82.
[125] Bilby, B. A. and Heald, P. T., *Proceedings of the Royal Society*, London, Series A, PRLAA, Vol. A305, 1968, pp. 429–439.
[126] Tomkins, B., *Philosophical Magazine*, PHMAA, Vol. 18, 1968, pp. 1041–1066.
[127] Yokobori, T. and Ichikawa, M., "Effect of Elastic-Plastic Stress Distribution Near the Crack Tip on the Nucleation Theory of Fatigue Crack Propagation," Research Institute for Strength and Fracture Materials, Tohoku University, Sendai, Japan, Vol. 4, 1968, pp. 45–53.
[128] Fleck, W. G. and Anderson, R. B., "A Mechanical Model for Fatigue Crack Propagation," *Fracture 1969*, Proceedings of the Second International Conference on Fracture, Brighton, England, April 1969.
[129] Lui, H. W. and Iino, N., "A Mechanical Model for Fatigue Crack Propagation," *Fracture 1969*, Proceedings of the Second International Conference on Fracture, Brighton, England, April 1969.
[130] Bilby, B. A., Cottrell, A. H., and Swinden, K. H., *Proceedings of the Royal Society*, London, Series A, PRLAA, Vol. A272, 1963, pp. 304–314.
[131] Rice, J. R. and Rosengren, G. F., *Journal of Mechanics and Physics of Solids*, JMPSA, Vol. 16, 1968, pp. 1–12.
[132] Hutchinson, J. W., *Journal of Mechanics and Physics on Solids*, Vol. 16, 1968, p. 13–31.
[133] Hutchinson, J. W., *Journal of Mechanics and Physics of Solids*, JMPSA, Vol. 16, 1968, pp. 337–347.
[134] Dixon, J. R., *International Journal of Fracture Mechanics*, IJFMA, Vol. 1, 1965, pp. 224–243.
[135] Dixon, J. R. and Strannigan, J. S., *Journal of Mechanical Engineering Science*, JMESA, Vol. 7, 1965, pp. 312–317.
[136] Neuber, H., *Journal of Basic Engineering, ASME Transactions*, JBAEA, Vol. 83, 1961, pp. 544–550.
[137] Topper, T. H., Wetzel, R. M., and Morrow, J., *Journal of Materials*, JMLSA, Vol. 4, 1969, pp. 200–209.
[138] Wetzel, R. M., *Journal of Materials*, JMLSA, Vol. 3, 1968, pp. 646–657.
[139] Borik, F., Justusson, W. M., and Zackay, V. F., *Transactions*, American Society for Metals, TASEA, Vol. 56, 1963, pp. 327–338.
[140] Matheny, J. E., "Low Cycle Fatigue Properties of an Ausformed Steel," TAM Report No. 308, Department of Theoretical and Applied Mechanics, University of Illinois, Urbana, Ill., Feb. 1968.
[141] Forsyth, P. J. E., George, R. N., and Ryder, D. A., *Applied Materials Research*, AMRSA, Vol. 3, 1964, pp. 223–228.
[142] Ham, R. K. and Place, T. A., *Journal of Mechanics Physics of Solids*, Vol. 14, 1966, pp. 271–280.
[143] Baker, A. A., *Journal of Materials Science*, JMTSA, Vol. 3, 1968, pp. 412–423.

M. Gell,[1] *G. R. Leverant,*[1] *and C. H. Wells*[1]

The Fatigue Strength of Nickel-Base Superalloys

REFERENCE: Gell, M., Leverant, G. R. and Wells, C. H., **"The Fatigue Strength of Nickel-Base Superalloys,"** *Achievement of High Fatigue Resistance in Metals and Alloys, ASTM STP 467*, American Society for Testing and Materials, 1970, pp. 113–153.

ABSTRACT: The service lives of nickel-base superalloy components in gas turbine engines are frequently limited by their fatigue properties. This paper reviews what is known about the fatigue behavior of nickel-base superalloys and suggests methods for improving their properties. Low-temperature crack initiation occurs preferentially at microstructural defects such as pores and brittle phases in cast materials and at defects such as brittle phases and annealing twin boundaries in wrought materials. The brittle phases may contain inherent cracks or be cracked during working operations or service exposures. Plastic deformation at low temperatures is concentrated in coarse planar bands, and as a result matrix cracking is predominantly transgranular and crystallographic. Techniques are discussed for increasing the low-temperature fatigue properties by minimizing the role of microstructural defects and achieving a more homogeneous distribution of deformation.

At elevated temperatures, intergranular cracking predominates and methods are discussed for improving fatigue properties through grain size control, the use of columnar-grained and single-crystal materials, and the application of oxidation-resistant and fatigue-resistant coatings.

KEY WORDS: fatigue, fatigue strength, nickel alloys, nickel-base superalloys, Stage I fracture, Stage II fracture, crack initiation, crack propagation, microstructure, environment, coatings, temperature, frequency, grain size, single crystal

Nickel-base superalloys are used extensively in the gas turbine industry for applications where good elevated temperature creep and tensile strength are required. Although these alloys possess relatively good oxidation resistance, they must be used with protective coatings in the hotter parts of modern engines. The advanced nickel-base superalloys exhibit unique temperature-dependent strength properties in that their strength is constant or even increases slightly from room temperature up to about 1400 F. These alloys are

[1] Group leader, senior research associate, and assistant director, respectively, Advanced Materials Research and Development Laboratory, Pratt & Whitney Aircraft, Middletown, Conn. 06458.

also unusual for engineering load-carrying materials in that they are used at temperatures in excess of 80 percent of their absolute melting temperature.

In many applications for these materials in gas turbine engines, fatigue damage limits their useful life. Table 1 shows the fatigue strengths (endurance limits) for a number of materials at room temperature [*1–6*].[2] In general, the endurance limits for nickel-base superalloys are a low fraction of the flow stress, much lower than those for relatively pure single-phase materials and lower than those for most other classes of engineering materials, except for some high-strength aluminum alloys and ultrahigh-strength ferrous alloys. While the endurance limit increases somewhat with increasing temperature [*1*], it is still considerably below the yield stress. Thus, in certain applications, the excellent high-temperature static strength of these materials is compromised by poor fatigue properties.

TABLE 1—*Fatigue strength of various materials at room temperature.*

Class of Material	Alloy	0.2% Offset Yield Stress, ksi	Endurance Limit at 10^7 Cycles, ksi	Normalized Endurance Limit	Type of Test	Reference
Nickel-base superalloy..	Inconel X	122	30	0.25	reversed bending	[5]
	Inco 718	145	63	0.43	reversed bending	[2]
	Incoloy 901	128	25	0.20	reversed bending	[3]
	Udimet 700	142	35	0.25	reversed bending	[4]
Aluminum alloy.....	2024-T4	50	24	0.48	reversed bending	[5]
	7075-T6	75	25	0.33	rotating beam	[1]
Titanium alloy.....	Ti-6Al-4V	130	43	0.33	reversed bending	[5]
High-strength ferrous alloy	4340	130	72	0.55	rotating beam	[1]
	18Ni maraging steel (1)	205	100	0.49	roating beam	[1]
	(2)	280	84	0.30	axial	[1]
Pure metals..	Ni	16	15	0.94	rotating beam	[6]
	Al	5	5	1.00	rotating beam	[6]
	Cu	7.5	7	0.93	reversed bending	[6]
	Fe (0.2% Ti)	18	26	1.44	rotating beam	[6]

There has been relatively little research directed at gaining an understanding of the fatigue properties of nickel-base superalloys. However, in recent years, a number of studies have been reported that begin to shed light on the nature

[2] Italic numbers in brackets refer to the list of references at the end of this paper.

of cyclic deformation and fracture in these materials, and these studies will be the subject of this review. Most of this work has been conducted on specimens cycled isothermally. The important and more complicated problem of thermal fatigue, where both the strain and temperature are cycled, has received even less careful attention and therefore will not be treated at length in this paper. Following a brief review of the microstructure of nickel-base superalloys, the fatigue characteristics and mechanisms at low and elevated temperatures will be described, and then the possibilities for improving the fatigue strength will be explored.

Microstructure of Nickel-Base Superalloys

Gamma and Gamma Prime Phases

Nickel-base superalloys, in general, consist of two principal phases: a face centered cubic (fcc) solid-solution-strengthened matrix (γ) and a coherent, ordered, intermetallic submicron precipitate, Fig. 1. Some high-temperature nickel-base alloys such as Hastelloy X are single phase, but these will not be considered in this review. The type and amount of precipitate in the two-phase alloys depend on the particular superalloy composition and heat treatment. The most common precipitate is fcc and of the form A_3B (γ'), where A

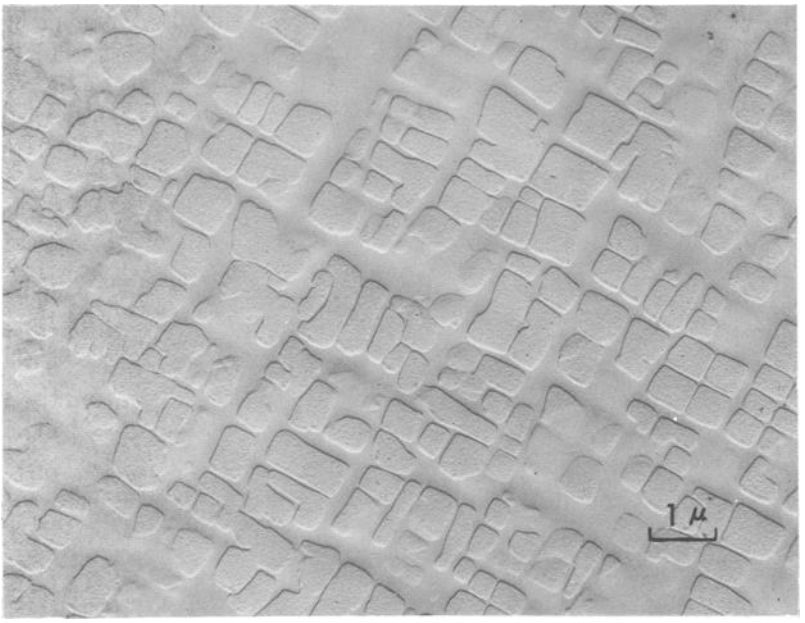

Courtesy E. Gajdusek, Pratt & Whitney Aircraft

FIG. 1—*A typical nickel-base superalloy microstructure consisting of a γ' precipitate in a γ solid-solution matrix.*

is primarily nickel and cobalt, *B* is primarily aluminum and titanium, and where other alloying additions substitute for either *A* or *B*. Gamma prime is found in most high-strength cast alloys, such as MAR-M200, Inconel 713C, In 100, and B-1900, and in some wrought alloys such as Udimet 700 and the Nimonic 80 through Nimonic 115 series of alloys. Some alloys contain more than one precipitate as well as precipitates with crystal structures other than fcc. The volume percent of γ' varies widely, ranging from about 15 percent for some wrought alloys to greater than 50 percent for cast alloys [7]. Some typical superalloy compositions are given in Table 2.

TABLE 2—*Compositions of several nickel-base superalloys, weight percent.*[a]

Alloy	Al	Ti	Cr	Co	W	Mo	Fe	Cb	Ta	B	Zr	C	Ni
Nimonic 80A	1.4	2.4	20	...	...	...	...	...	...	...	...	0.08	balance
Nimonic 90	1.4	2.4	20	17	...	...	...	...	...	...	...	0.08	balance
Nimonic 115	4.9	3.9	15	15	...	3.5	...	...	...	...	...	0.15	balance
Inconel 718	0.6	0.9	19	...	...	3.0	18.0	[b]	[b]	...	...	0.10	balance
Incoloy 901	...	2.6	12.5	...	...	6.0	34.0	...	...	0.015	...	0.10	balance
Udimet 700	4.3	3.3	15	18.5	...	5.0	...	...	...	0.03	...	0.07	balance
MAR-M200	5.0	2.0	9	10	12.5	...	...	1.0	...	0.015	0.05	0.15	balance
B-1900	6.0	1.0	8	10	...	6.0	...	...	4.3	0.015	0.07	0.11	balance

[a] Source: *Nickel-Base Superalloys*, International Nickel Co., Inc., 1964.
[b] Cb + Ta 5.0.

Minor Phases

In addition to the γ and γ' phases, most superalloys contain a number of other phases, several of which are potentially detrimental to fatigue strength. Carbon is added to superalloys to form carbides at grain boundaries and thereby enhance creep rupture properties [*8*]. The carbides formed include MC, M_7C_3, $M_{23}C_6$, and M_6C, where *M*, the metal atom, is primarily chromium in M_7C_3 and $M_{23}C_6$, and is usually titanium, tungsten, columbium, molybdenum, and tantalum in MC and M_6C; cobalt and nickel are also found in M_6C [*9*]. Impurities in superalloy melts result in the formation of very small amounts of titanium nitrides [*10*] and sulfides [*11*], and the deliberate addition of boron to improve creep rupture properties can lead to boride formation [*12*].

Effect of Brittle Phases and Defects on Crack Initiation

The initiation of fatigue cracks in nickel-base superalloys is almost always associated with defects in the microstructure, such as brittle phases, casting pores, coherent annealing twin boundaries, and, at elevated temperatures, grain boundaries. Possible exceptions to this statement are the slipband

cracking of wrought, recrystallized material and carbide-free single crystals oriented for single slip in low-cycle fatigue near room temperature (see the sections on Low-Cycle Fatigue of Polycrystals and Fatigue Behavior of Single Crystals). In general the cast alloys fail by propagation or linkup of cracks from brittle inclusions or pores at low temperatures and along grain boundaries at high temperatures. Linking of cracks between multiple initiation sites is favored by high strain ranges, whereas at low strain ranges a single defect dominates the fracture process. The same generalizations apply to wrought alloys, with the exception noted above, and with the addition of coherent twin boundaries as a major source of cracking at long lives and low temperatures. With this general background, let us examine the role of specific types of defects in detail. Except where specified, discussion will be concerned with room temperature properties.

Preexisting Cracks in Brittle Phases

The brittle minor phases in the nickel-base superalloys, notably carbides, nitrides, sulfides, and borides, may become cracked at some point during the processing history of the material. Cracks in MC carbides have been observed in the as-cast microstructure of directionally solidified MAR-M200 [*13*] and Udimet 700.[3] The cracks always run parallel to the long dimension of the carbide (Fig. 2*a*) and can closely follow the contour of an irregularly shaped particle (Fig. 2*b*). Since these carbides are the first product of solidification upon cooling a melt, and differential contraction between these phases and the solid matrix places the particles in compression, the cracks must form prior to the solidification of the matrix. It has been suggested [*13*] that the cracks result from sharp compositional gradients in the carbide during growth from the melt, and in Udimet 700 the cracks have now been found to occur at the interface between an MC carbide and another phase believed to be a carbosulfide.[3]

Owing to the residual compressive stress, the cracks in the carbides of the directionally solidified materials cannot be revealed by mechanical polishing. It has been found by replicating the surface of a mechanically polished specimen under increasing tensile stress that these cracks commence to open up, and slip is generated at the crack tips at about one fifth of the yield stress [*13*]. It is interesting to note that the 10^7 cycle endurance limit occurs at maximum stresses of about the same value. At higher stress levels, the precracked carbides are the sites of slip and crack initiation (Fig. 3) and the fatigue life is a strong function of carbide size at room temperature and at 1400 F. For example, at room temperature the material containing large

[3] Gell, M., Leverant, G. R., and Organ, F. E., Advanced Materials Research and Development Laboratory, Pratt & Whitney Aircraft, Middletown, Conn., unpublished research. Note that all references to unpublished research are for work done at this laboratory.

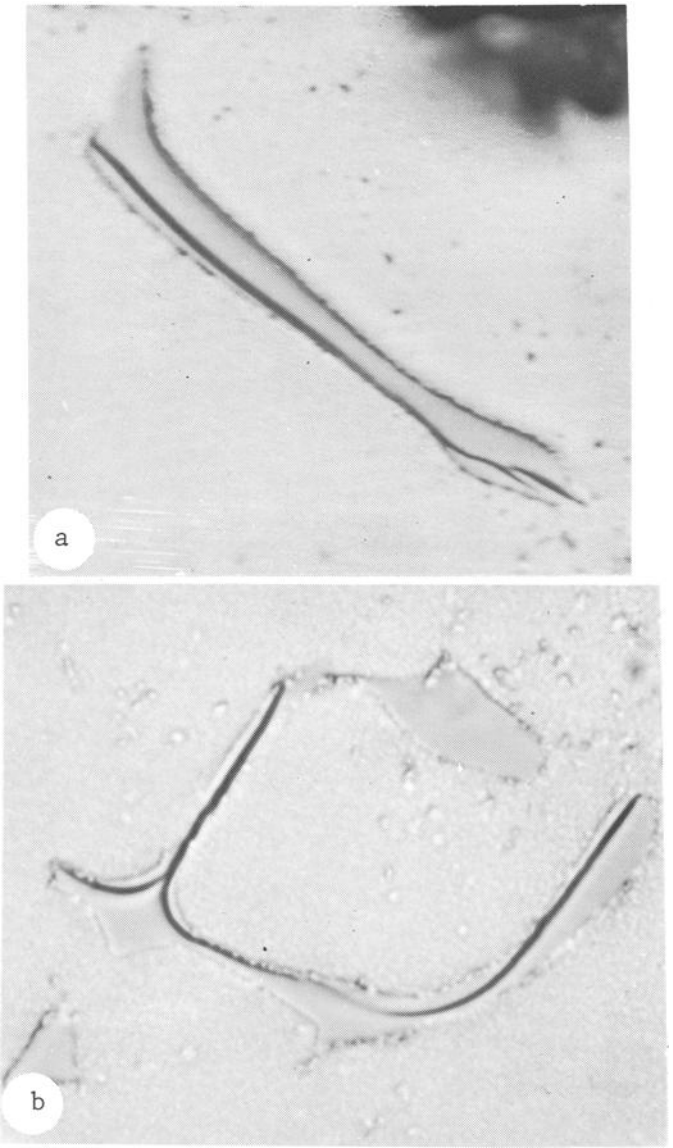

FIG. 2—*MC carbides containing cracks in as-cast single crystals of MAR-M200 (X2000); after Gell and Leverant* [13].

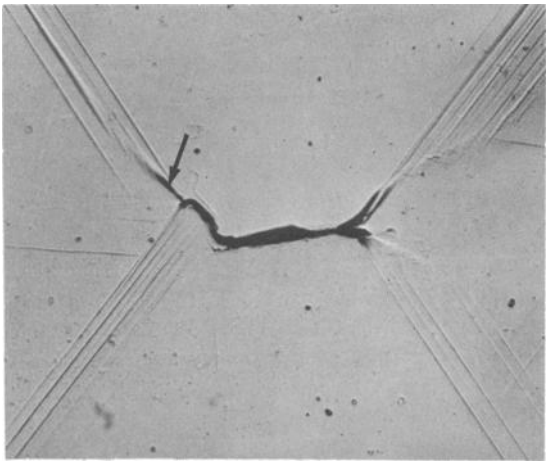

FIG. 3—*Preferential matrix slip and crack initiation* (arrow) *at the tips of a precracked carbide in a single crystal of MAR-M200; stress axis vertical (X200); after Gell and Leverant* [13].

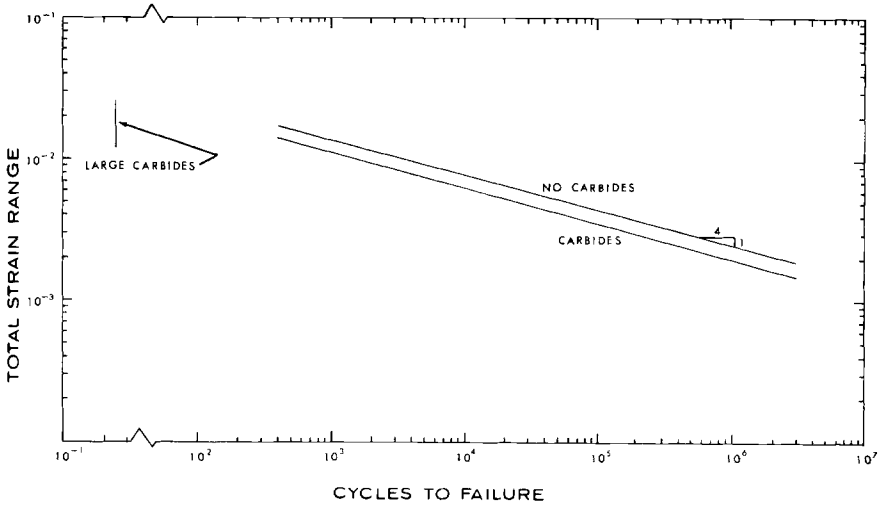

FIG. 4—*The effect of carbide size on the fatigue life of directionally solidified MAR-M200 at room temperature.*

carbides (0.25 to 0.30 mm) fails upon loading above the proportional limit, whereas materials having somewhat smaller carbides (0.12 to 0.14 mm) exhibit much improved fatigue lives (Fig. 4). Complete removal of the MC carbides further improves the fatigue life by a factor of 2.

Deformation-Induced Cracking

Initially sound particles can be fractured by impingement of slipbands [*14–16*] or by a sufficiently large tensile strain in the matrix, similar to the manner of fiber fracture in a composite. Under these circumstances, the crack in an elongated particle always forms across the short dimension and so may be distinguished from preexisting cracks in directionally solidified alloys (see previous section on Preexisting Cracks). Carbide fracture has also been observed in glass-bead blasted surfaces, presumably from impact [*4*]. Certain machining operations, for example, grinding and turning, have been found to produce fractured particles at the surface. The residual compressive stress associated with such operations may offset any harmful effects by (*a*) preventing the particle fractures from opening up in tension or (*b*) inhibiting the shearing displacement along the fractures through surface friction. Any relative motion of the two halves of a fractured particle will propagate one or more slipbands from the crack tip, which are the precursors to a Stage I fatigue crack. The only effective way of suppressing this process at lower temperatures is to achieve a surface compressive stress, for the particle cracks are sharp and necessarily enforce plastic relaxation in the matrix. Dispersal of the shear displacements by means of cross slip is exceedingly difficult because deformation in these $\gamma + \gamma'$ alloys proceeds by the motion of superlattice pairs [*17*].

Some amelioration of the effect of brittle phases is obtained at high temperature. The chief benefit is probably obtained from oxidation of the particles at the free surface, which may reduce the stress concentration at the crack tips, with perhaps some tendency towards slip dispersal as a consequence of thermally activated cross slip. The endurance limit, which may be taken as an indication of the severity of defects, increases from 0.2 to 0.5 of the flow stress between room temperature and 1400 F [*13*, *18*]. Another possibility is rupture of the particle matrix interface at locations of slip impingement, thus avoiding fracture of the particle. The decreasing strength of such interfaces with increasing temperature is an element in the transition to intergranular cracking (see section on Grain Size and Grain Boundary Structure). While we have observed instances of carbide-matrix interfacial rupture, mainly in elevated temperature low-cycle fatigue, it has not been identified as the critical mechanism of transgranular crack initiation.

Porosity

Gas or shrinkage porosity may be of equal importance to brittle phases in initiating fatigue cracks in cast superalloys (Fig. 5) and is the chief source of cracking in carbide-free single cyrstals. Surface-connected pores are more damaging than internal pores; this could be the result of the greater stress

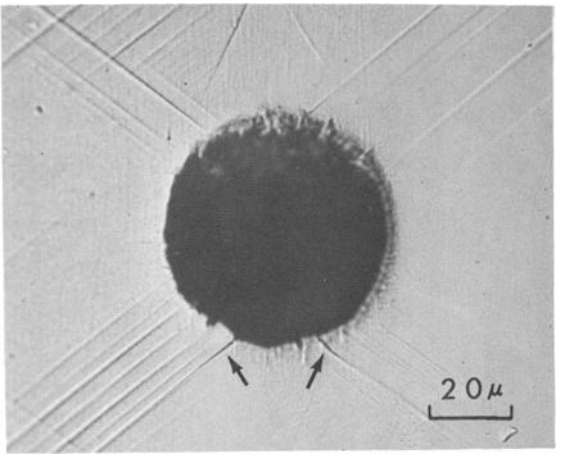

FIG. 5—*Preferential slip and crack initiation* (arrows) *at the periphery of a surface pore in single crystal MAR-M200.*

concentration of the surface pore or the effect of the environment. Large pores are much more damaging than small ones, primarily because the stress decays more slowly with distance from a large pore; consequently the length of the slipband emanating from the pore and the amplitude of shear displacement are greater, resulting in more rapid crack initiation and propagation. There may be in addition a true size effect in these materials such that defects smaller than some critical dimension are not capable of initiating slip or cracking [*19*].

Coherent Annealing Twin Boundaries

Coherent twin boundaries are significant sites of crack initiation in wrought alloys at room temperature [*4*] and in low-cycle fatigue in the temperature range below the transition from slipband to grain boundary cracking [*20*] (Fig. 6). In the case of wrought Udimet 700, surface twin boundary cracking in low-cycle fatigue was prominent from 600 to 1000 F. Internal twin boundary cracks were observed at 1200 F, but none at 1300 F where the cracking was predominantly intergranular. The absence of γ' precipitation across the twin boundary may explain the rapid falloff of twin boundary strength with temperature that is suggested by the preceding results.

Low-Temperature Fatigue

In this section we review the cyclic deformation and fracture behavior of nickel-base superalloys below the creep range. Much of the discussion deals

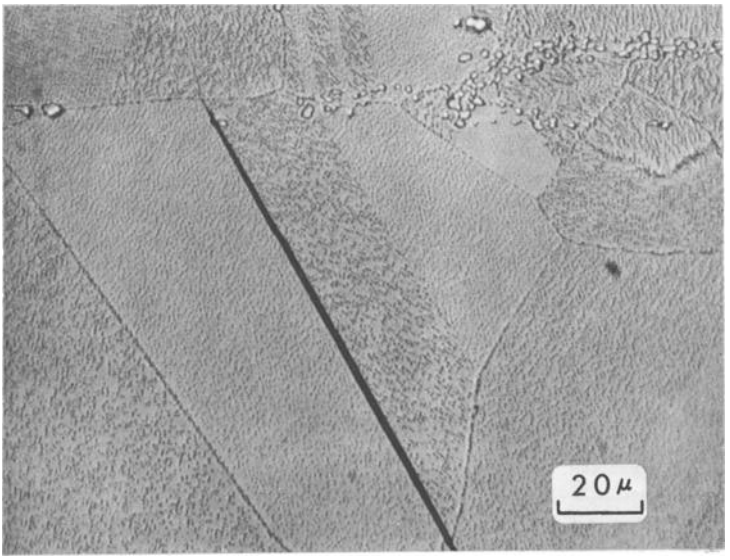

FIG. 6—*Cracking along a coherent annealing twin boundary in the interior of a low-cycle fatigue specimen of Udimet 700 tested at 1200F; stress axis horizontal; after Wells and Sullivan.*[6]

with wrought, polycrystalline Udimet 700 [*4, 20, 21*] and single crystal MAR-M200 [*13, 22*]. These are the materials which have been studied most extensively to date and their properties are believed to be typical of those to be found in other $\gamma + \gamma'$ nickel-base superalloys.

Deformation at low temperatures in these materials is characterized by the shear of both γ and γ' phases by $a/2\ \langle 110 \rangle$ superlattice dislocation pairs [*17*], where a is the lattice parameter (Fig. 7*a*). Since cross slip of the superlattice pairs at low temperatures is difficult, deformation in all forms of these materials proceeds by the generation of coarse, planar bands containing a high density of dislocations (Figs. 7 and 9). No indication of any difference between bulk and surface slip behavior has been revealed by comparing surface slip offsets with internal plastic deformation revealed by a slipband etching technique [*23*].

Low-Cycle Fatigue of Polycrystals

In low-cycle fatigue of wrought Udimet 700 at room temperature [*21*], there is an initial brief period of cyclic strain hardening and this is followed by cyclic strain softening over the remainder of the life of a specimen (Fig. 8). The strain hardening is accompanied by dispersal of slip onto neighboring planes and the softening implies increasing concentration of cyclic slip in the active bands. Figures 9*a* and *b* show that there is a high degree of reversi-

bility of slip in certain bands in the first cycle. The slip offsets are generally greatest at the center of surface grains, and cracking is observed to initiate there. Slipband or Stage I cracking (Fig. 9*c*) develops gradually, but is always observed at a low fraction of life (usually 5 to 10 percent). At large strains, characterized by strong intersecting slip, cracking may be very segmented along short lengths of slip traces. At small strains the slipbands and subsequent microcracks extend completely across the grains with little deviation. Most of the life of a specimen is occupied by microcrack extension and

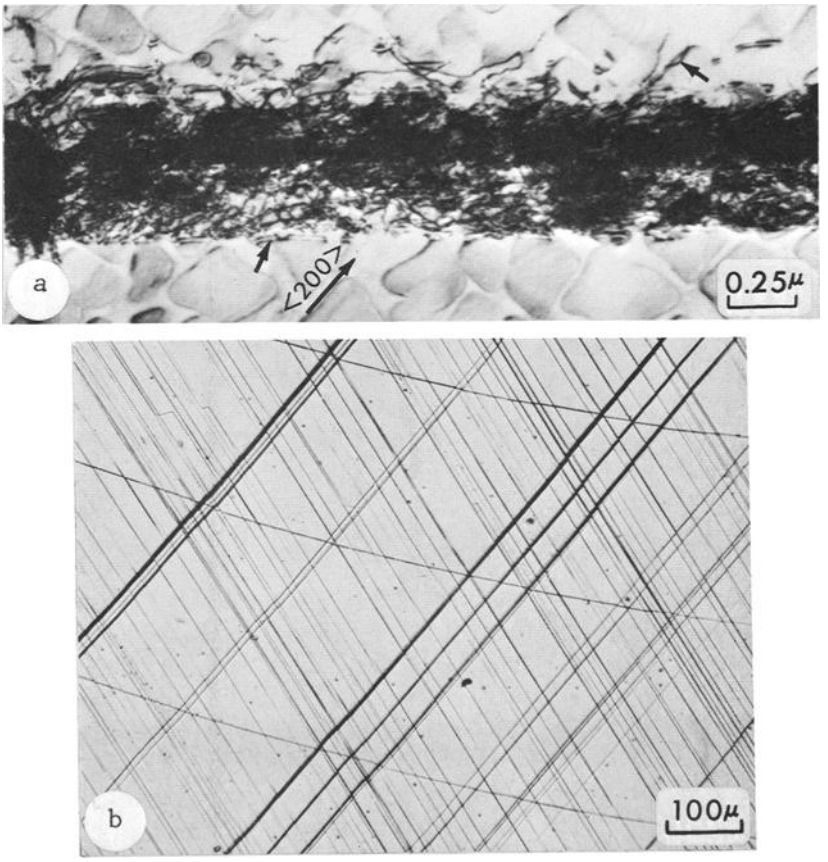

(*a*) Transmission electron micrograph showing dense dislocation structure of bands and superlattice dislocations (*arrows*) generated during low-cycle fatigue; after Gell and Leverant [*32*].

(*b*) Planar slip offsets on the surface of a carbide-free single crystal.

FIG. 7—*The planar character of room temperature cyclic plastic deformation in single crystals of MAR-M200.*

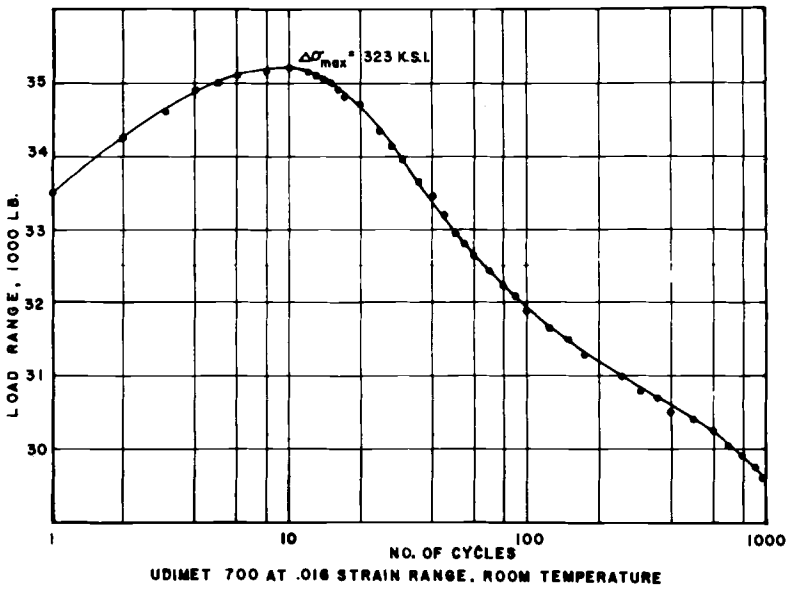

FIG. 8—*The variation of load range with cycling for a low-cycle fatigue specimen of Udimet 700 tested at room temperature; after Wells and Sullivan* [21].

linkup, with linking governing the lifetime at high strain range. Figure 10 shows an example of the progressive linking of surface cracks, which propagate into the specimen volume and then form a Stage II macrocrack. The area of crystallographic cracking (Stage I) is limited to the outermost layer of grains at high strain, but may be very extensive at low amplitudes. The transition to Stage II is marked by ductile striations and the absence of crystallographic facets. The tensile overload region of the fracture surface is a mixture of ductile rupture and smooth grain boundary surfaces. The grain boundaries are believed to be easy paths for crack propagation at high strain rates because of the presence of brittle carbide and boride particles in the boundaries.

At temperatures between 200 and 1200 F, cyclic strain aging occurs in wrought Udimet 700 and is accompanied by simultaneous slip dispersal and rapid strain hardening [*20*]. Crack initiation and propagation between 600 and 1000 F occur predominantly at coherent twin boundaries both at the surface and in the interior, and crystallographic facets are observed on the fracture surface in the tensile overload region. In a cast alloy [*24*] where there are no coherent twin boundaries, cracking occurs along slipbands at 1200 F. Presumably, carbide precipitation in active slipbands in the wrought material is responsible for hardening and for the erratic variation of cyclic life with temperature (Fig. 11). The size of the fatigue zone is reduced and

the amount of crystallographic cracking during tensile overload is increased by the aging that accompanies cycling in tests at 200 F and above. It is interesting to note that a small amount of aging is beneficial to life, while a large amount is detrimental.

High-Cycle Fatigue of Polycrystals

As was discussed in the section on Effect of Brittle Phases and Defects on Crack Initiation, high-cycle fatigue generally involves the growth of a crack from a single dominant defect in both wrought and cast materials. In the former case, coherent annealing twin boundaries are the chief sites of crack initiation [*4*]. The cracks when first observed in cantilever bend specimens are a finite size, that is about 1/10 to 1/4 of a grain diameter. It has been reasoned that these cracks must grow at a rapid rate up to the point at which they are first observed, because careful observations earlier in life showed no cracking and extrapolation of subsequent crack growth data indicates the crack would have to exist prior to cycling. Once detected, the rate of growth of these surface *microcracks* is independent of crack length and varies with the fourth power of the total strain range.

This work [*4*] also demonstrated the large influence of mean stress on the rate of surface microcrack extension. For example, the propagation rate in an electropolished specimen cycled between zero and a maximum value in compression was a hundred times smaller than that in a specimen cycled about zero mean stress through the same stress range, and the ratio of crack propagation rates between an electropolished specimen and a glass-bead blasted specimen having a surface residual compressive stress was of the order of 10^4 (Fig. 12). In all cases the cracks initiated at the surface along twin boundaries which were oriented for maximum in-plane shear.

There was little difference in the number of cycles to first detection of the coherent twin boundary cracks in the glass-bead blasted and electropolished specimens. In addition to the reduction in the rate of surface crack propagation by glass-bead blasting, there also was a doubling of the endurance limit at 10^7 cycles. On the other hand, a cold-worked specimen with no long-range residual stress did not show an improvement in endurance limit. This indicates that the improvement in fatigue properties from glass-bead blasting results from the residual stress rather than from any effect of cold work.

The rate of propagation of a *macroscopic* fatigue crack in polycrystalline Udimet 700 at room temperature obeys a $\Delta K^{3.4}$ law (Fig. 13), where ΔK, the change in stress intensity factor, is proportional to the change in stress range and the square root of the crack length.[4] Similar behavior has been found for other alloys [*25*]. The macroscopic path of the crack in a pulsating tension

[4] Hopkins, S. W. and Landes, J. D., unpublished research.

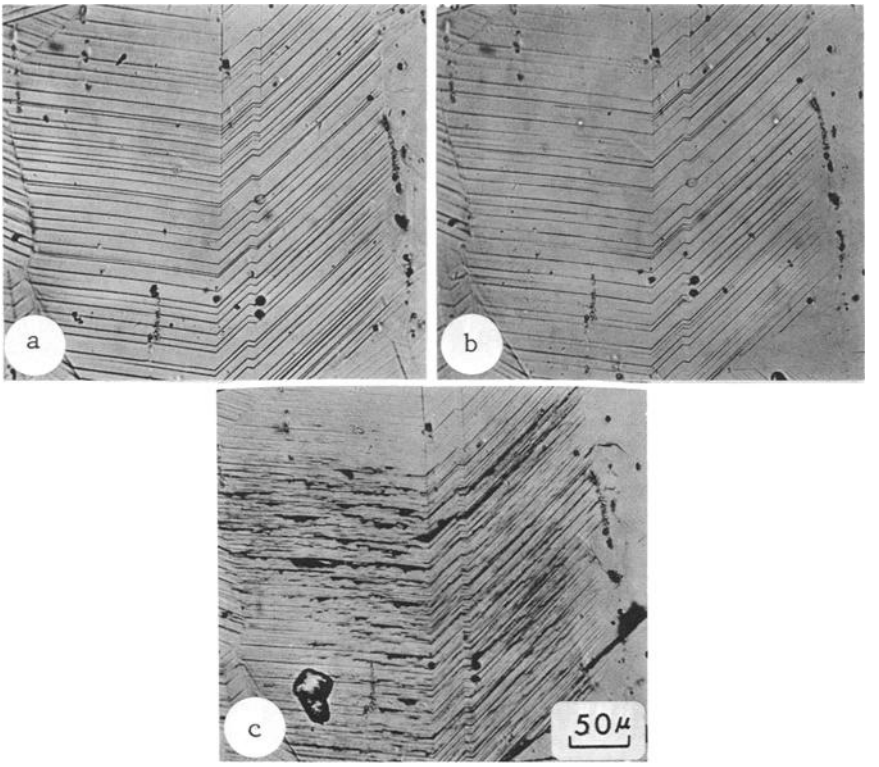

(*a*) ½ cycle.
(*b*) 1 cycle.
(*c*) 764 cycles; N_f = 765 cycles.

FIG. 9—*The development of surface slip and cracking during low-cycle fatigue of Udimet 700 at room temperature; stress axis is vertical; extrusion-like markings are caused by penetration of replicating material into cracks; after Wells and Sullivan* [21].

fatigue test follows approximately the plane of maximum normal stress. However, at low values of stress intensity, individual microcrack segments are crystallographic and follow coarse, planar slipbands (Stage I cracking). At high stress intensity, slip lines and crack surfaces are distorted and ductile striations are observed on the fracture surfaces, indicating crack propagation in the Stage II mode. The variation of stress intensity apparently alters only the degree of strain hardening and not the crack propagation law. In torsion,[5] the crack shows very little tendency toward branching and closely follows a direction of maximum resolved shear stress. Possibly because of a reduction in branching, the propagation rate in torsion is considerably greater than in

[5] Wells, C. H. and Hopkins, S. W., unpublished research.

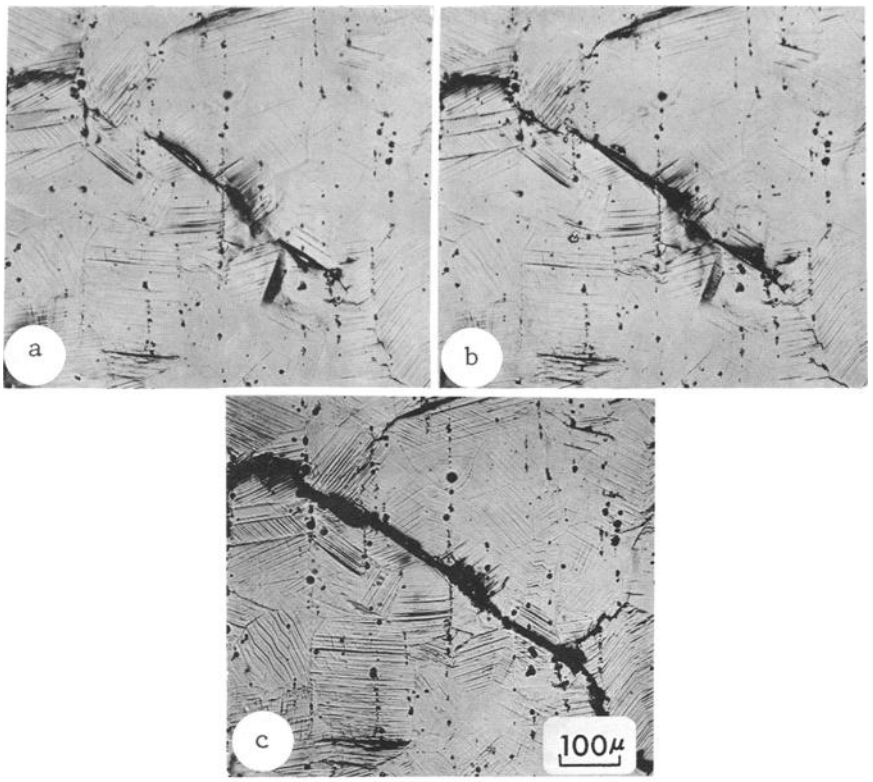

(*a*) 290 cycles.
(*b*) 400 cycles.
(*c*) 764 cycles; N_f = 765 cycles.

FIG. 10—*Linkup of cracks on the surface of a low-cycle fatigue specimen of Udimet 700 tested at room temperature; stress axis vertical; after Wells and Sullivan* [21].

tension when the maximum resolved shear stress is the same in torsion and tension.

Fatigue Behavior of Single Crystals

The cyclic deformation of single crystals results in relatively more dispersal of slip than in the wrought alloy and no apparent reversibility of the displacement. Figure 7*b* shows the planar surface slip offsets early in the life of a low-cycle fatigue specimen of MAR-M200 and Figure 7*a* reveals the high density of dislocation loops and dipoles concentrated in these bands. Crack initiation in ⟨100⟩ oriented crystals occurs at MC carbides or micropores, but slipband initiation has been observed in carbide-free crystals oriented for single slip. There is some linking of individual slipband cracks; however,

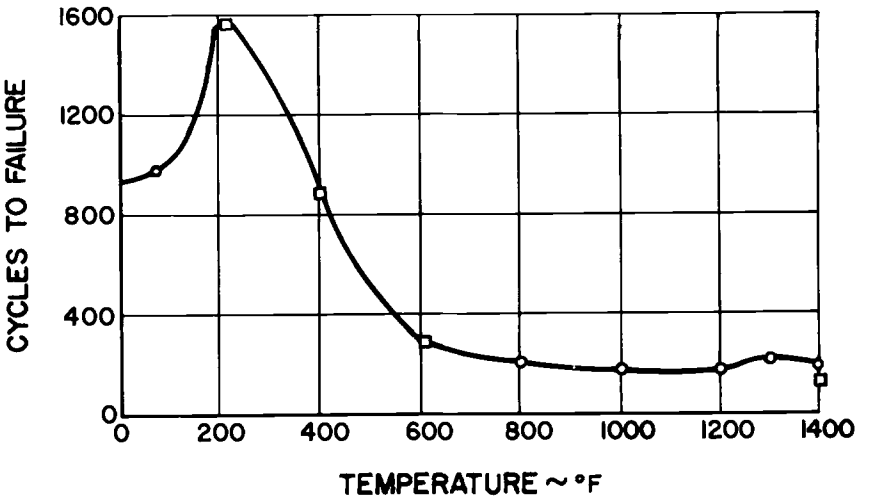

FIG. 11—*Variation of low-cycle fatigue life of Udimet 700 with temperature at a total strain range of 0.016; after Wells and Sullivan* [20].

the rate-controlling mechanism of fracture is the propagation of a single crack over a large fraction of the specimen cross section, resulting in large Stage I facets which have been identified as {111} planes [*13*, *22*]. There is normally no transition to Stage II cracking. The Stage I facets in high-cycle fatigue are highly reflective and contain distinct fracture steps and river lines (Fig. 14*a*). Those in low-cycle fatigue are less reflective, and the most distinct features are equiaxed dimples less than 1 μm in size (Fig. 14*b*). In order to explain the features on Stage I fractures and the absence of evidence for rubbing, it has been proposed [*13*] that cyclic slip activity either lowers the cohesive energy of the slipband or that there is a local enhancement of the normal stress across the band by the accumulation of dislocation dipoles and multipoles [*26*]. Final separation then occurs under the influence of the local normal stress at the crack tip.

Comparison of Fatigue Behavior of Single Crystals and Polycrystals at Room Temperature

The mechanism of Stage I cracking has not been positively identified, but it is suggested that the key to understanding its behavior is the reversibility of slip. Two limiting points of view are possible: If slip is completely reversible, no defect accumulation, strain hardening, or degradation of the cohesive strength would be expected, and crack initiation would have to be governed by oxidation of surface slip offsets by the environment [*27*]. On the other hand, if slip is irreversible, then the possibility exists for strain

hardening, dispersal of slip activity onto neighboring planes, defect accumulation, and a decrease in the fracture energy of slip planes. There is evidence that suggests the behavior of polycrystals is closer to the former case and single crystals to the latter.

In the polycrystalline material, direct observation of reversibility of slip-band displacements has been made. Reversibility of strain hardening is supported by measurements of the Bauschinger effect: a simple analogy between the deformation of a blocked slipband and the extension of a parallel arrangement of spring and friction block provides a very accurate prediction of the hysteresis loop shape from the initial stress-strain curve [*28*]. The displacement of a slipband is equivalent to that of a shear crack in an elastic

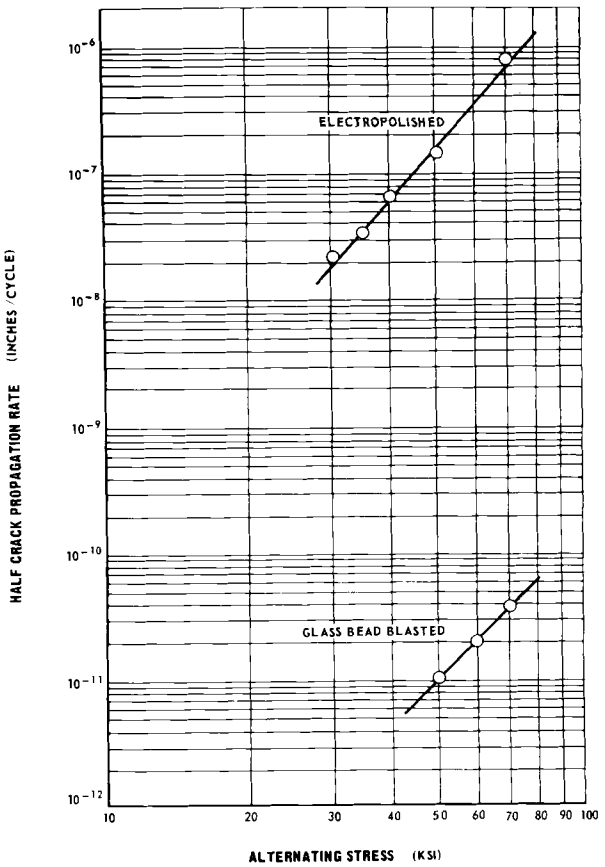

FIG. 12--*Surface crack growth rate as a function of alternating stress amplitude in Udimet 700 at room temperature for electropolished and glass-bead blasted specimens; after Burck et al* [4].

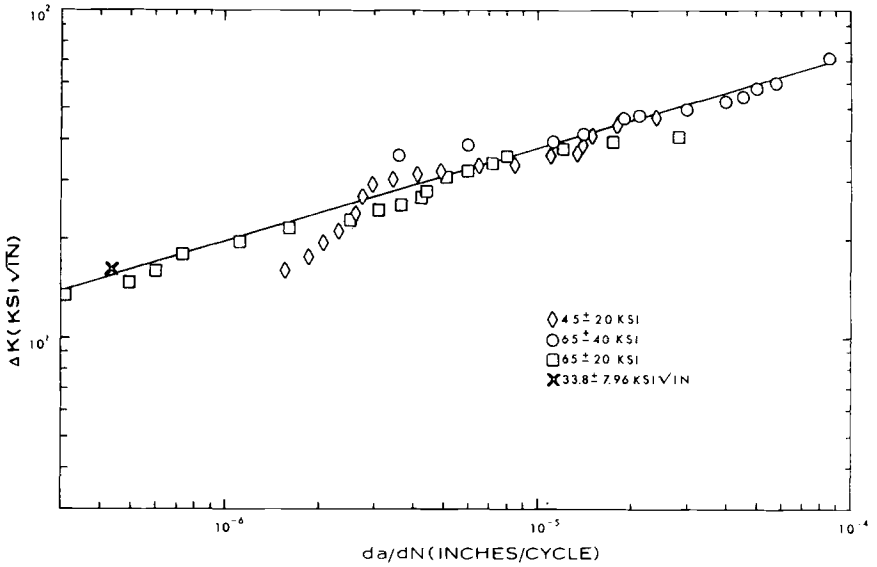

FIG. 13—*The effect of stress intensity factor range on the crack growth rate in Udimet 700 at room temperature; after Hopkins and Landes.*[4]

body with friction on the crack surfaces; therefore these displacements should be proportional to the total strain, and it is found that the cyclic life correlates with total strain range [*21*].

It has also been shown theoretically that under the assumptions of planar slip and impenetrable grain boundaries the stress-strain curve should be independent of grain size [*29*], and this has been found to be the case in limited testing (Table 3). In this model, the range of slip displacement is proportional to the rate of Stage I crack initiation and, for a given total strain range, should be proportional to grain diameter. Table 3 shows that a reduction in grain size significantly improves the low-cycle fatigue life of Udimet 700. While the effects of grain size and total strain range on the range of slipband displacement should be identical, it has been found that changes in total strain range have a much larger effect on fatigue life than changes in grain size. This can be explained by the fact that much of the specimen life is occupied in microcrack linkup and as the grain size is reduced, the density of microcracks increases and linking has to occur over relatively shorter distances.

In support of the hypothesis of slip reversibility in the polycrystalline material, internal crack initiation and crystallographic facets in the tensile overload stage are never observed at room temperature. In contrast, cyclic strain aging of this material in the temperature range of 200 to 1200 F (clearly

TABLE 3—*Effect of grain size on the stress-strain curve and fatigue life of wrought Udimet 700* [29].

Average Linear Intercept, mm	Flow Stress, ksi			Cycles to Failure at 0.016 Strain Range
	0.02% Offset	0.2% Offset	1.0% Offset	
0.095.....	122	142	153	970
0.043.....	125	145	155	2470

an example of irreversible slip) results in internal cracking and facets on the overload fracture surface.

Investigations on single crystals suggest a smaller degree of reversibility of slip[3] [*13*] than in polycrystals. At the same plastic strain range, there is greater dispersal of slip, the amount of cyclic strain softening is negligible, and there is a much smaller Bauschinger effect. This difference is reasonable in the light of the absence of strong obstacles to slip in the single crystal. The features on the Stage I fracture surfaces (Fig. 14) and the observation of tensile fracture along slipbands formed by cyclic prestrain would suggest glide band decohesion (see section on Fatigue Behavior of Single Crystals).

High-Temperature Fatigue

With increasing temperature, additional factors must be considered in describing the fatigue behavior of nickel-base superalloys. These include the effect of the gaseous environment and the effects of mean stress, time, cyclic frequency, and temperature on thermally activated deformation processes and the tendency to intergranular cracking. As was true of the description of low-temperature fatigue, much of our knowledge of the elevated temperature behavior of nickel-base superalloys comes from studies of wrought, polycrystalline Udimet 700 [*30*, *31*] and single crystal MAR-M200 [*18*, *32*]. In the following discussion, the mode of crack initiation and propagation will be considered to be intergranular or transgranular. The mode of transgranular cracking will be further described as crystallographic (Stage I) or noncrystallographic (Stage II).

Effect of Temperature

Numerous investigators [*18*, *20*, *33–38*] have found in many different superalloys that intergranular crack initiation and propagation occur much more readily with increasing temperature. The transition temperature from transgranular to intergranular surface crack initiation is a function of the particular alloy composition, heat treatment, test frequency, and stress history, and falls approximately in the range 900 to 1400 F.

Wrought Udimet 700 has been studied most extensively. Some indication of surface intergranular crack initiation in isothermal low-cycle fatigue was found at 1200 F [*20*], while all crack initiation at the surface was intergranular at 1400 F [*30*]. At the latter temperature, the intergranular cracks propagated at the most one grain diameter into the sample before a transition to transgranular cracking occurred. At 1700 F, where time-dependent damage (creep) is more extensive, crack initiation (Fig. 15) and propagation are predominantly intergranular [*31*]. In thermal fatigue tests of many different

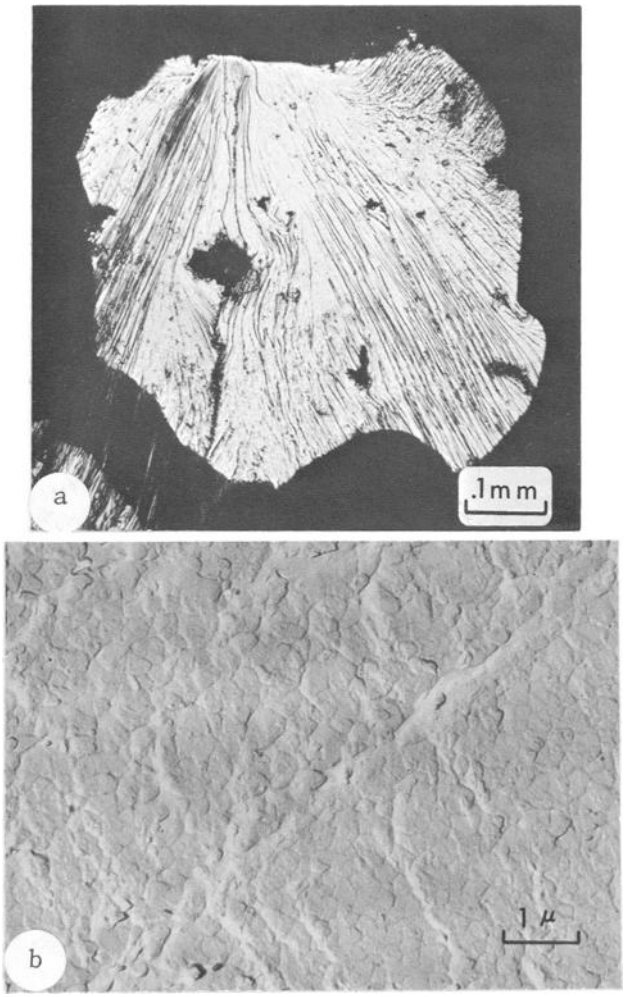

FIG. 14—*Stage I facets on the fracture surfaces of directionally solidified MAR-M200 specimens tested at room temperature:* (a) *high-cycle fatigue* (b) *low-cycle fatigue; after Gell and Leverant* [13, 22].

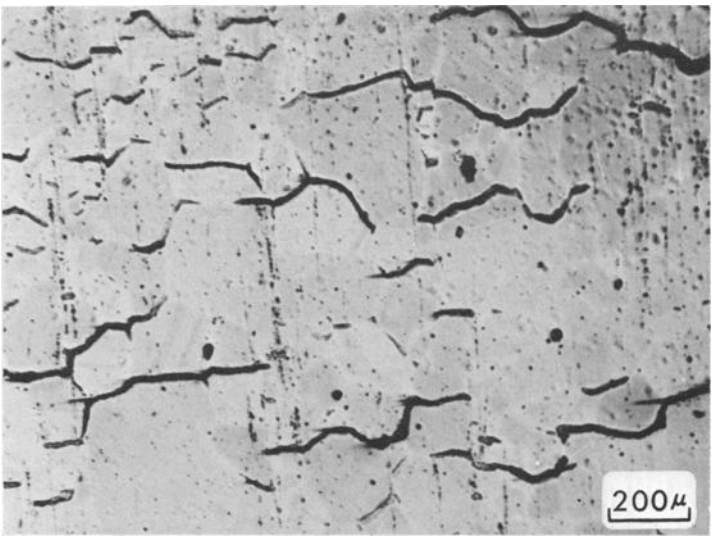

FIG. 15—*Intergranular cracking on the surface of a specimen cycled at 1700 F; stress axis vertical. Specimen surface was etched following removal of oxide scale by mechanical polishing. After Wells and Sullivan* [31].

superalloy compositions [*33–35*, *37*, *38*], the transition to primarily intergranular cracking has been found to occur at peak temperatures of 1500 to 1600 F in reasonable agreement with the isothermal low-cycle tests on Udimet 700.

The mode of fatigue cracking in single-crystal and columnar-grained materials is also a function of temperature. In low-cycle fatigue tests of MAR-M200 at 1400 F, deformation is concentrated in [111] slipbands (Fig. 16*a*). Although the dislocation density in the bands is lower than at room temperature (Fig. 7*a*), cracking is in the Stage I mode. As the temperature is increased to 1700 F, deformation becomes more homogeneous (Fig. 16*b*) and irreversible, and noncrystallographic cracking occurs on a surface normal to the stress axis (Stage II mode, Fig. 17). Cracking at both temperatures originates at carbides or micropores.

Effect of Grain Size and Grain Boundary Structure

Under conditions where intergranular cracking occurs, the grain size has an effect on fatigue life. The general observation has been that thermal fatigue life decreases with increasing grain size [*33*, *35*, *37*], although isothermal low-cycle fatigue tests on Udimet 700 at 1400 F[6] have shown the opposite result. The problem that arises in assessing the significance of these experiments is that the different heat treatments required to produce various grain sizes

[6] Wells, C. H. and Sullivan, C. P., unpublished research.

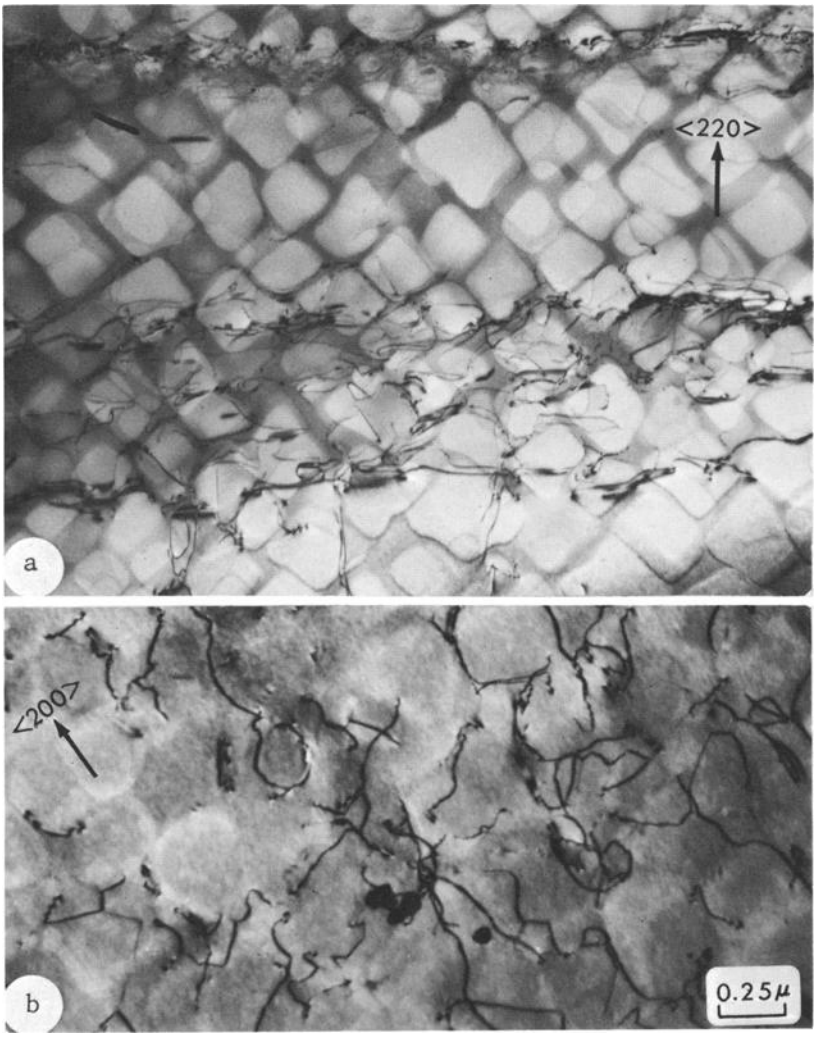

FIG. 16—*Dislocation structures typical of single-crystal MAR-M200 specimens cycled to failure at a high strain range at* (a) *1400 F and* (b) *1700 F; after Gell and Leverant* [32].

simultaneously change the structure of the grain boundary and its immediate vicinity, which could affect resistance to both crack initiation and propagation. For example, in Nimonic 80A [*8*], Cr_7C_3 is found in the grain boundaries of specimens solutionized at 1975 F and aged at 1290 F to produce small grains (ASTM grain sizes 4 and 5) but is not found in the grain boundaries after a 2190 F solutionizing and the same aging treatment to produce large grains. An attempt was made to separate the effects of grain size from grain

boundary structure by thermal-fatigue testing a Ni-20Cr binary alloy [*8*], however, the carbon content of the alloy was sufficient to produce carbide precipitation in grain boundaries [*39*], which precludes an unambiguous result.

As is obvious from the above discussion, additional research is needed to separate the effect of grain size from concomitant changes in grain boundary structure. It is also necessary to distinguish the separate effects of grain size on crack initiation, propagation, and linkup; a possible framework for accomplishing this is considered in the section on discussion of Intergranular Cracking.

Certain elements such as carbon, boron, and zirconium are known to have significant effects on creep rupture behavior of superalloys through their

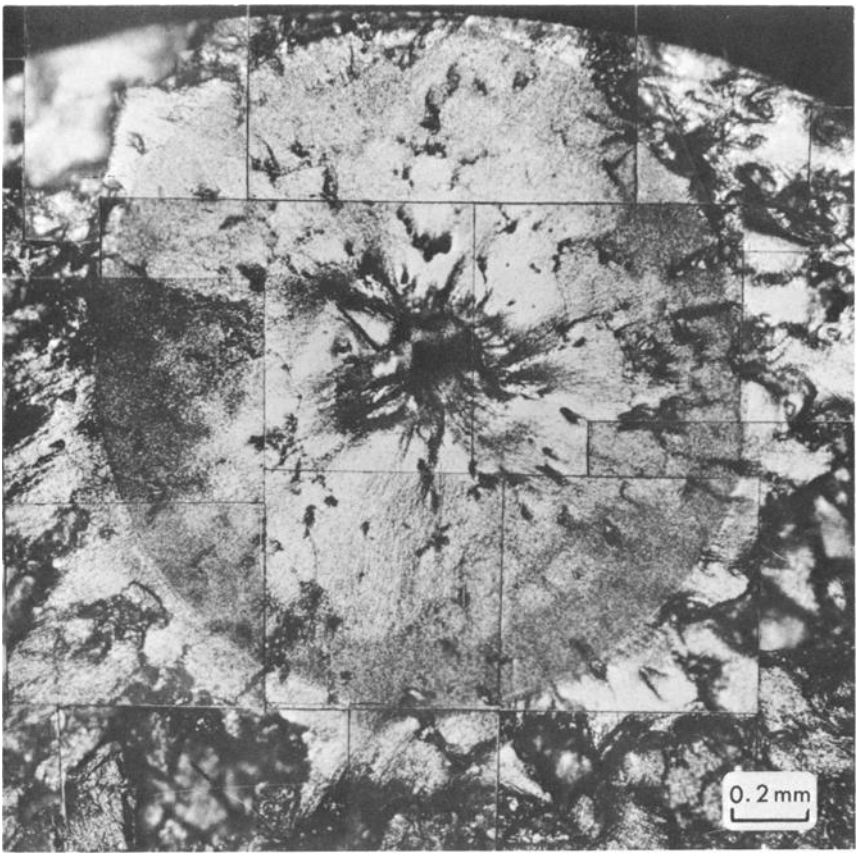

FIG. 17—*Montage of an internally initiated Stage II crack responsible for specimen failure at a low strain range at 1700 F; after Gell and Leverant* [32].

influence on grain boundary properties [*40*, *41*]. These elements were also found to increase individually the resistance to thermal fatigue crack initiation in a nominal Nimonic 80A composition [*33*]. The compositions which exhibited the best resistance to thermal fatigue crack initiation had the best elevated temperature tensile ductility. The source of crack initiation at grain boundaries has not been as carefully documented in elevated temperature fatigue tests as it has been in creep [*42*, *43*]. It is likely that the formation of cavities at the interface between the matrix and carbides or other hard particles that occurs during creep is also present during elevated temperature fatigue.

Directional Solidification

Columnar-grained and single-crystal forms of cast nickel-base superalloys offer a distinct advantage over polycrystalline materials in elevated temperature fatigue through elimination of intergranular cracking [*18*]. For example, columnar-grained and single-crystal MAR-M200 have low-cycle fatigue lives at 1400 and 1700 F that are 10 to 100 times greater than the polycrystalline form of the same material (Fig. 18) [*44*]. The improvement in fatigue life is due to the predominance of the slower modes of transgranular crack propagation in these materials. If a crack is initiated in a grain boundary in the

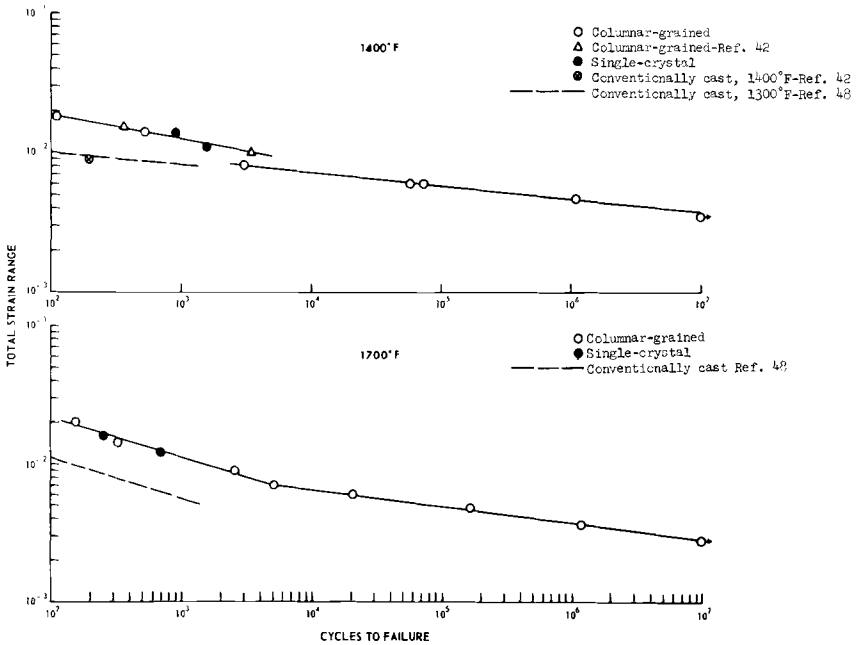

FIG. 18—*Fatigue lives of conventionally cast, columnar-grained, and single-crystal MAR-M200 as a function of total strain range at 1400 and 1700 F; after Leverant and Gell* [18].

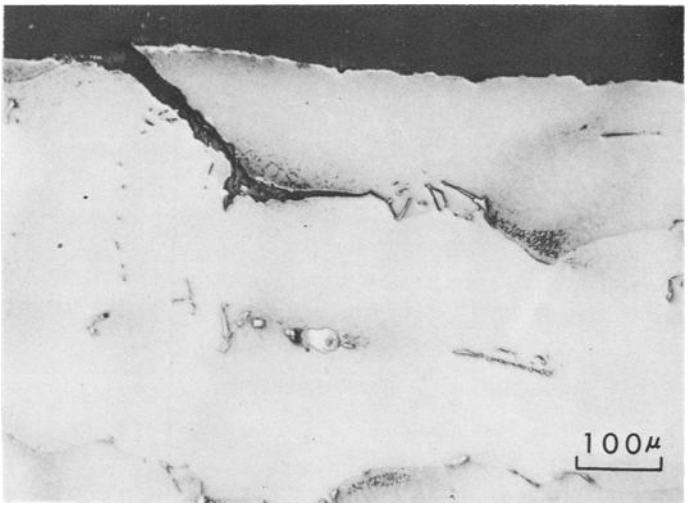

FIG. 19—*Surafce intergranular crack initiation and propagation in columnar-grain MAR-M200 tested in low-cycle fatigue at 1700 F; stress axis is horizontal; after Leverant and Gell* [18].

columnar-grained material, it cannot propagate intergranularly over a large distance because the grain boundaries become parallel to the stress axis, Fig. 19. Single-crystal Udimet 700 similarly shows an improvement in life at 1400 F[3] over wrought polycrystalline material, although the improvement is not as large as that for MAR-M200. An explanation is that in the polycrystalline Udimet 700, crack propagation was primarily in the slower transgranular mode, whereas much of the cracking was intergranular in polycrystalline MAR-M200.

Effect of Frequency

The frequency of cycling has been found to have a significant effect on both the fatigue life and the mode of crack propagation at elevated temperatures. However, little influence of frequency on surface intergranular crack initiation has as yet been observed[3] [*45*, *46*].

In a study of the effect of cyclic frequency on the fatigue life of Nimonic 90 at 1650 F for frequencies of 0.12, 10, and 8000 cpm, it was found that fatigue lives increased with frequency [*36*]. A similar observation has been made on directionally solidified MAR-M200 at frequencies of 2 and 600 cpm at 1400 and 1700 F [*18*]. Fatigue lives were greater at the higher frequency by a factor of 5 at 1400 F and 175 at 1700 F. In this case, the incidence of surface secondary cracks was investigated as well and it was found that more intergranular

and transgranular cracks were initiated at the lower frequency at each temperature (Table 4) which is indicative of the importance of creep-induced damage at low frequencies in the directionally solidified materials. It has also been demonstrated for Nimonic 90 tested at 1650 F and 10 cpm that the fatigue life is almost an order of magnitude greater for push-pull cycling than for repeated-tension cycling [*36*]. Since the mean stress is higher in the repeated-tension cycling, this also emphasizes the importance of creep effects. In addition, several investigators [*24, 45, 46*] have found that crack propagation is primarily transgranular at temperatures up to 1750 F for cyclic frequencies ranging from 1800 to 8700 cpm, whereas it is primarily intergranular at frequencies less than 10 cpm. Figure 20 shows a comparison of the crack propagation mode for Udimet 700 tested at 1700 F at 2 and 1800 cpm.[7]

TABLE 4—*Effect of cyclic frequency on secondary cracking and fatigue life of directionally solidified MAR-M200* [18].

Temperature, deg F	Stress Range, ksi	Frequency, cpm	Number of Surface Secondary Cracks per cm	Cycles to Failure
1400.....	5 to 135	600	0	3.0×10^3
1400.....	5 to 135	2	8.2	6.1×10^2
1700.....	5 to 65	600	1.7	1.7×10^5
1700.....	5 to 65	2	4.2	9.7×10^2
1700.....	5 to 92.5	600	0.5	5.2×10^3
1700.....	5 to 92.5	2	10	2.9×10^1

The mode of transgranular crack propagation at these temperatures also depends on the frequency of cycling. For example, in columnar-grained MAR-M200 at 1400 F [*18*], crack initiation and propagation at 2 cpm are primarily in the Stage II mode, whereas at 600 cpm crack initiation and the initial portion of crack propagation occur in the Stage I mode. In addition, at 1700 F in carbide-free MAR-M200 single crystals, 50 percent of the fatigue zone was Stage I at 600 cpm, but 90 percent was Stage I at 36,000 cpm.[3] The type of transgranular crack propagation that occurs may be related to the rate at which dislocations move out of slipbands. For example, at high frequencies many cycles are accumulated, while the dislocations at a crack tip remain in a planar band; this is conducive to Stage I cracking. On the other hand, at low frequencies, dislocation dispersal out of bands occurs during a single loading cycle and, therefore, leads to a more homogeneous strain field and consequently to Stage II cracking.

[7] Boone, D. H. and Paskiet, G. F., unpublished research.

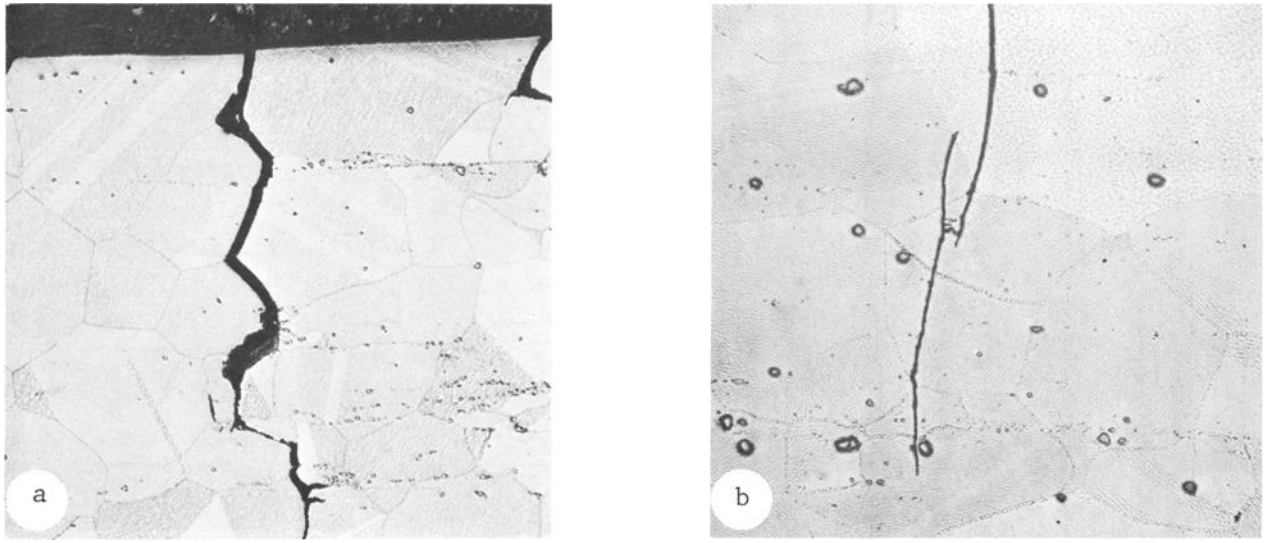

FIG. 20—*The effect of frequency on the mode of fatigue crack propagation in Udimet 700 at 1700 F:* (a) *2 cpm, intergranular* (×*110*); (b) *1800 cpm, transgranular* (×*220*); *after Wells and Sullivan*[6] *and Boone and Paskiet*,[7] *respectively.*

Environmental Effects

Both advantageous and detrimental effects of oxidation on surface crack initiation and propagation have been reported [*32*, *34*, *46–48*]. A number of possibilities exist: for example, crack initiation may be retarded by the oxidation of deleterious phases or accelerated by preferential intergranular attack [*46*]. Crack propagation may be retarded by crack-tip blunting and by the wedging open of the oxide-filled cracks during compression or accelerated by a brittle layer at the crack front. It is also possible that surface intergranular crack initiation at elevated temperatures may not be related to oxidation at all. In Udimet 700 tested in low-cycle fatigue at 1400 F, it was found that interior as well as surface cracks were intergranular [*30*]. This result suggests that intergranular initiation is related to the decrease in the inherent grain boundary strength with increasing temperature rather than to oxidation.

A clear example of oxidation retarding crack growth is found in the tests on columnar-grained MAR-M200 at 1700 F and 600 cpm [*32*]. It was observed that most cracks were surface-initiated, and that these surface cracks were formed first; yet, the crack that eventually led to failure was initiated in the specimen interior (Fig. 17). Cracks initiated in the interior were narrow and had sharp tips (Fig. 21*a*); whereas, surface cracks were wide and contained oxide both at the crack tip and between the crack faces (Fig. 21*b*). It is likely that the oxide increases the crack-tip radius and reduces the amount of crack resharpening that is possible on unloading from peak stresses, and these effects should retard surface crack growth [*49*]. Other nickel-base superalloys in polycrystalline form tested at high frequencies at temperatures between 1300 and 1700 F show similar effects in that failure originates at an internal site even though there is surface intergranular cracking [*45*].[3,8]

Investigations of the fatigue of Inconel 550 [*47*] and Inconel X [*48*] at 1500 F and frequencies of 1970 and 300 cpm, respectively, show that the fatigue lives of both materials are longer in vacuum than in air. The fatigue lives of both materials in the different environments converge at long lives and the point of convergence occurs at shorter lives for higher ratios of mean to alternating stress. Not enough metallographic evidence is presented in either of these studies to assess the importance of environmental effects on crack initiation and crack propagation. Investigations of the effect of other corrosive environments on the high-frequency fatigue strength of several Nimonic alloys at 1200 and 1380 F have indicated no significant change in life from air tests, suggesting that both the cycles to crack initiation and transgranular crack propagation rates are unaffected by these environments [*50*].

[8] Ellison, E. G. and Sullivan, C. P., unpublished research.

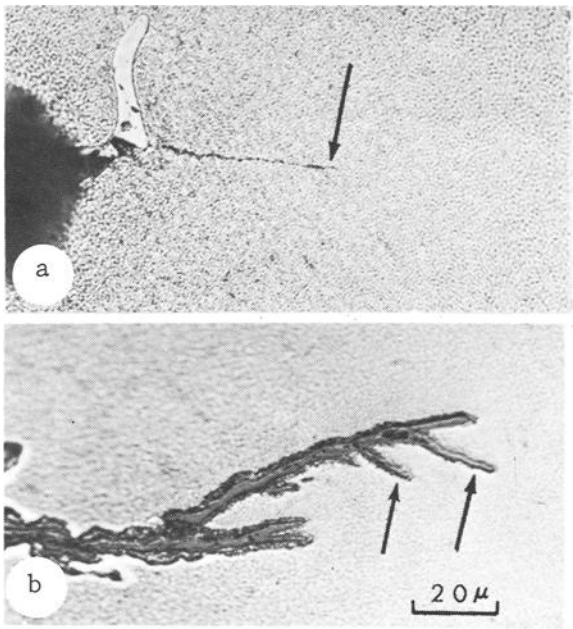

(*a*) Interior crack (*arrow*) initiated at MC carbide and micropore.
(*b*) Surface-initiated crack showing oxide, a light region denuded of γ' precipitate, and crack branching (*arrows*).

FIG. 21—*Secondary cracks in low-cycle fatigue specimens of single-crystal MAR-M200 tested at 1700 F; stress axis is vertical; after Gell and Leverant* [32].

Oxidation-Resistant Coatings

Aluminide coatings are normally used on nickel-base superalloys that operate at temperatures above 1500 F. Figure 22 shows a typical coating, the principal phase of which is NiAl [*51*]. Measurements of the tensile strain to first crack in some conventional nickel-aluminide coatings have indicated a brittle-ductile transition at about 1400 to 1500 F [*52*]. Below this temperature range, tensile elongation is less than 2 percent, whereas it increases rapidly with increasing temperature above the transition. Coatings can influence fatigue life depending on the substrate material and the testing conditions, as discussed below.

At temperatures where the coating is brittle, coating cracks are initiated in the first half-cycle in high-strain fatigue and may lead to reduced fatigue lives compared to uncoated material (Fig. 23). For example, the low-cycle fatigue life of Udimet 700 at 1400 F is reduced 20 percent by a nickel-aluminide coating.[6] On the other hand, at low strain ranges, plastic deformation in the coating is quite limited, and Udimet 700 with an electropolished

FIG. 22—*The structure of a typical nickel-aluminide coating on a nickel-base superalloy (×1000); after Fornwalt and Boone* [51].

coating actually has a higher endurance limit at room temperature than electropolished, uncoated material.[9] At 1700 F, where these coatings are relatively ductile, the low-cycle fatigue life of Udimet 700 is improved with a coating because early surface intergranular crack initiation in the substrate is prevented [*31*]. A nickel-aluminide coating had no effect on the 1400 and 1700 F low-strain fatigue life of columnar-grained MAR-M200 tested in pulsating tension at 600 cpm [*18*], because the cracks which led to failure in both the coated and uncoated materials were initiated in the specimen interior. It should be realized that the coating could affect the fatigue life in low strain range tests where the stress is biased to the surface, such as in bending.

[9] Burck, L. H., unpublished research.

The metallurgical structure of both the coating and the coating-affected substrate zones must be considered in order to optimize fatigue properties. For example, the ductility of a coating can be increased by heat treatment, which improves the low-cycle fatigue life of Udimet 700 at 1400 and 1700 F [*30, 31*]. In this alloy, a thin layer containing sigma phase is formed near the coating-matrix interface during heat treatment [*51*]. Some preferential crack propagation was observed along the boundaries of this phase, but there was no evidence that it served as a crack initiation site. Surface irregularities in the coating can have an important influence on coating crack initiation, such that cracks are frequently found at surface depressions [*31*] (Fig. 24). Also, topographical features of the substrate surface prior to coating have been found on the coating surface [*52*].

Discussion

The purpose of this section is to summarize those aspects of the behavior of nickel-base superalloys that directly affect their fatigue strength, and to suggest approaches by which the strength of these materials may be improved. A number of these approaches are relatively new, and in some cases there is no information available to evaluate their potential. In other instances, it is necessary to understand the processes of crack initiation, propagation, and linkup under the specific conditions of interest before deciding how fatigue properties may be improved. In these cases, a framework for considering the various possibilities is attempted.

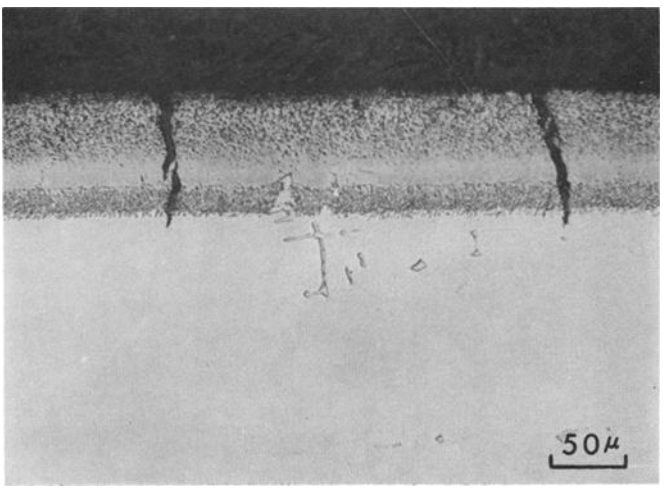

FIG. 23—*Cracks formed in an aluminide coating below the ductile-to-brittle transition; after Boone and Paskiet.*[7]

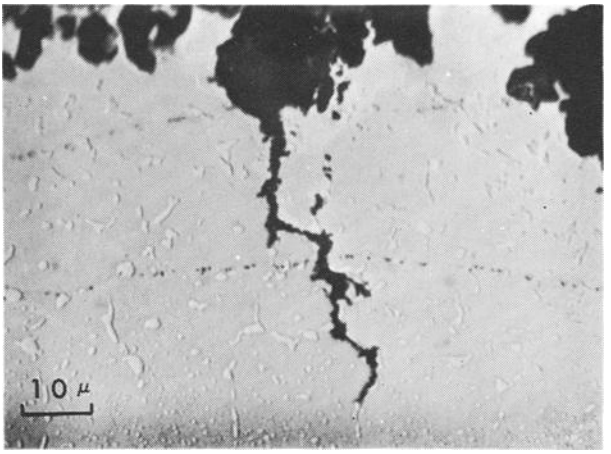

FIG. 24—*The initiation of a crack at a coating surface defect on a low-cycle fatigue specimen of Udimet 700 tested at 1700 F; stress axis horizontal; after Wells and Sullivan* [31].

The relatively poor fatigue strength of nickel-base superalloys can be attributed to the planar slip character, to lack of slip dispersal and the presence of defects at low temperatures, and to intergranular cracking and defects at elevated temperatures. Table 5 summarizes some potentially fruitful approaches for improving the fatigue properties of these materials that will be discussed below. For this discussion, low temperatures are those at which crack initiation and propagation are transgranular in polycrystals, and high temperatures are those at which initiation or propagation or both are intergranular.

TABLE 5—*Approaches for increasing fatigue strength of nickel-base superalloys.*

Temperature Range	Improving Crack Initiation Resistance	Improving Crack Propagation Resistance
Low Temperatures..	1. Eliminate or reduce size of defects. 2. Reduce grain size. 3. Use fatigue resistant surface coatings. 4. Obtain more homogeneous deformation.	1. Impart residual compressive stress to surface. 2. Obtain more homogeneous deformation.
High Temperatures..	1. Retard intergranular initiation in polycrystals. 2. Use fatigue- and oxidation-resistant surface coatings. 3. Use single crystals.	1. Retard intergranular propagation in polycrystals. 2. Use single crystals.

Role of Defects

Once the defect responsible for crack initiation has been determined, crack initiation and, to a lesser extent, crack propagation resistance can be improved by removal of the defect or a reduction in its size. Depending on the type of the defect, this may be accomplished in a given material by alloying, casting, or heat-treating modifications. The cracking of brittle phases may also be eliminated by better fabrication or surface-finishing practices. Where crack initiation along annealing twin boundaries is the limiting factor, the density and length of the twins can be controlled by the amount of deformation prior to recrystallization and by the grain size, respectively. The twins can be entirely avoided by using cast materials. The improvement in fatigue properties obtained by reducing the size of a defect or eliminating it from the microstructure will be greatest for low-temperature applications and for conditions where the defects remaining in the structure are not nearly as deleterious as those that were removed.

Slip Homogeneity

In low-strength, single-phase metals and alloys, good fatigue properties have been associated with a planar slip character and a high degree of slip dispersal [*6*, *53–56*]. In nickel-base superalloys, the concentration of slip in coarse, planar bands and the absence of a high degree of slip dispersal contributes to the relatively poor fatigue properties. It should be possible to improve the fatigue properties by dispersal of the planar slip or by a change in slip character from planar to wavy. There has not been much research done to achieve either of these objectives, so discussion will be centered around possible avenues of approach.

Slip dispersal can be achieved by increasing the number of active slip nucleating sites or the cyclic strain hardening rate [*57*]. Both objectives may be achieved by introduction of a finely spaced, hard, incoherent dispersoid at the surface or throughout the volume of the material. Alloying and heat treatment can effect a change in slip dispersal or the cyclic work hardening rate only insofar as they change the density, size, and location of hard second-phase particles. It is also possible to disperse slip in surface grains by surface working treatments, although in the case of glass-bead blasting of Udimet 700, slip dispersal was not the cause of improved fatigue life (see section on Deformation-Induced Cracking).

Grain size refinement should also provide an improvement in crack initiation resistance, although slip dispersal in most cases is less important than a reduction in the mean free slip distance. It has been shown that the rate of slipband crack initiation should be proportional to the range of shear band displacement and, consequently, inversely proportional to grain size [*29*].

This grain size effect requires slipbands or slip along annealing twin boundaries to extend completely across a grain and this condition is most likely to be satisfied when the maximum stress in a cycle exceeds a large fraction of the proportional limit. If the mean free slip distance could be reduced to approximately the size of γ' particles or less, then the slip character would essentially become more wavy.

Intergranular Cracking

As is true of most polycrystalline materials, the elevated temperature fatigue properties of nickel-base superalloys are limited by intergranular initiation and propagation. The intergranular cracking is initiated preferentially on grain boundaries normal to the stress axis (the conditions favoring this were discussed in the section on High-Temperature Fatigue). Assuming a constant grain boundary structure, the effect of grain size on fatigue life can be hypothetically arranged into two broad categories (Fig. 25).

In the first case, likely to be found at low stress ranges, a single intergranular crack is initiated and propagates to failure with little or no crack linking. It can be seen in Figs. 25*a* and *c* that a crack on a transverse boundary in a fine grain material is much smaller before it reaches a triple point than a crack in a coarse grain material. At the triple point the cracks must undergo the more difficult processes of crack reinitiation, branching, and propagation on a boundary not normal to the stress axis if it continues intergranularly (Fig. 25*a*), or the cracks must propagate in a much slower transgranular mode (Fig. 25*c*). Under these circumstances, the fatigue life should increase with reduced grain size.

In the second case, likely to be found at high strain ranges, cracks are initiated on transverse grain boundaries, with the number of cracks increasing with reduced grain size. If crack linking is the critical step in the fracture process, whether it be intergranular (Fig. 25*b*) or transgranular (Fig. 25*d*), the rate of linkup should be inversely proportional to grain size. Hence, the fatigue life should increase with grain size.

Just as the brittle phases and casting pores that initiate cracks are considered defects, so too should grain boundaries under conditions of intergranular failure be considered defects. It has been possible by reducing or eliminating their effect through directional solidification of materials into either columnar-grained or single-crystal forms to improve significantly the creep, stress rupture, thermal shock [*58–60*], and elevated temperature fatigue properties (section on Directional Solidification). The use of materials in single-crystal forms has the added advantage that they can be made carbide-free; there is no need for carbides whose sole purpose is grain boundary strengthening. The use of defect-free, single-crystal materials appears to be the ultimate solution to the problem of achieving improved elevated temperature fatigue properties of nickel-base superalloys.

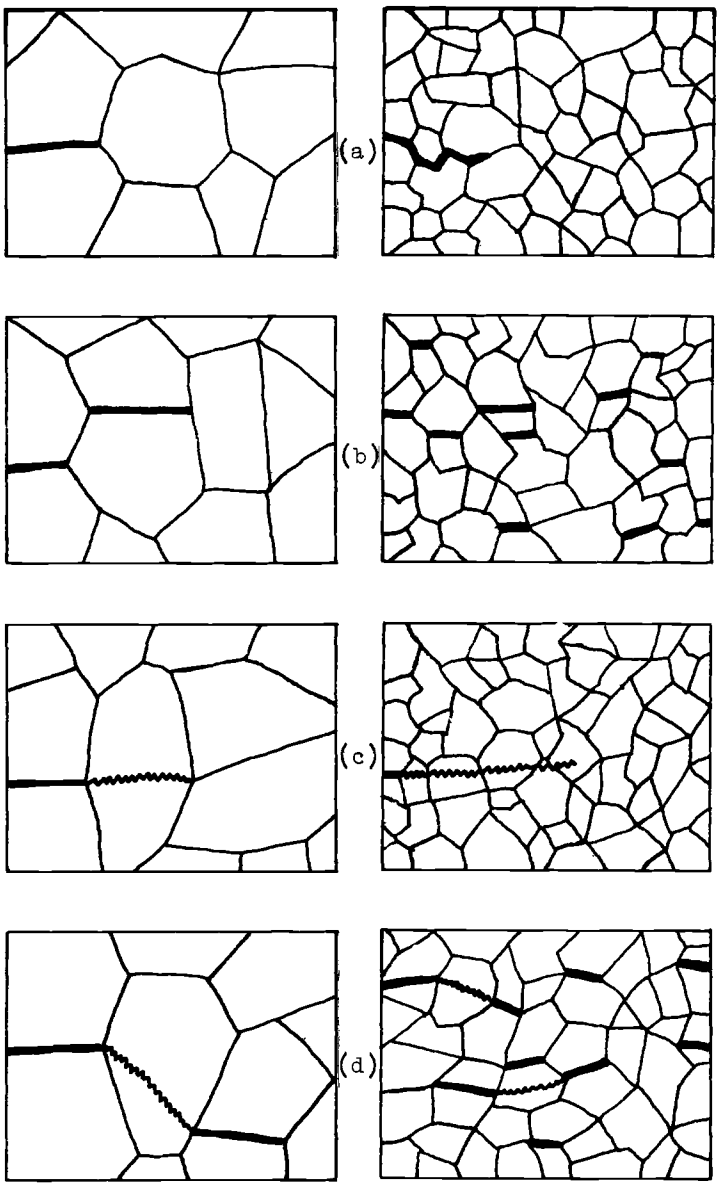

(*a*) Intergranular initiation and propagation; linkup unimportant.
(*b*) Intergranular initiation and propagation; linkup important.
(*c*) Intergranular initiation, transgranular propagation; linkup unimportant.
(*d*) Intergranular initiation, transgranular propagation; linkup important.

FIG. 25—*A schematic drawing comparing elevated temperature surface cracking in* (left) *coarse- and* (right) *fine-grained polycrystalline materials.*

Fatigue-Resistant Coatings

Since most fatigue cracking is initiated at an external surface, the use of a coating with physical and mechanical properties different from those of the substrate can have a marked effect on the fatigue behavior of the coating-substrate combination. Coatings are not presently used on nickel-base superalloys for low-temperature applications such as turbine shafts and disks; however, the life of these components is often limited by fatigue and could benefit by the application of fatigue-resistant coatings. The discussion will, therefore, deal with desirable characteristics of both low- and high-temperature coatings.

Low Temperatures—At low temperatures, the important considerations for coating selection, assuming a tightly adherent coating can be made, are the elastic modulus, yield strength, ductility, and fatigue strength of the coating relative to that of the substrate. The most important consideration is that the coating have superior fatigue properties at a given stress range as compared to that of the substrate. Additional advantage can be obtained by a low elastic modulus of the coating when cycling is totally in the elastic range, because the coating and the substrate undergo the same total strain range, and the stress range experienced in the coating, $\Delta\sigma_c$, is given by: [10]

$$\Delta\sigma_c = (E_c/E_s)\Delta\sigma_s$$

where E_c and E_s are the elastic moduli of the coating and substrate, respectively, and $\Delta\sigma_s$ is the stress range of the substrate (Fig. 26*a*). If the substrate or coating or both are plastically yielded then, in addition to the above considerations, the relative yield strengths and cyclic work hardening and softening rates are needed to determine the magnitudes of the stress and plastic strain ranges in the coating and substrate. Figures 26*b* and 26*c* illustrate, for the first cycle, two of the many possible cases.

Elevated Temperatures—For elevated temperature applications, nickel-base superalloys must be used in conjunction with an oxidation-resistant surface coating. This is normally of nickel-aluminide type, the exact structure of which can be complex and is dependent on the initial aluminum concentration at the surface, subsequent heat treatments, and service exposures. Coating performance on a substrate is normally evaluated on the basis of the oxidation resistance as measured in static or dynamic tests. However, it is known that if the aluminum concentration of a coating is high, which is desirable for oxidation resistance, brittle cracks extending to the substrate can be formed under stress at temperatures below the brittle to ductile transition for the coating (section on Oxidation-Resistant Coatings). Under these circumstances, not only may the oxidation protection of the coating be impaired, but the brittle cracks in the coating can lead to cracking of the substrate. On the other

[10] Rau, C. A., unpublished research.

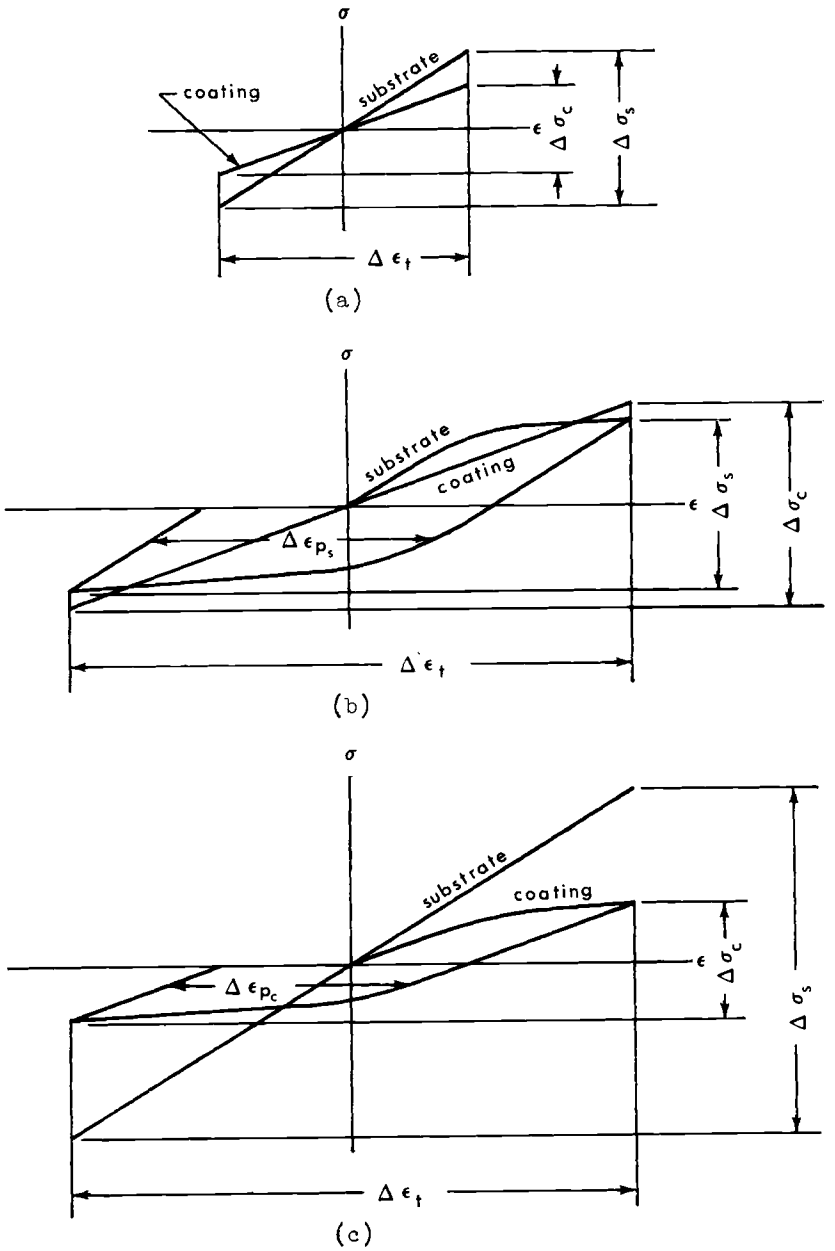

(*a*) Coating and substrate are both in elastic region.
(*b*) Coating is elastic and substrate has plastically yielded.
(*c*) Coating has plastically yielded and substrate is elastic.

FIG. 26—*The stress range* ($\Delta\sigma$) *and plastic strain range* ($\Delta\epsilon_P$) *response of a coating and substrate for a given applied total strain range* ($\Delta\epsilon_T$). *It is assumed that the elastic modulus of the coating is less than that of the substrate.*

extreme, it is possible to prepare more ductile coatings by lowering the aluminum concentration during heat treatment. The oxidation protection is then reduced and, after long time exposures at elevated temperatures, intergranular cracking in the substrate can occur following preferential oxidation and γ' denudation at grain boundaries. It would therefore be desirable to design coatings so that consideration is given to the fatigue properties of the coating as well as to protection of the substrate from the environment. This is an extremely difficult problem, but certain desirable characteristics of a coating from a fatigue-resistance viewpoint, in addition to those discussed above for low temperatures, are clear. A discussion of the oxidation resistance and structure of coatings may be found elsewhere [*52*, *61*].

The most important aspect is to insure that the fracture strain of the coating exceeds the maximum applied strain at all temperatures of interest. This can be accomplished by lowering the ductile-to-brittle transition of the coating by heat treatment. Crack initiation in a ductile coating can be retarded by minimizing surface irregularities on the substrate prior to coating and by polishing the coating surface itself (section on Oxidation-Resistant Coatings). Once a crack has propagated through a coating, it is still possible to retard substrate initiation by deflecting the crack along the coating-matrix interface. This requires a relatively weak interface relative to the strength of the substrate matrix [*62*]. If interface cracking is extensive, then spalling of the coating could become a problem.

Residual Compressive Stress

It has been shown for polycrystalline Udimet 700 at room temperature that a residual compressive stress obtained by glass-bead blasting the surface has little effect on crack initiation but markedly reduces the Stage I crack propagation rate while the crack is in the residual stress zone (see section on High-Cycle Fatigue of Polycrystals). The improvement in crack propagation resistance is proportional to the magnitude of the residual compressive stress and its depth. It is important that the surface working treatment confer complete coverage in order to prevent premature failure in those surface areas having a lower residual stress.

There is some evidence to indicate that a surface working treatment leads to sharply reduced fatigue properties at elevated temperatures [*46*]. The temperature of testing (1382 F) may have produced a surface stress relief but this would only have reduced or eliminated the improvement in fatigue properties conferred by the residual stress. Rather, it is likely that surface working has a deleterious effect on the intergranular initiation that would be expected at this temperature. In the absence of stress relief, the beneficial effects of residual compressive stress should be present at all temperatures at which crystallographic cracking occurs.

Acknowledgments

We appreciate the permission by many of our colleagues to use their unpublished results and are grateful to G. W. Goward and C. P. Sullivan for a critical review of the manuscript.

References

[1] *Aerospace Structural Metals Handbook*, Third Revision, Syracuse University Press, March, 1966.

[2] Malin, C. O. and Schmidt, E. H., "Tensile and Fatigue Properties of Alloy 718 at Cryogenic Temperatures," Technical Report No. C7-23.3, American Society for Metals, Metals Park, Ohio, 1967.

[3] Slack, R. B., Jr., "The Effect of Several Variables on Fatigue of a Nickel-Base Alloy," MSc thesis, Hartford Graduate Center, Rensselaer Polytechnic Institute of Connecticut, 1967.

[4] Burck, L. H., Sullivan, C. P., and Wells, C. H., "Room Temperature Fatigue of Udimet 700 Including Effects of Cold Work and Residual Stress," *AMRDL Report No. 69-012*, Pratt & Whitney Aircraft, Middletown, Conn., 1969.

[5] Favor, R. J. et al, "Investigation of Fatigue Behavior of Certain Alloys in the Temperature Range Room Temperature to −423°F," WADD, TR61-132, Wright Air Development Div., June 1961.

[6] McEvily, A. J., Jr., and Johnston, T. L., *International Journal of Fracture Mechanics*, IJFMA, Vol. 3, 1967, pp. 45–73.

[7] Kriege, O. H. and Baris, J. M., *Transactions Quarterly*, American Society for Metals, ASMQA, Vol. 62, March 1969.

[8] Betteridge, W. and Franklin, A. W., *Journal of the Institute of Metals*, London, JIMEA, Vol. 85, 1956-57, pp. 473–479.

[9] Smashey, R. W. and Piearcey, B. J., *Transactions of the Metallurgical Society of AIME*, American Institute of Mining, Metallurgical, and Petroleum Engineers, TMSAA, Vol. 239, 1967, pp. 451–457.

[10] Betteridge, W., *The Nimonic Alloys*, Edward Arnold Ltd., London, 1959, p. 32.

[11] Betteridge, W., *The Nimonic Alloys*, Edward Arnold Ltd., London, 1959, p. 44.

[12] Lund, C. H. and Wagner, H. J., "Identification of Microconstituents in Superalloys," DMIC Redort 160, Defense Metals Information Center, Battelle Memorial Institute, Columbus, Ohio, 1962.

[13] Gell, M. and Leverant, G. R., *Transactions of the Metallurgical Society of AIME*, American Institute of Mining, Metallurgical, and Petroleum Engineers, TMSAA, Vol. 242, 1968, pp. 1869–1879.

[14] McMahon, C. J., Jr., and Cohen, M., *Acta Metallurgica*, AMETA, Vol. 13, 1965, pp. 591–604.

[15] Gell, M. and Worthington, P. J., *Acta Metallurgica*, AMETA, Vol. 14, 1966, pp. 1265–1271.

[16] Smith, E. and Barnby, J. T., "Nucleation of Grain-Boundary Cavities During High-Temperature Creep," *Metal Science Journal*, Vol. 1, pp. 1–4.

[17] Kear, B. H., Copley, S. M., and VerSnyder, F. L., *Proceedings*, International Conference on the Strength of Metals and Alloys, published as *Supplement to Transactions of the Japan Institute of Metals*, TJIMA, Vol. 9, 1968, pp. 672–680.

[18] Leverant, G. R. and Gell, M., *Transactions of the Metallurgical Society of AIME*, American Institute of Mining, Metallurgical, and Petroleum Engineers, TMSAA, Vol. 245, 1969, pp. 1167–1173.

[19] Cottrell, A. H., *The Mechanical Properties of Matter*, Wiley, New York, 1963.

[20] Wells, C. H. and Sullivan, C. P., *Transactions Quarterly*, American Society for Metals, ASMQA, Vol. 60, 1967, pp. 217–222.

[21] Wells, C. H. and Sullivan, C. P., *Transactions Quarterly*, American Society for Metals, ASMQA, Vol. 57, 1964, pp. 841–855.

[22] Gell, M. and Leverant, G. R., *Acta Metallurgica*, AMETA, Vol. 16, 1968, pp. 553–561.
[23] Gell, M. and Field, T. T., *Transactions of the Metallurgical Society of AIME*, American Institute of Mining, Metallurgical, and Petroleum Engineers, TMSAA, Vol. 245, 1969, pp. 1666–1669.
[24] Drake, J. R., "Rotating-Beam Fatigue Strength of Cast Nickel-Base Alloys at Elevated Temperatures," Paper 63-WA-214, American Society of Mechanical Engineers, 1963, pp. 1–9.
[25] Rice, J. R. in *Fatigue Crack Propagation, ASTM STP 415*, American Society for Testing and Materials, 1967, p. 247.
[26] McNeil, M. B. and Grosskreutz, J. C., *Philosophical Magazine*, PHMAA, Vol. 16, 1967, pp. 1115–1118.
[27] Fujita, F. E. in *Fracture of Solids*, D. C. Drucker and J. J. Gilman, Eds., Interscience Publishers, New York, 1963, p. 657.
[28] Wells, C. H., *Journal of Basic Engineering*, ASME Transactions, Series D, JBAEA, Vol. 89, 1967, pp. 893–896.
[29] Wells, C. H., *Acta Metallurgica*, AMETA, Vol. 17, 1969, pp. 443–449.
[30] Wells, C. H. and Sullivan, C. P., *Transactions Quarterly*, American Society for Metals, ASMQA, Vol. 58, 1965, pp. 391–402.
[31] Wells, C. H. and Sullivan, C. P., *Transactions Quarterly*, American Society for Metals, ASMQA, Vol. 61, 1968, pp. 149–155.
[32] Gell, M. and Leverant, G. R., "The Effect of Temperature on Fatigue Fracture in a Directionally Solidified Nickel-base Superalloy," *Fracture 1969*, Proceedings of Second International Conference on Fracture, Brighton, England, Chapman and Hall Ltd., London, 1969.
[33] Franklin, A. W., Heslop, J., and Smith, R. A., *Journal of the Institute of Metals*, London, JIMEA, Vol. 92, 1963–64, pp. 313–322.
[34] Glenny, E. and Taylor, T. A., *Journal of the Institute of Metals*, London, JIMEA, Vol. 88, 1959–60, pp. 449–461.
[35] Glenny, E. and Northwood, J. E., *Foundry Trade Journal*, FUTJA, Vol. 119, 1965, pp. 607–620.
[36] Tilly, G. P., *Proceedings of the Institution of Mechanical Engineers*, London, PIMLA, Vol. 180, 1965–66, pp. 1045–1058.
[37] Forrest, P. G. and Armstrong, K. B., *Journal of the Institute of Metals*, London, JIMEA, Vol. 94, 1966, pp. 204–213.
[38] Baron, H. G. and Bloomfield, B. S., *Journal of the Iron and Steel Institute*, London, JISIA, Vol. 197, 1961, pp. 223–232.
[39] Robinson, A. T. and Dorn, J. E., "The Effect of Grain Size on the Fatigue and Creep Properties of Stainless Steel and Inconel at Elevated Temperatures," WADC Technical Report 54-40, Wright Air Development Center, Dayton, Ohio, 1954.
[40] Decker, R. F., Rowe, J. P., and Freeman, J. W., *Transactions of the Metallurgical Society of AIME*, American Institute of Mining, Metallurgical, and Petroleum Engineers, TMSAA, Vol. 212, 1958, pp. 686–694.
[41] Bieber, C. G. and Decker, R. F., *Transactions of the Metallurgical Society of AIME*, American Institute of Mining, Metallurgical, and Petroleum Engineers, TMSAA, Vol. 221, 1961, pp. 629–636.
[42] McLean, D., *Journal of the Institute of Metals*, London, JIMEA, Vol. 85, 1956–57, pp. 468–472.
[43] Weaver, C. W., *Journal of the Institute of Metals*, London, JIMEA, 1959–1960, pp. 296–300.
[44] LaMothe, E., Phippen, C., and Bublick, A., MDL Report B-14537 and Correction, Pratt & Whitney Aircraft, East Hartford, Conn., 1966.
[45] Northwood, J. E., Smith, R. S., and Stephenson, N., "The Effect of Alternating Stresses at Elevated Temperatures on Structural Changes in Nimonic 90," Memorandum No. M.325, National Gas Turbine Establishment, Pyestock, Hants., England, 1959.
[46] Betteridge, W., *The Nimonic Alloys*, Edward Arnold Ltd., London, 1959, p. 214.

[47] Danek, G. J., Smith, H. H., and Achter, M. R., *Proceedings*, American Society for Testing and Materials, ASTEA, Vol. 61, 1961, pp. 775–788.
[48] Nachtigall, A. J. et al, "The Effect of Vacuum on the Fatigue and Stress-Rupture Properties of S-816 and Inconel 550 at 1500°F," NASA TN D-2898, National Aeronautics and Space Administration, 1965.
[49] Laird, C. in *Fatigue Crack Propagation, ASTM STP 415*, American Society for Testing and Materials, 1967, p. 131.
[50] Betteridge, W., *The Nimonic Alloys*, Edward Arnold Ltd., London, 1959, pp. 219–222.
[51] Fornwalt, D. E. and Boone, D. H., "Metallographic Characterization of Phases Associated with Aluminide Coated Udimet 700," *Proceedings*, First Annual Meeting International Metallographic Society, Denver, 1969, pp. 97–111.
[52] Boone, D. H. and Goward, G. W., "The Use of Nickel-Aluminum Intermetallic Systems as Coatings for High Temperature Nickel-Base Alloys," Third Bolton Landing Conference on Ordered Alloys, Claitor's Publishing Division, Baton Rouge, La.
[53] McEvily, A. J., Jr., and Boettner, R. C., *Acta Metallurgica*, AMETA, Vol. 11, 1963, pp. 725–743.
[54] Avery, D. H. and Backofen, W. A. in *Fracture of Solids*, Wiley, New York, 1963, pp. 339–382.
[55] Boettner, R. C. and McEvily, A. J., Jr., *Acta Metallurgica*, AMETA, Vol. 13, 1965, pp. 937–946.
[56] Miller, G. A., Avery, D. H., and Backofen, W. A., *Transactions of the Metallurgical Society of AIME*, American Institute of Mining, Metallurgical, and Petroleum Engineers, TMSAA, Vol. 236, 1966, pp. 1667–1673.
[57] Ashby, M. F. in *Oxide Dispersion Strengthening*, Gordon and Breach, New York, 1968, pp. 143–212.
[58] VerSnyder, F. L. and Piearcey, B. J., *Journal of Aircraft*, American Institute of Aeronautics and Astronautics, JAIRA, Vol. 3, 1966, pp. 390–397.
[59] Piearcey, B. J. and VerSnyder, F. L., *Journal*, Society of Automotive Engineers, SAEJA, Vol. 74, 1966, pp. 36–43.
[60] Piearcey, B. J. and Terkelsen, B. E., *Transactions of the Metallurgical Society of AIME*, American Institute of Mining, Metallurgical, and Petroleum Engineers, TMSAA, Vol. 239, 1967, pp. 1143–1150.
[61] Goward, G. W., Boone, D. H., and Giggins, C. S., *Transactions Quarterly*, American Society for Metals, ASMQA, Vol. 60, 1967, pp. 228–241.
[62] Cook, J. and Gordon, J. E., *Proceedings of the Royal Society*, London, Series A, PRLAA, Vol. A282, 1964, pp. 508–520.

DISCUSSION: See page 296.

J. F. Throop[1] *and G. A. Miller*[2]

Optimum Fatigue Crack Resistance

REFERENCE: Throop, J. F. and Miller, G. A., "**Optimum Fatigue Crack Resistance,**" *Achievement of High Fatigue Resistance in Metals and Alloys, ASTM STP 467*, American Society for Testing and Materials, 1970, pp. 154–168.

ABSTRACT: An evaluation is made of the influence of mechanical properties on fatigue crack growth rate. Data representing SAE 4340 and modified 4330 steels show that for levels of the stress intensity factor, K, below about 40 ksi$\sqrt{\text{in.}}$ mechanical properties have little influence on growth rate. However, at higher K levels both the product of Young's modulus, yield strength, and fracture toughness and the product of Young's modulus, tensile strength, and true strain at fracture seem to be reasonable indexes of crack growth resistance. For K levels above 40 ksi$\sqrt{\text{in.}}$ the fatigue crack growth rate is minimized by tempering 4340 and modified 4330 steel at temperatures of about 1000 and 1100 F, respectively.

KEY WORDS: fatigue (materials), crack propagation, crack initiation, fracture strength, temper annealing, stress analysis, fracture properties, materials specifications, evaluation

Fatigue fracture has been characterized as including the stages of crack nucleation, stable crack growth under cyclic loading, and unstable crack growth during the final load cycle. In principle, optimization of fatigue performance might be expected to involve control over each stage in the fracture process. However, the difficulty of detecting small cracks less than 0.001 in. in length, coupled with the fact that such cracks can occur as early as the first 10 percent of life, suggests that in practice little control can be exercised over the nucleation stage. Consequently, the best chance for controlling fatigue performance should involve control of both the stable crack growth rate and the onset of unstable crack growth.

According to the principles of fracture mechanics, control of unstable crack growth is defined in terms of the fracture toughness of the material, in particular K_{Ic}, for conditions where plane strain prevails. Optimum resistance to unstable crack growth is provided by achieving the maximum fracture toughness.

[1] Research mechanical engineer, Maggs Research Center, Watervliet Arsenal, Watervliet, N. Y. 12189. Personal member ASTM.

[2] Research engineer, Homer Research Laboratories, Bethlehem Steel Corp., Bethlehem, Pa. 18016. Personal member ASTM.

Numerous investigations have attempted to provide insight regarding control of stable crack growth during cyclic loading by establishing the dependence of growth rate on the stress intensity factor K [*1–3*][3] or the crack size and gross stress S_g [*4–8*]. The growth rate dependence on K may be expressed by the equation, $Rate = C(K_{max})^m$, where *Rate* is the change in crack length per cycle, K_{max} is the stress intensity factor at maximum cyclic load, m is an invariant integer, and C is an explicit function of mechanical properties [*9–14*] (Table 1). Frost and Dugdale's expression [*15*] differs from the above equation in that C is inversely proportional to crack size. For a given material, crack rate depends upon K_{max}, which is in turn a function of crack size and applied load. If stable crack growth is well represented by the above equation, then optimization of crack growth resistance should simply involve minimizing C to minimize growth rate.

TABLE 1—*Models of crack growth kinetics.*

$Rate = C(K_{max})^m$ or $C'(\Delta K)^m$

Rate = $d(2a)/dN$ for center notch, da/dN for compact tension.
K_{max} = $\alpha S_g(\pi a)^{1/2}$ is the stress intensity factor at maximum tensile load.
ΔK = $(K_{max} - K_{min})$; K_{min} is evaluated at the minimum cyclic load.
α = correction for finite specimen width.
S_g = gross section stress.
C = a constant for a given material.
m = an invariant integer.

Model	Mechanical Properties in C	Value of m
McClintock [*12*]	$(ES_u)^{-1}$	2
Pearson [*13*]	$(E)^{-3.6}$	3.6
Krafft [*14*]	$(E^3K^2_{1c}n)^{-1}$	4
McEvily and Johnston [*10*]	$[E(S_y + S_u)\epsilon_u S_u^2]^{-1}$	4
McClintock [*12*]	$(ES_u\epsilon_f)^{-2}$	4

NOTE—S_y = yield strength 0.2 percent offset,
S_u = ultimate tensile strength,
ϵ_u = engineering strain at necking,
ϵ_f = "true strain" at fracture,
n = strain hardening exponent,
E = Young's modulus,
K_{1c} = plane strain fracture toughness, and
ρ = size of a region for which the average strain satisfies the fracture criterion.

The objective of the present effort was to determine if the various expressions for C [*9–15*] or some other parameter can be used as an index of a

[3] Italic numbers in brackets refer to the list of references at the end of this paper.

material's resistance to stable crack growth during cyclic loading. To this end, C functions will be compared with experimental data which include both crack growth rates and mechanical properties.

Crack Growth Resistance and Mechanical Properties

The problem of primary interest in this study is to determine what combination of mechanical properties is most useful in describing fatigue crack growth resistance. As a starting point we assume that stable crack growth during cyclic loading and unstable crack growth for monotonically increasing load are related. If this assumption is valid, then fatigue crack rate should be inversely related to fracture toughness as suggested by Krafft's model [*9*]. For a given application, however, the choice of a material or treatment to provide maximum fracture toughness may serve to reduce other properties, such as yield strength and hardness, below acceptable levels. Consequently, optimization of crack resistance might be expected to involve a balance between strength and crack toughness.

An illustration of such a trade-off in mechanical properties is presented in Fig. 1. This is an idealization (surfaces faired through the actual data) of the results of Hays and Wessel [*16*] for 1-in.-thick 4340 steel plate in which yield strength and fracture toughness are presented as functions of tempering and service (test) temperature. For the 1050 F tempering temperature, room temperature yield strength, S_y, and fracture toughness are both high and have values of about 160 ksi and 160 ksi$\sqrt{\text{in.}}$, respectively. For lower tempering temperatures crack toughness is reduced, whereas higher temperature results in a rapid decrease in yield strength. This figure also suggests that the tempering temperature which provides a balance between room temperature strength and toughness may also provide optimum properties at other test temperatures. For example, in the case of the 1050 F temper both yield strength and toughness remain at relatively high levels as service temperature is varied from -200 to $+200$ F. If tempering temperature is lowered by only 50 deg to 1000 F, crack toughness falls sharply at a service temperature of -100 F. Such a drop in toughness in the expected range of service temperature must be avoided if brittle fracture is to be prevented.

If the concept of a balance between strength and crack toughness has merit in describing a material's resistance to crack growth during cyclic loading, then growth rate should be inversely related to the strength and toughness product. In addition to strength and toughness, the other material property which we believe important in influencing crack growth resistance is Young's modulus E. An inverse relation between crack rate and E is the only common characteristic of all of the crack growth models [*9–15*]. Therefore, we suggest that the parameter $(ES_yK_{Ic})^{-1}$ may be of use in assessing the influence of material properties on fatigue crack growth. Unfortunately,

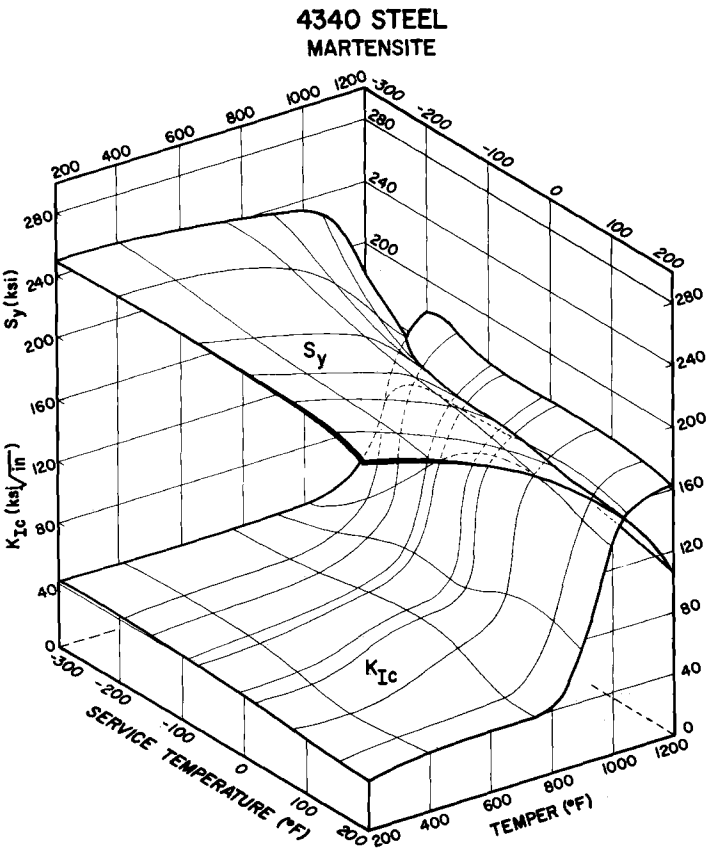

FIG. 1—*Idealized relationships of yield strength and fracture toughness of 4340 steel to both tempering temperature and service temperature. Surfaces have been faired through actual test results of Hays and Wessel, Ref* 16.

this parameter is proposed without benefit of a mathematical model because we have not found an acceptable basis for one. However, it appears from what follows that $(ES_yK_{Ic})^{-1}$ does express empirically the effects of heat treatment on crack growth, at least for the materials examined in this study.

Restrictions on the Expression Rate = $C(K_{max})^m$

Experimental results over a period of time have raised some questions regarding the universal applicability of the equation *Rate* = $C(K_{max})^m$. In the first place, plots of log *Rate* versus log K_{max} are not always the straight lines required by the equation. In some cases the data can be better represented by a sigmoidal relation [*17*, *18*] wherein the derivative of crack rate with respect to K_{max} is much greater at both low and high levels of K_{max} than it is at intermediate levels.

Secondly, when data representing a wide variety of materials, as in Table 2, are fitted using the method of least squares, the exponent m is not an invariant integer as required by many of the crack growth models but, rather, is found to vary from about 2.2 to 6.7 (Fig. 2). The median, average, and standard deviation of m for the plotted data are 3.3, 3.5, and 0.65, respectively. This figure represents the dispersion in 69 values of m from eight sources of data [*20–27*].[4]

TABLE 2—*Least squares fit of crack growth data.*

Materials	Number of Observations of m	Average m	Range in m	References[a]
Low- and medium-strength steels	30	3.5	2.3 to 5.2	[*21*], [*22*]
High-strength steels	20	3.3	2.2 to 6.7	[*20*, *23–25*]
Titanium	2	3.5	3.68 and 3.31	[*24*]
2024 aluminum	6	3.4	2.7 to 3.8	[*27*]
305 stainless steel	6	3.3	2.8 to 4.5	[*26*]
70-30 brass	5	4.1	3.6 to 4.9	[*26*]
Total sample	69	3.5	2.2 to 6.7	8

[a] See Ref. *19*.

Finally, implicit in the equation $Rate = C(K_{max})^m$ is the assumption that m and C are separate and independent quantities which express the growth rate's dependence on K_{max} and the material's influence on growth, respectively. Experimental findings for steels suggest that m may be related to material properties. The results of one study of high-strength steel [*23*] show an inverse relation between m and fracture toughness. Data for low- to medium-strength steels follow a similar trend in that m appears to be inversely related to the Charpy upper-shelf energy [*22*].

These observations suggest that different fracture mechanisms or processes can operate during crack growth in different materials, or even at different K levels for a given material. Thus, the equation $Rate = C(K_{max})^m$ should not be construed to be a long-range forecaster of crack growth rate, but, rather, a useful tool for assessing the effects of material treatments on growth rate for a limited range in K.

Model Predictions

Several models have been used as the bases for derivations of the crack rate equation. The C expressions for some of these are listed in Table 1.

[4] *ASTM Book of Standards*, Part 31, American Society for Testing and Materials, 1969, pp. 1099–1114.

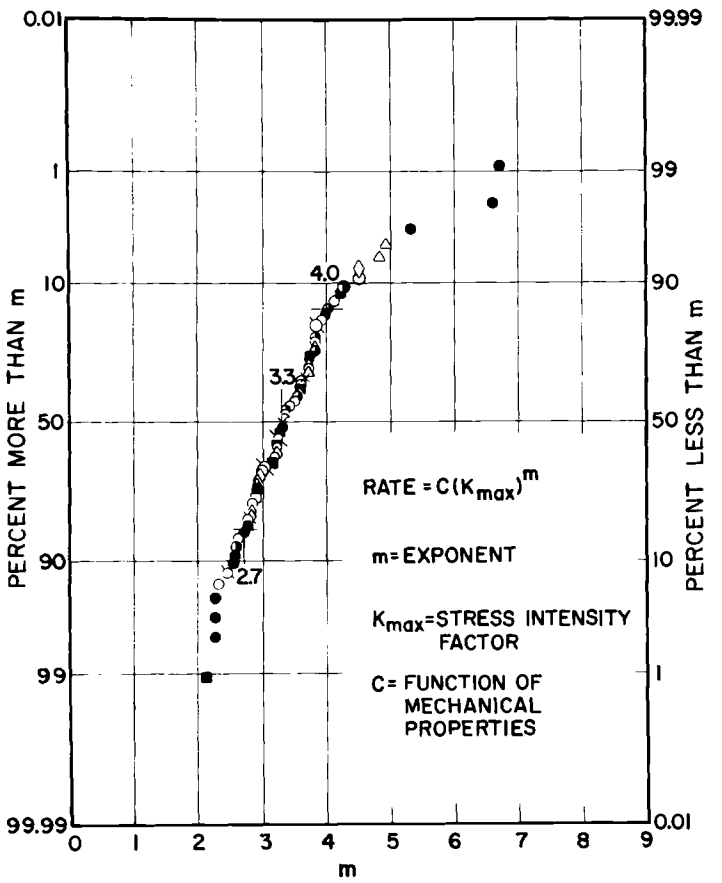

FIG. 2—*A normal probability plot of the crack rate exponent* m *for center-cracked specimens. The median and mean* m *values are 3.3 and 3.5, respectively.*

The Frost and Dugdale [*15*] expression is not listed but has the form $d(2a)/dN$ = constant $(K_{max})^3/aE(S_y + S_u)$, in which the property dependence of crack rate is related to $1/E^2(S_y + S_u)$ and is similar to others that are listed. As indicated, each model predicts a specified fixed value for the exponent.

There should then be a linear correlation between the value of C for different materials or different conditions of a particular material and the crack rates measured at a given K level. This was explored at K_{max} levels of 20 and 50 ksi$\sqrt{\text{in.}}$ using crack rate results on several high-strength steels [*20, 23–25*] and aluminum alloy [*19, 28*] reported in the literature. A large variability was evident in the plots of crack rate versus C from most of the C expressions.

This variability was not surprising—the difficulty in obtaining coherent information on all variables needed in the comparison, since the reported results were from several sources, testing was done on center-cracked specimens of different sizes in different machines, etc., almost precluded any consistency. The C-expressions of McEvily and Johnston]*10*] and of Krafft [*14*] were not thoroughly explored, because much of the available data did not supply the engineering strain at maximum load, ϵ_u, and the strain hardening exponent, n, respectively. The variability in the data precluded the possibility of ruling out the expressions $(E)^{-3.6}$, $(ES_u)^{-1}$, and $(ES_u\epsilon_f)^{-2}$ as adequate descriptions of the material's influence on crack growth rate. Compared with these expressions, however, a better example of a linear trend between the fixed K_{max} crack rate and the values of C was obtained in plots of $d(2a)/dN$ versus $(ES_yK_{Ic})^{-1}$; thus, it seemed appropriate to examine the expressions $(ES_u\epsilon_f)^{-2}$ and $(ES_yK_{Ic})^{-1}$ to a further extent.

Crack Growth Rates for 4340 Steel

In an effort to reduce the variation in crack rate associated with including data from different sources, we chose to make model comparisons with growth rate data from a single source representing a wide range in growth rate, K_{max}, and material properties. This choice, while restricting the base from which conclusions could be drawn, should have served to eliminate sources of variation such as testing machine and specimen dimensions.

Growth rate data for 4340 steel [*23*] representing four conditions of heat treatment are shown in Fig. 3. The plotting position on the abscissa for spheroidized 4340, designated 1400 F in Table 3, was chosen to reflect the strength of this material rather than a single treatment temperature. For K_{max} levels below 40 ksi$\sqrt{\text{in.}}$ crack rate decreases continuously as tempering temperature increases. For K_{max} levels above 40 ksi$\sqrt{\text{in.}}$ curves connecting

TABLE 3—*Fabrication of steel test specimens.*

	Alloy Composition, wt. %								
Alloy	C	Mn	P	S	Si	Cr	Mo	V	Ni
4340..	0.40	0.72	0.011	0.014	0.33	0.84	0.23	...	1.72
4330..	0.34	0.50	0.012	0.011	0.22	1.15	0.58	0.13	3.08

NOTE—*Heat Treatment*

4340: Austenitize 1500 F for ½ h, oil quench; temper for 2 h at 200, 500, 1000, and 1400 F (held at 1400 for 2 h, furnace-cooled to 1210 and held for 8 h, then air-cooled; designated as Spheroidized 4340).

4330: Austenitize 1550 F for 2 h, oil quench; temper for 4 h, then water quench at 600, 800, 900, 1000, 1050, 1200, 1275, and 1300 F.

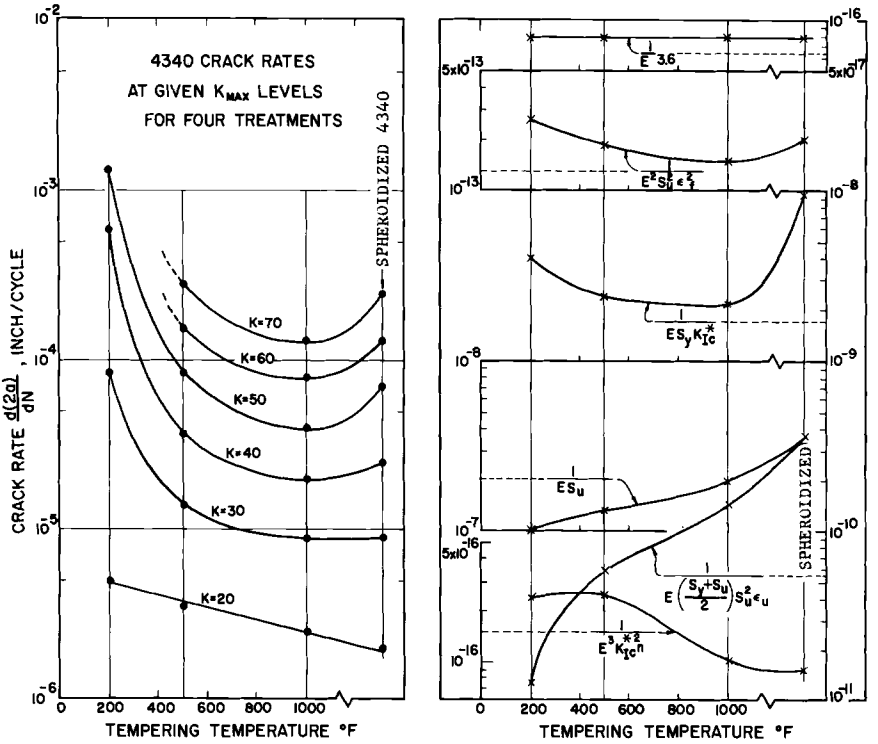

FIG. 3—*Crack rates in center-cracked plate specimens of 4340 steel at several* K *levels and* C *functions are plotted versus the tempering temperature. At high* K *levels these show that minimum rates correspond to the 1000 F temper.*

growth rates for the various heat treatments have a minimum in the rate at about 1000 F. This minimum becomes more sharply defined as the K_{max} level increases from 40 to 70 ksi$\sqrt{\text{in.}}$ The accentuation of the minimum as K_{max} increases stems from the fact that the m exponents were not constant but also reached a minimum value at 1000 F. For the 200, 500, 1000, and 1400 F treatments the m values [*23*] were 6.73, 3.29, 3.17, and 3.95, respectively.

At the right in Fig. 3 the various C expressions are plotted as a function of tempering temperature for the four heat treatments of 4340 steel. The expression $(E^3 K^{*2}_{Ic} n)^{-1}$, where K^*_{Ic} denotes fracture toughness values based on specimens too thin to satisfy plane strain conditions [*23*], describes a continuous decrease in growth rate with increasing tempering temperature, a trend which agrees with the data for K_{max} levels less than 30 ksi$\sqrt{\text{in.}}$ For the higher K levels the variation of observed crack rate with tempering temperature is in accord with the $(ES_u \epsilon_f)^{-2}$ from McClintock's model [*12*] and the $(ES_y K^*_{Ic})^{-1}$ that we suggested. Both expressions describe the trend of the

data from the 200 to the 1400 F condition, with a minimum in the rate at about 1000 F. In plotting McClintock's expression we have assumed that the region of structural size, ρ, is independent of the treatment temperature. If ρ is related to the substructure [*11*], this assumption may be invalid because the substructure would be influenced by the treatment. On the other hand, if ρ is a function of the density of inclusions [*12*], the assumption would seem to be reasonable. The other expressions are either insensitive to the property changes from the treatments, such as $(E)^{-3.6}$, or have the wrong trend for describing these experimental results for the 4340 steel.

Our interpretation is that for this alloy the minimum crack rate is obtained by minimizing either $(ES_u\epsilon_f)^{-2}$ or $(ES_yK^*_{Ic})^{-1}$ and that the dependence of crack rate upon material properties is approximated by either expression, with the latter being the more sensitive indicator. It is noteworthy that the minimum in rate at 1000 F closely corresponds to the 1050 F temper, which was referred to in discussing Fig. 1 as that temper providing the best combination of strength and crack tolerance under static loads. As suggested by the above expressions, for a given material, minimum crack rate should correspond to the maximum product of tensile strength and true strain at fracture or to the maximum product of yield strength and fracture toughness. Since many product designs are concerned with elastic behavior and the prevention of brittle fracture, we believe the latter expression should be used whenever fracture toughness data are available. The criterion for optimum fatigue crack resistance is thereby defined as the combination of high elastic modulus, high yield strength, and high fracture toughness, the maximum product of which should result in a low rate of fatigue crack propagation.

Optimization of Cracking Resistance for 4330 Steel

An additional test of the utility of $(ES_u\epsilon_f)^{-2}$ and $(ES_yK_{Ic})^{-1}$ in predicting the fatigue crack growth resistance of a material is provided by some preliminary data on a modified 4330 martensitic steel. The relation between mechanical properties and tempering temperature for this grade differ somewhat from that of 4340 steel because of the difference in composition. The alloy composition and the heat treatments used are shown in Table 3.

Specimens of modified 4330 steel were made from sections taken from a large forging heat-treated prior to final machining. Plots of yield strength and crack toughness, evaluated at room temperature, versus tempering temperature are shown in Fig. 4. The yield strength, S_y, was evaluated at 0.1 percent offset and the crack toughness, K^*_{Ic}, was evaluated using the secant load from specimens evaluated for compact tension in accordance with ASTM Proposed Method of Test for Plane Strain Fracture Toughness of Metallic Materials.[4] The symbol K^*_{Ic} is used because the 1-in. specimen thickness was not sufficient for valid K_{Ic} results for some of the test condi-

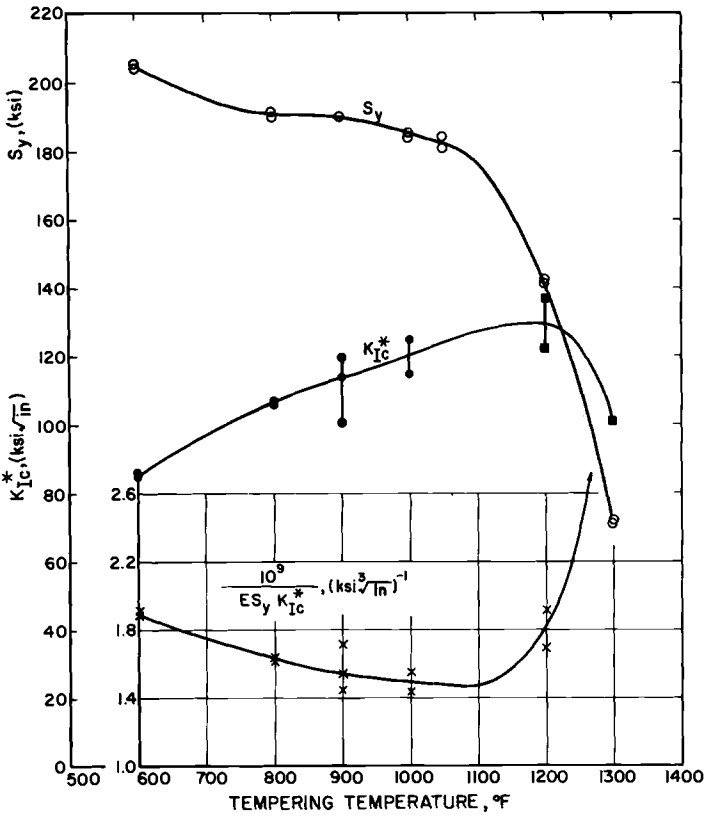

FIG. 4—*Yield strength and fracture toughness versus tempering temperature of modified 4330 steel. The parameter* $10^9/(ES_yK^*_{Ic})$ *appearing in the lower portion of this figure has a minimum value at about 1100 F.*

tions. This applies to the values for tempering temperatures higher than 1000 F. Each plotted point in this figure represents a single test result. The circles represent valid results and the squares represent invalid results.

At the bottom of Fig. 4 is a graph of the quantity $10^9/(ES_yK^*_{Ic})$ plotted for E = 30,000 ksi and values of S_y and K^*_{Ic} obtained from the two upper curves. The crosses show the range in this quantity at each temper. At tempering temperatures over 600 F, the quantity decreases to a minimum at about 1100 F and then rises sharply for tempers of 1200 F and higher.

In Fig. 5 are plots of ultimate strength S_u and percent reduction of area versus tempering temperature of the 4330 steel. Each plotted point represents a single test result. At the bottom of the figure is a graph of the quantity $10^{13}/(ES_u\epsilon_f)^2$, representing the C expression from the McClintock model, plotted for E = 30,000 ksi and values of S_u and $\epsilon_f = \ln [1/(1 - RA)]$ obtained

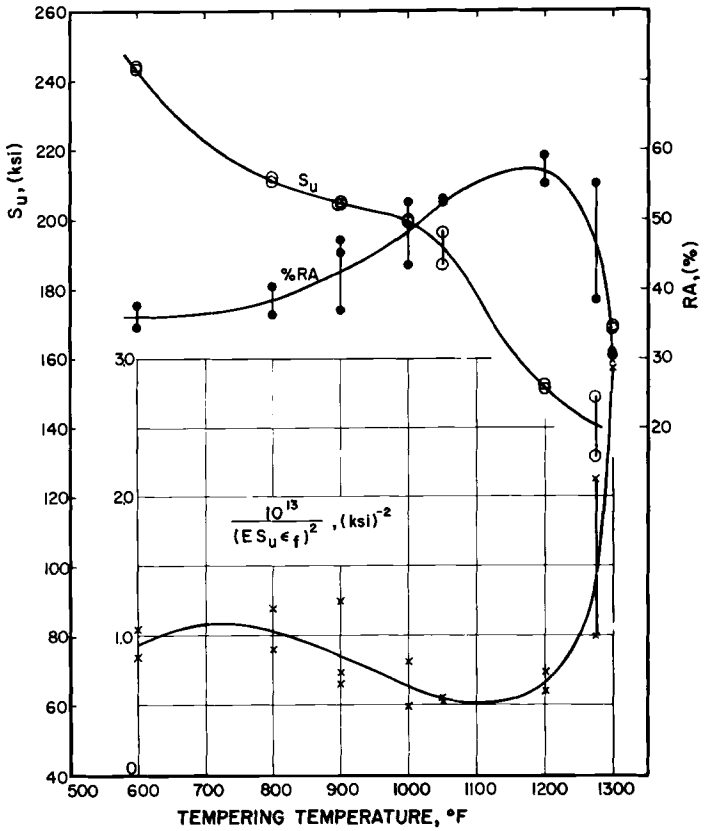

FIG. 5—*Ultimare strength and percent R.A. versus tempering temperature of modified 4330 steel. The parameter* $10^{13}/(ES_u\epsilon_f)^2$ *appearing in the lower portion of this figure has a minimum value at about 1100 F.*

from the two upper curves. The crosses show the range in the quantity at each temper. At tempering temperatures over 600 F, the curve rises somewhat, falls to a minimum at about 1100 F, and then rises sharply for tempers of 1200 F and higher.

The variation of these two functions of the static test results with tempering temperature in the 4330 steel is similar to that for the 4340 steel, but in this case their minimum values correspond to about an 1100 F tempering temperature. This variation suggests that optimum fatigue crack resistance is to be obtained by tempering the 4330 steel at about 1100 F. A test of this prediction is provided by data taken in zero-to-tension loading of ASTM compact tension specimens of 1-in. thickness at 5 cycles per second (Fig. 6).

Fatigue Crack Rate in 4330 Steel

Values of da/dN from the ASTM compact tension specimens at K_{max} levels ranging from 30 to 80 ksi$\sqrt{\text{in.}}$ are indicated by different symbols in Fig. 6. Data are not yet available for the 1100 F temper, but it appears from the graph that minimum crack rates will be found between 1050 F and 1150 F. Rates on either side of this range, especially for K_{max} levels of 50 ksi$\sqrt{\text{in.}}$ and higher, are greater than the values measured at 1050 F temper. (Data obtained subsequent to paper submission show that the minimum in crack rates corresponds to 1125 F tempering temperature, see Table 4.)

TABLE 4—*Crack growth rate of 4330 steel, 1125 F tempering temperature.*

				Crack Rate, in./cycle, at K_{max} =				
K^*_{Ic}, ksi$\sqrt{\text{in.}}$	S_y, ksi	S_u, ksi	R.A., %	30	40	50	60	70
122.0	153.0	162.0	49.8	...	...	12.6×10^{-6}	39.5×10^{-6}	60×10^{-6}
129.0	150.9	157.9	55.3	8.4×10^{-6}	21.0×10^{-6}	...	...	...

Most of the data represent room temperature results. Performance at low temperatures is also important and some results are shown for the 1050 F temper at −40 and −65 F achieved by immersion of specimens in alcohol and dry ice. These low-temperature crack rates do not differ greatly from the room temperature values for this temper. This finding could be of special importance because it indicates that optimizing crack rate through control of room temperature mechanical properties may also serve to provide good crack growth resistance at other test temperatures, an observation suggested earlier in discussing Fig. 1 for 4340.

The curves in Fig. 6 were constructed from equations expressing the *expected* form of crack rate versus tempering temperature for various K levels in the 4330 steel. The equations are used to illustrate the expected trends in this case because the 4330 data are incomplete. The solid curves represent the McClintock model expression $da/dN = 70\,(ES_u\epsilon_f)^{-2}K_{max}{}^4$. The exponent $m = 4$ is specified by the model, and the constant 70 was obtained from the average crack rates at K levels of 50 and 60 ksi$\sqrt{\text{in.}}$ for the 1050 F tempering temperature. The dashed curves represent the equation $da/dN = 0.020\,(ES_yK^*_{Ic})^{-1}K_{max}{}^{3.5}$. The exponent $m = 3.5$ was selected because this is the average for the data shown in Fig. 2. The constant 0.020 was obtained from the average crack rates at K_{max} levels of 50 and 60 ksi$\sqrt{\text{in.}}$ for the 1050 F tempering temperature.

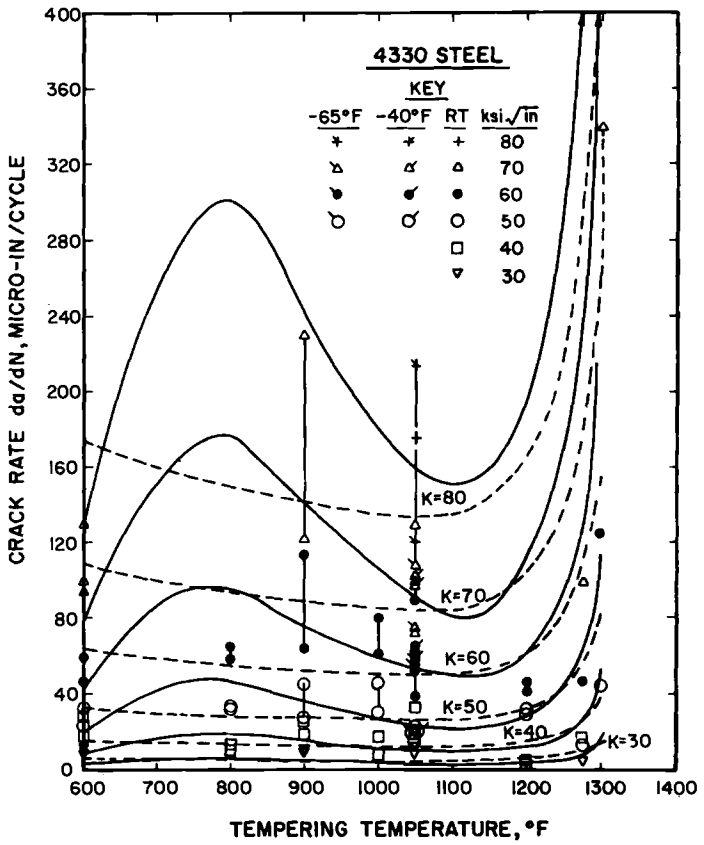

FIG. 6—*Crack rate* da/dN *versus tempering temperature for 1-in.-thick compact tension specimens of modified 4330 steel. Dashed curves represent the expression* $da/dN = 0.020 (ES_yK^*_{Ic})^{-1}(K_{max})^{3.5}$; *solid curves represent* $da/dN = 70(ES_{u\epsilon_f})^{-2}K_{max}^4$.

These curves and the data indicate that tempering temperature has little effect on growth rate for K_{max} levels below 40 ksi$\sqrt{in.}$; consequently, test results at relatively high K levels will be required to evaluate the effects of various treatments on crack rate. Comparison of the curves with the data indicates that both equations are in reasonable accord with the data in the tempering range from 1050 to 1300 F and that a minimum in rates is evident at about 1100 F. The equation from McClintock's model predicts the high crack rates experienced in the tempering range from 800 to 900 F, while the equation we propose does not. It may possibly be the case that some specimens tempered in this range incurred temper embrittlement and that this is reflected more strongly by $(S_u\epsilon_f)^{-2}$ in the former expression than by $(S_yK^*_{Ic})^{-1}$ in the latter expression. The latter has a somewhat better agreement with measured crack rates at the low temper of 600 F and at the higher tempers from 1050 to 1300 F.

Completion of more tests at higher K levels for the appropriate tempers will undoubtedly aid the interpretation of this comparison. Our purpose here, however, is not to present completed experimental results but rather to illustrate and test a concept for optimizing fatigue crack resistance.

Summary

This study supports the view that for certain levels of the stress intensity factor K the fatigue crack resistance of a material is related to other mechanical properties. Data representing 4340 and modified 4330 steel show that for K_{max} levels below the range of 30 to 40 ksi$\sqrt{\text{in.}}$ substantial differences in mechanical properties, resulting from tempering at different temperatures, have little influence on crack growth rate. However, for K_{max} levels greater than 40 ksi$\sqrt{\text{in.}}$, useful indexes of crack growth rate are provided by the parameters $(ES_yK_{Ic})^{-1}$ and $(ES_u\epsilon_f)^{-2}$, where E is Young's modulus, S_y is yield strength, S_u is tensile strength, ϵ_f is the true strain at fracture, and K_{Ic} is the plane strain fracture toughness.

At high K levels the optimum fatigue crack resistance, namely the minimum fatigue crack growth rate, is provided by tempering 4340 and modified 4330 steel at temperatures of 1000 F and 1100 F, respectively. The condition for minimum fatigue crack rate may be predicted from static test results for these alloys from the variation of the quantities $(ES_yK^*_{Ic})^{-1}$ and $(ES_u\epsilon_f)^{-2}$ with tempering temperature. It is hoped that other investigators find these expressions useful for other metals and alloys as well.

Acknowledgments

We gratefully acknowledge the technical assistance of J. J. Miller in metallurgical control, of R. R. Fujczak in testing and data analysis, and of D. J. Corrigan in crack growth experiments.

References

[1] Paris, P. C., "A Note on the Variables Affecting the Rate of Growth Due to Cyclic Loading," Boeing Co. Document No. D-17867, Addendum N, Sept. 1957.
[2] Paris, P. C. and Erdogan, F., *Journal of Basic Engineering*, American Society of Mechanical Engineers, JBAEA, Vol. 85, 1963, p. 528.
[3] Paris, P. C., "Crack Propagation Caused by Fluctuating Loads," ASME Paper No. 62-MET-3, American Society of Mechanical Engineers, ASMSA, 1962.
[4] Head, A. K., *Philosophical Magazine*, PHMAA, Vol. 44, 1963, p. 925.
[5] Frost, N. E. and Dugdale, D. S., *Journal of Mechanics and Physics of Solids*, JMPSA, Vol. 6, 1958, p. 92.
[6] McEvily, A. J. and Illg, W., "The Rate of Crack Propagation in Two Aluminum Alloys," NACA Technical Note 4394, National Advisory Committee for Aeronautics, NACNA, Sept. 1958.
[7] Weibull, W., *Acta Metallurgica*, AMETA, Vol. 11, 1963, p. 745.
[8] Liu, H. W., *Applied Materials Research*, AMRSA, Vol. 3, 1964, p. 229.
[9] Krafft, J. M., *Transactions Quarterly*, American Society for Metals, ASMQA, Vol. 58, 1965, p. 691.

[10] McEvily, A. J. and Johnston, T. L., "The Role of Cross Slip in Brittle Fracture and Fatigue," *Proceedings*, First International Conference on Fracture, Sendai, Japan, 1966.

[11] McClintock, F. A., "On the Plasticity of the Growth of Fatigue Cracks," *Fracture of Solids*, D. C. Drucker and J. J. Gilman, Eds., Interscience Publishers, New York, 1963, p. 65.

[12] McClintock, F. A., discussion of paper by C. Laird, "The Influence of Metallurgical Structures on the Mechanism of Fatigue Crack Propagation," *Fatigue Crack Propagation, ASTM STP 415*, American Society for Testing and Materials, 1967, pp. 170–174.

[13] Pearson, B. S., *Nature*, NATUA, Vol. 211, 1966, pp. 1077–1078.

[14] Krafft, J. M., discussion of paper by R. P. Wei et al, "Fatigue Crack Propagation in Some Ultrahigh-Strength Steels," *Fatigue Crack Propagation, ASTM STP 415*, American Society for Testing and Materials, 1967, pp. 483–484.

[15] Frost, N. E. and Dixon, J. R., *Nature*, NATUA, Vol. 212, 1966, pp. 1569–1570.

[16] Hays, L. E. and Wessel, E. T., *Applied Materials Research*, AMRSA, Vol. 2, April 1963, pp. 99–108.

[17] Forman, R. G., Kearney, V. E., and Engle, R. M., "Numerical Analysis of Crack Propagation in Cyclic-Loaded Structures," ASME Paper No. 66-WA-MET-4, American Society of Mechanical Engineers, ASMSA, 1966.

[18] Johnson, R. E., "Application of Fracture Mechanics to Fatigue Failure Prevention," presented at the 1969 Spring Meeting of the Metallurgical Society of AIME, Pittsburgh, Pa., 12 May 1969, abstract in *Journal of Metals*, JOMTA, March 1969, p. 16A.

[19] Wilhelm, D. P. in *Fatigue Crack Propagation, ASTM STP 415*, American Society for Testing and Materials, 1967, pp. 363–380.

[20] Carman, C. M. and Katlin, J. M., "Low-Cycle Fatigue Crack Propagation Characteristics of High Strength Steels," ASME Paper No. 66-MET-3, American Society of Mechanical Engineers, ASMSA, 1966.

[21] Brothers, A. J. and Yukawa, S., *Journal of Basic Engineering*, American Society of Mechanical Engineers, JBAEA, Vol. 89, 1967, p. 19.

[22] Heiser, F., "Anisotropy of Fatigue Crack Propagation in Hot-Rolled Banded Steel Plate," Report No. WVT-6931, Benet Laboratories, Watervliet Arsenal, N. Y., Oct. 1969.

[23] Miller, G. A., *Transactions Quarterly*, American Society for Metals, ASMQA, Vol. 61, 1968, pp. 442–448.

[24] Hanna, G. L. and Steigerwald, E. A., "Influence of Work Hardening Exponent on Crack Propagation in High-Strength Materials," Technical Report AFML-TR-66-139, Air Force Materials Laboratory, Dayton, Ohio, May 1966.

[25] Anctil, A. A. and Kula, E. B., "Fatigue Crack Propagation in 4340 Steel as Affected by Tempering Temperature," Technical Report AMMRC-TR-69-15, Army Materials and Mechanics Research Center, Watertown, Mass., June 1969.

[26] Weber, J. H., "Effects of Crystallography and Thermomechanical Treatment on Fatigue Crack Propagation," PhD dissertation, Lehigh University, Bethlehem, Pa. 1969.

[27] Donaldson, D. R. and Anderson, W. E., "Crack Propagation Behavior of Some Airframe Materials," Cranfield Crack Propagation Symposium, Cranfield, England, 1961, pp. 375–442.

[28] Smith, S. H., Porter, T. R., and Sump, W. D., "Fatigue and Fracture Toughness Characteristics of 7079 Aluminum Alloy Sheets and Plates in Three Aged Conditions," NASA CR-996, National Aeronautics and Space Administration, Washington, D. C., Feb. 1968.

F. G. Ostermann[1] *and W. H. Reimann*[1]

Thermomechanical Processing and Fatigue of Aluminum Alloys

REFERENCE: Ostermann, F. G. and Reimann, W. H., "**Thermomechanical Processing and Fatigue of Aluminum Alloys,**" *Achievement of High Fatigue Resistance in Metals and Alloys, ASTM STP 467*, American Society for Testing and Materials, 1970, pp. 169–187.

ABSTRACT: A review is made of the available information on thermomechanical processing of aluminum alloys, especially with respect to their fatigue behavior. An attempt is made to evaluate from the scarce and sometimes contradictory experimental evidence the possibility of improving the fatigue resistance of high-strength aluminum alloys by these treatments. To do so, it is also necessary to review the important microstructural features and deformation characteristics of these alloys, which seem to control the various stages of fatigue, and which may be influenced by the thermomechanical treatments. The discussion is limited to thermomechanical treatments subsequent to solution annealing. It is concluded that suitable processing offers the advantage of improving both strength and ductility in Al-Cu and Al-Zn-Mg-Cu alloys. If the effects of inclusions can be minimized, significant benefits are possible in fatigue, at least in Stage I crack resistance, by thermomechanical processing.

KEY WORDS: mechanical properties, fatigue (materials), fatigue tests, deformation, aluminum alloys, evaluation, microstructure, process variables, heat treatment

For aluminum alloy applications in aircraft structures the problem of fatigue response is second in importance only to stress corrosion; thus, there exists a considerable impetus to improve the fatigue resistance of these alloys. In the past, aluminum alloy development has concentrated successfully on the achievement of high static strength, but has resulted in little improvement in fatigue properties. At present, there seems to exist no well-defined approach to improve the fatigue resistance by compositional changes. Another approach to the problem of fatigue improvement is the use of thermomechanical treatments. It is the object of this paper to review the possibilities of applying this approach to the age-hardened aluminum alloys.

[1] Materials research engineers, Air Force Materials Laboratory, Wright-Patterson Air Force Base, Ohio 45433.

Thermomechanical processing can be conveniently divided into two classes —high-temperature and low-temperature processing. High-temperature thermomechanical processing may be defined as working in or near the recrystallization temperature range to achieve a hot-worked structure which is largely retained during the subsequent thermal treatments for age-hardening alloys and which will interact with the aging processes. The improved fatigue strength of extrusions of certain aluminum alloys is an example of the possible beneficial influence of high-temperature thermomechanical processing [*1*, *2*].[2] The avoidance of recrystallization when working at low and medium temperatures necessarily limits the temperature for subsequent thermal treatments. For age-hardening aluminum alloys, low-temperature thermomechanical processing is usually applied after solution annealing and is characterized by working prior to or during the aging cycle. At present, low-temperature working after solution annealing and quenching is predominantly done for dimensional control rather than for the achievement of a suitable microstructure, and it appears worthwhile to exploit the low-temperature processing in this latter respect.

To develop fatigue-oriented thermomechanical treatments for age-hardening aluminum alloys it is at first necessary to consider the various processes that participate in the development of fatigue damage, to examine the influence of the existing microstructure on each of the stages involved, and to isolate from this evidence the important features which appear to control each stage. It is further necessary to understand the structural conditions basic to high-strength, age-hardened aluminum alloys and to know their deformation characteristics. This task will be attempted in the next section. The published information on thermomechanical treatments of age-hardened aluminum alloys is very scant and sometimes contradictory. What is available and relevant will be discussed in the section on thermomechanical processing. It will become apparent that most of the work concerned with thermomechanical processing of aluminum alloys hardly explores the full potential of this method, which lies in the possibility of changing the common strength-ductility relationship. Such a change probably reflects significant alterations of the strengthening and deformation mechanisms and should affect both static and dynamic properties.

Age-hardening, Deformation, and Fatigue

Vast efforts have been devoted to research and development of age-hardened aluminum alloys and several extensive reviews of this subject are available [*3–7*]. Since the behavior of the age-hardened aluminum alloys during thermomechanical processing depends on both the decomposition reactions

[2] Italic numbers in brackets refer to the list of references at the end of this paper.

and the deformation mechanisms, a thorough understanding of both is a necessary prerequisite. Obviously, however, such a detailed review is outside the intent of this volume and only a brief summary of the most salient points will be made here. An extended review by the present authors can be found elsewhere [*8*].

It has been found that for most alloys, the observed age-hardening phenomena are based on nonequilibrium decomposition reactions involving one or more, often sequential, steps. In general, the type and kinetics of decomposition reactions of a supersaturated alloy matrix depend strongly on temperature. At or near room temperature, decomposition of aluminum-copper (Al-Cu) and aluminum-zinc-magnesium (Al-Zn-Mg) alloys proceeds by the formation of Guinier-Preston (G-P) zones. Yield and ultimate strength values increase with aging time, and fracture elongation remains relatively unaffected [*6*, *9*, *10*]. G-P zone formation (the "natural aging" process) can also occur at elevated temperatures prior to the onset of precipitation or "artificial aging." The presence of inflection points in the age-hardening curves may be cited as evidence of this [*9*]. In contrast to aging by coherent G-P zone formation, artificial aging is characterized by precipitation of "intermediate" phases that are generally semicoherent with the matrix and may constitute a transition phase to the equilibrium precipitate phase. Artificial aging produces higher strength characteristics and is generally accompanied by a pronounced increase in yield strength to ultimate strength ratio and by a significant loss in fracture elongation.

The aging reactions and structural changes during aging depend strongly on the alloy system and alloy composition. In the following paragraphs a brief description is given of the reactions occurring in the Al-Cu and Al-Zn-Mg systems, since these two systems form the bases of the commercial heat-treatable alloys of interest here. It will be shown in the section on processing that the different responses of these two alloy systems to thermomechanical treatments are a direct result of differences in precipitation behavior.

In the aluminum-copper alloys [*3–5*, *11–13*], hardening during natural aging is caused by G-P I zones, which form spontaneously after quenching at room temperature and can already be detected by X-ray diffraction techniques after only 15 min of aging. G-P I zones can exist at temperatures below 200 C although their numbers decrease above 130 C. Depending on the model derived from X-ray diffraction, G-P I zones are segregations of one [*14*, *15*] or a few [*7*, *16*] layers of copper atoms on {100} matrix planes in complete coherence with the aluminum lattice. The lateral size of the zones depends on aging temperature and ranges from 40 Å at room temperature to 100 Å at 130 C [*5*, *14*, *15*, *17*].

Artificial aging involves the following decomposition sequence: solid solution $\rightarrow \theta'' \rightarrow \theta' \rightarrow \theta$ ($CuAl_2$), although the various stages are overlapping. In the

highest strength condition Al-Cu alloys are essentially strengthened by θ'' [*18*] and much less by θ', while the stable θ phase is relatively unimportant for age hardening. However, the fraction of θ' relative to the total of the decomposition products increases as the aging temperature approaches the limit of existence of θ''.

The structure of θ'' is not fully known but it is characterized by a periodic stacking of monatomic copper layers parallel to the cube face of the aluminum matrix with which it is completely coherent [*19*]. The θ'' particles have a thickness to diameter ratio of 1:10, and at 150 C they obtain thicknesses of 10 to 40 Å [*16*, *20*]. The θ' platelets are coherent on {100} matrix faces and have a diameter of 1000 Å and a thickness of 100 to 300 Å during aging at 200 C [*21*, *22*] but grow to larger dimensions at higher aging temperatures.

In the Al-Zn-Mg system two types of G-P zones have been observed during natural aging depending on the Zn:Mg ratio [*23*, *24*]. Both types of zones have an arrangement of Zn and Mg atoms such that the overall atomic size misfit is minimized and the zones take on a spherical shape. The lattice distortions limit the size of G-P zones in the Mg-rich alloys to less than 50 Å. At aging temperatures above 100 C the zones start to disappear [*24*, *25*, *26*, *27*] and revert completely at 175 C.

At temperatures above room temperature the decomposition process is characterized by the formation of $\eta(MgZn_2)$. Hardening appears to be related to the intermediate phase η' or the nuclei of the η phase [*24*, *26–33*]. The η' phase is coherent with the lattice on {111} planes and has a platelet shape. The η phase forms from the η' phase after loss of coherency but retains the original orientation relationship.

There is a discrepancy between X-ray diffraction and electron microscopy observations regarding the existence of G-P zones and their importance for hardening during artificial aging. To reconcile the disagreement it has been suggested [*5*] that the apparent G-P zones observed by transmission electron microscopy [*31*, *33*] during aging at or above 120 C are either nuclei of the η phase or the initial stage of η' formation. It appears that the maximum hardness obtained above room temperature is essentially caused by η' or an early stage of η phase formation, which is in agreement with the previously mentioned aging phenomena [*9*] at elevated temperatures, for instance, inflection points in the age-hardening curves, decrease of fracture elongation.

Plastic deformation in these age-hardened aluminum alloys is markedly nonhomogeneous. Aging inhomogeneities lead to the formation of precipitate-free zones along grain boundaries, and slip will therefore concentrate into these regions [*31*]. However, in addition to slip concentrations resulting from the presence of precipitate-free zones, slip may also be concentrated by precipitate-dislocation interactions. In order to become active a dislocation source must first shear through the existing precipitate structure. Once

sheared, the second-phase particles offer considerably less resistance to dislocation motion. It is therefore energetically favorable for the following dislocations to remain on these same glide planes than to initiate elsewhere in the matrix.

Most of the fundamental studies of plastic deformation in age-hardened aluminum alloys have been done on the relatively simple Al-Cu system [*34*, *35*]. However, the work of Speidel [*36*] and Jacobs [*37*] shows that the same influences exist in commercial SAE 7075.

It is well known that the fatigue strengths of high-strength, age-hardened aluminum alloys are inherently poor in relation to their static strengths. Unfortunately, however, the relationship between the fatigue processes and the microstructure in these alloys is not clearly understood owing to the complexity of the metallurgical structure and the fineness of the precipitate (approaching the limit of resolution of the electron microscope). In addition, if the aluminum alloys are considered in general, it will be seen that while the static strengths show considerable variations, the fatigue strengths remain fairly constant, particularly in the notched condition [*38*]. This suggests that a relationship between static and dynamic behavior is not straightforward but must be sought by more subtle considerations.

The poor performance of the aluminum alloys in fatigue has generally been attributed to the presence of "soft" regions at grain boundaries and throughout the matrix in which the fatigue deformation can take place. The precipitate-free zones along grain boundaries are formed by solute or vacancy denudation, while the formation of these zones within the matrix has been attributed to either overaging [*39*, *40*] or reversion [*41*, *42*] taking place during the cyclic stressing. Recently Laird and Thomas [*43*] have demonstrated that these soft matrix regions can exist prior to cycling as a result of aging inhomogeneities. Some care should be exercised, however, in extrapolating the observations from simple laboratory-prepared binary and ternary alloys to commercial alloys in which precipitate-free zones are less marked, presumably due to the beneficial nucleating effects of the impurity and trace elements present.

From a review of the general mechanisms of fatigue,[3] and of some specific aspects of fatigue of aluminum alloys, one may attempt to isolate the important features controlling the development of each stage of fatigue of age-hardened aluminum alloys in two categories: microstructural features and fundamental deformation characteristics. We have attempted to do this in Table 1. Obviously, the whole fatigue process will be influenced by such external conditions as stress range and environment for example, but these considerations are outside the intent of the table. Likewise, the influence of

[3] For a review of the basic mechanisms of fatigue, see paper by Feltner and Beardmore, pp. 77–112.

surface condition has not been considered in the initiation stage. In cases where a single feature may influence more than one stage of the fatigue process (as in the case for inclusions, for example), we have tried to indicate its most critical influence.

TABLE 1—*Correlation of fatigue stages with microstructure and deformation characteristics.*

Fatigue Stage	Microstructural Features	Fundamental Deformation Characteristics
Initiation	heterogeneities (inclusions, precipitate-free zones) grain boundaries	slip mode, cyclic elastic limit (high-cycle fatigue)
Stage I propagation	cell structures slipband formation grain size (high-cycle fatigue)	slip mode dynamic recovery homogeneous deformation
Stage II propagation	hardness heterogeneities	gross plastic behavior (work hardening capacity, ductility, fracture toughness)

In the commercial aluminum alloys [*44*] inclusions are known to play a dominant role in crack nucleation. Their importance in nucleation probably relates to three factors: in the first place, a hard inclusion can act as a stress concentrator thereby localizing deformation in much the same way as a notch; secondly, debonding may occur along the inclusion-matrix interface; and thirdly, the relative brittleness of intermetallic compounds allows the possibility of precracking during forming operations. In addition to their effect on nucleation, inclusions can also increase the rate of Stage II propagation by nucleating cracks ahead of the main advancing crack [*45*, *46*]. Grosskreutz et al [*47*] have also demonstrated the importance of inclusions by a laboratory-prepared, inclusion-free 2024 alloy. Their results showed significant improvements in the fatigue strength of this alloy over the normal 2024. Similar improvements had been reported earlier by Brenner [*48*].

The recent work of Feltner and Laird [*49*, *50*, *51*] has reemphasized the importance of slip mode on the development of fatigue cracks. Materials with a planar slip mode show inherently better fatigue properties than those materials exhibiting wavy-type slip. In planar slip materials the lower stacking fault energy inhibits the ease of cross slip and, by preventing the formation of sharp surface discontinuities, extends the initiation and Stage I phases of crack development. The apparent sharpness of slip observed on the surface of deformed aluminum alloys [*34*, *37*] is deceptive and does not mean that the aluminum alloys deform by a planar slip mode. Detailed transmission electron microscopy studies [*36*] reveal that these bands consist of dense

patches of very short dislocations indicative of a large amount of localized cross slip within the bands. This localization of slip possibly results from difficulties in initiation, as described earlier in this section.

It is also worthwhile to elaborate on what we have termed the cyclic elastic limit. For fatigue damage to accumulate, plastic deformation must occur, at least on a local scale. There is a tendency to overlook the microplastic straining that takes place below the conventional 0.2 percent yield stress. Its importance in high-cycle fatigue can be readily seen by the fact that the endurance limit (10^8 cycles) of most high-strength aluminum alloys occurs below the 0.2 percent yield stress, even in high-purity alloys where inclusions would not dominate. Clearly, then, these microstrains are still sufficient to build up enough damage to initiate and propagate a fatigue crack. It follows that an increase in the 0.2 percent yield stress without an equivalent increase in the true elastic limit will not result in improved fatigue strength. This may perhaps explain the similarities of the fatigue strengths in age-hardened aluminum alloys.

It is also necessary to consider the variation of the elastic limit with cyclic deformation, that is, cyclic strain hardening (or softening). In materials showing a high rate of work hardening, the mobile dislocations are rapidly pinned and the elastic limit will increase. This is also important in explaining the improved fatigue performance of materials in which cross slip is difficult. Confining dislocations to their original glide planes would be of no advantage unless the dislocations could be locked (and in so doing, tend to deactivate the source). It is interesting to note here, too, that the aluminum alloys showing the highest fatigue ratio, that is, the ratio of endurance strength to ultimate strength, are the alloys capable of showing strain aging [*40*]. Here the cyclic elastic limit could be expected to be relatively high.

In Stage I crack propagation the controlling factor becomes essentially the degree of homogeneity of deformation. A highly heterogeneous deformation structure (slipbands, cell walls) will provide paths along which Stage I growth will be facilitated. In this view, a material capable of a high degree of dynamic recovery would be expected to behave poorly in fatigue, since the recovery accelerates the formation of intense cell walls.

It is important here to distinguish between homogeneous structure and homogeneous deformation. The production of a more homogeneous structure in the age-hardened aluminum alloys will not be of any benefit in fatigue unless the accompanying deformation is also homogenized. The structure must be stable enough to resist reversion or overaging that could again lead to localized softening.

In Stage II crack propagation, attempts to relate the behavior to microstructural details have not been too successful because of the gross plastic yielding taking place immediately ahead of the advancing crack. However,

heterogeneities such as precipitate-free zones and inclusions will influence the crack growth by providing preferential sites. Most empirical equations for Stage II crack growth have attempted to relate the process to the parameters listed, and these are essentially the parameters that influence the plastic behavior of the material (see, for example, Refs *52* and *53*). The exact relationship is, however, still far from clear, the main problem being to engineer definitive experiments in which the parameters can be independently varied.

The value of a table such as that given here must lie in its ability to point the way towards improvements in the fatigue performance of the material being considered. From the analysis shown here, it would appear that a good place to concentrate a fatigue improvement effort for the aluminum alloys would be on the parameters controlling Stage I crack growth. This stage depends essentially on the degree of heterogeneity of the microdeformation, and, if techniques such as thermomechanical processing are to be successful in improving fatigue strengths, this is the aspect they must improve.

Thermomechanical Processing

The discussion of thermomechanical processing in this section is limited to low-temperature processing as defined in the introduction. The temperature range required for mechanical working and heat treatments comprises temperatures up to common aging temperatures that do not induce recrystallization. Most of the available information on low-temperature thermomechanical processing effects, however, is concerned with working at room temperature.

In general terms, any combination of mechanical deformations and thermal treatments during the final processing of age-hardened aluminum can be considered thermomechanical processing. In this respect the common straightening or mechanical stress-relieving operations, which involve only a few percent of plastic deformation prior to natural or artificial aging, must be regarded as thermomechanical treatments, although the influence of such operations on the mechanical properties is generally negligible. A well-known exception are the alloys of the Al-Cu system, which respond to deformations prior to artificial aging with considerable strength increases. For example, the yield strength of 2024-T6 aluminum can be increased from 57,000 to 71,000 psi by a 6 percent cold reduction between solution annealing and artificial aging [*54*]. A thermomechanical treatment of this type, which derives some strength benefits from the working operation, has been given the T8 temper designation.

The high-cycle fatigue properties of many commercial age-hardened aluminum alloys in various tempers, including the T8 temper condition, have been obtained and reviewed by Lyst [*55*]. The data reveal a total lack of sensitivity of the fatigue strength of both smooth and notched specimens to the thermo-

mechanical T8 treatment. More recently, however, Krause and Laird [*56*] have found a considerable improvement of the fatigue strength of a high-purity, binary Al-4Cu alloy, which was swaged 31 percent after solution annealing and quenching. They showed that the improved fatigue resistance was clearly above the band of data for conventionally treated aluminum alloys. The data of Krause and Laird are reproduced in Fig. 1. The striking similarity between the *S-N* curves of the materials in the aged and unaged conditions was interpreted in terms of two competing mechanisms: in the unaged condition the strength was caused by solid-solution strengthening, which was almost precisely balanced by the strengthening effects of the precipitate phases in the aged condition where the solute atoms were drawn from solid solution. It appears likely, however, that natural aging and possibly strain aging will also be of some influence in the unaged conditions.

The results of Krause and Laird for the high-purity Al-Cu alloy are significant enough to consider the microstructural and deformation characteristics of the thermomechanically treated material in greater detail. The effects of deformation on the aging reactions in binary Al-Cu alloys and the qualitative relationship between the resulting microstructure and static strength properties appear to be well understood [*56–63*]. The uniform dislocation structure

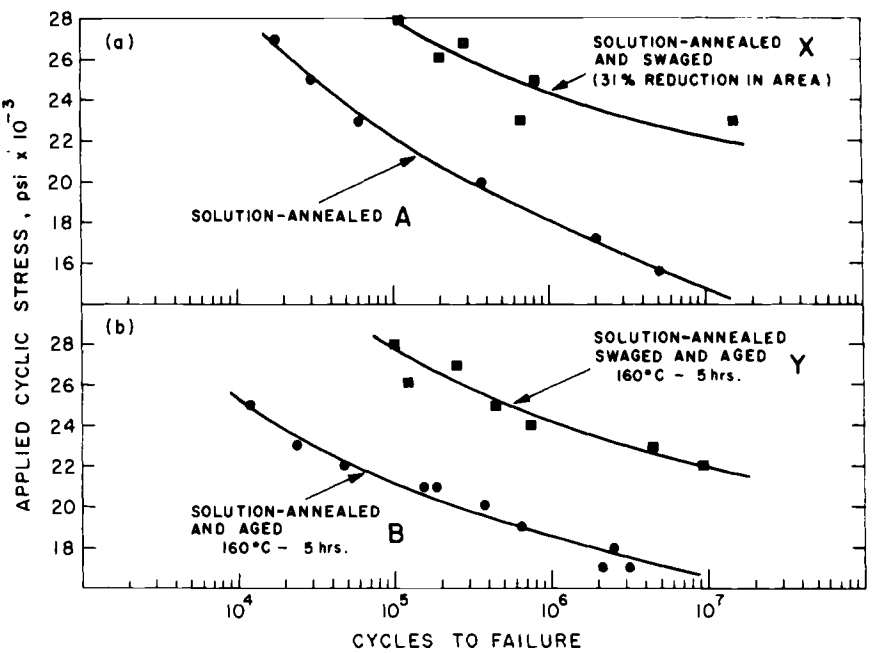

FIG. 1—S-N *curves showing the effects of various thermomechanical treatments on the fatigue properties of Al-4Cu alloy* (*Ref* 56).

after a few percent of plastic deformation of solution-annealed and quenched Al-Cu alloys helps to overcome the nucleation difficulty of the θ' phase and induces a uniform distribution of small θ' platelets during artificial aging. The rate of θ'' formation is decreased due to the reduction of thermal (quenched-in) vacancies by the deformation-induced dislocation structure. The increase in strength properties by this thermomechanical treatment can be safely attributed to the higher density of fine θ' platelets in the structure, which at the same time should be more stable than the θ''-hardened structure. The same observations have been made on commercial alloys of the Al-Cu-Mg system although the details of aging of commercial alloys are not as well documented as for the binary Al-Cu alloys. A comparison of the structures of 2024-T6 and T8 alloys shows that the S′ phase becomes much more uniformly distributed, finer, and more numerous when the alloy is deformed prior to artificial aging [*54*].

Deforming the solution-treated Al-Cu alloys by more than about 15 percent produces dense bands of dislocations in addition to the general dislocation distribution. These bands of highly disturbed lattice serve as nucleation sites for the stable θ phase. Graf [*60*] and von Heimendahl [*58*, *59*] have shown that an inversion of the usual precipitation sequence can occur after large deformations, that is, the stable θ phase can form prior to the intermediate θ' phase. The microstructure of Krause and Laird's thermomechanically treated Al-Cu alloy should therefore contain uniformly distributed θ' and possibly θ particles in deformation bands, whereas the microstructure of conventionally heat-treated Al-Cu material should primarily reveal a high density of zones of θ''. A further important distinction of the thermomechanically treated Al-Cu alloy is the absence of aging inhomogeneities [*56*], which are commonly found in conventionally heat-treated, high-purity alloys as described in the previous section.

The presence of some dispersed θ particles in Krause and Laird's Al-Cu material cannot explain its superior fatigue properties relative to the commercial 2024-T86 data from Lyst's work. Moreover, aging inhomogeneities appear to play a minor role in commercial materials and should be remedied anyway in 2024 aluminum by the T86 treatment. It is likely, then, that an explanation for this difference in fatigue response of the high-purity Al-4Cu and the commercial 2024 alloys to thermomechanical treatments of the T8-type can be found in the overriding detrimental influence of inclusions in commercial material. Work is in progress at the Air Force Materials Laboratory to determine the fatigue properties of a thermomechanically treated, high-purity 2024 aluminum alloy.

The work of Krause and Laird suggests another important effect of the T8-type thermomechanical processing. The strength increase of commercial 2024 aluminum between the T6 and T86 condition is generally accompanied by a

decrease of elongation to fracture. This behavior would be expected from the commonly observed inverse strength-ductility relationship, which also applies to age-hardened aluminum alloys [*48*]. While Krause and Laird did not report fracture elongation, the reduction-in-area values indicate a significant increase in ductility for the thermomechanically treated alloy *despite* the considerable strength increase. This effect may partly be attributed to the lack of aging inhomogeneities in the latter condition and partly to a change in the deformation characteristics. As described in the previous section, Al-Cu alloys as well as other age-hardened aluminum alloys deform in a pseudoplanar mode and exhibit large and straight, narrow slip steps at the surface. In contrast to this behavior, Krause and Laird [*56*] found homogeneous slip with a wavy slipband appearance at larger deformations of thermomechanically treated foil of the same Al-Cu alloy. Perhaps the larger degree of cold-working (30 to 50 percent) in the case of the high-purity Al-4Cu alloy was responsible for this increased ductility and the apparent change in deformation characteristics.

McEvily and co-workers [*64*, *65*] provide some further aspects of this T8-type of thermomechanical processing. Precipitation of the intermediate phase β' in Al-Mg alloys is difficult and heterogeneous [*4*, *66*]. Precipitate-free zones at grain boundaries in Al-Mg alloys have been related to the propensity towards intercrystalline, brittle fracture. Investigating a binary Al-10Mg alloy which was cold-worked 50 percent prior to aging at 200 C, McEvily et al [*64*] found improved static strength and fatigue resistance and a change in fracture mode from brittle intercrystalline to more ductile transcrystalline fracture. A similar change in fracture mode was also observed for an Al-Zn-Mg alloy when cold-worked 50 percent prior to aging at 121 C [*65*]. In this case, the precipitate-free zones at grain boundaries were not entirely removed, instead the grain boundaries became strongly jogged. Due to the cold-working operation there was a small improvement of tensile strength values (about 5 percent) and fatigue resistance of the Al-Zn-Mg alloy; but contrary to the behavior of the thermomechanically processed Al-10Mg alloy, the fracture elongation was less in the T8 than in the T6 condition. In both instances the microstructures became more homogeneous after working and aging by providing nucleation sites at dislocations for the formation of β' and η' in the binary and ternary alloys, respectively. These examples of thermomechanical processing effects serve to illustrate the further possiblity of changing the mode of fracture from brittle to more ductile fracture. On the other hand, it becomes apparent that this route of thermomechanical processing does not invariably produce improved properties, but that the type of alloy with its characteristic aging behavior must be considered individually.

In comparison with Al-Cu alloys and their commercial modifications the Al-Zn-Mg and Al-Zn-Mg-Cu alloys do not respond favorably to the T8 treat-

ment. This behavior has been attributed to the fact that they harden by zone formation, which is apparently not affected in the same way by the presence of dislocations as the semicoherent, intermediate phases [*54*]. If one accepts, however, the other view (see preceding section) that age-hardening at standard T6 aging temperatures (110 to 135 C) is predominantly caused by the formation of fine and rather uniformly distributed intermediate phases, such as η' (M′), then another explanation has to be sought. It is known that η' phases can nucleate on dislocations [*67*]. In the absence of dislocations, however, η' appears to precipitate rather uniformly, and after aging to maximum hardness at 120 C, it is barely resolvable in the electron microscope. The distribution of θ' in the T6 condition is much less uniform than that for η'. Therefore, the effect of deformation prior to aging on the size and distribution of η' will be small, but considerable in the case of θ'. Furthermore, since the strength values of Al-Zn-Mg-Cu alloys are not significantly different after T6 or T8 treatments, the effect of strengthening by work hardening is either lost or counterbalanced by a loss of age-hardening capacity. The transmission electron micrograph in Fig. 2 of commercial alloy 7075-T86 which was strained 6 percent in tension prior to aging at 250 F (120 C) indicates that some recovery may have occurred during aging. According to Averbach [*68*] the Laue diffraction spots from a cold-worked Al-Cu alloy become sharper during precipitation heat treatment, indicating that recovery has taken place. Further

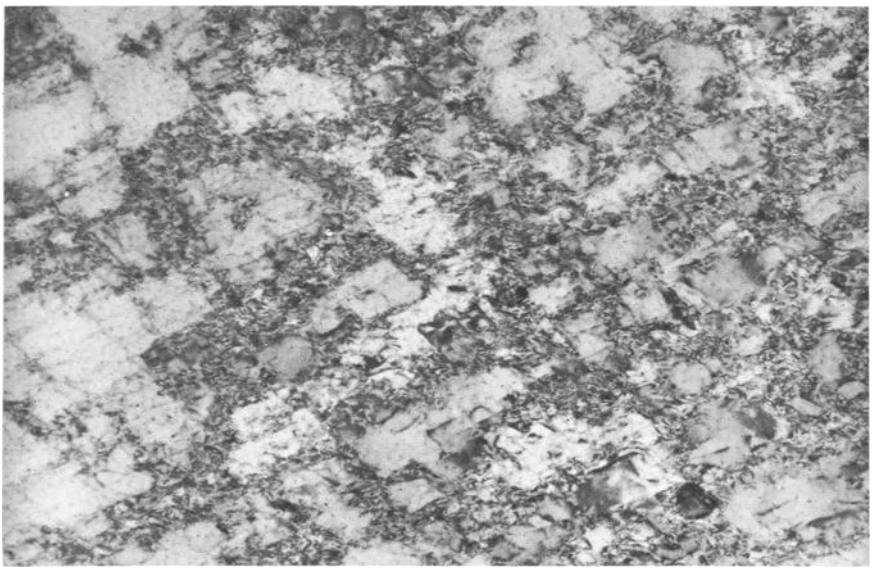

FIG. 2—*Transmission electron micrograph of the structure of aluminum alloy 7075 bar that was stretched 6 percent after quenching and aged 24 h at 120 C (T86 condition ×25,500).*

work is evidently necessary to establish the relative contributions to strength from work hardening and age-hardening for the T8-type treatments.

Low-temperature thermomechanical processing, however, offers a broader and more sophisticated scope of treatments than discussed above. Partial aging of the material after solution annealing and quenching should influence the dislocation structure resulting from a cold- or warm-working operation and should retard recovery processes during final aging. The complex aging sequences of aluminum alloys, which were discussed in the previous section, and the various interaction mechanisms of dislocations with existing decomposition products offer a multitude of thermomechanical treatment possibilities.

The available information on this route of low-temperature thermomechanical processing is scant. Some work on the effects of simultaneous deformation during aging on the kinetics of θ' precipitation in Al-Cu alloys has been reported in the recent literature [*61*, *62*] and has revealed, surprisingly, that θ' precipitation is retarded under simultaneous creep deformation, whereas it is accelerated if deformation occurs prior to aging. This retardation of θ' precipitation was interpreted in terms of dislocation loops around existing θ' particles, which trapped Cu atoms and released them only after climbing over the precipitate particle. However, no evidence was furnished on the resulting strength, ductility, and deformation characteristics.

On the other hand, work performed at the Air Force Materials Laboratory [*69*] indicated interesting property changes of commercial 7075 aluminum alloy, when the aging treatment was interrupted by cold working. A more detailed investigation by F. G. Ostermann into these treatments is presently being conducted at AFML, and a comprehensive description of the results has to await the completion of this project. This route of thermomechanical processing is highlighted by the static properties reported in Table 2. The increase in yield and tensile strength of the same 7075 bar would not be too significant if it were not for the simultaneous increase of fracture elongation. An explanation for these results is speculative at this point. From the transmission electron micrograph in Fig. 3 of a specimen of 7075 treated to the TX condition, one observes a much more uniform distribution of dislocations when compared with the structure of 7075-T86 alloy in Fig. 2. This difference in dislocation structure indicates a lower degree of recovery during final aging or lesser dynamic recovery during working in the 7075-TX material, which is undoubtedly caused by the precipitation structure present in the underaged condition. The increased strength values of 7075-TX alloy may thus be explained in terms of strengthening by retained work hardening. It is also conceivable that a uniform dislocation structure may permit more homogeneous deformation to occur, which should benefit ductility. Quite recently, similar results have been reported by Conserva et al [*70*] for ternary

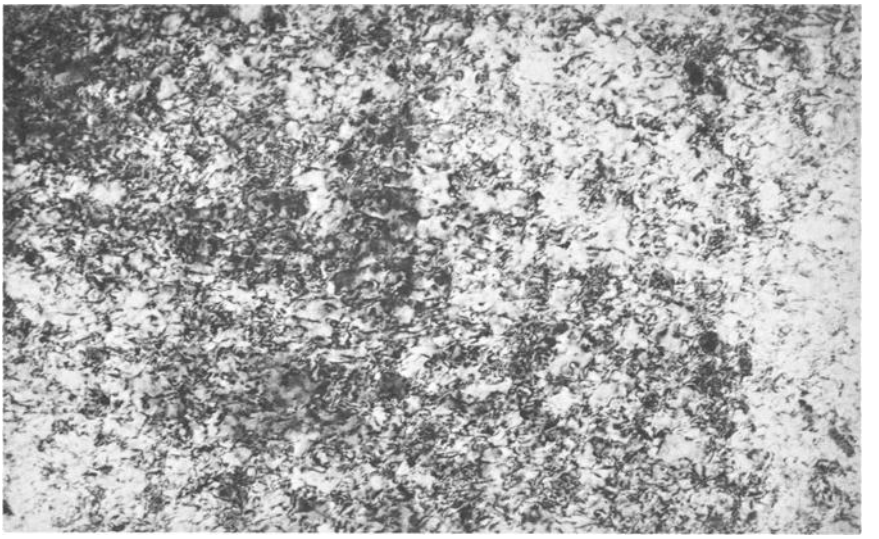

FIG. 3—*Transmission electron micrograph of the structure of aluminum alloy 7075 bar deformed at room temperature during an interrupted aging treatment* (×25,500).

Al-Zn-Mg alloys that had been deformed between low-temperature aging and subsequent high-temperature aging treatments. The dislocation structures obtained by these workers are very similar to those in Fig. 3 for the thermomechanically treated 7075 alloy.

TABLE 2—*The effects of thermomechanical processing of 7075 bar.*

Treatment	0.2% Yield Strength, ksi	Ultimate Tensile Strength, ksi	Elongation, % in 1 in.
T6.....	69.3	79.8	13.3
TMT-TX.....	80.5	84.1	16.4

As is known from ferrous metallurgy, thermomechanical processing has the potential to improve both strength and ductility, and the results given in Table 2 indicate as much for the age-hardened aluminum alloys. Supporting evidence of similar results for alloys of the Al-Cu system has recently been obtained by others.[4] The observed improvement of strength and ductility suggests that the above-described thermomechanical treatments may bring

[4] Private communication with E. Gold, Aeronutronic Division, Philco-Ford Corp., Philadelphia, Pa.

about a change of the deformation characteristics in addition to providing the beneficial features of the T8-type treatment. Whether this change is significant, and in the desirable direction to improve the fatigue processes, remains to be shown.

Low-temperature thermomechanical processing of age-hardened aluminum alloys hence provides improvement of strength and ductility; and, where fatigue resistance is strongly affected by microstructural inhomogeneities, improved fatigue strength can be achieved. There appear to be indications which suggest that, apart from improving the microstructural homogeneity, plastic deformation may also become more homogeneous.

Conclusions

Apart from the important effects of inclusions, perhaps the most characteristic feature related to fatigue crack initiation and Stage I propagation in age-hardened aluminum alloys is the inhomogeneity of deformation. Nonhomogeneous deformation has been considered an important factor in the fatigue cracking of other metals and alloys, but the problem appears to be more acute for age-hardened aluminum alloys. The observed phenomena of soft, precipitate-free zones at grain boundaries and within the matrix, and of reversion and overaging during cyclic stressing are one part of the problem. The other part appears to be nonhomogeneous deformation of an otherwise homogeneously age-hardened matrix, which is related to both the difficulty of slip initiation and the relative ease of slip propagation.

Thermomechanical processing will provide a possibility for preventing aging inhomogeneities and the associated phenomena of reversion and overaging by introducing nucleation sites for more stable precipitate phases. Proper thermomechanical treatments may also provide the opportunity for obtaining more homogeneous deformation by facilitating slip initiation throughout the matrix and perhaps by inhibiting slip propagation. The effects on the fatigue stages of strain hardening introduced during the mechanical processing step and retained, at least in part, during the subsequent aging treatments have hardly been studied. While there are indications for the beneficial effects of thermomechanical treatments on the behavior of aluminum alloys during Stage I cracking, virtually no information has been generated regarding the effects on notch sensitivity and crack propagation.

It is realized that thermomechanical processing of aluminum alloys will often be impractical or expensive and cannot be regarded as a substitute for further alloy development. On the other hand, the possibilities of thermomechanical processes, which involve a multitude of interrelated parameters, have hardly been explored enough to establish the limitations.

References

[1] Bungardt, W. and Osswald, E., *Zeitschrift für Metallkunde*, ZEMTA, Vol. 39, 1948, pp. 185–189.

[2] Rosenkranz, W., *Metall, Zeitschrift für Technik, Industrie und Handel*, MTLLA, Vol. 20, 1966, pp. 227–232.

[3] Franz, H., *Über die Aushärtung von Aluminium—Kupfer—Legierungen*, Aluminium-Verlag G.m.b.H., Düsseldorf, 1957.

[4] Kelly, A. and Nicholson, R. B., *Progress in Materials Science*, PRMSA, Vol. 10, 1963, pp. 151–391.

[5] Altenpohl, D., *Aluminium and Aluminium Legierungen*, Springer-Verlag, Berlin/Göttingen/Heidelberg/New York, 1965.

[6] Van Horn, K. R., Ed., *Aluminum*, Vol. I Properties, Physical Metallurgy and Phase Diagrams, published by American Society for Metals, 1967.

[7] Shakov, Yn. A., *Metallovedenie i Termicheskaya Obrabotka Metallov*, MTOMA, Vol. 5, 1967, pp. 26–40.

[8] Ostermann, F. and Reimann, W. H., "Thermo-Mechanical Processing and Fatigue of Aluminum Alloys," Air Force Materials Laboratory, AFML-TR-69-262, 1969.

[9] Köster, W., *Aluminium, Fachzeitschrift der Deutschen Aluminiumindustrie*, ALUMA, Vol. 34, 1958, p. 694.

[10] Nock, Jr., J. A. and Wooll, A. C., *Iron Age*, IRAGA, Vol. 159, 1947, pp. 57–59.

[11] Hardy, H. K. and Heal, T. J., *Progress in Metal Physics*, PMPHA, Vol. 5, 1954, pp. 143–278.

[12] Guinier, A., *Solid State Physics*, SSPHA, Vol. 9, 1959, pp. 293–398.

[13] Gerold, V., *Ergebnisse der exakten Naturwissenschaften*, EENAA, Vol. 33, 1961, pp. 105.

[14] Gerold, V., *Zeitschrift fuer Metallkunde*, ZEMTA, Vol. 45, 1954, pp. 593–599 and 599–607.

[15] Baur, R. and Gerold, V., *Zeitschrift fuer Metallkunde*, ZEMTA, Vol. 57, 1966, pp. 181–186.

[16] Toman, K., *Acta Crystallographica*, ACCRA, Vol. 10, 1957, p. 187.

[17] Nicholson, R. B. and Nutting, J., *Philisophical Magazine*, PHMAA, Vol. 3, 1958, pp. 531–535.

[18] Silcock, J. M., Heal, T. J., and Hardy, H. K., *Journal of the Institute of Metals (London)*, JIMEA, Vol. 82, 1953–54, pp. 239–248.

[19] Thomas, G. and Nutting, J., *Journal of the Institute of Metals (London)*, JIMEA, Vol. 86, 1957, pp. 1–7.

[20] Castaing, R. and Lenoir, G., *Academie des Sciences, Comptes Rendus*, CRADA. Vol. 239, 1954, pp. 972–974.

[21] Gerold, V., *Acta Crystallographica*, ACCRA, Vol. 11, 1958, p. 230.

[22] Guinier, A., *Zeitschrift fuer Elektrochemie*, ZEELA, Vol. 56, 1952, p. 468.

[23] Gerold, V. and Haberkorn, H., *Zeitschrift fuer Metallkunde*, ZEMTA, Vol. 50, 1959, pp. 568–574.

[24] Schmalzried, H. and Gerold, V., *Zeitschrift für Metallkunde*, ZEMTA, Vol. 49, 1958, pp. 291–301.

[25] Lambot, H., *Revue de Metallurgie (Paris)*, REMEA, Vol. 47, 1950, pp. 709–726.

[26] Graf, R., *Academie des Sciences, Comptes Rendus*, Vol. 242, 1956, pp. 1311–1313 and 2834–2836.

[27] Spiridonov, V. B., Vlasova, T. A., and Iordanskii, V. N., *Metallovedenie i Termicheskaya Obrabotka Metallov*, MTOMA, Vol. 8, 1966, pp. 6–11.

[28] Mondolfo, L. F., Gjostein, N. A., and Levinson, D. W., *Journal of Metals*, American Institute of Mining, Metallurgical and Petroleum Engineers, TMENA, Vol. 206, 1956, pp. 1378–1385.

[29] Graf, R., *Academie des Sciences, Comptes Rendus*, Vol. 244, 1957, pp. 337–340.

[30] Graf, R., *Journal of the Institute of Metals (London)*, JIMEA, Vol. 86, 1957-58, pp. 535–36.

[31] Thomas, G. and Nutting, J., *Journal of the Institute of Metals* (*London*), JIMEA, Vol. 88, 1959-60, pp. 81–90.
[32] Durer, A. and Köster, W., *Zeitschrift für Metallkunde*, ZEMTA, Vol. 30, 1958, pp. 311–319.
[33] Embury, J. and Nicholson, R. B., *Acta Metallurgica*, AMETA, Vol. 13, 1965, pp. 403–417.
[34] Thomas, G. and Nutting, J., *Journal of the Institute of Metals* (*London*), JIMEA, Vol. 86, 1957-58, pp. 7–13.
[35] Carlsen, K. and Honeycombe, R. W. K., *Journal of the Institute of Metals* (*London*), JIMEA, Vol. 83, 1954-55, pp. 449–454.
[36] Speidel, M. O., *Fundamental Aspects of Stress Corrosion Cracking*, National Association of Corrosion Engineers, Texas, 1969, pp. 561–579.
[37] Jacobs, A. J., *Fundamental Aspects of Stress Corrosion Cracking*, National Association of Corrosion Engineers, Texas, 1969, pp. 530–557.
[38] Templin, R., *Proceedings*, American Society for Testing and Materials, ASTEA, Vol. 54, 1954, pp. 641–699.
[39] Hanstock, R., *Journal of the Institute of Metals* (*London*), JIMEA, Vol. 83, 1954-55, pp. 11–15.
[40] Broom, T., Molineux, J., and Whittaker, V., *Journal of the Institute of Metals* (*London*), JIMEA, Vol. 84, 1955-56, pp. 357–363.
[41] Clark, J. and McEvily, A., *Acta Metallurgica*, AMETA, Vol. 12, 1964, pp. 1359–1372.
[42] Polmear, I. and Bainbridge, I., *Philosophical Magazine*, PHMAA, Vol. 4, 1959, pp. 1293–1304.
[43] Laird, C. and Thomas, G., *International Journal of Fracture Mechanics*, IJFMA, Vol. 3, 1967, pp. 81–97.
[44] Grosskreutz, J. C. and Shaw, G. G., "Critical Mechanisms in the Development of Fatigue Cracks in 2024-T4 Aluminum," Air Force Materials Laboratory Report AFML-TR-68-137, 1968.
[45] Piper, D. E., Quist, W. E., and Anderson, W. E., *Metallurgical Society Conferences*, Metallurgical Society, American Institute of Mining Metallurgical and Petroleum Engineers, Vol. 31, 1966, pp. 227–272.
[46] Erhardt, K., Pelloux, R. M. N., and Grant, N. J., "The Role of Structure, Low Strain Rates, High Strain and Temperature on the Low-Cycle Fatigue Behavior of 2024-T4 Aluminum," Air Force Materials Laboratory Report AFML-TR-69-85, 1969.
[47] Grosskreutz, J. C., Shaw, G. G., and Benson, D. K., "The Effect of Inclusion Size and Distribution on Fatigue of 2024-T4 Aluminum," Air Force Materials Laboratory Report AFML-TR-69-121, 1969.
[48] Brenner, P., *Aluminium*, ALUMA, Vol. 32, 1956, pp. 756–768.
[49] Laird, C. and Feltner, C. E., *Transactions of Metallurgical Society*, American Institute of Mining, Metallurgical and Petroleum Engineers, TMSAA, Vol. 239, 1967, pp. 1074–1083.
[50] Feltner, C. E. and Laird, C., *Transactions of the Metallurgical Society*, American Institute of Mining, Metallurgical and Petroleum Engineers, TMSAA, Vol. 242, 1968, pp. 1253–57.
[51] Feltner, C. E. and Laird, C., *Acta Metallurgica*, AMETA, Vol. 15, 1967, pp. 1621–1653.
[52] McEvily, A. J. and Johnston, T. L., *Proceedings*, First International Conference on Fracture, Sendai, Vol. 2, 1965, p. 515.
[53] Tomkins, B., *Philosophical Magazine*, PHMAA, Vol. 17, 1968, pp. 1041–1066.
[54] Van Horn, K. R., Ed., *Aluminum*, American Society for Metals, 1967, p. 149ff.
[55] Lyst, J. O., *Journal of Materials*, JMLSA, Vol. 3, No. 4, 1968, pp. 996–1017.
[56] Krause, A. R. and Laird, C., *Materials Science and Engineering*, MSCEA, Vol. 2, 1967-68, pp. 331–347.
[57] Hornbogen, E., *Zeitschrift für Aluminium*, ALUMA, Vol. 43, 1967, pp. 41–47, 115–121, and 163–170.

[58] von Heimendahl, M., *Metall, Zeitschrift für Technik, Industrie und Handel*, MTLLA, Vol. 21, 1967, pp. 606–611.
[59] von Heimendahl, M., *Acta Metallurgica*, AMETA, Vol. 15, 1967, pp. 417–419.
[60] Graf, R., Publ. Scient. Techn. Ministère de l'Air, No. 318, 1956.
[61] Driver, D. and Barrand, P., *Philosophical Magazine*, PHMAA, Vol. 14, 1966, pp. 657–665.
[62] Noble, B. and Holmes, E., *Philosophical Magazine*, PHMAA, Vol. 17, 1968, pp. 7–19.
[63] Laird, C. and Aaronson, H. I., Report No. SL-67-54, Ford Motor Co., 1967.
[64] McEvily, A. J., Snyder, R. L., and Clark, J. B., *Transactions of the Metallurgical Society*, American Institute of Mining, Metallurgical and Petroleum Engineers, TMSAA, Vol. 227, 1963, pp. 452–458.
[65] McEvily, A. J., Clark, J. B., and Bond, A. B., *Transactions*, American Society for Metals, TASEA, Vol. 60, 1967, pp. 661–71.
[66] Saulnier, A. and Mirand, P., *Memoires Scientifique de la Revue de Metallurgie*, MRMTA, Vol. 57, 1960, pp. 91–95.
[67] Thomas, G., *Philosophical Magazine*, PHMAA, Vol. 4, 1959, pp. 606–611.
[68] Averbach, B. L. in *Cold Working of Metals*, American Society for Metals, 1949, p. 262.
[69] Dickerson, L. E., "A Study of the Effects of Prior Heat Treatment on the Fatigue Strength of 7075 Aluminum," M.S. thesis, Air Force Institute of Technology, 1968.
[70] Conserva, M., DiRusso, E., and Gatto, F., *Alluminio*, ALLUA, 1969, pp. 441–445.

DISCUSSION

Alfred Fox[1] (*written discussion*)—The authors are to be commended for a real contribution toward providing a better understanding of processes which improve the fatigue strength of metals. At Bell Telephone Laboratories we have been studying the effect of combining extreme cold work and low-temperature heat treatment on the fatigue strength of Copper Alloy 510 (5 percent tin phosphor bronze) strip. We have been able to achieve in this widely used spring material significant increases in the 0.01 percent offset yield strength, good stress relaxation properties, and an improvement in the fatigue strength at 10^8 cycles of approximately 20 percent over that of unheat-treated hard temper material having the same thickness and grain size. While the ductility was significantly reduced by the extreme cold work, the subsequent low-temperature heat treatment restored it to a level satisfactory for many spring applications.

This work, as well as our own unpublished work, shows that processing can do much to improve significantly a metal's fatigue strength.

[1] Bell Telephone Laboratories, Murray Hill, N. J. 07974.

D. K. Benson[1]

Surface Treatments for Fatigue Strengthening*

REFERENCE: Benson, D. K., "**Surface Treatments for Fatigue Strengthening,**" *Achievement of High Fatigue Resistance in Metals and Alloys, ASTM STP 467*, American Society for Testing and Materials, 1970, pp. 188–208.

ABSTRACT: Three broad categories of surface treatments are considered: discrete coatings, surface diffusion treatments, and thermomechanical treatments. From the standpoints of reliability and versatility, surface diffusion treatments appear to be best suited for fatigue strengthening. A surface treatment which truly strengthens must not, on the other hand, increase the susceptibility to other forms of damage such as wear, corrosion, and oxidation. It is shown that surface diffusion coatings have the potential capability of providing an increased resistance to all of these forms of damage. Some guidelines are developed for the design of such all-around protective treatments.

KEY WORDS: surface finishing, fatigue (materials), oxidation, corrosion, cracking (fracturing), diffusion coating, wear, evaluation, fatigue crack

Fatigue fracture usually begins at, and is frequently confined near, an external surface throughout a sizeable portion of the lifetime of a structure. Surface treatments can consequently be effective in increasing fatigue strength. However, the surface is also the front with which a metal meets an adverse environment. Oxidation, corrosion, and wear may become separate hazards as well as aggravators of the fatigue problem; thus, a surface treatment which strengthens against fatigue damage while making the metal more susceptible to these other forms of damage is not generally acceptable. An optimally designed surface treatment should strengthen against all these adverse influences.

In the first part of this paper, some basic principles of fatigue will be surveyed for guidelines to the design of optimal surface treatments. In the second part, guidelines for protection against oxidation, corrosion, and wear are discussed and found to be compatible with fatigue strengthening by surface diffusion coatings. Some examples of the application of these guidelines will also be discussed.

[1] Senior physicist, Midwest Research Institute, Kansas City, Mo. 64110.

* The work covered in this paper was supported by the Air Force Materials Laboratory, Wright-Patterson Air Force Base, Ohio, under Contract No. F33615-67-C-1547.

Guidelines

Fatigue

Generally, fatigue cracks are initiated at surfaces and grow at a rate which is initially very slow; hence, a fatigue crack may be confined to a volume of the material near a surface for a large portion of the total fatigue life. Manson [*1*][2] has shown that for a wide variety of metals the fraction of life occupied in developing a crack of length ~0.010 in. is given approximately by

$$N_0/N_f \sim 1 - 2.5N_f^{-1/3} \quad \ldots\ldots\ldots\ldots\ldots\ldots\ldots\ldots (1)$$

where N_0 is the number of cycles for the crack to reach 0.010 in. and N_f is the total life. Thus, in long-life fatigue, the environment, composition, and condition of the metal surface may play disproportionately large roles in determining the total fatigue life of a structure.

In single-phase metals fatigue cracks are usually initiated in regions of highly concentrated plastic strain at the surface. In such materials fatigue strength may be increased by surface hardening. Most structural metals, however, are multiphase alloys in which crack initiation usually occurs at interphase interfaces.

Hard inclusions or nonequilibrium second-phase particles are frequently the sites of premature crack initiation in commercial alloys. Figure 1 shows an example of the initiation of a fatigue crack at a second-phase particle in 2024-T4 aluminum alloy [*2*]. Surface treatments which remove, bridge over, or strengthen the region around these surface inhomogeneities can increase the fatigue strength. However, the effectiveness of a surface layer in supressing fatigue cracking may depend strongly on its thickness. The importance of surface layer thickness is illustrated schematically in Fig. 2. A layer thinner than the second-phase particles may have little or no effect on the crack nucleation, *A*. A hard layer slightly thicker than the second-phase particles may actually cause premature cracking (*B* and *C*). Only if the layer is much thicker than the second-phase particles will the concentrated stress be borne entirely by the layer *D*.

Once a microcrack is initiated in a hard, semibrittle layer, the rate at which it grows to a macroscopic fatigue crack depends upon the local hardness of the material. An approximate expression [*3*] for the crack propagation stress, σ_f, in a nearly brittle material containing a small crack is

$$\begin{aligned} \sigma_f &\sim \{(2E\gamma/\pi c)[1 + (2\gamma/\pi b\sigma_y)]\}^{1/2} \\ &\sim \{(2E\gamma/\pi c)[1 + (2\gamma/3\pi b\mathrm{HV})]\}^{1/2} \quad \ldots\ldots\ldots\ldots (2) \end{aligned}$$

where E is Young's modulus, γ is the surface energy, c is the crack length,

[2] Italic numbers in brackets refer to the list of references at the end of this paper.

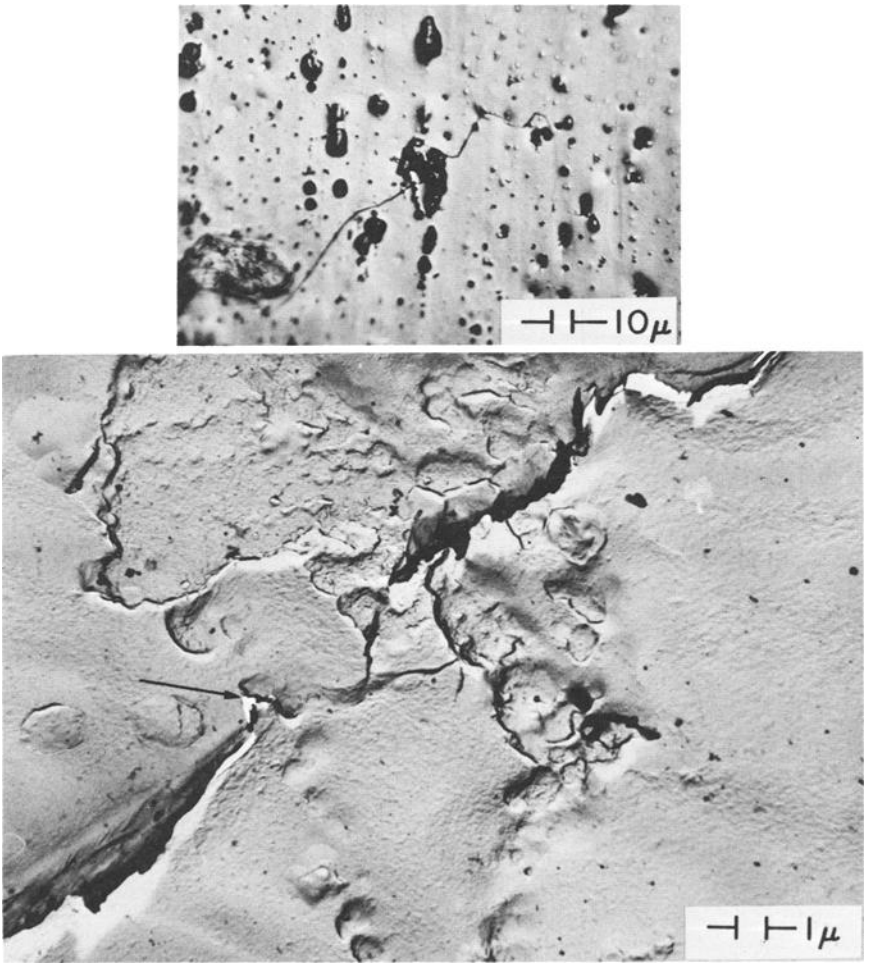

FIG. 1—*Fatigue crack initiation at a nonequilibrium second-phase particle in 2024-T4 aluminum alloy. Bottom is high-resolution micrograph of area at top.*

b is the Burger's length, and σ_y is the yield strength, approximately equal to three times the Vicker's hardness HV [*4*]. Thus, the stress required to cause a crack to propagate in a surface layer is less if the layer is hard. The benefit of a hard coating in delaying crack initiation must be weighed against the decrease in the time required for a crack to grow to macroscopic size.

In ductile metals a mechanism of shear decohesion appears to be a general characteristic of all stages of fatigue growth. Fatigue crack growth in ductile surface layers should be controlled by the same mechanism. Tomkins [*5*] has shown that the Dugdale model of a plastic shear zone ahead of the crack

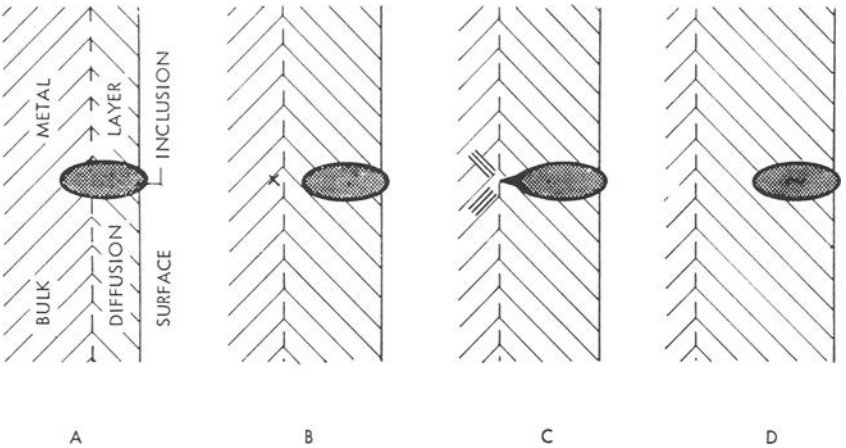

The inclusion acts as a stress concentration when the metal is placed under tensile stress. A thin diffusion coating, *A*, does not affect the region of stress concentration. A coating slightly thicker than the inclusion, *B* and *C*, may still allow the soft matrix at Point x, *B*, to yield under the concentrated stress. When yielding occurs at x, the hard diffusion layer can crack, *C*. If the diffusion layer is much thicker than the inclusion, *D*, then the entire region of intense stress is borne by the hard coating and no yielding occurs.

FIG. 2—*Schematic illustration of an inclusion near the surface of a diffusion-coated metal.*

can be used to derive expressions for fatigue crack growth rates in terms of easily measured material properties. The incremental crack growth rate, δ, is assumed to be equal to the total shear strain displacement along the plastic zone (Fig. 3):

$$\delta = \Delta\gamma_p D \sim \Delta\epsilon_p D \quad (3)$$

where D is the plastic zone length and $\Delta\epsilon_p$ is the net plastic strain imposed on the specimen. Using the expression for D given by Hahn and Rosenfield [6], the growth rate under quasi-static conditions becomes

$$\delta = dl/dN = \sqrt{2}\, l\Delta\epsilon_p[\sec(\pi/4)(\sigma/\sigma_u) - 1] \quad (4)$$

where σ_u, the ultimate tensile stress of the metal, is taken as the approximate value of the effective tensile stress across the plastic shear zone during crack advance and σ is the maximum applied tensile stress. By using the empirical expression for cyclic strain hardening

$$\Delta\sigma = k\Delta\epsilon_p^{\beta} \quad (5)$$

Eq 4 can be written as

$$dl/dN \sim \frac{\pi^2\sqrt{2}}{32}\, l(2/k)^{1/\beta}(1/\sigma_u)^2\sigma^{2\beta+1/\beta} \quad (6)$$

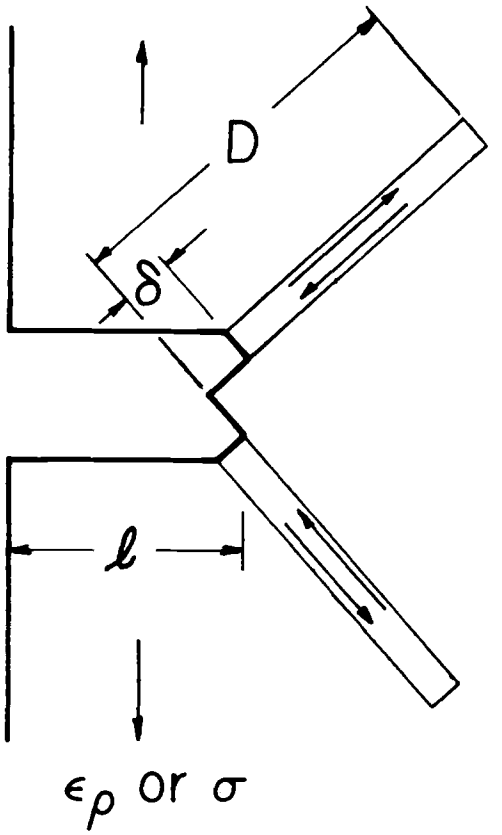

FIG. 3—*Schematic diagram of crack propagation model, after Tomkins* [5]. *Crack length is* l, *shear band length* D, *and incremental crack advance* δ.

for constant stress amplitude fatigue or

$$dl/dN \sim \frac{\pi^2\sqrt{2}}{128}(k/\sigma_u)^2\Delta\epsilon_p{}^{1+2\beta} \quad \ldots\ldots\ldots\ldots\ldots\ldots\ldots\ldots (7)$$

for constant strain amplitude fatigue [assuming $(\sigma/\sigma_u) \ll 1$]. Under both constant stress amplitude and constant strain amplitude conditions, the fatigue crack growth rate is inversely proportional to the square of the ultimate tensile stress, σ_u. Thus, a surface treatment should be selected which produces a high ultimate tensile stress.

The surface layer may be thought of as experiencing the strain cycling imposed upon it by the response of the bulk to service loads. Thus, it may be more important for a surface layer to resist strain cycling rather than stress cycling. Equation 7 shows that for maximum strain resistance, k, the cyclic strain hardening coefficient should be as small as possible.

In summary, the surface treatment should produce a surface layer thicker than any second-phase particles, which has a high ultimate tensile stress, with a low, cyclic strain hardening coefficient. Once a crack is formed, the resistance to its propagation (Eq 2) is promoted by a high surface energy and a low value of hardness. There are several different kinds of surface treatments. The advantages and disadvantages of a few are discussed briefly below.

Work Hardening—This can be accomplished by rolling, impact, or shock deformation. The resulting tangle of dislocations restricts further dislocation glide and increases the stress required to produce the local yielding that leads to crack initiation. Perhaps as important as the barriers to dislocation glide are the residual, elastic compressive strains that are left in the surface volume.

Shot peening is the most widely used method of suppressing fatigue by surface work hardening. Shot peening a metal produces a residual compressive stress in a thin surface layer, which is balanced by a residual tensile stress deeper in the metal. The stress gradients between these two regions are usually quite large. During cyclic stressing the residual stresses are relaxed in the neighborhood of large residual stress gradients [*7*]. In spite of this relaxation, considerable improvement in fatigue endurance is common throughout the high cycle ($N_f > 10^4$ cycles) portion of the *S-N* curve. A particularly large improvement in the fatigue strength of weldments is produced by careful shot peening: typical are 50 percent increases in the fatigue strength of butt welds in an 18 percent nickel (18Ni) maraging steel and in an aluminum-zinc-magnesium (Al-Zn-Mg) alloy [*8*].

At temperatures above about one half of the absolute melting temperature, the residual stresses and dislocation tangles will be relaxed by diffusion. Thus, the work-hardening treatments are not very useful for high temperature applications. In addition, the elastic strain energy of the work-hardened surface increases the corrosion susceptibility.

Surface Constraint—A coating such as an oxide or a plating can alter the dislocation interactions at a surface [*9*]. If the elastic modulus of the coating is greater than that of the metal, then dislocations may be repelled from the coating and the surfacc made more resistant to fatigue crack initiation. An interesting example of this effect is the influence of an oxide coating on aluminum. The amorphous anodic aluminum oxide has an elastic modulus that is extremely sensitive to its degree of hydration [*10*]. In dry air or vacuum the oxide becomes dehydrated and exhibits an elastic modulus of about 1.9×10^{11} N/m^2 (approximately 3 times the modulus of aluminum), whereas the modulus is only 2×10^{10} N/m^2 in moist air. Thus, in the dehydrated state the anodic oxide is effective in suppressing fatigue crack initiation. The fact that the fatigue strength of anodized aluminum alloys is higher in dry air or vacuum than in moist air has been reported often [*11*]. At least part of

this effect is due to the constraint of the dry oxide. Some commercial anodization treatments such as Mar-M Seal,[3] which significantly increase the fatigue strength of aluminum alloys, may also work on this principle.

The thin, natural oxide on aluminum may also restrain surface slip when it is dehydrated. Table 1 summarizes the results of experiments designed to test the effect of the natural oxide on fatigue crack initiation. Electropolished, polycrystalline sheets of aluminum were heated to 200 C and covered with various protective coatings. The metal was then cycled in reversed bending for 10^5 cycles and examined for Stage I fatigue cracks. The fraction of grains containing Stage I cracks (persistent slipbands) was compared for coated and uncoated portions of the same sheet. As shown in the table, conditions which preserved the dehydrated state of the oxide led to a large reduction in the number of Stage I cracks. An electroplate of high elastic modulus can also restrain surface slip and increase fatigue strength. Part of the fatigue strength increase produced by plating treatments such as the Chrome-ite[4] treatment is probably a result of this effect [*12*].

TABLE 1—*Effect of coatings on persistent slip in aluminum.*[a]

Coating, treatment	Average Number of Grains with Persistent Slip, Deviation at 95% Confidence Level: Control, f_0	Coated Specimen, f_c	$(f_0 - f_c)/f_0$, at 95% confidence level
2000 Å evaporated aluminum film (applied in vacuum)	0.79 (±0.08)	0.06 (±0.14)	0.66
Polyethylene (applied to "dry" oxide)[b]	0.82 (±0.06)	0.48 (±0.06)	0.36
Polyethylene (soaked in H_2O 36 h)	0.87 (±0.03)	0.82 (±0.08)	no significant difference
Poly(vinyl chloride) (applied to "dry" oxide)[b]	0.76 (±0.09)	0.23 (±0.15)	0.54
Poly(vinyl chloride) (applied in laboratory air)	0.83 (±0.08)	0.86 (±0.04)	no significant difference

[a] All tests: 10^5 cycles at $\pm 0.0006\ \epsilon$, 6 Hz at room temperature in air; examination at 4×10^{-4} cm below original surface.

[b] All specimens electropolished and heated to 200 C before testing. "Dry" oxide produced by heating to 200 C in dry atmosphere and coating before re-exposure to moist air.

Discrete coatings are beneficial only as long as they remain intact. Any macroscopic strain which produces a fracture in the coating creates an efficient fatigue crack initiation source. Thus, discrete coatings may pose a

[3] Martin-Marietta Corp., Denver, Colo.

[4] Chrome-ite Co., Gardena, Calif.

serious problem for the designer who is never sure how well he can rely on the increased fatigue strength of the coated material.

Alloying—This process can alter both crack initiation and growth rates. Although it is not usually thought of as alloying, eliminating certain impurity elements can prevent the formation of inclusions and thereby improve fatigue strength. This fact is well known for the case of steels which are processed in vacuum to prevent the formation of oxide inclusions. Less well known is the fact that excluding impurities such as iron and silicon from the high-strength aluminum alloys can also reduce their content of nonequilibrium second-phase particles and increase their fatigue strength [*13*].

A metal can also be altered superficially by various surface alloying treatments. The surface diffusion coatings can have a strong influence on fatigue strength while changing the gross mechanical properties only slightly; such surface diffusion treatments include nitriding, carbonizing, chrome alumizing, vapor plating, and electrodiffusion. Except for vapor plating and electrodiffusion, these treatments are well known and will not be discussed in detail here.

The principal advantage of the diffusion coatings is that they are an integral part of the base metal rather than a discrete coating. The concentration of the alloying element naturally varies gradually from a maximum at the surface to zero at some depth below the diffusion coating. Thus, there is a graded transition in composition. The coatings are tenacious and generally not susceptible to flaking or the "pest" effect.

Vapor plating is a high-temperature process by which a metal is deposited onto a substrate by the thermal decomposition of a metallo-organic compound vapor. Some refractory elements such as tungsten, molybdenum, and columbium, which are very difficult to plate by any other process, can be deposited by this technique [*14*]. However, because the base metal oxide is left as a barrier to diffusion, the vapor-plated coatings are generally not as tenacious as other diffusion coatings and, therefore, not as reliable.

The electrodiffusion process [*15*] is a unique high-temperature electroplating technique in which a molten fluoride salt bath is the electrolyte. The temperature and plating rate are selected so that the plating rate matches the diffusion rate; hence the name "electrodiffusion." Because the base metal oxide is dissolved in the fluoride salt, especially uniform and tenacious coatings are produced. A great variety of elements can be applied as diffusion coatings to the common structural metals (with the possible exception of aluminum). Figure 4, for example, shows some of the elements which can be applied as diffusion coatings to iron-, cobalt-, nickel-, or copper-based alloys by electrodiffusion.

Because of the versatility of surface diffusion coatings, and their desirable tenacity and relative freedom from catastrophic failure, they appear to provide the most promising type of surface treatment for strengthening alloys

against fatigue damage. In the following sections other forms of damage which contribute to the fatigue problem are examined. Guidelines are established for the selection of surface diffusion coatings that provide a measure of protection against wear, oxidation, and corrosion, as well as fatigue.

Fretting

The kind of wear most often implicated in metal fatigue is called fretting. It is caused by small-amplitude oscillating slippage of one surface over another. Usually the slip is unintended and frequently of such small amplitude that it goes undetected. The effect of fretting on fatigue strength, however, is quite dramatic. Examples of 50 percent reduction in fatigue strength due to fretting are quite common [*16*, *17*, *18*].

Figure 5 illustrates the mechanism of fretting wear. Even a very small oscillatory displacement in a structure such as a lap joint, *A*, may be large in comparison to the size of the surface asperities which form the real areas of contact, *B*. Under the combined pressure and shear stresses asperities adhere and occasionally shear off, *C*. If the wear particle remains adherent, then no macroscopic wear occurs although material is transferred from one surface to the other. However, under some circumstances, a wear particle can peel off as it relaxes elastically, *D*. When this happens, wear occurs.

Fretting wear is a general mechanical effect which has been observed in glass, sapphire, platinum, structural metals, etc., at displacement amplitudes as low as 2.5×10^{-6} cm [*19*]. In the case of structural metals, oxidation of the small wear particles can increase their size and cause abrasive wear as a secondary effect. If loose wear particles are not created by fretting, then the subsequent abrasive wear will not occur.

Rabinowicz [*20*] has considered the energetics of the formation of loose wear particles and found that for pressures below a certain threshold, the

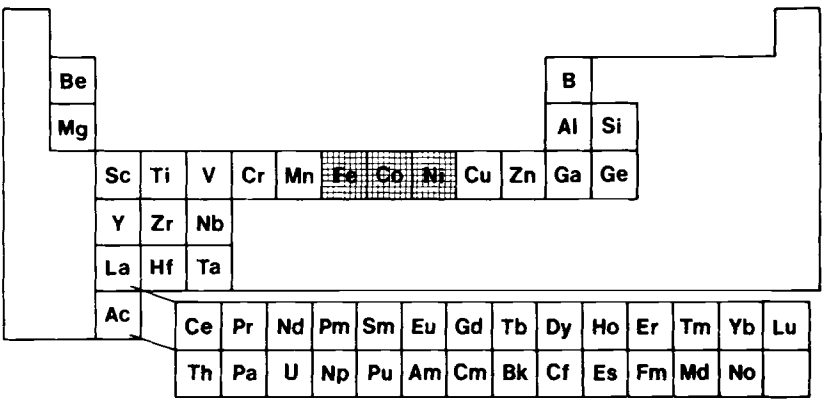

FIG. 4—*Periodic table of the elements.*

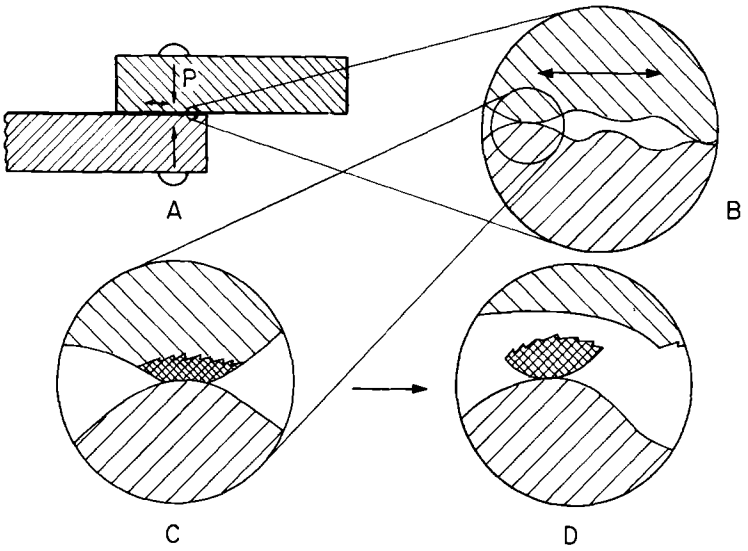

FIG. 5—*Schematic diagram of fretting wear mechanism.*

wear particles will remain adherent. For contact between identical metals, the threshold pressure above which fretting wear occurs is given by

$$P \propto E^2\gamma^2/\sigma_y{}^3 \propto E^2\gamma^2/\mathrm{HV}^3 \quad \ldots\ldots (8)$$

where E is Young's modulus, γ is the surface-free energy of the solid metal, and σ_y is the yield stress at the surface which is proportional to the penetration hardness, HV, at the surface. Thus resistance to fretting is promoted by high values of Young's modulus and surface energy and by low values of surface hardness.

Oxidation

The oxidation resistance of metals depends upon a number of factors. The mechanical compatibility of the oxide coating with the metal is one of these factors. If when a volume, V_m, of metal oxidizes it forms a greatly different volume, V_0, of oxide, then the resulting strains may prevent the oxide from providing a continuous protective barrier against further oxidation. The interfacial mismatch strain in the oxide,

$$\epsilon_I \sim (V_0/V_m)^{1/3} - 1 \quad \ldots\ldots (9)$$

is an indication of how serious the mechanical incompatibility will be. The quantity

$$V_0/V_m = (1/a)(W_0/W_m)(d_m/d_0) \quad \ldots\ldots (10)$$

is the well-known Pilling-Bedworth ratio, where W_0 and W_m are the molecular

weights of the oxide and metal, respectively, d_0 and d_m are the densities of the oxide and metal, respectively, and a is the number of metal atoms in a molecule of the oxide. Some room temperature values of ϵ_I for several metals are listed in Table 2.

TABLE 2—*Metal-oxide interfacial strain.*

Metal Oxide-Metal	Pilling-Bedworth Ratio, $(V_0/V_m) = (1/a)(W_0/W_m)(d_m/d_0)$	Interfacial Strain, $\epsilon_I \approx (V_0/V_m)^{1/3} - 1$
Li_2O-Li	0.57	−0.17
MgO–Mg	0.81	−0.07
CdO-Cd	1.21	+0.07
SnO-Sn	1.28	+0.09
Al_2O_3-Al	1.29	+0.09
NiO-Ni	1.51	+0.15
ZnO-Zn	1.62	+0.18
Cu_2O-Cu	1.67	+0.19
CuO-Cu	1.75	+0.21
BeO-Be	1.71	+0.20
TiO_2-Ti	1.75	+0.21
FeO-Fe	1.77	+0.21
Fe_2O_3-Fe	2.15	+0.29
Fe_3O_4-Fe	1.06	+0.02
Cr_2O_3-Cr	2.02	+0.27
Co_3O_4-Co	2.00	+0.26
Ta_2O_5-Ta	2.32	+0.32

Because the thermal expansion of a metal is greater than its oxide, ϵ_I decreases as the temperature is increased. Thus, metals like lithium and magnesium have little oxidation resistance even at moderate temperatures, whereas titanium, beryllium, and nickel retain protective oxides at high temperatures. Alloying can be used to modify the oxide and make it more mechanically compatible with the metal; however, alloying can have a much stronger influence on the kinetics of oxidation than on the mechanical compatibility. Alloy additions introduce substitutional defects in the oxide lattice which can affect the electrical conductivity and also the diffusion rates in the oxide.

Figure 6 schematically illustrates the steps in the incremental growth of a thick, continuous oxide on a pure metal. In *B*, a metal ion vacancy is shown forming at the oxide surface and finally being filled at the oxide-metal interface. As the metal ion vacancy is annihilated, a new vacancy is formed. This vacancy is either an oxygen ion vacancy which migrates to the surface, *C*, or a metal lattice vacancy which migrates into the metal, *E*. The oxide lattice vacancies are charged defects. If the oxide has the formula MO, where M is a metal atom, then the metal ion vacancy M_{V}^{++} has a net −2e charge

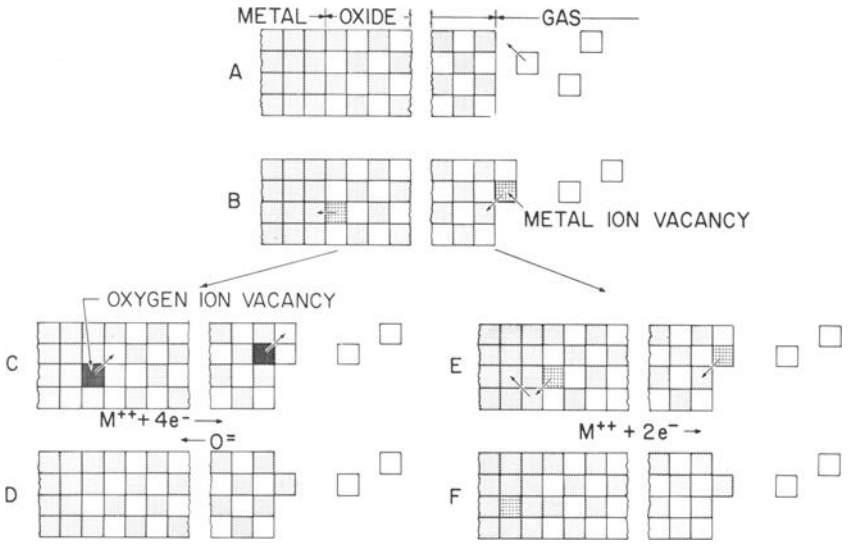

Metal atoms diffuse to the oxide surface by the migration of vacancies, *B*. Oxygen ions may move to the metal-metal oxide interface by vacancy diffusion, *C*, or the metal may absorb vacancies, *F*, without oxygen ion diffusion.

FIG. 6—*Incremental growth of an ideal oxide film.*

and the oxygen ion vacancy $O_{v=}$ has a net +2e charge. Thus, the diffusion steps shown in *B* and *C* lead to a positive space charge buildup at the oxide surface which tends to retard further vacancy migration. In good insulators such as CdO, TiO_2, and Al_2O_3, this space charge is not readily neutralized by electron flow, so the oxidation at low temperatures may be limited by the low electrical conductivity of the oxide. At high temperatures the electrical conductivity of the normally impure oxides is high enough to neutralize the space charge. In semiconducting oxides, such as Cu_2O, FeO, ZnO, and NiO, the space charge is readily neutralized even at low temperatures, so the oxidation rate is only limited by the rate of diffusion of the less mobile ion (usually the larger oxygen ion).

Figure 7 shows how alloying affects the oxidation rate of zinc, which is probably limited by the rate of oxygen ion diffusion. A monovalent element such as lithium enters substitutionally into the ZnO lattice carrying a net −e charge. Overall charge conservation requires that the total electronic charge throughout the oxide be zero. Consequently the average concentrations of charged defects are interdependent, that is,

$$(2e)Zn_{v^{++}} + (e)Li_{s^{+}} = (2e)O_{v=}$$

(charge on zinc vacancies) + (charge on substitutional lithium ions) = (charge on oxygen ion vacancies)

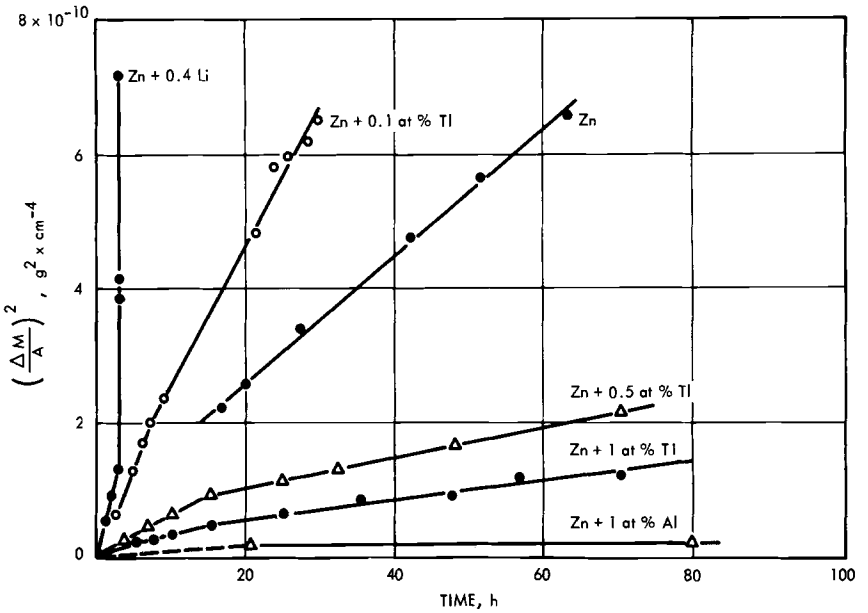

FIG. 7—*The effect of alloy additions on the oxidation rate (weight change per unit area, ΔM/A) of zinc* [21].

Since $(2e)Zn_{v}^{++}$ is essentially a function of temperature only and, therefore, a constant at any particular temperature, the presence of the Li_{s}^{+} ion must increase the concentration of oxygen vacancies and the oxidation rate. Similarly, the addition of trivalent aluminum to the ZnO lattice produces a substitutional defect with a net charge of +e, so that charge conservation leads to the equation:

$$(2e)Zn_{v}^{++} = (2e)O_{v}^{=} + (e)Al_{s}^{+++}$$

This shows that the presence of the trivalent ions decreases the concentration of oxygen ion vacancies and thus retards oxidation. Thallium, which can be either monovalent or trivalent, appears to behave more like lithium at low concentrations and like aluminum at higher concentrations.

Another example of the effect of alloying on oxidation rate is shown in Fig. 8. The oxidation rate of titanium (valence 4) was decreased by about 30 times as a result of the addition of 1 atom percent niobium (valence 5). Of course, the oxidation reactions in many alloys are much more complicated. Further alloying in these cases may produce subtle effects contrary to what might be expected from these simple considerations. Nevertheless, a useful, general guideline is that the addition of a higher valence element to a metal can retard oxygen ion diffusion in the oxide and reduce the oxidation rate,

whereas addition of a lower valence element can be expected to increase the oxidation rate.

Corrosion

Corrosion is essentially a dissolution process whose tendency (the corrosion susceptibility) is proportional to the negative free energy of the dissolution reaction. Thus, the corrosion susceptibility is not simply determined by the elemental makeup of the metal and the corrodant but is also influenced by whatever affects the free energy of the reaction. For example, strain energy in the metal is released when it dissolves so that the total decrease in free energy is greater when a strained portion of the metal dissolves than when an unstrained portion dissolves. Thus, strained portions of a metal, such as a crack tip or grain boundary, are more susceptible to corrosion.

The difference in the free energies of reaction produces a chemical potential difference between two dissimilar parts of a surface. A net ion current results with positive metal ions migrating away from the more active region toward

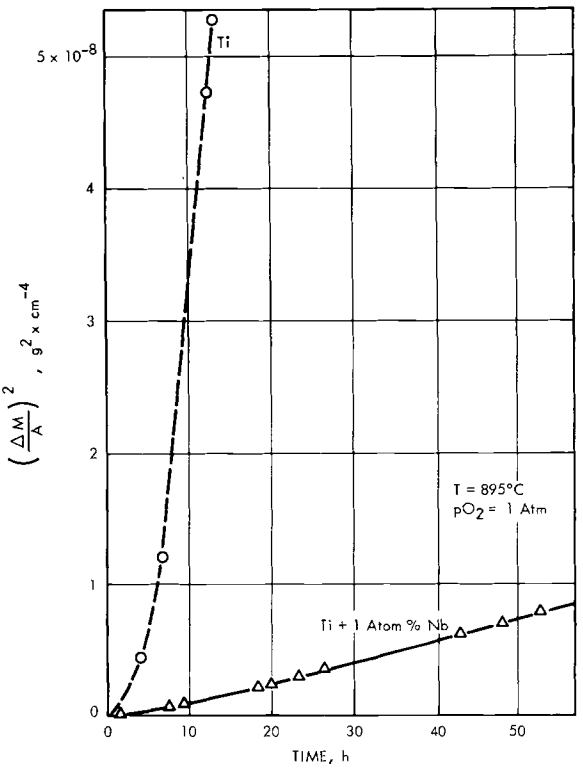

FIG. 8—*The effect of niobium additions on the oxidation rate of titanium* [22].

the less active. Thus, there is an electrical potential difference ΔU proportional to the difference in the free energies of reaction ($-\Delta W$). Under ideal (reversible) conditions ΔU and ΔW are related by the equation

$$\Delta W = Fn\Delta U \quad (11)$$

where n is the oxidation state of the dissolved metal ion, F is Faraday's constant $\sim$ 96,500 C mol^{-1}, and ΔU is expressed in volts and ΔW in joules per mole (1 kcal/mol equals 4.184 $\times$ 10^3 J/mol). The exact value of the change in molar free energy, ΔW, will depend on the details of the corrosion reaction, but a useful estimate is provided by the molar free energy of reaction under standard conditions. If, for example, the reaction involves the dissolution of the metal as the chloride in salt water, then a useful, but rough, approximation to the relative free energies of reaction can be obtained from a comparison of the free energies of formation of the metal chlorides.

The kinetics of dissolution determine the seriousness of the corrosion problem. If a stable, insoluble corrosion product forms in the corrodant, the corrosion is self-limiting and not much of a problem. If no such passive layer is formed, or if the passive layer is repeatedly ruptured by stresses, then the rate of corrosion is usually limited only by polarization. The dissolution of a metal atom leaves a net negative charge on the metal and a net positive charge in the corrodant. Thus, an ionic space charge, or polarization, builds up and retards further dissolution. Depolarization occurs when this space charge is neutralized by a compensating flow of electrons into the corrodant.

In acidic corrodants, electrons may flow from the metal to adsorbed hydrogen ions reducing them to atomic hydrogen and compensating the polarization space charge. The adsorption of hydrogen ions occurs preferentially where the positive metal ion concentration is lowest, that is, in cathodic areas of lowest corrosion activity. If the rate of hydrogen reduction is restricted, then the corrosion rate is similarly decreased. In neutral or basic corrodants the space charge may be neutralized by the reduction of dissolved oxygen at the metal surface; thus, the corrosion rate may be limited by the concentration of dissolved oxygen or the rate of its reduction to oxygen ions.

Alloying can affect the corrosion rate by promoting the formation of a passive layer or by altering the rate-determining depolarization reactions. The formation of a passive layer usually occurs when an oxide forms which is stable, and therefore protective, in the corrosive environment. An alloy addition which can form such a stable oxide is preferable to one whose oxide is not stable in the corrodant.

There are also some general guidelines for selecting alloy additions to suppress the depolarization reactions. The depolarization reactions, reduction of oxygen atoms or hydrogen ions, both require that electrons be removed from the metal. Thus, the facility with which depolarization proceeds

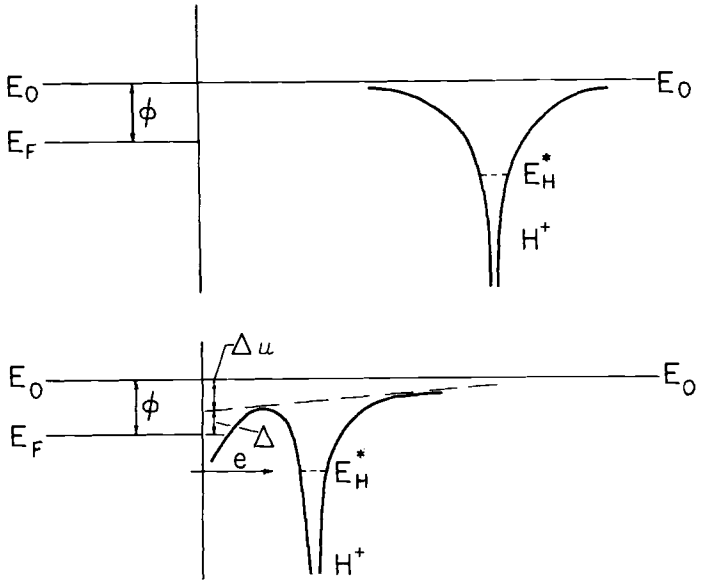

FIG. 9—*Schematic energy level diagram for the reduction of a hydrogen ion at a metal surface.*

is inversely related to the electronic work function of the metal. The electrochemical potential difference between the anodic and cathodic regions produces a field which promotes the electron transfer. Figure 9 shows schematically the energy level diagram of hydrogen ion reduction at a metal surface. An electron must tunnel from the Fermi level, E_F, through a potential barrier into an excited state of the hydrogen atom, $E_H{}^*$. The electrochemical potential lowers this barrier by an amount $\sim\Delta U$. Thus, the height of the tunneling barrier is closely related to the difference, Δ, between the metal work function, φ, and the electrochemical potential difference, ΔU; that is,

$$\Delta \sim \varphi - \Delta U \quad \ldots\ldots\ldots\ldots\ldots\ldots\ldots\ldots\ldots\ldots (12)$$

The corrosion resistance can be improved by a properly selected surface alloy addition that provides an oxide which is stable in the corrodant or one which minimizes the rate of depolarization. To minimize the rate of depolarization, it is useful to make the difference between the electronic work function and the maximum electrochemical potential as large as possible.

Summary of Guidelines for Surface Treatments

The general guidelines for selecting an element to be used in a surface diffusion coating can be summarized as follows:

Fatigue

Alloying should be designed to (1) increase σ_u, ultimate tensile stress of the diffusion coating, and γ, its surface energy; (2) decrease σ_y, surface yield stress (with the possible exception of single-phase, pure metals for which an increased surface hardness is desirable); and (3) control the diffusion coating thickness so that it is greater than the largest second-phase particle diameter.

Fretting

Alloying should be designed to (1) increase γ and (2) decrease σ_y.

Oxidation

The alloying element should be selected to have (1) higher valence (oxidation state) than the major constituent of the base metal and (2) a Pilling-Bedworth ratio which tends to compensate for the strains at the base metal-metal oxide interface.

Corrosion

The alloying element should be selected to (1) provide a stable oxide passivating layer or (2) maximize the barrier to depolarization reactions, that is, maximize $\Delta = \varphi - \Delta U$, where φ is the electronic work function and ΔU is the maximum electrochemical potential difference between alloy constituents.

Example

As an example of the use of these guidelines, consider the problem of selecting a diffusion coating for Ti-8Al-1Mo-1V alloy which could be expected to improve the wear (fretting), oxidation, and saltwater corrosion resistance as well as increase the fatigue strength. Table 3 lists the pertinent data for three candidate elements, beryllium, aluminum, and tantalum, in addition to the basic constituents of the alloy, titanium, molybdenum, and vanadium. For fatigue resistance a large surface energy, γ, is desirable (Eq 2); thus, on this basis tantalum should be selected, with beryllium appearing to be nearly as good. The resistance to oxidation depends upon the stability of the metal oxide, which is indicated by the interfacial strain and the nature of the impurities. The stability of the aluminum and beryllium oxides is considerably greater than that of the tantalum oxide. If a tantalum coating were applied to the titanium alloy, then the titanium, aluminum, vanadium, and molybdenum of the Ti-8Al-1Mo-1V alloy could become substitutional impurities of lower valence in the tantalum oxide. As previously discussed, such lower valence additions are expected to increase oxidation susceptibility. On the other hand, if a beryllium coating were applied to the alloy, all of the substitutional impurities in the beryllium oxide would be of

higher valence than the beryllium and might therefore increase oxidation resistance. A beryllium coating appears most likely to afford oxidation resistance.

TABLE 3—*Evaluation of elements for use on Ti-8Al-1V-1Mo.*

Metal, melting point	γ, erg cm^{-2}	Valence	Work Function, eV	Free Energy of Formation, W, kcal/mol-bond	Depolarization Barrier Potential, Δ Relative ro			
					Ti	Be	Al	Ta
Titanium..... (1998 K)	1470	+4	4.07	1/4($TiCl_4$) = 52.5 1/4(TiO_2) = 57.3	...	3.7	3.9	3.7
Beryllium..... (1556 K)	1250	+2	3.37	1/2($BeCl_2$) = 60.0 1/2(BeO) = 67.0	3.7	...	3.7	3.5
Aluminum.... (932 K)	1030	+3	3.74	1/3($AlCl_3$) = 59.7 1/6(Al_2O_3) = 67.3	3.9	3.7	...	3.5
Tantalum..... (2150 K)	3000	+5	4.12	1/5($TaCl_5$) = 45.0 1/10(Ta_2O_5) = 49.0	3.7	3.5	3.5	...
Molybdenum..	...	+3	4.27	1/3($MoCl_3$) = 15.3 1/6(MoO_3) = 31.0	2.7	3.2	2.5	3.0
Vanadium....	...	+3	4.11	1/3(VCl_3) = 40.0 1/6(V_2O_3) = 50.5	1.8	3.2	3.3	3.9

In the sixth column (Table 3) the stability of the metal oxide in a chloride environment is indicated by a comparison of the metal oxide bond strength to the metal chloride bond strength. The titanium and tantalum oxides appear to be marginally stable in the presence of the chloride ion, whereas the aluminum and beryllium oxides appear stable. Thus either the beryllium or aluminum coatings could improve chloride corrosion resistance, so long as the coatings remain intact. Once the coating is breached, the resistance to saltwater corrosion will depend on the potential barrier to depolarization (columns 7 to 10, Table 3). If the uncoated Ti-8Al-1Mo-1V alloy were exposed to salt water, then the titanium and aluminum would dissolve preferentially, leaving molybdenum and vanadium behind. The vanadium which is least active, would be the site of the depolarization reaction since the potential barrier relative to titanium dissolution is only ~1.8 V. If a beryllium coating were applied, then this more active metal would dissolve preferentially. Thus, the depolarization reaction at any exposed vanadium would be controlled by the electrochemical potential between beryllium and vanadium. The barrier to the depolarization reaction in the beryllium-coated alloy would therefore be ~3.2 V rather than ~1.8 V for the uncoated alloy. Similarly, if an aluminum coating were used, the minimum depolarization barrier would be ~2.5 V. A tantalum coating would not dissolve preferentially. Thus the

controlling depolarization barrier in the tantalum-coated alloy would be the same as the uncoated alloy, ~1.8 V. From these considerations, it appears that the beryllium coating would provide the best protection against salt-water corrosion even under circumstances in which the integrity of the coating was breached.

A diffusion coating of beryllium on Ti-8Al-1Mo-1V was tested. The coating was applied by electrodiffusion in a molten electrolyte of $BeF_2 \cdot LiF$ eutectic at 680 C in 4 h. The current density was 2 mA/cm^2. The diffusion coating extended to a depth of about 4 mils and contained about 1.35 milligrams of beryllium per square centimeter of surface. Notched fatigue specimens and uncoated control specimens were duplex annealed by heating for 15 min at 1000 C in vacuum, quenching in argon gas, and aging at 800 C for 8 h in vacuum. Figure 10 shows the microhardness of the coating measured on a taper section. Note the relatively soft layer at the surface which would be expected to improve resistance to fretting. Figure 11 shows a comparison of the *S-N* curves for notched, beryllium diffusion-coated (Beryllided) specimens and for uncoated control specimens. A significant increase in the fatigue strength in long-life fatigue was achieved. The oxidation, corrosion, and fretting resistance of the beryllium diffusion-coated titanium alloy have not yet been tested.

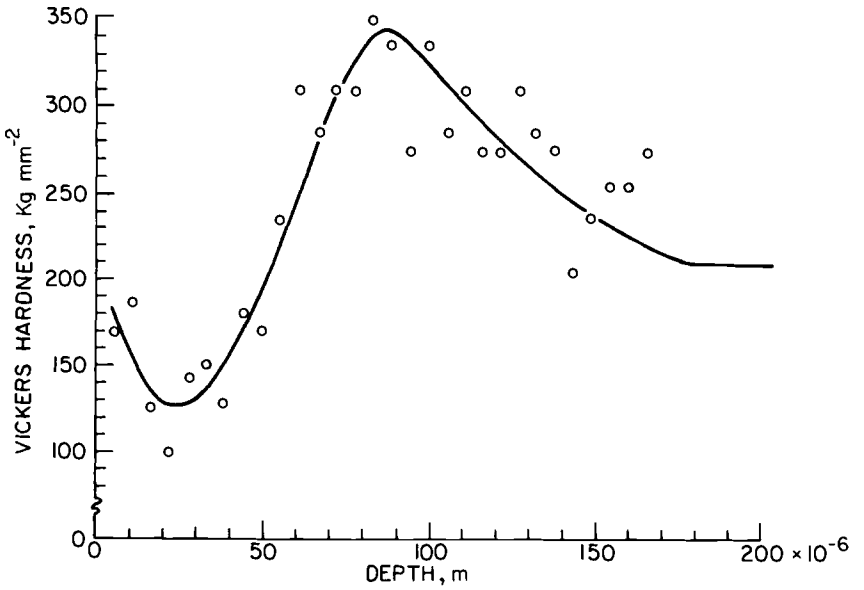

FIG. 10—*Microhardness of a beryllium diffusion layer on a Ti-8Al-1Mo-1V alloy.*

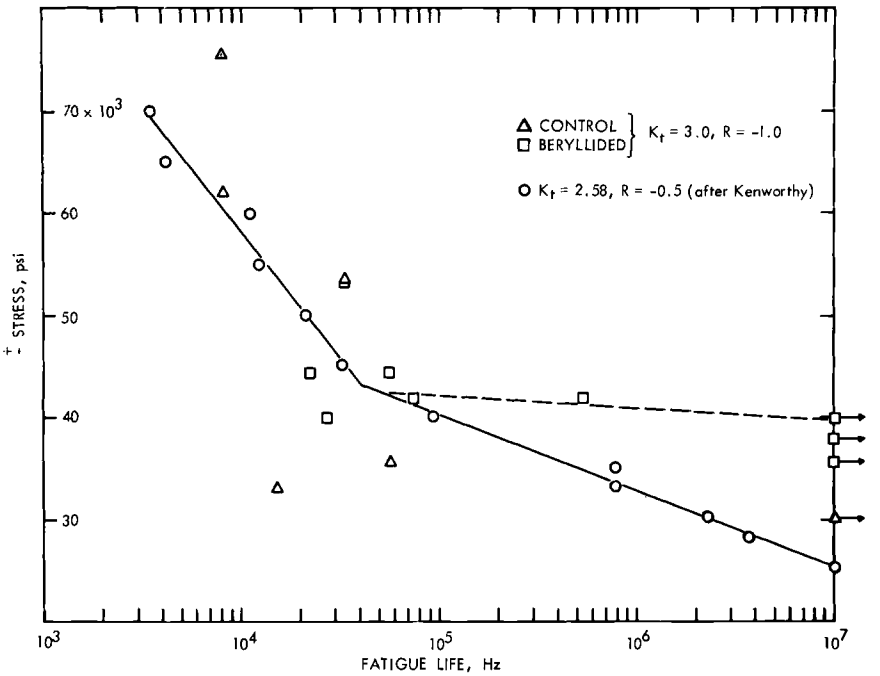

FIG. 11—S-N *curve showing the effect of a beryllium diffusion layer on the fatigue of Ti-8Al-1Mo-1V alloy.*

Conclusions

We have shown that there are some, albeit crude, guidelines by which one can make a preliminary selection of candidate surface alloying elements. These guidelines suggest that it is possible to tailor a diffusion coating to resist fretting wear, corrosion, and oxidation as well as increase fatigue strength. Obviously much more work needs to be done before the design engineer can specify the optimum surface treatment for any particular application. Perhaps the suggestion that this is a possibility will encourage others to explore it further.

References

[1] Manson, S. S., *Experimental Mechanics*, EXMCA, Vol. 5, 1965, p. 193.
[2] Grosskreutz, J. C. and Shaw, G. G., "Critical Mechanisms in the Development of Fatigue Cracks in 2024-T4 Aluminum," AFML-TR 68-137, Air Force Materials Laboratory, Dayton, Ohio, May 1968.
[3] Tegart, S. J. M., *Elements of Mechanical Metallurgy*, Macmillan, New York, 1966, pp. 206–208.
[4] Rabinowicz, E., *Friction and Wear of Materials*, Wiley, New York, 1965, p. 21.
[5] Tomkins, B., *Philosophical Magazine*, PHMAA, Vol. 18, No. 155, 1968, p. 1041.

[6] Hahn, G. T. and Rosenfield, A. R., *Acta Metallurgica*, AMETA, Vol. 13, 1965, p. 293.
[7] Esquival, A. L. and Evans, K. R., *Experimental Mechanics*, EXMCA, Vol. 8, No. 11, 1968, p. 496.
[8] Brine, E. R., Webber, D., and Baron, H. G., *British Welding Journal*, BRWJA, Vol. 15, No. 11, 1968, p. 541.
[9] Conners, G. H., *International Journal of Engineering Science*, IJESA, Vol. 5, 1967, pp. 25–38.
[10] Grosskreutz, J. C., *Journal of the Electrochemical Society*, JESOA, Vol. 116, No. 9, 1969, pp. 1232–1237.
[11] Eeles, E. G., *Journal of the Institute of Metals*, JIMEA, Vol. 95, 1967, p. 156.
[12] Smith, C. R., "Evaluation of Fatigue Life of Chrome-ite Plated Specimens," AFFDL-TR-65-166, Air Force Flight Dynamics Laboratory, Dayton, Ohio, Dec. 1965.
[13] Grosskreutz, J. C., Shaw, G. G., and Benson, D. K., "The Effect of Inclusion Size and Distribution on Fatigue of 2024-T4 Aluminum," AFML-TR-69-121, Air Force Materials Laboratory, Dayton, Ohio, March 1969.
[14] Burcal, G. J., "Metal-Organic Compounds for Vapor-Plating Applications," ML-TDR-64-206, Part 1, Air Force Materials Laboratory, Dayton, Ohio, June 1964.
[15] U.S. Patent Nos. 3,024,175 through 3,024,177, 6 March 1962.
[16] Sachs, G. and Stefan, P., *Transactions*, American Society for Metals, TASEA, Vol. 29, 1941, p. 373.
[17] Teed, P. L., *Metallurgical Reviews*, MREVA, Vol. 5, 1960, p. 267.
[18] Liu, H. W., Corten, H. T., and Sinclair, G. M., *Proceedings*, American Society for Testing and Materials, ASTEA, Vol. 57, 1957, p. 623.
[19] Tomlinson, G. A., Thorpe, P. L., and Gough, H. J., *Proceedings of the Institution of Mechanical Engineers*, PIMLA, Vol. 141, 1939, p. 223.
[20] Rabinowicz, E., *Friction and Wear of Materials*, Wiley, New York, 1965, p. 153.
[21] Hauffe, K., *Oxidation of Metals*, Plenum Press, New York, 1965, p. 206.
[22] Hauffe, K., *Oxidation of Metals*, Plenum Press, New York, 1965, p. 223.

E. R. Speakman[1]

Fatigue Life Improvement Through Stress Coining Methods

REFERENCE: Speakman, E. R., **"Fatigue Life Improvement Through Stress Coining Methods,"** *Achievement of High Fatigue Resistance in Metals and Alloys, ASTM STP 467*, American Society for Testing and Materials, 1970, pp. 209–227.

ABSTRACT: The use of a quick and economical new process, stress coining, results in an aircraft structure with a more balanced fatigue strength than was previously possible. Basically, the stress coining procedure, a proprietary method of the Douglas Aircraft Co., involves controlling the yielding of material inside holes and in the material surrounding holes and slots. Stress coining induces residual compressive stresses that offset load-induced tensile stresses concentrated around these load-carrying areas. The procedure can be used in highly stressed areas to increase fatigue life and resistance to stress corrosion of structural members. Salvage rework by reaming, stress coining, and installing an oversize fastener increases the remaining fatigue life to approach that of a virgin stress-coined structure. Fatigue life of test specimens for various aircraft has been improved by a factor of approximately four.

KEY WORDS: fatigue strength at N cycles, fatigue life, stress relieving, residual stress, stress corrosion, hole size, joints (junctions), tensile stress, fasteners, aircraft equipment, evaluation, tests

One goal of the design engineer is to increase the fatigue life of bolted joints without drastic alteration of established design concepts. The fatigue life of the joint, however, is limited by the eventual formation of cracks, which tend to propagate from the edge of the bolt hole in a direction perpendicular to the direction of the load carried by the bolted assembly. There are three major causes that contribute to the formation of cracks:

1. High tensile stresses at the edge of the holes perpendicualr to the loading direction. The presence of a hole in a load-carrying member causes a significant increase of tensile stress at the edge of the hole when the member is tension loaded.

2. Inadequate tightness and fit of the bolt in the joined members, particularly at the faying surfaces. It is practically impossible to ream a hole accurately enough to cause a uniform fit of the bolt through the member. As a

[1] Senior engineer and scientist, Douglas Aircraft Co., Long Beach, Calif. 90405.

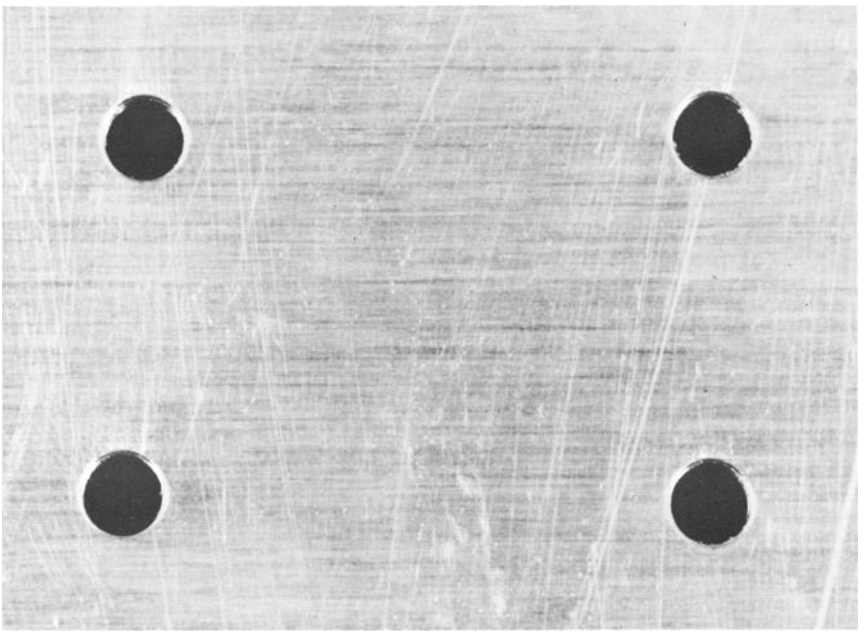

FIG. 1—*Radius stress-coined, loose fit holes in thin material.*

result, there is frequent relative movement of the joined members because the bolt is not tight enough at the faying surfaces.

3. Fretting at the faying surfaces. Fretting damage occurs both between mating surfaces of the structure and in the countersink mating with the flush head of the attachment.

Description of Stress Coining[2]

Test results have proved that aircraft parts without holes have a longer fatigue life than those with attachments or open holes. The stress coining process is a new hole preparation technique that increases the fatigue strength of open and fastener-filled holes. There are three methods of stress coining used at present for production applications:

1. *Radius stress coining* increases the fatigue strength of loose fit holes and slots in material thicknesses to 0.188 in. This process cold-works a highly polished 0.030-in. radius around the edges of the hole or slot in the material (Fig. 1).

[2] Stress coining is a proprietary method for which a patent, No. 3,434,327, was issued on 25 March 1969. A license should be obtained from the Douglas Aircraft Co. before performing the stress coining procedures, and for this reason none of the techniques are explained in the paper.

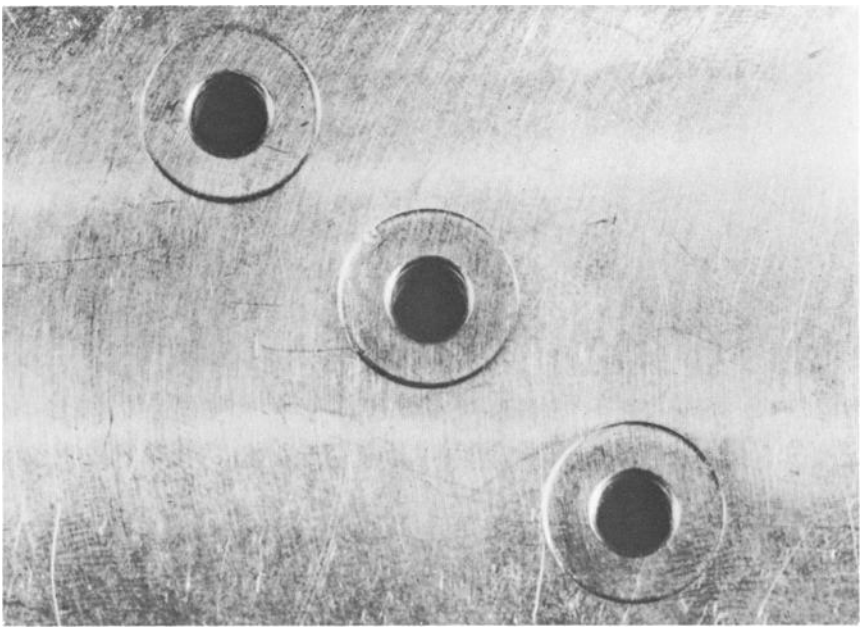

FIG. 2—*Pad stress-coined, loose fit holes in thick material.*

2. *Pad stress coining* increases the fatigue strength of loose fit holes in door doublers and fuel transfer slots in wing stringers. The pad recess is an impression formed approximately 0.004 in. deep in the surface material surrounding the hole or slot. This process is applicable to materials of thicknesses of 0.188 in. and above (Figs. 2 and 3).

3. *Stress coin hole expansion* increases the fatigue strength of close tolerance holes for bolts, rivets, bushings, and bearings. This process starts with an undersized hole that is plastically expanded to the final diameter by a lubricated expanding pin. This procedure is adaptable to any material thickness combinations on final aircraft assembly (Fig. 4).

Stress coining produces local residual compressive stresses in the material surrounding the hole. The residual compressive stresses prolong the fatigue life from N_1 to N_2 by decreasing the local mean stress (as well as the maximum stress) at Point A where the crack begins, while the amplitude remains approximately the same (Fig. 5 top and bottom).

Material Thickness Effect on Fatigue

The fatigue strength of a riveted aircraft structure decreases with an increase in material thickness. The designer may increase the material thickness to lower the applied stress level in the structure, but he may, at the same time,

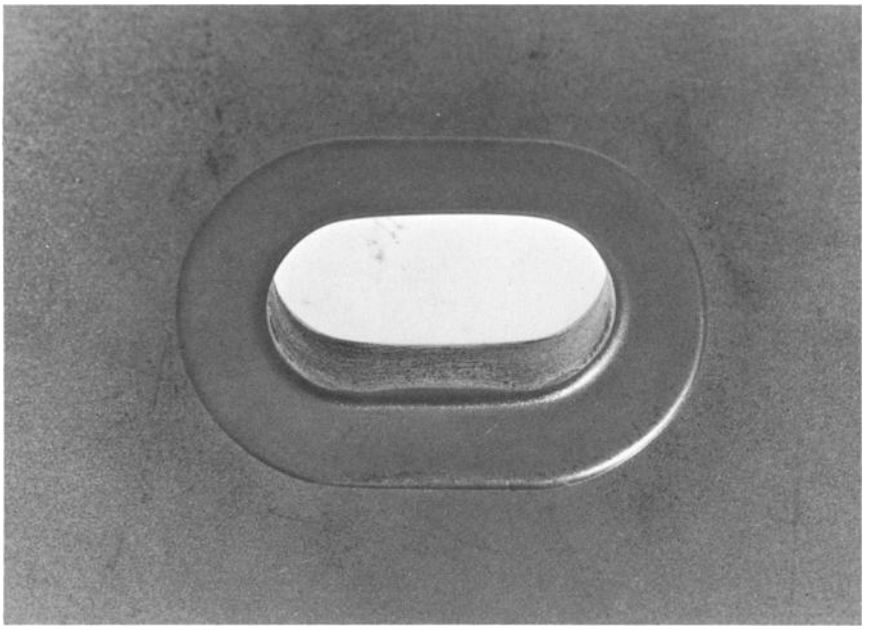

FIG. 3—*Pad stress-coined fuel transfer slot.*

inadvertently create a fatigue problem with the attachments. This situation will prevail in the design of aluminum heavy transport aircraft. One of the primary origins of fatigue failure in aircraft structures is associated with open holes, access cutouts, fuel transfer slots, and attachment holes. The *S-N* curves in Fig. 6 show the relative fatigue life for these conditions.

Conventional aluminum aircraft structure is assembled with mechanical attachments that produce varying degrees of fatigue strength. Therefore, it has become necessary to coin open holes for screws in lower wing access doors and fuel transfer slots. Application of coining in these areas extends the fatigue life into the range of that for lockbolts and slug rivets. This design concept provides a more balanced fatigue strength for light basic structure. Combinations of materials up to 0.500 in. thick are considered light structure and combinations above 0.500 in. are considered heavy structure.

The jumbo jets and heavy subsonic transports are in the category of heavy structural combinations. Attachments installed in thick combinations cause a severe reduction in fatigue life for the reasons: (1) insufficient swelling of the slug rivet inside the hole (Fig. 7), (2) difficulty in installation of 0.004-in. interference fit lockbolts, and (3) fatigue failure in the countersink. As the material thickness increases for slug rivets, the hole experiences lesser amounts

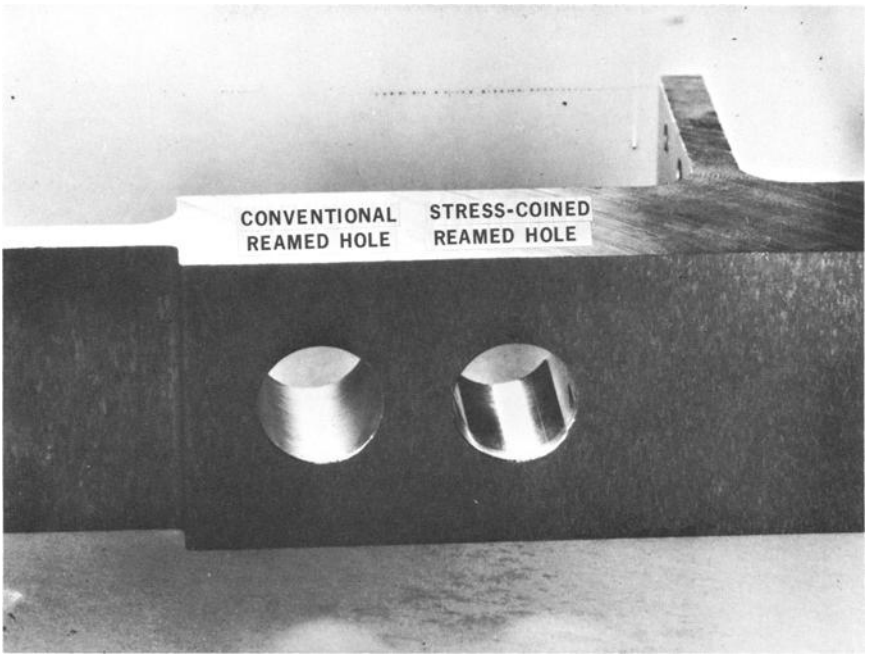

FIG. 4—*Visual comparison of conventional and stress-coined holes.*

of prestressing from hole filling. A point is soon reached where the hole prestress becomes negligible and the fatigue strength approaches that of an open hole. The fatigue strength for lockbolt installations increases with an increase in interference fit. Installation of lockbolts in heavy structure with high interference causes the fastener to gall and seize into a partially installed position, and removal of the lockbolt in this condition is very difficult. To overcome this problem, the practice has been to prepare the hole to the low interference limit; but this can result in lower fatigue life and occasional loose fit holes that permit fuel leakage. Countersink fatigue failures are typical for interference fasteners such as lockbolt and Taper-Lok fasteners whose fit prestresses the hole upon installation. The countersink is not prestressed because this is not possible with the clamp-up pressure of fastener installation.

An improvement in fatigue life for heavy structure can be achieved by applying the stress coining technique prior to fastener installation. Stress coin expansion of the hole for slug rivets induces favorable residual compressive stresses through plastic deformation inside the hole. Stress coining prior to lockbolt installation in thick material increases the fatigue strength because it is then possible to expand the hole to a controlled, low interference fit. The mirror finish inside the hole eases the lockbolt installation, while the residual

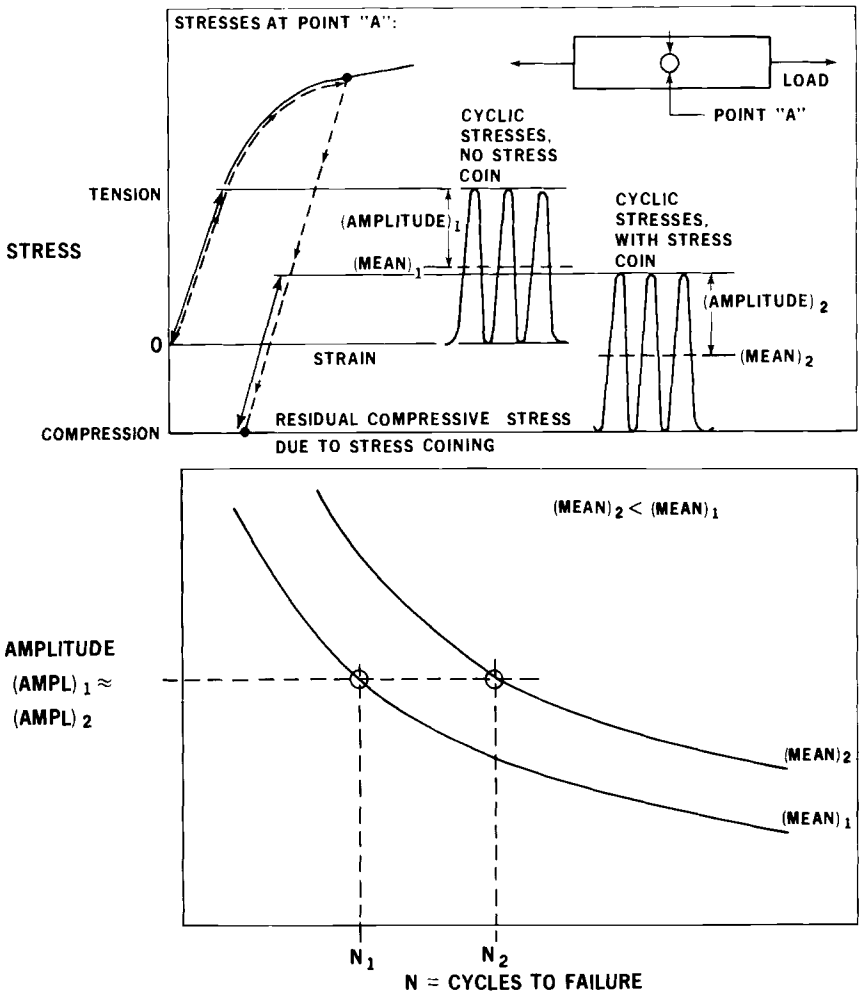

FIG. 5—*Fatigue life improvement due to stress coining in terms of local stresses.*

compressive stresses offset the low interference effect on fatigue strength. The weakness of countersink failures may be overcome by stress coining the countersink. This procedure prestresses the cone of the countersink and cold-works a small radius at the juncture of the countersink and hole.

Stress Coining Applications

The stress coining procedure is not restricted by material thickness. It is possible to stress coin for a Class A bolt installation that would equal the

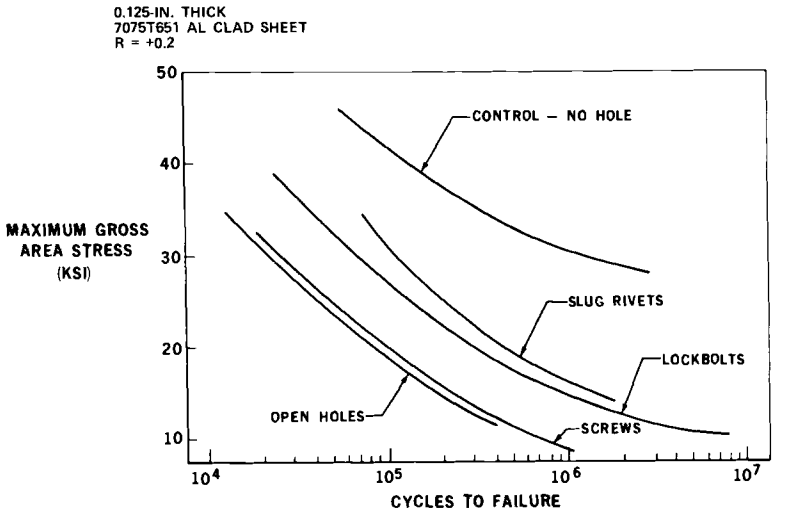

FIG. 6—*Summary of fatigue data for light basic structure.*

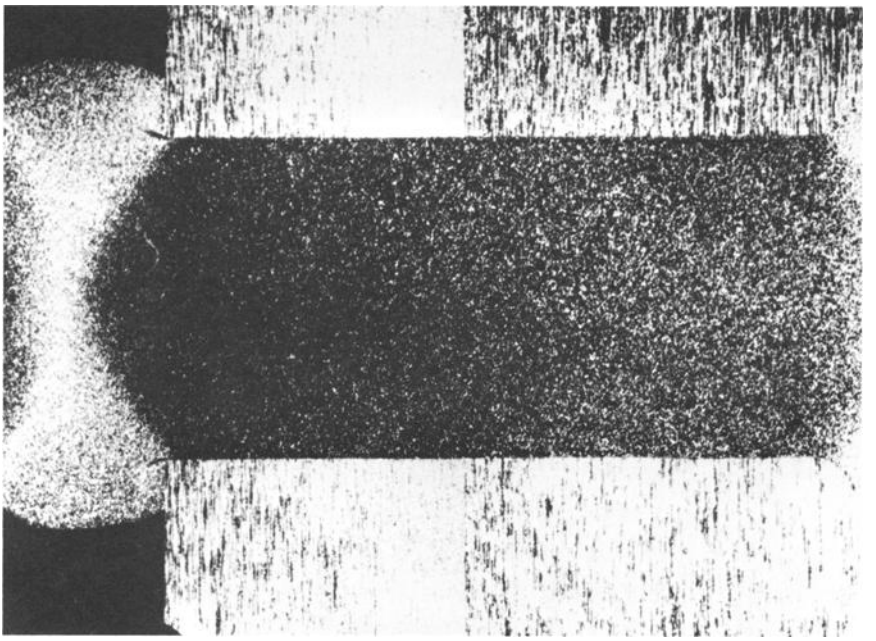

FIG. 7—*Slug rivet grain structure.*

fatigue strength of lockbolts. To illustrate this statement, a service life extension program (SLEP) was conducted for the Douglas C-124 airplane, in which a 0.750-in-thick 2014-T6 aluminum plate was used to represent the C-124 lower spar cap. The test results of the fatigue specimens are shown in Fig. 8.

A-4 B/C Airplane Front Spar Stress Coin Rework

Small, tension fatigue specimens and fuel surge tests were performed to evaluate the stress coin rework of the A-4C front spar access door cutouts in the spar web. The purpose of these tests was to increase the service life of the aircraft, because fatigue cracking occurs in the spar web under catapult and heavy loads. The edges of both sides of the holes around the cutout were stress coined to a 0.030-in. radius. Portable coining tools were designed for a simplified rework procedure that required a minimum amount of time (Fig. 9). Test results indicated a substantial increase in service life for airplanes if cracks had not occurred (Figs. 10, 11, and 12).

DC-9 Pylon Engine Mount Fitting

Specimens with conventionally reamed holes were compared to coined holes in various material thicknesses. Test results indicated that stress coining is an inexpensive method which provides superior fatigue strength for the DC-9 engine pylon fitting. Stress coining plastically expands an undersized hole to final dimensions by pushing a lubricated expanding pin through it, as shown in Fig. 13. Approximately one half of the interference between the

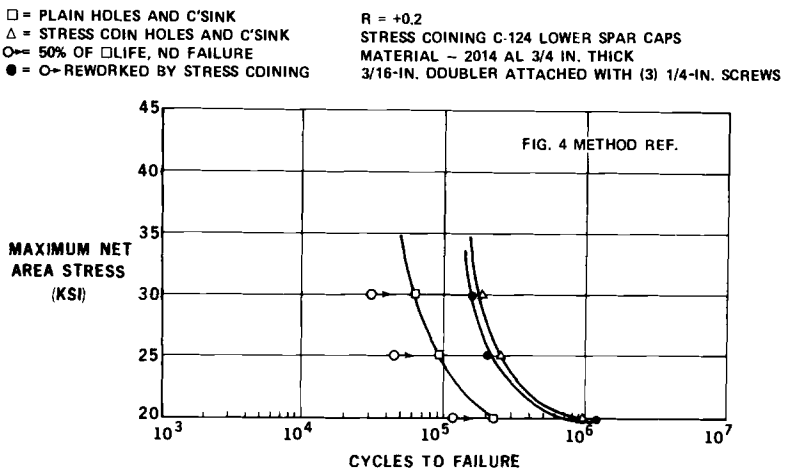

FIG. 8—*C-124 specimen fatigue test.*

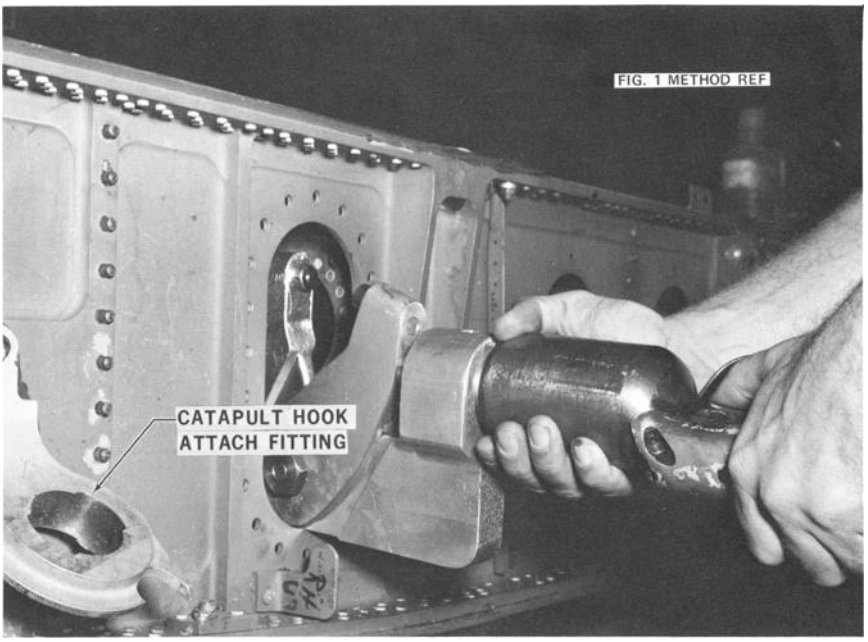

FIG. 9—*Alligator coining tool and wing front spar.*

undersized hole and the expanding tool springs back to the final hole diameter. The resulting residual compressive stresses thereby increase fatigue strength. An approximate pressure of 2500 lb is required to push the expanding pin through the hole in the fitting. The resulting highly polished mirror finish inside the hole is evidence that the hole has been stress coined. Manufacturers requested pull-broach sizing holes prior to stress coining as an optional method to reaming for production. Test data from these specimens indicated that broached, stress-coined holes have superior fatigue strength compared to reamed, stress-coined holes. Specimens were cycled to failure at various stress levels at a stress ratio of +0.2 by a Sonntag Model 10-U fatigue machine, and the cycles were recorded. *S-N* curves were plotted for the various configurations, and the results are shown in Fig. 14.

Fuel Transfer Slots

Slots for fuel transfer are machined in the vertical web of the integral fuel tank lower wing panel stringers. Located every 4 in. along the length of the stringers, the slots create stress concentrations that cause fatigue cracks. Flight of the aircraft builds up a concentrated tensile stress in the area around each slot, reducing fatigue strength. An improvement of fatigue life can be achieved by pad stress coining each of the fuel transfer slots. The coining

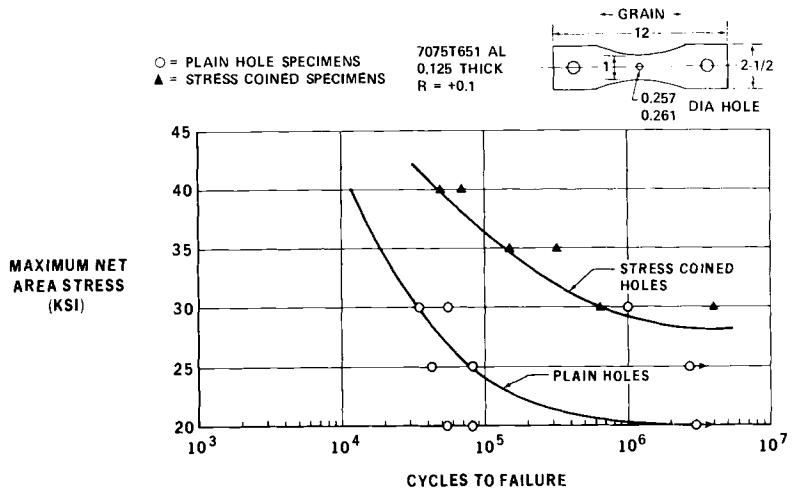

FIG. 10—*Comparison test of specimens with a conventional, plain hole and a stress-coined hole.*

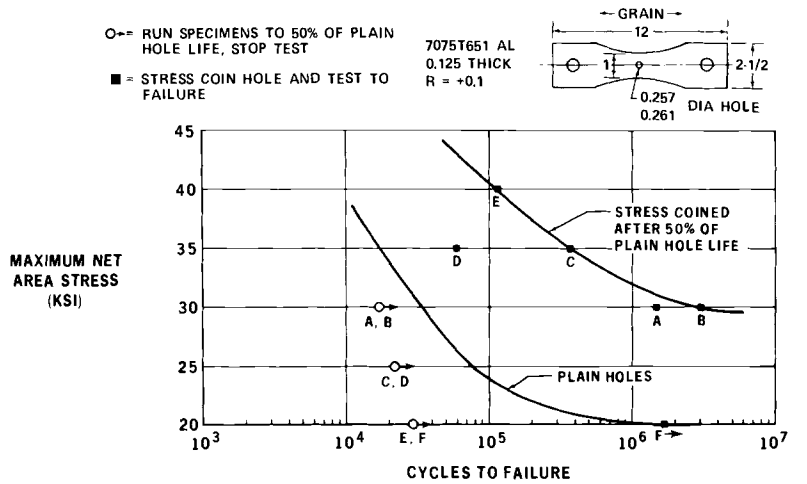

FIG. 11—*Stress coin rework after 50 percent fatigue life.*

process cold-works and plastically deforms the material surrounding the slot. When the coining pressure is released, the springback of the material induces residual compressive stresses around the slot, which offset tensile stresses concentrated there, thus increasing service life of the stringer (Fig. 15).

DC-9 Lower Wing Skin Access Door Fatigue and Failsafe

Several small, dog-bone fatigue specimens were tested to evaluate various coining methods to improve the fatigue life of the lower wing access door

doublers. Specimen variables included material (7075-T651 and 2024-T351 nonclad aluminum), material thickness, and hole preparation method. Attachment hole preparation was effected by stress coin and Douglas Process Standard (DPS) ring coin techniques.

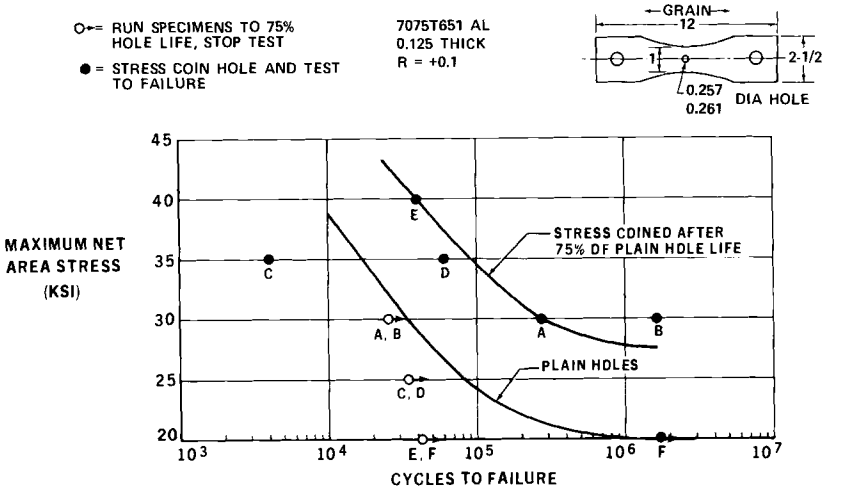

FIG. 12—*Stress coin rework after 75 percent fatigue life.*

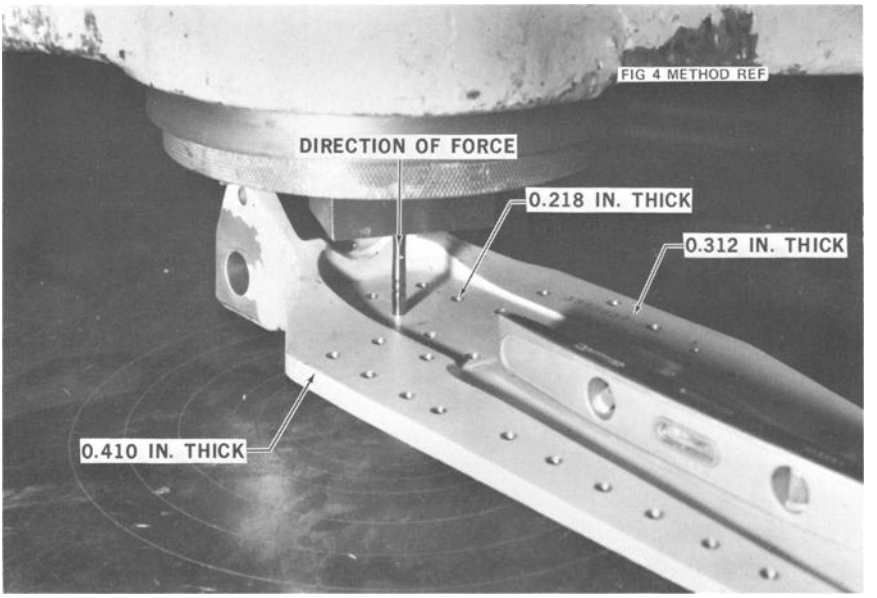

FIG. 13—*Stress-coined (expansion) DC-9 engine pylon fitting.*

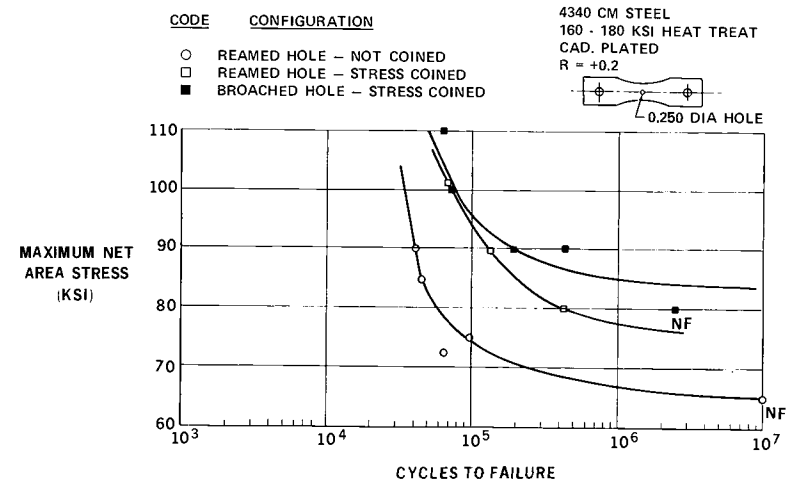

FIG. 14—*Fatigue test of 0.410-in.-thick DC-9 engine pylon beavertail fitting.*

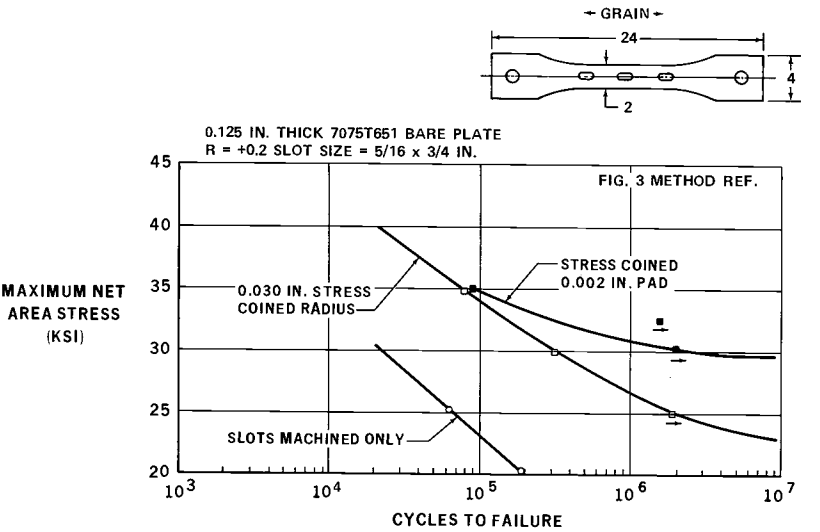

FIG. 15—*Fuel transfer slot fatigue improvement (0.125-in. 7075-T651).*

Testing of the two large access door specimens shown in Fig. 16 revealed relatively low fatigue life. Fatigue failure occurred in the oversize screw holes in the large, machined door doublers. The purpose of these tests was to compare the relative fatigue life of open holes in various thicknesses of material to similar specimens that were ring and stress coined. Another consideration was to develop a coining method that would permit sealing between the door

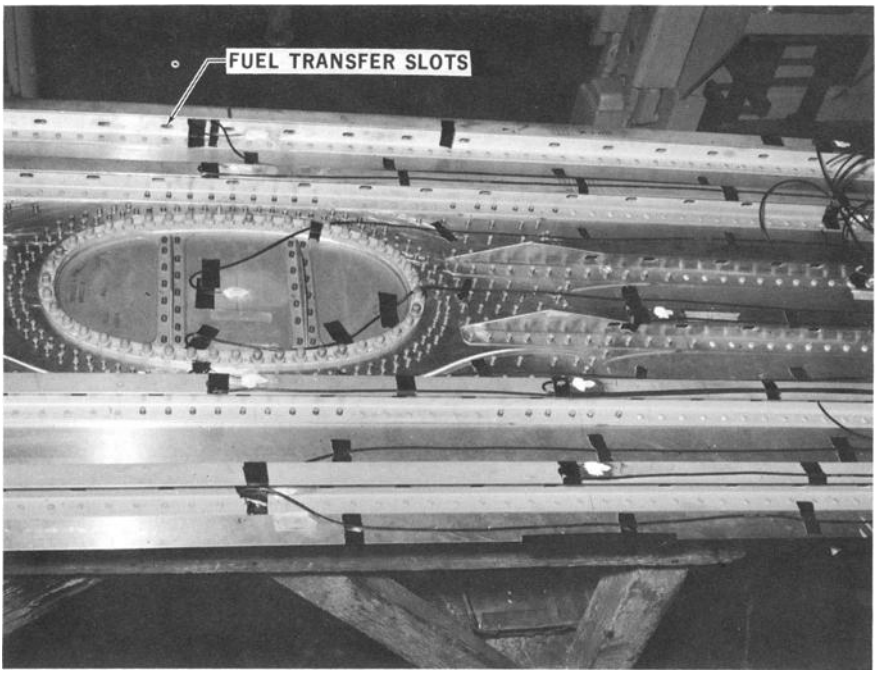

FIG. 16—*Fatigue test specimen of DC-9 lower wing skin access door.*

doubler and the rubber O-ring seal dome nuts in the retainer nutstrips. Stress corrosion cracking would also be improved by the stress coining process. This test covered the problem of increasing fatigue life of access door doublers that have oversize holes with a loose hole tolerance of 0.257 to 0.261-in. for 0.250-in.-diameter screws.

The original stress coin process by which the hole was expanded plastically to final dimensions was not adaptable to the existing design. For this application a new method was developed that considered existing design, possible rework of completed aircraft, the sealing problem around the door, increased fatigue life, and the economical feasibility of the stress coin technique. The revised method plastically deforms a circular pad, 9/16 in. in diameter and approximately 0.004 in. deep, and cold-works the sharp edge of the hole to an 0.030-in. radius (Fig. 17). This operation is performed to both sides of the material by inexpensive steel dies in a portable hydraulic gun, Fig. 18.

Test specimens were fabricated from 7075-T651 aluminum bare plate in thicknesses of 0.125 to 0.500 in. and from 2024-T351 aluminum bare plate 0.250 to 0.500 in. thick. All specimens were chromic anodized after the coining operation, then cycled to failure at various stress levels, at a stress ratio of +0.2, by a Sonntag Model 10-U fatigue machine, and the cycles recorded. Test results are presented in the form of *S-N* curves in Figs. 19–23.

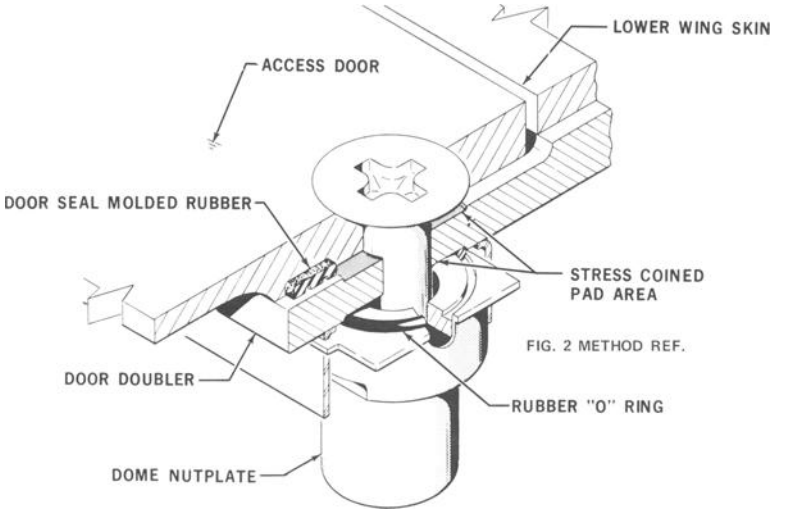

FIG. 17—*DC-9 lower wing skin access door.*

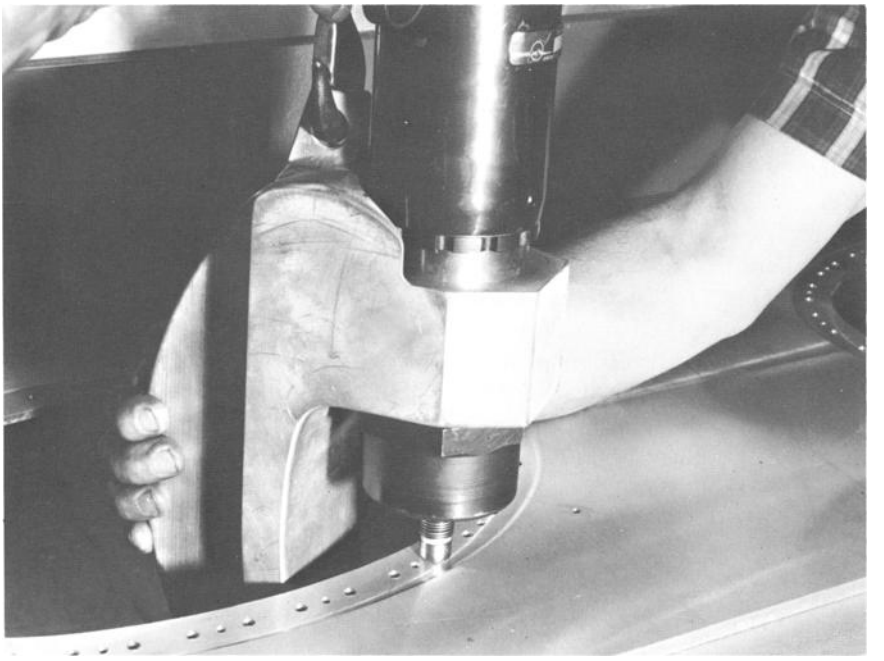

FIG. 18—*Portable, hydraulic stress coin tool.*

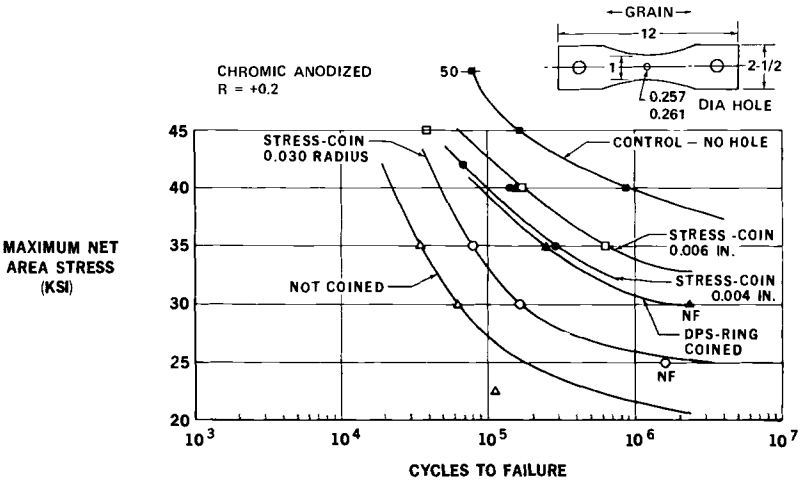

FIG. 19—*Fatigue test of 0.250-in. 2024-T351 nonclad aluminum.*

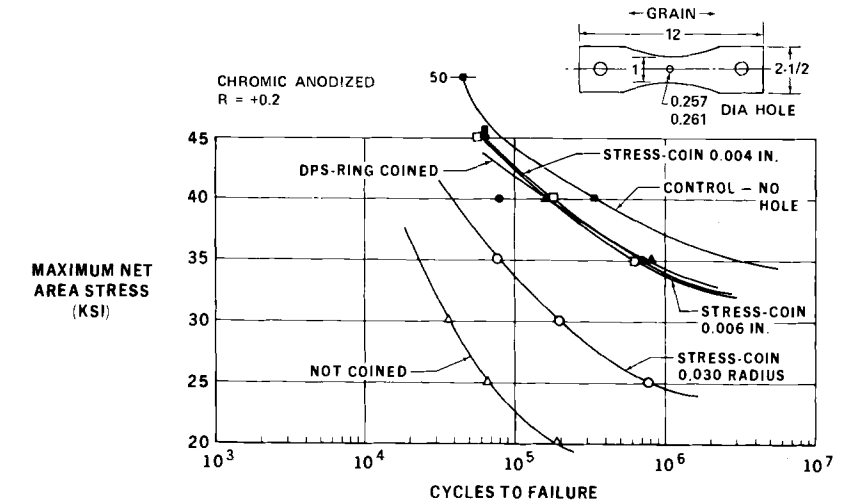

FIG. 20—*Fatigue test of 0.250-in. 7075-T651 nonclad aluminum.*

Conclusions

The fatigue strength of an aircraft structure is only as strong as its weakest link, which is usually an open or a fastener-filled hole. The fatigue strength of an open hole can be improved by various methods of coining. Stress coining the holes prior to fastener installation prolongs the fatigue life of a joined structure. The fatigue strength of riveted structures decreases with increases

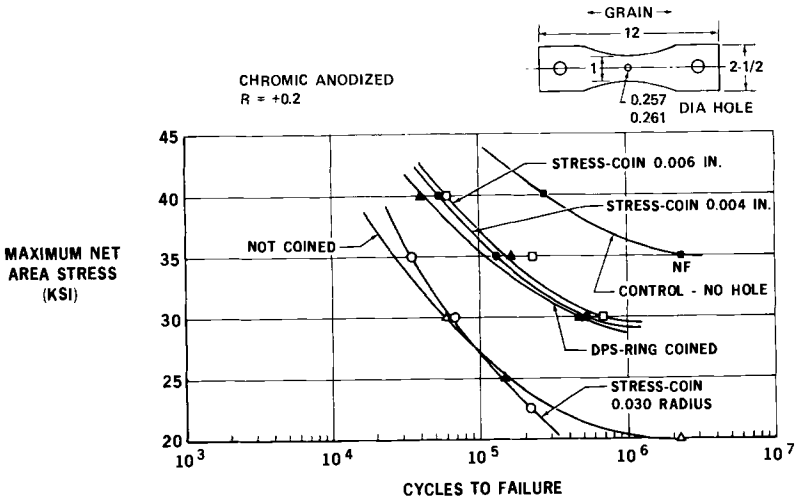

FIG. 21—*Fatigue test of 0.500-in. 2024-T351 nonclad aluminum.*

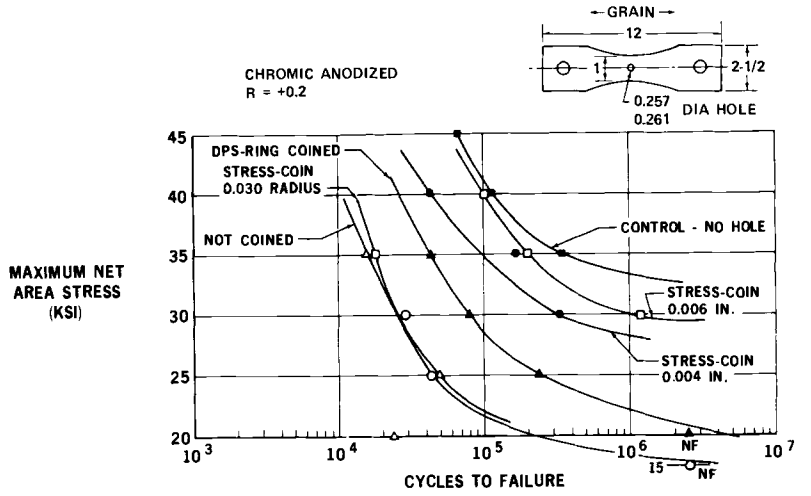

FIG. 22—*Fatigue test of 0.500-in. 7075-T651 nonclad aluminum.*

in material thickness. A method to correct this deficiency would be to expand the holes by stress coining prior to rivet installation. In general, the fatigue strength of expansion stress-coined holes is relatively unaffected by material thickness.

The stress coining development program is directed toward creating new techniques to achieve a more balanced fatigue strength for aircraft structure. The following areas deserve further study:

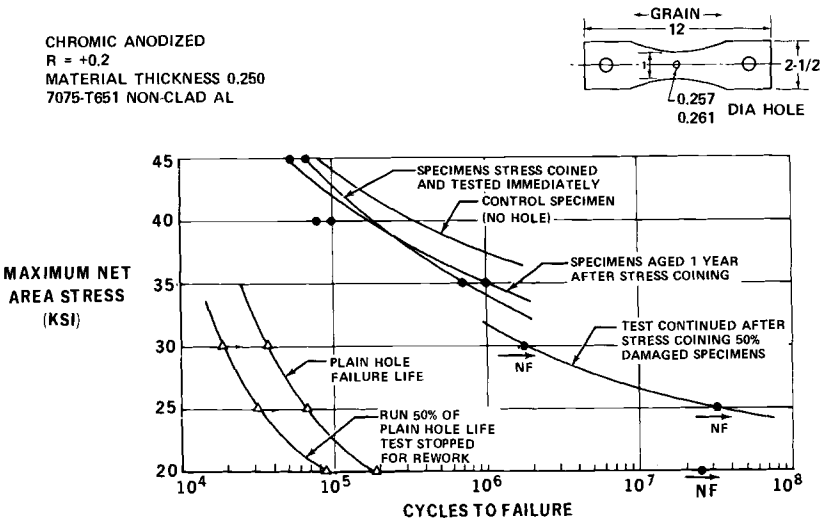

FIG. 23—*Comparison of fatigue of plain and stress-coined holes.*

1. Effect of stress coining various thicknesses of material for possible weight saving in a new heavy-transport design concept.

2. Development of field service methods for stress coin rework of delivered aircraft.

3. Cost comparisons of coining procedures so that the most economical manufacturing method can be recommended.

4. Loss in fatigue strength from attachment holes required to assemble aircraft structure.

5. Relative fatigue values of various fasteners for structural design information.

6. Stress-coined test data comparisons with conventional fatigue test data. (Results of this program would be utilized to design and rework aircraft for increased service life.)

7. Resistance-spot-welded and fusion-welded structure. (Preliminary test data indicate that stress coining resistance-spot-welded and fusion-welded structures greatly increase the fatigue strength necessary for future supersonic and hypersonic vehicle concepts.)

Bibliography

[1] Speakman, E. R., "Stress Coin Improvement of Structural Fatigue Strength," Report DAC-66668, Development Tests, Vol. 1, Douglas Aircraft Company, 29 Dec. 1967.

[2] Speakman, E. R., "Stress Coining Applications," Report DAC-66876, Douglas Aircraft Company, 2 Feb. 1968.

[3] Yen, S. W., "Stress Coin Improvement of Structural Fatigue Strength," Report DAC-66668, Mathematical Analysis, Vol. 2, Douglas Aircraft Company, 29 Dec. 1967.

[4] Yen, S. W., "Computer Solutions of Stress Distribution at a Hole Due to Stress Coining and Loads," Report DAC-67515, Douglas Aircraft Company, March 1969.

DISCUSSION

C. S. Yen[1] (*written discussion*)—From the years 1951 to 1961 I was fortunate enough to participate continuously in the development of the hole expansion and coining methods with A. Phillips, J. L. Waisman, C. Hedges, and others at Douglas Aircraft Co. These methods were used in aircraft DC-6, -7, and -8. A portion of the methods and results were presented (and subsequently published) in a paper entitled "Improvements of Fatigue Life of Aircraft Components by Coining," by A. Phillips, in the ASME National Aviation Division Conference, March 1960.

I should like to congratulate Mr. Speakman and Douglas Aircraft Co. on the new stress coining methods developed more recently. I wonder what relations and differences there are between the new methods and the previously developed hole expansion and ring coining methods? How do they compare in fatigue life improvements? Can one use both new and old methods at one hole for greater improvement?

E. R. Speakman (*author's closure*)—The recent design of airbus-type aircraft has created the necessity for new coining methods adaptable to thick materials. The ring coining method developed at the Douglas Aircraft Co. from 1951 to 1961 increases the fatigue life of single members 0.125 to 0.400 in. thick; ring coining thicknesses above 0.400 in. are restricted, as they lead to reduction of fatigue life. As the thickness increases, the effect of ring-coined grooves around the hole at the surface of the material diminishes toward the center of the material. Squeeze pressures of 20,000 to 35,000 lb are required to form the ring grooves in single members on a hydraulic press. Multiple members in aircraft joints cannot be ring coined on final assembly, whereas diassembly of aircraft structure after setup and then drilling to be ring coined proves to be impractical.

Stress coining was developed at the Douglas Aircraft Co. from 1960 to 1970 for use on final assembly, utilizing standard lightweight portable tools such as rivet guns and drill motors. Hole diameters from 0.188 to 1.500 in. have been expansion stress coined in thickness combinations up to 5 in. using portable tools.

[1] Research projects engineer, Hughes Tool Co., Aircraft Division, Culver City, Calif. 90230.

The effect of ring coining and stress coining for fatigue improvement could be considered equal in thicknesses from 0.125 to 0.400 in. Application of the coining method has to be the main consideration to obtain increased fatigue strength at reduced cost.

In some cases it would be possible to combine the methods of ring and stress coining, but the improvement gained would not justify the costs. Either coining method would improve fatigue life relative to the noncoined surrounding structure. For this reason coining is used only in areas of high tension-stress concentrations in an effort to obtain a uniform, balanced fatigue life structure.

D. V. Nelson,[1] *R. E. Ricklefs*,[1] *and W. P. Evans*[1]

The Role of Residual Stresses in Increasing Long-Life Fatigue Strength of Notched Machine Members

REFERENCE: Nelson, D. V., Ricklefs, R. E., and Evans, W. P., "**The Role of Residual Stresses in Increasing Long-Life Fatigue Strength of Notched Machine Members,**" *Achievement of High Fatigue Resistance in Metals and Alloys, ASTM STP 467*, American Society for Testing and Materials, 1970, pp. 228–253.

ABSTRACT: High compressive residual stress and high hardness were utilized to obtain high fatigue strength in nonrotating bending. A compressive residual stress of 250 ksi, obtained in a 0.25-in. notch in SAE 1045 specimens of 1.50-in. diameter, resulted in a one million-cycle fatigue strength of ±230 ksi. An investigation showed that, over the range studied, maximum residual stress from heat treatment was produced with maximum hardness, medium carbon content, maximum section size (to 4-in. diameter), and minimum hardenability. At high hardness, cold working by shot peening was found to decrease the high residual stress from heat treatment. Fatigue tests were run on peened and unpeened specimens of various hardnesses with a machine that had provisions for applying a mechanical mean stress. Various net mean stress conditions, residual plus mechanical, could then be obtained. The fatigue strength of hard specimens with a tensile, applied mean stress was reduced by the presence of crack-like defects created by peening. Data were interpreted in terms of a theory in the literature involving crack initiation, crack propagation, and yielding.

KEY WORDS: fatigue strength at N cycles, residual stress, notch sensitivity, steels, heat treatment, shot peening, crack initiation, crack propagation, yield strength, fatigue (materials), hardness, tests, evaluation, residual stress relaxation

The purpose of this investigation was to develop the maximum possible fatigue strength in a specimen simulating a notched machine member. The hypothesis was that high strength could be achieved in conventional commercial steels by combining high compressive residual stresses with high hardness in the material. Accordingly, methods for producing high compressive residual stresses were studied and the effect of these stresses on the fatigue strength of steels of varying hardness was determined.

[1] Research engineer, research physicist, and staff physicist, respectively, Research Dept., Caterpillar Tractor Co., Peoria, Ill. 61602.

The advantage of increased hardness in increasing fatigue strength has been demonstrated many times in the literature [*1*].[2] The existence of an optimum hardness for maximum fatigue strength has frequently been observed in steels: an example is the well-known data of Garwood et al [*2*]. The concept was studied by Morrow et al [*3*]. An extensive review of the literature and critical, uniaxial push-pull fatigue tests on unnotched SAE 1045 steel have demonstrated an optimum hardness in the finite life region that depends on the cyclic strain amplitude. This effect was believed to be due to a transition from a shear-governed fatigue failure mode to a tension-governed failure with increasing hardness. It was stated that the resistance to shear increased with increasing hardness while the resistance to tension decreased. This concept explains why compressive residual stresses are beneficial in the fatigue of hardened steels: algebraic addition to the applied tensile stress results in a decreased net stress. The increased shear strength of hard steels can then be utilized because the decreased resistance to tensile stresses is avoided.

A systematic investigation was carried out to determine the factors that contribute to high residual stress. The effects of composition, heat treatment, and cold working were explored primarily on SAE 86B45 and SAE 1045 steels, with some other plain carbon and boron steels used to broaden the range of variables. Specifically, the variables were carbon content, hardness, temper, hardenability, and size as they affect residual stresses from heat treatment. Induced stress by shot peening was investigated as a function of hardness. Residual stresses were measured by X-ray diffraction.

Fatigue tests were run in nonrotating bending on SAE 86B45 and SAE 1045 specimens with a minimum diameter of 1.5 in. and a 0.25-in.-radius notch. A fatigue machine was used on which it was possible to vary the magnitude of the mean mechanical stress. This stress was combined with the residual stresses produced by hardening and shot peening to give varying desired values of net mean stress at or near the surface of the fatigue specimen. The variables studied in fatigue were then the net stress and the hardness of the material being tested.

Utilizing the principle, developed in a previous investigation [*4*], that a mean mechanical stress is the equivalent of a stable residual stress of the same magnitude, fatigue strength at long lives was determined for various values of net stress. The results of the fatigue tests were interpreted in terms of a theory of Fuchs [*5*], which relates net stress to fatigue crack initiation, propagation, and yielding.

[2] Italic numbers in brackets refer to the list of references at the end of this paper.

Methods

Specimen Preparation

Steels used in this investigation are listed with their chemical compositions in Table 1. Residual stress specimens were machined from rolled bar stock to approximately 2-in. diameter by 6-in. length. Austenitizing temperature was varied between 1440 and 1600 F depending on the carbon level. All specimens were water quenched except those of SAE 86B45 steel which were quenched in oil. Fatigue specimen configuration is shown in Fig. 1. The notch geometry, corresponding to a stress concentration factor of 1.5, was the most severe that would allow X-ray stress measurements in the notch in the longitudinal direction. These specimens were finish ground in the notch after heat treatment. Those to be used unpeened were then electropolished to a depth of 0.002 to 0.005 in. in the notch to remove the worked layer. A bath of concentrated 60 percent phosphoric plus 40 percent sulfuric acid was used with a current density of about 10 A/in.^{2}. Electropolishing was also used to remove the worked material, after layer removal by grinding, for stress measurements in depth. In some cases a decarburized or oxidized layer was removed by electropolishing before the surface stress was measured. Some specimens were shot peened using S330 steel shot for 0.024-in. Almen A-2 intensity or S550 shot for 0.016-in. C-2 intensity. (These designations are explained in Society of Automotive Engineers Standard J442 and Recommended Practices J443, J444, and J827 [*6*].)

TABLE 1—*Chemical compositions of steels (weight percent).*

SAE Number	Composition, %		
	C	Mn	B
Plain Carbon Steels:			
1018	0.20	0.79	...
1035	0.35	0.82	...
1042	0.45	0.76	...
1045	0.44 to 0.50	0.70 to 0.85	...
1078	0.80	0.41	...
1095	1.00	0.26	...
Plain Carbon-Boron Steels:			
10B35	0.32 to 0.36	0.74 to 0.85	0.0004 to 0.0007
10B39	0.43	1.09	0.0014
10B45	0.43	0.85	0.0011
10B45 (elevated Mn)	0.43	1.56	0.0009
Alloy Steel:			
86B45[a]	0.42 to 0.46	0.78 to 0.94	0.0014 to 0.0016

[a] 0.45 to 0.54 Ni, 0.54 to 0.58 Cr, 0.20 to 0.22 Mo, in percent.

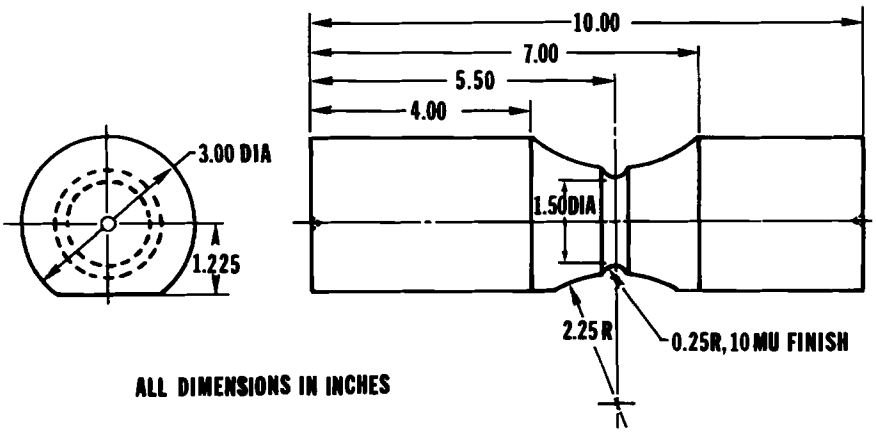

FIG. 1—*Fatigue specimen.*

X-ray Stress Technique

X-ray diffraction, residual stress measurements were made by the two-exposure method described by Christenson et al [*7*]. The stress factor was calculated from elastic constants using 30×10^6 psi for Young's modulus and 0.29 for Poisson's ratio. Both a diffractometer and a film unit were used with filtered chromium radiation and the 211 diffraction peak of iron. The film unit was built for determining stress in large parts, although the beam size could also be decreased by collimation for measuring stress in small specimens. Special cylindrical cameras were used to provide a technique closely approximating that used with the diffractometer. The machine and cameras are described in detail elsewhere [*8*]. Stresses reported in this paper were in the longitudinal direction, measured at midlength of the cylindrical specimens, and in the critical section of the fatigue specimens. Measurements in depth were corrected for the effect of the removed stressed layers [*9*].

Fatigue Test Procedure

The fatigue machine used in these investigations is described in Refs *4* and *10*. It utilizes the principle of inertial force compensation to apply a non-rotating, alternating bending stress to the specimen at 30 Hz. A mean bending stress can also be applied to produce the desired net mean stress at the surface. The quoted longitudinal bending stresses are the surface principal stresses in the notch, normal to the plane of bending, as determined with 1/32-in. strain gages. Bending produced a biaxial stress state in the notch—the ratio of tangential to longitudinal stress was 0.26.

Results

Variables Affecting Residual Stress

Heat Treatment—Surface residual stress in plain carbon steels of varying carbon content was measured after each of the successive tempers until the stress had decreased to a low value. Residual stress versus tempering temperature is plotted in Fig. 2 for the various bars. The stress was highest in the as-quenched condition for all carbon levels. The two high carbon steels showed an immediate and severe reduction in stress as the tempering temperature was increased. This was in contrast to the three lower carbon steels, which showed a more gradual decrease in stress for the lower tempers, attributable to auto-tempering.

Corresponding residual stress versus hardness plots are shown in Fig. 3. Shown also are approximate isothermals obtained by cross-plotting the data in Fig. 2. The stress versus hardness plots show a progressive displacement to the right because of the higher hardness attainable with increasing carbon. The isothermals show a maximum stress occurring in a range of 0.35 to 0.45

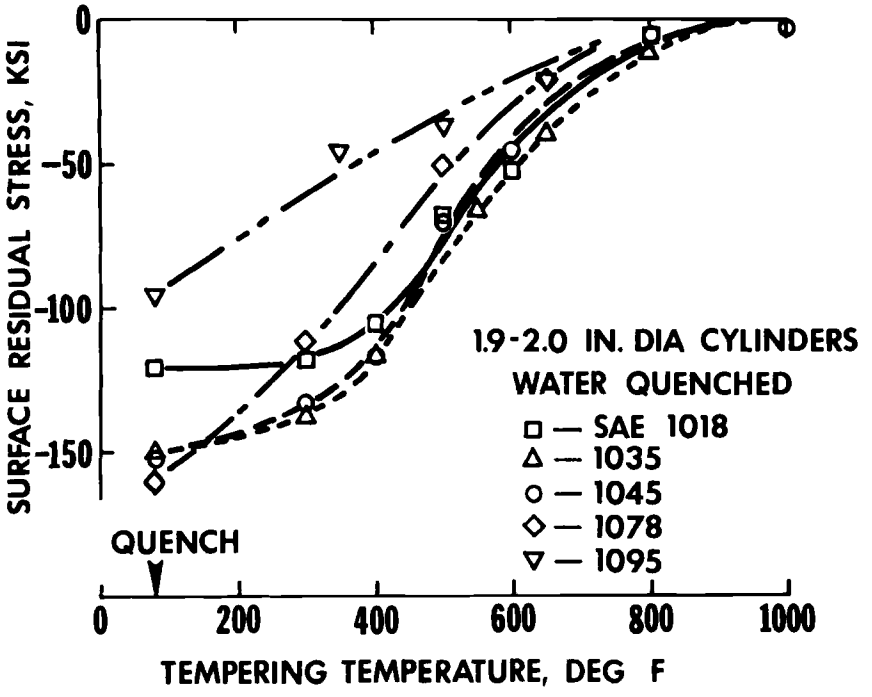

FIG. 2—*Surface residual stress as a function of tempering temperature for various plain carbon steels.*

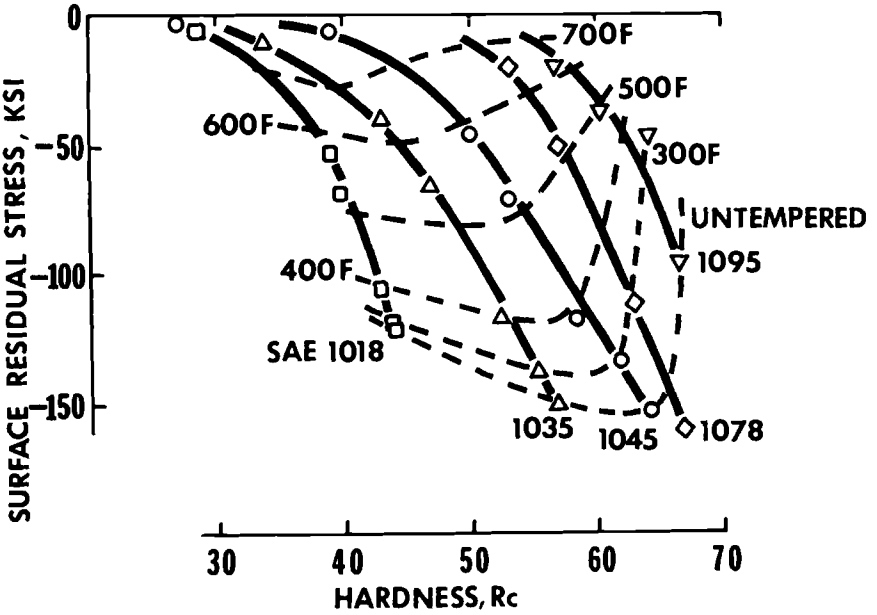

FIG. 3—*Residual stress data of Fig. 2 plotted as a function of hardness. The dotted lines represent temper isothermals, showing optimum carbon content for each given temper.*

percent carbon. Compressive residual stress induced by heat treatment increases as the carbon decreases for given hardness. This is shown specifically by the cross-plots of Fig. 4.

Residual stresses in depth were compared for steels in which hardenability had been varied by changing the manganese and boron content, but where carbon content had been maintained at approximately the same level. Figure 5 shows markedly higher compressive stress in the plain carbon steel over that of the boron steel at 58 to 59 HRc. Peak stress near the surface was 185-ksi compression for the plain carbon steel in contrast to only 125-ksi compression for the similar steel with boron. There is a general trend leading to the conclusion that "compressive stress decreases with hardenability," which is illustrated further by the peak stress versus case depth plots of Fig. 6, taken from stress versus depth curves for several steels. Case depth as used here is defined as the depth corresponding to the mean hardness between that of case and core.

The effect of section size is shown by the plot of surface stress as a function of bar diameter in Fig. 7. The induced stress due to heat treatment increased with bar diameter over the range investigated. The highest stress was nearly 200-ksi compression on the surface of a 3.75-in.-diameter bar at high hardness. A limit was to be expected, however, at very large sections because self-tempering during the quench had begun to have an effect. It is significant that

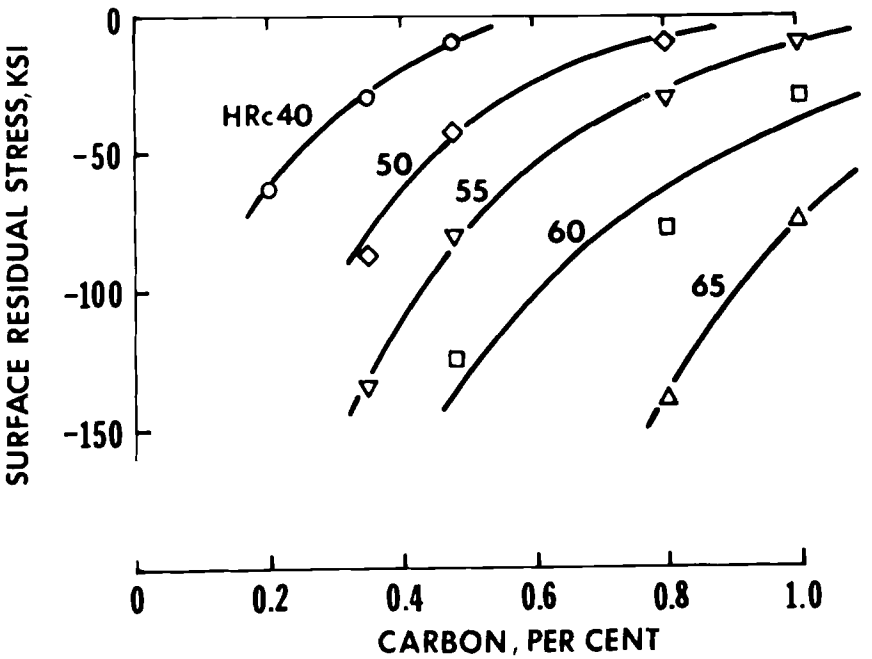

FIG. 4—*Cross-plot of the data of Fig. 3. Maximum compressive residual stress is obtained at a given hardness with minimum carbon content.*

residual stresses were greatly reduced at small sections; this occurred because transformation and thermal gradients were minimal.

Shot Peening—Surface residual stresses in SAE 1045 cylinders and representative SAE 86B45 fatigue specimens are compared in Fig. 8. The stress before peening in the alloy steel was low at all hardnesses due to the oil quenching and high hardenability, in contrast to that in the plain carbon steel. The significant fact was observed, however, that a single curve could be drawn through the data points for peening stresses induced in specimens of either prior-stressed condition for a given peening intensity.

Residual stress versus depth curves are shown in Fig. 9 for a typical fatigue specimen of SAE 1045 steel. Because the specimens were not tempered, the residual stresses due to heat treatment alone were very high in the notch. The value at the surface after removing 0.010 in. by electropolishing was 250-ksi compression. This value is considerably higher than that shown in Fig. 7 for a cylindrical specimen of the same diameter. The difference indicates a residual stress concentration or constraining effect in the notch. When a similar specimen was shot peened, the stress in the disturbed surface layer was replaced by the much lower peening stress of 60-ksi compression, in agreement with the data at high hardness in Fig. 8. This reduction in sur-

face residual stress due to peening has considerable significance in fatigue, as will be shown.

Fatigue

The SAE 1045 specimens were fatigue tested in both the peened and unpeened condition. In these tests "initiation" means that the crack can be seen with the unaided eye; "failure" means fracture of the specimen into two pieces. As shown in Fig. 10, the one million-cycle fatigue strength was in excess of ±230 ksi; the five million-cycle life to failure corresponded to approximately ±215 ksi. A significant difference existed in the crack initiation lives of peened and unpeened specimens, but the lives to failure were similar. This suggests that a crack propagation failure criterion was controlling the lives of all specimens. This supposition was further evaluated with fatigue tests in which a high tensile, mean bending stress was imposed. Figure 11 shows the *S-N* curves. The fatigue strength of peened specimens was greatly reduced.

The possibility of the compressive residual stresses in unpeened SAE 1045 specimens relaxing in the compression part of the fatigue cycle was investi-

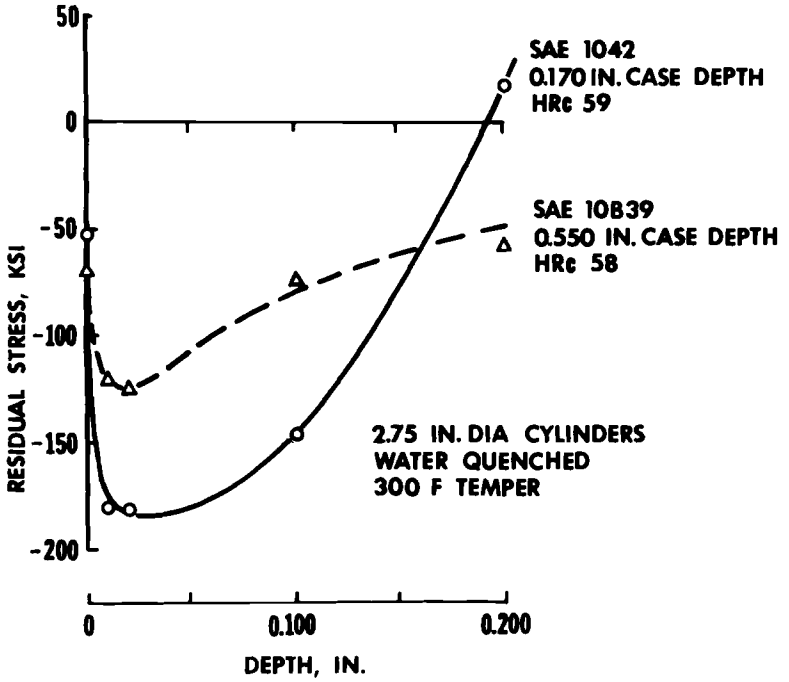

FIG. 5—*Comparison of residual stresses induced by water quenching and tempering of plain carbon and boron steels of approximately equal carbon content and hardness.*

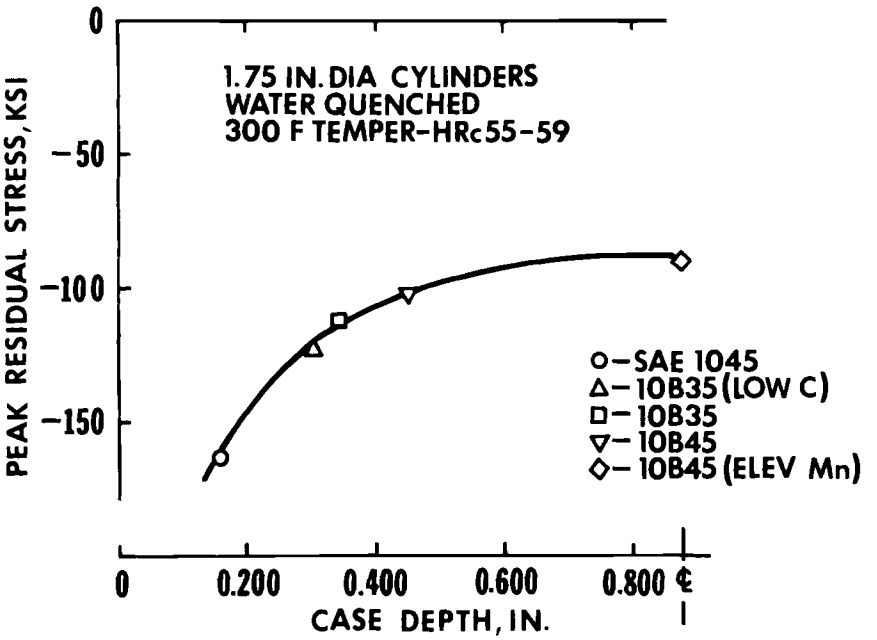

FIG. 6—*Comparison of peak residual stresses near the surface for steels of various hardenabilities.*

gated. Residual stresses were measured in a specimen after cycling at increasing stress levels. Figure 12 shows the residual, maximum, and minimum longitudinal stresses in the fatigue cycle as a function of the alternating stress. The number of cycles at each stress level ranged from 2.3 to 7.3 million. As shown in the figure, the longitudinal residual stress relaxed; tangential stress did not change.

Discussion

Variables Affecting Residual Stress

Hardness increased with increasing carbon content for a given temper, as the curves in Fig. 3 show. Therefore, to achieve a given level of residual stress, an increase in hardness was required as the carbon level was increased. Residual stress increased rapidly with hardness at all carbon levels investigated; the gradient was approximately 10 ksi per HRc point change. A carbon level of 0.35 to 0.45 percent gave maximum compression for a given temper. This is believed related to the M_s temperature, the temperature corresponding to the start of transformation of austenite to martensite. Transformation evidently occurs at a temperature resulting in a maximum thermal stress-transformation stress combination. A criterion of significance is that the highest compressive residual stress is induced when the carbon is the minimum

required to provide a given hardness, as shown in Fig. 4. This is explained by the higher tempering temperatures (and accompanying stress relief) for a given hardness as carbon increases.

Limited data on plain carbon-boron steels (not reported) showed similar trends although the stress levels induced were somewhat lower. Boron increased hardenability greatly, but residual compression was greatly reduced (Fig. 5). A definite case-core with a sharp hardness transition was necessary for high compressive stress. This optimized the transformation stress and gave the highest compression. A particular instance would need to be evaluated, however, to weigh the significance and desirability of deeper hardening and strength against increased effective fatigue strength confined to a shallower surface layer. Stress relaxation can occur in the finite life region in axial or bending stress applications due to subsurface yielding, in which case the greater core strength may be of more advantage.

The effect of quench severity can be seen by comparing the stress of 90-ksi compression in the through-hardened bar of Fig. 6 with the low stress

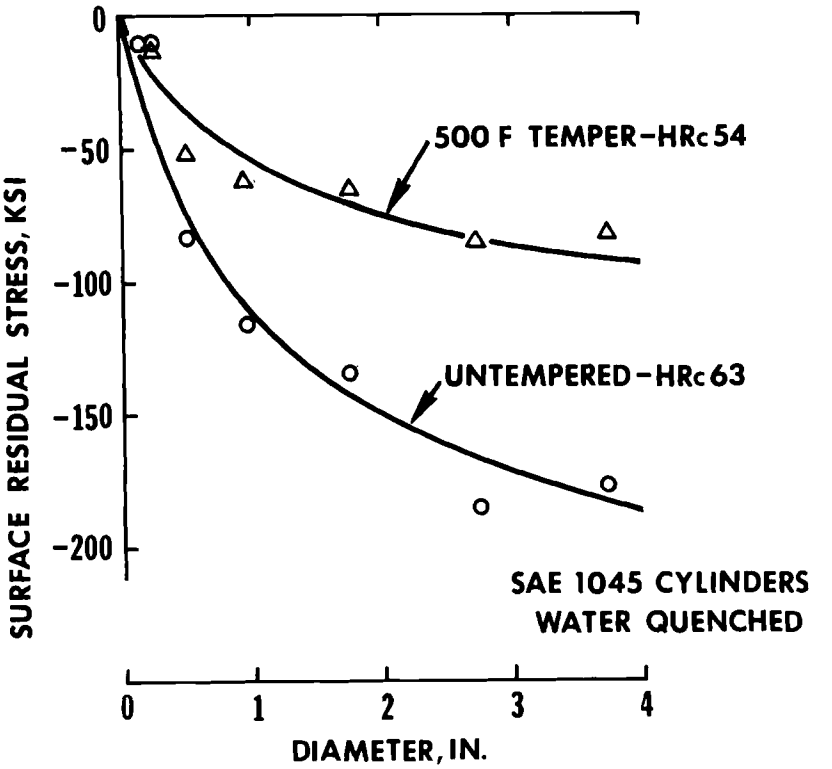

FIG. 7—*Graph showing the effect of section size on residual stress induced by heat treatment at two levels of hardness.*

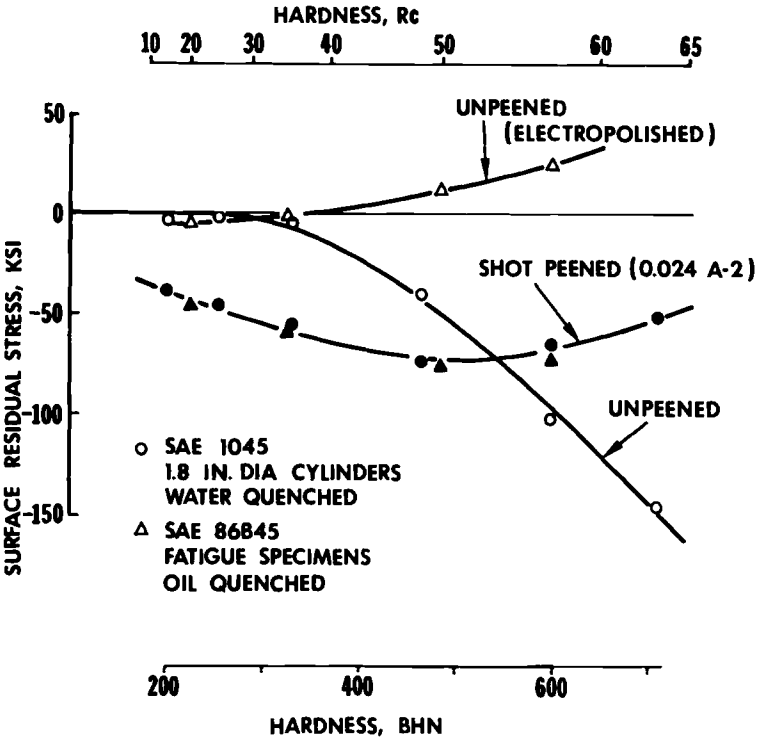

FIG. 8—*Plot showing surface residual stresses from hardening and shot peening. Note the common curve resulting from peening for two different, prior residual stress states.*

shown in Fig. 8 for the SAE 86B45 specimen of the same hardness. Both specimens hardened through the section, so no transformation stress resulted from a case-core relationship. However, the more severe water quench resulted in substantially higher residual stresses because of the higher thermal gradients.

Section size is of considerable significance, as shown by Fig. 7. When attempting to enhance fatigue strength through compressive residual stresses, large sections should be used to induce higher compression by heat treatment. This demonstrates the inadequacy of using small fatigue specimens to predict long-life fatigue performance of large parts that contain significant residual stresses. This, furthermore, relates directly to areas of practical importance where the machine members of critical interest are usually large. It is indeed fortunate that compressive stresses due to heat teratment increase with size; this helps offset brittle tendencies aggravated by both size and hardness.

Shot peening is a very practical means of cold working and is often used to strengthen the surface layers by the introduction of residual compressive stress. The "crossover" of the plots for SAE 1045 steel in Fig. 8 is believed to

be of considerable significance. It is generally known that peening stretches the surface and causes tensile yielding, leaving the surface in residual compression. Compressive residual stresses similar to those shown to the left of the crossover at lower hardness are usually expected. In the hardness range of 20 to 50 HRc the stress is usually increased in compression by peening. This also holds to the right of the crossover at 50 HRc when the prior residual stress is low. It is of considerable interest to note, however, that shot peening high-hardness steels greatly reduced the compressive residual stress when this prior stress was very high in compression. The stress induced by peening depends upon hardness and peening intensity to some extent but is quite independent of prior stress state. This has been repeatedly demonstrateed in our laboratory for a variety of prior residual stress conditions.

Interpretations of Fatigue Results

Influence of Hardness and Residual Stress—The general results of the investigations on the through-hardened SAE 86B45 steel reported in Refs *4*

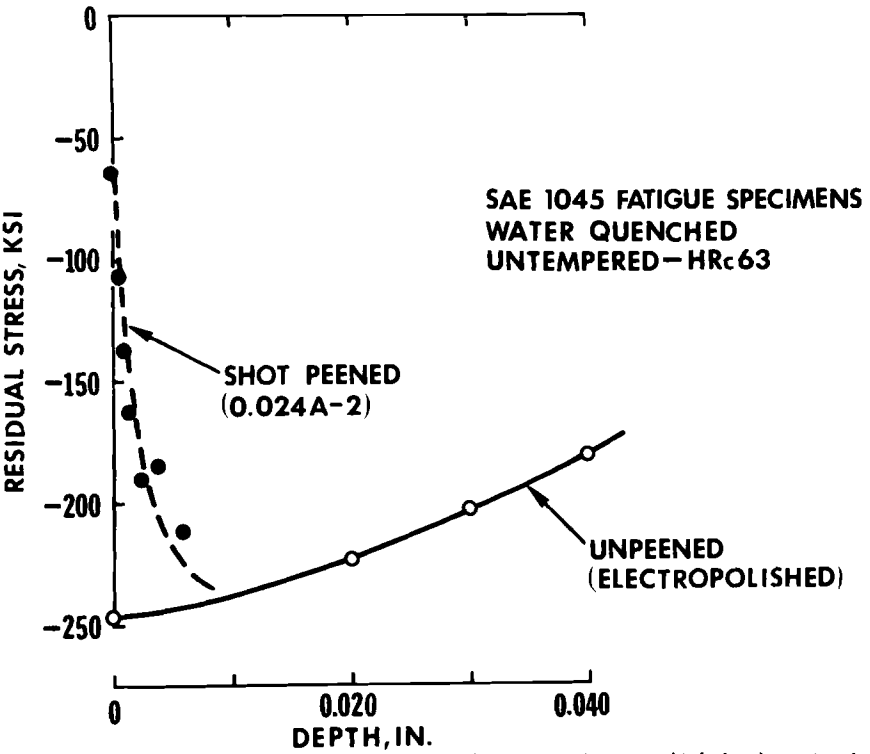

FIG. 9—*Residual stresses in depth for the fatigue specimen at high hardness in the hardened and shot-peened conditions. Note the decreased surface stress due to peening.*

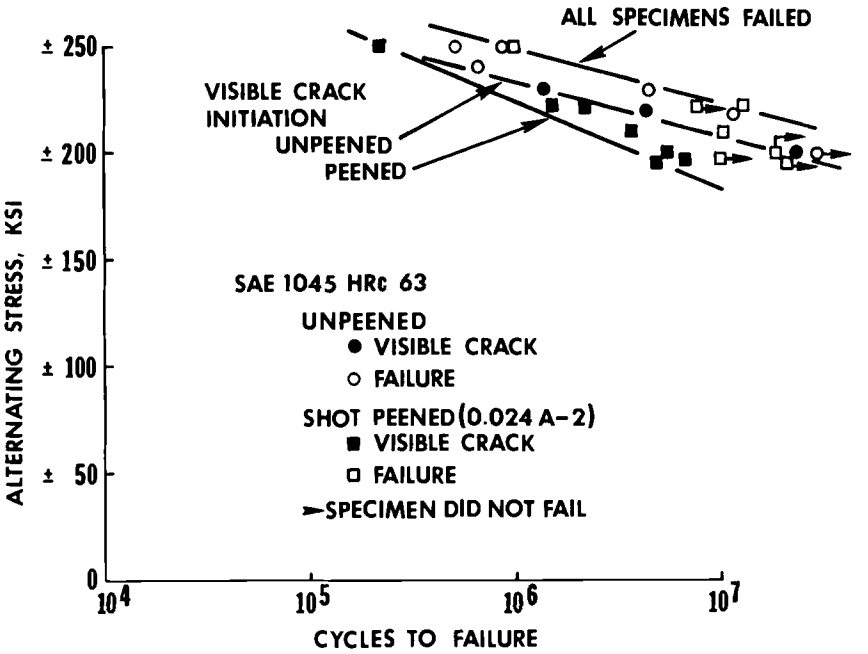

FIG. 10—S-N *curves for hardened and shot-peened specimens.*

and *10* are shown in Fig. 13. Fatigue limits are shown for hardnesses ranging from 20 to 57 HRc and for two peening intensities, all with zero mechanical mean stress and essentially zero residual stress. The data show a slight inclination toward a maximum fatigue limit for unpeened specimens between 50 and 57 HRc. The effect of compressive residual stress is to reduce the tendency toward an optimum hardness. The line defined by specimens peened to 0.016-in. Almen C-2 intensity and the SAE 1045 data represent approximately the maximum fatigue limit that can be obtained. When the surface of the specimen is protected with high compressive residual stress there is no tendency toward an optimum hardness for maximum fatigue limit. The tension-governed fatigue failure mode is avoided if compressive residual stress is present, because a very high alternating stress is required to put the surface in tension. Frequently a value of one half of the ultimate tensile stress (UTS) is used as the fatigue limit for machined surfaces. Note that a fatigue limit much greater than $\pm 1/2$ UTS can be obtained through the optimum use of compressive residual stresses.

When tensile mean stresses are applied during the fatigue cycle, specimens which have had the residual stresses imposed by shot peening frequently are much more sensitive to the mechanical mean stress than unpeened specimens. Figure 14 shows fatigue limit versus mechanical mean stress over a range of

hardness and peening intensity. The fact that shot peening increases sensitivity to tensile mean stress is certainly evident in Fig. 14; but if the data are analyzed in terms of the fatigue failure criteria advanced by Fuchs [5], the reasons for the trends become clear.

Fatigue Failure Criteria—Almen [*11*] provided the basic background for understanding and analyzing the effects of residual stress on fatigue failure when he pointed out that crack initiation and propagation are separate phenomena. He further asserted that fatigue failures result from tensile stresses and that surfaces are inherently weaker in fatigue than is subsurface material. The recognition by Fuchs that at least three separate failure criteria are needed to explain data on long-life fatigue provided a successful method for analyzing the effects of residual stress, hardness, and notches on fatigue strength. Fuch's criteria are related to the following stresses:

1. The alternating shear stress required to initiate a fatigue crack.
2. The alternating tensile stress required to propagate a fatigue crack.
3. The stress required for yielding.

An attempt is made in Fig. 15 to apply the principles of analysis of crack initiation and crack propagation behavior developed in Ref 5 to the data on

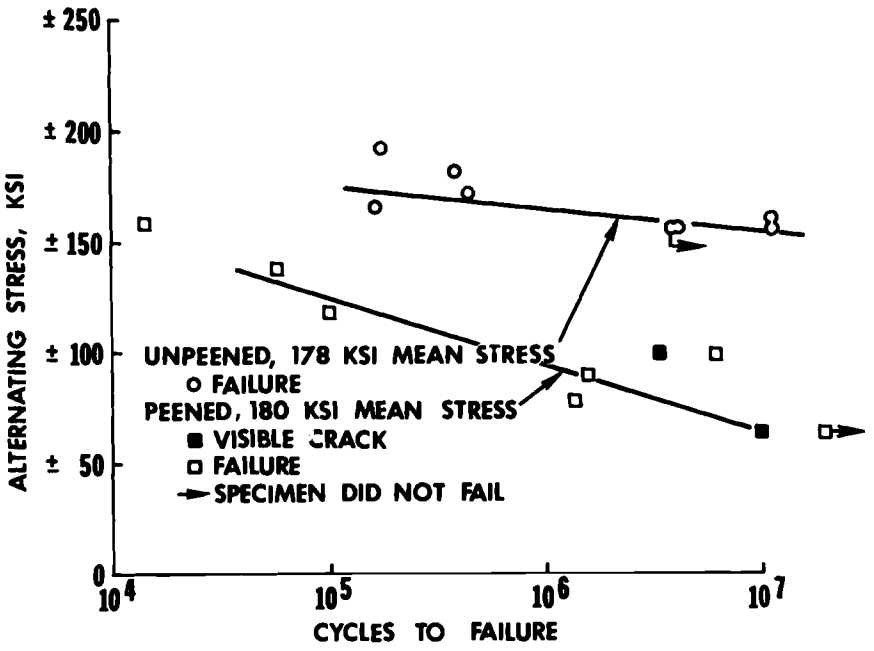

FIG. 11—S-N *curves for the conditions of Fig. 10 when a tensile mechanical mean stress is applied.*

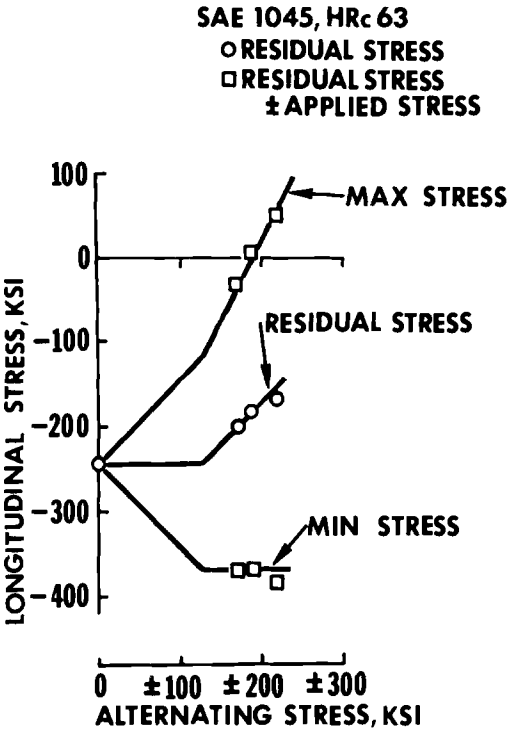

FIG. 12—*Relaxation of residual stress due to cycling at increasing stress levels.*

the SAE 86B45 material at 50 HRc. The net mean stress at the surface, as illustrated in Fig. 16, was used for those specimens plotted on the initiation line. It appeared logical on those specimens in which cracks stopped at a subsurface location—the points plotted on the propagation line—to use the peak, subsurface, net mean stress.

The steep slope of the propagation line indicates the great significance of compressive residual stresses in increasing fatigue strength in the presence of surface cracks. Such cracks might be present as a result of an intense peening operation. Observation confirmed the existence of the shaded nonpropagating crack region. Relaxation of residual stress was observed in the instance indicated by the arrow in the figure.

Crack Investigation—Cracks were examined in a peened SAE 1045 fatigue specimen which had been cycled at several increasing stress levels. Cracks were observed at the positions of maximum stress after a million cycles at the highest stress of ±221 ksi. After 7.6 million cycles at this stress level, the test was stopped so the cracks could be examined. Figure 17 shows these cracks. The specimen was then broken open by static bending. As shown in Fig. 18,

the depth of cracking is indicated by the discoloration due to fretting corrosion. It corresponds to about 0.050 in., compared to the case depth of approximately 0.150 in.

These nonpropagating cracks are explained in part by the stress versus depth curve in Fig. 9 for the peened specimens. The residual stress at the surface was not very high in compression, so fatigue cracks could initiate easily. As they propagated into regions of high compressive stress, however, their progress was slowed or stopped. This nonpropagating region is shown in Fig. 15 for SAE 86B45 at 50 HRc. A similar nonpropagating crack region existed for the SAE 1045 data.

Since unpeened specimens contained higher compressive residual stress near the surface, they may have been expected to perform even better in fatigue. Actually, as shown in Fig. 10, fatigue performance was approximately the same for the two groups; however, the unpeened specimens did not have nearly as many cracks at the surface. Both sets of specimens performed very well in fatigue because the high compressive residual stress near the surface put them in the nonpropagating crack region.

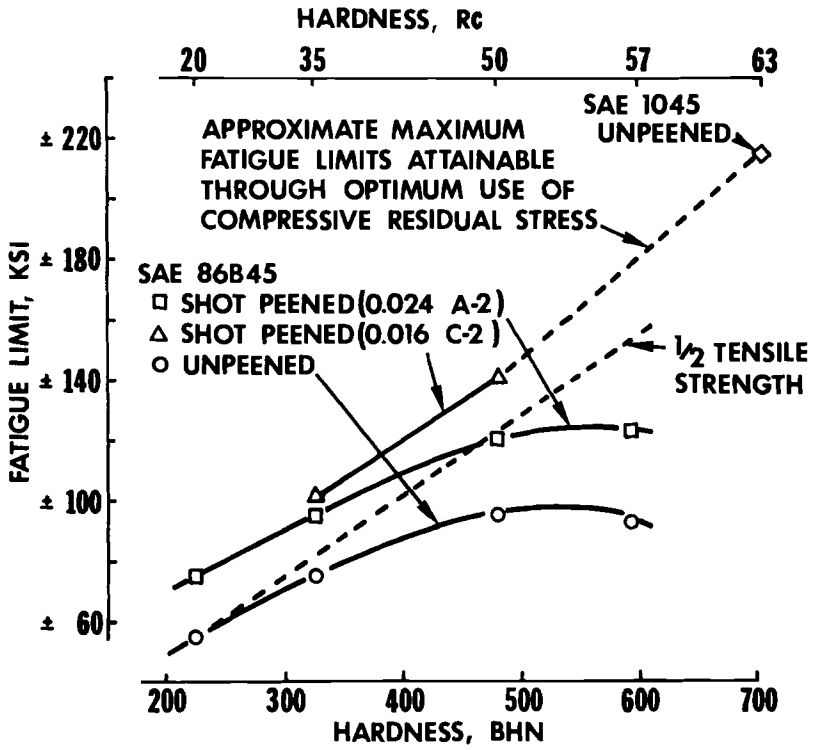

FIG. 13—*Fatigue limit as a function of hardness for hardened and shot-peened specimens —data obtained at zero mechanical stress.*

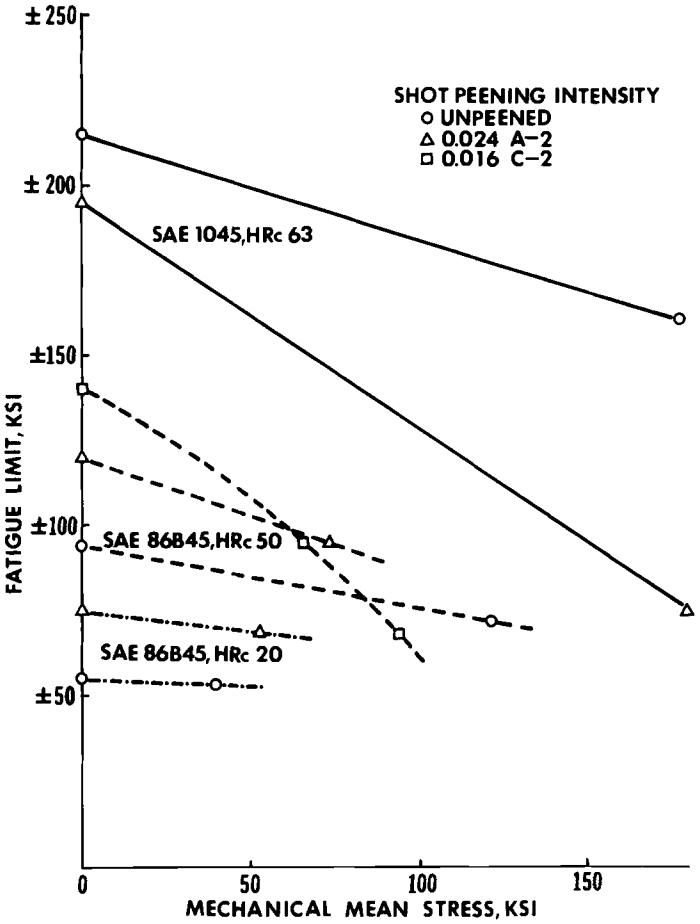

FIG. 14—*Effect of mechanical mean stress on fatigue limit for hardened and shot-peened specimens. Note the increasing sensitivity to mean stress as hardness and peening intensity increase.*

This lower surface stress could not completely explain the fact that the propagation criterion determines the fatigue strength of the peened specimens in the presence of a tensile, mechanical mean stress. The SAE 1045 specimens were examined to determine if cracks were produced by peening. Two-stage, plastic-carbon replicas were made of the surface of an electropolished specimen and of one that had been peened, and were examined by electron microscopy. The only surface feature seen after electropolishing in Fig. 19*a* is the etching at prior austenite grain boundaries. As shown in Fig. 19*b*, however, peening produced features which could be interpreted as laps or cracks. This was on a much smaller scale than the macroscopic roughening produced. The damaging effect of peening in the presence of a tensile, applied mean

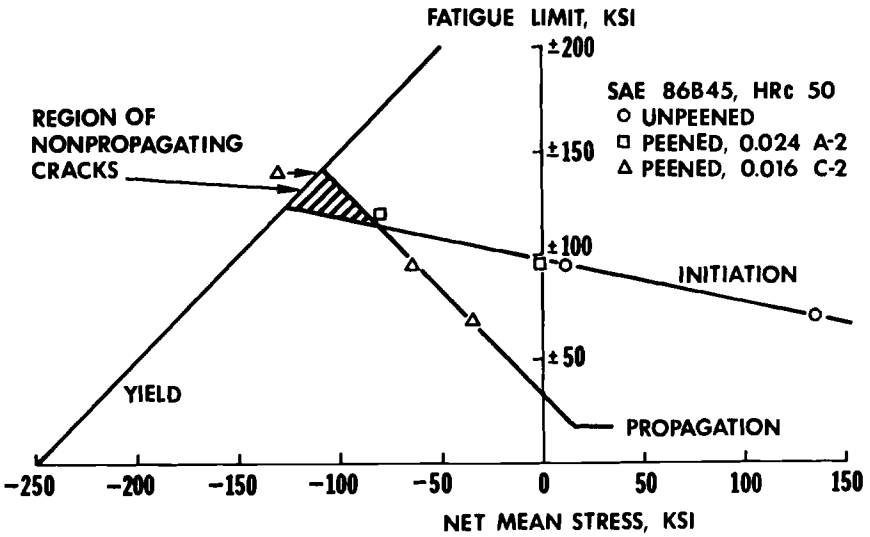

FIG. 15—*Example of the effect of mean stress on fatigue limit, showing three failure criteria.*

stress also occurred in SAE 86B45 specimens at lower hardness. At 50 HRc, peening intensity appeared to be the factor that determined sensitivity to mean stress.

An attempt was made to determine the depth of the crack-like defects. This was done by electropolishing and replicating the new surface. Data in Table 2 indicate that the depth of the crack-like defects depends upon hardness and peening intensity. Apparently, very superficial defects can cause the shot-peened surface to act in fatigue as a cracked surface.

TABLE 2—*Depth of defects produced by shot peening.*

Material	HRc	Peening Intensity	Electro-polishing Time, s	Approximate Depth, in.[a]	Defects Seen?
SAE 1045.....	63	0.024 A-2	0	Surface	Yes
			10	0.06×10^{-3}	No
SAE 86B45.....	50	0.024 A-2	0	Surface	Yes
			10	0.06	Yes
			20	0.12	Yes
			40	0.23	No
SAE 86B45.....	50	0.016 C-2	0	Surface	Yes
			10	0.06	Yes
			20	0.12	Yes
			40	0.23	Yes
			80	0.46	No

[a] From linear interpolation, based on a profilometer measurement of 0.00092-in. depth, after a 160-s polishing of the SAE 1045 specimen.

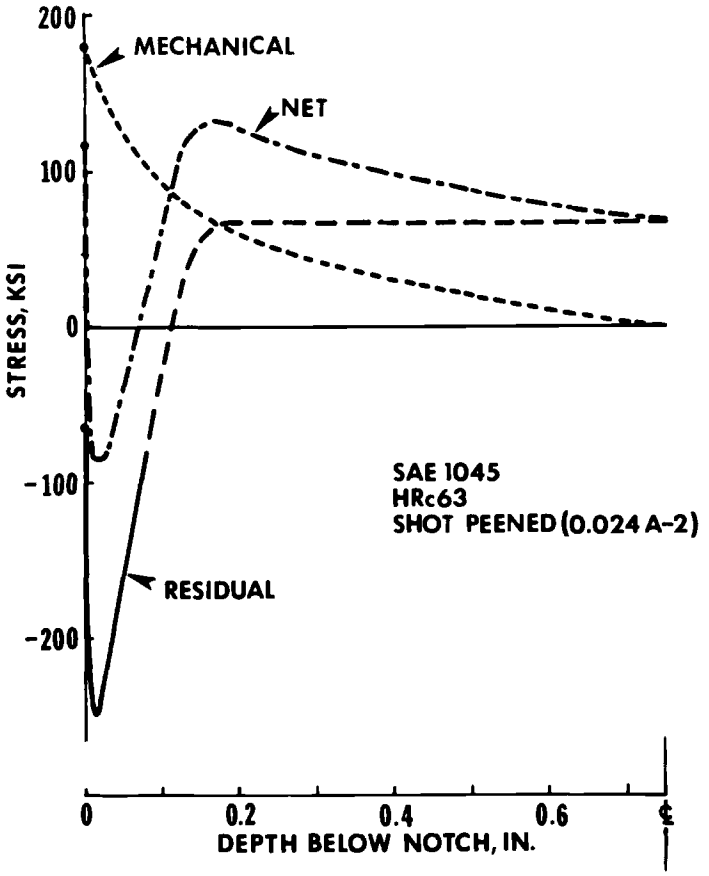

FIG. 16—*Mean stress distribution below the notch of a case-hardened, shot-peened fatigue specimen.*

Yielding—An important aspect of the yield criterion is the relaxation of residual stresses. The minimum stresses shown in Fig. 12 are replotted in Fig. 20 along with the maximum distortional energy ellipse for a uniaxial yield strength of 320 ksi. The data illustrate that yielding occurred because the minimum stress in the fatigue cycle could not exceed that permitted by the maximum distortional energy theory; consequently, the residual stress relaxed as shown in Fig. 12. In general, the effects of constraint on yielding in a notch and the possibility of cyclic softening must be considered. Cyclic softening becomes an increasingly important factor at stresses above the fatigue limit, but it can also be a factor at the fatigue limit.

The criteria for relaxation of residual stresses are often overlooked. For example, it is concluded in Ref *12* that near the fatigue limit the residual stress remains practically unchanged by fatigue loading, while at stresses

above the fatigue limit residual stresses may relax. This will usually be true, but a relationship is implied between fatigue limit and residual stress relaxation which is, in fact, incidental. Gross yielding is discussed in the SAE *Fatigue Design Handbook* [*13*] as the failure criterion that has to be considered. In notched members, however, there can be a large difference between the nominal stress required to produce gross yielding and that which causes the onset of yielding in the notch. The initial yielding is important in long-life fatigue because it can cause a redistribution of the residual stresses in the notch.

Effect of Residual Stress in Fatigue

The method of Fuchs is very helpful in extending the analysis to sharper notches. Data [*14*] on sharply notched, round, unidirectional bend specimens with a stress concentration factor of 3.6 illustrate that compressive residual stresses can greatly increase fatigue strength, as predicted with the crack propagation criterion.

The finding that the severely shot-peened surface of hard steel may have low resistance to fatigue crack initiation could imply a condemnation of shot peening. This is not the intent, and experience does not bear this out. If compressive residual stresses can be developed in a part by heat treatment,

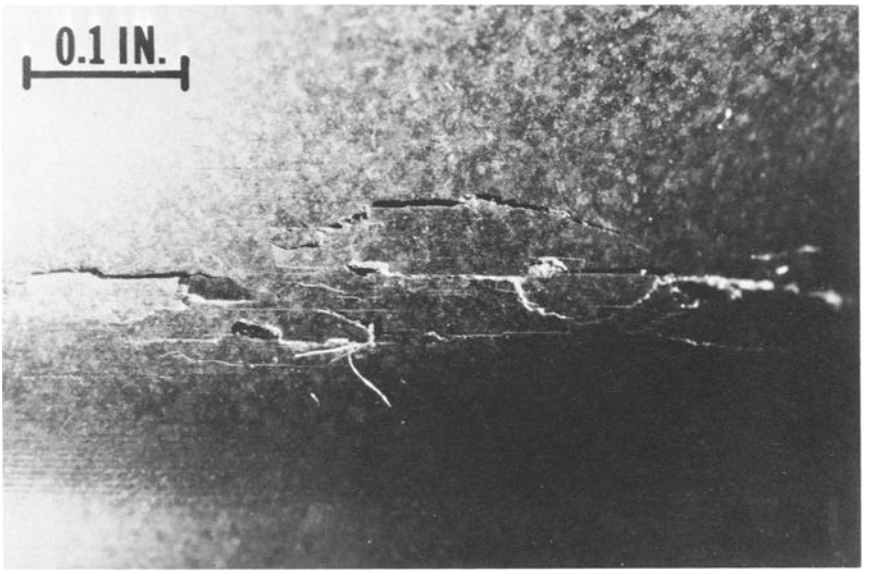

FIG. 17—*Cracks in the surface of a shot-peened SAE 1045 fatigue specimen at 63 HRc, after 7.6 million cycles at 221-ksi alternating stress. Multiple cracking and spalling are evident.*

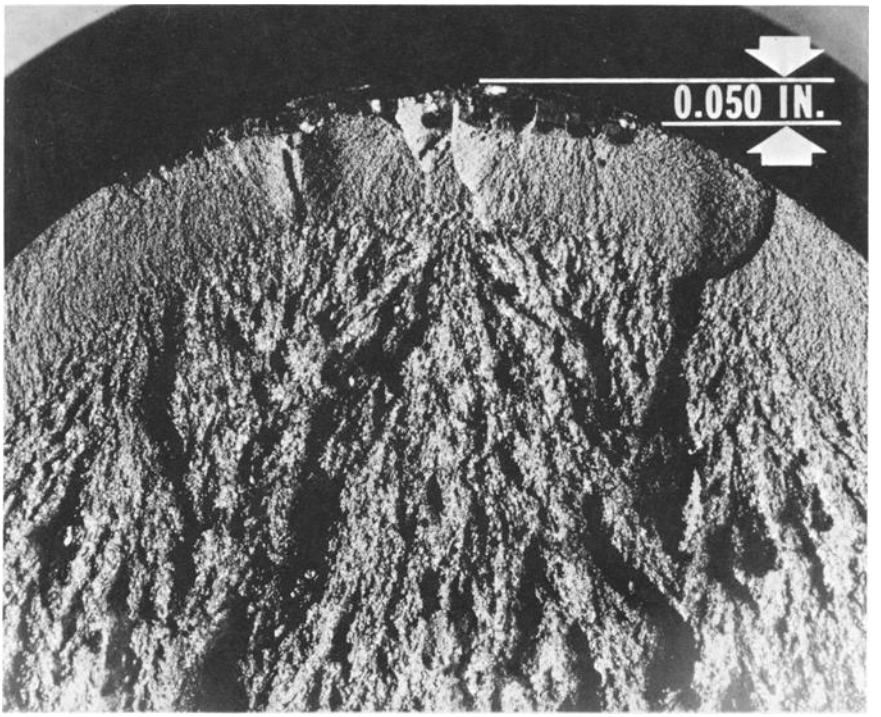

FIG. 18—*The specimen of Fig. 17 broken open. The depth of the cracking from cycling is shown by the discoloration due to fretting corrosion.*

then this is certainly the logical way to attain them, since the peening operation can be eliminated. Frequently, residual stresses developed by heat treatment will be relieved by a tempering operation required for other design considerations. In these cases there may be no alternative to shot peening. If the mechanical mean stress in a part in service is low, the implication that peening initiates a crack is irrelevant. Of far more commercial importance than the initiation of a crack by shot peening is the benefit that can be gained by the masking of prior surface weaknesses through compressive residual stresses induced by the peening.

Conclusions

Factors which contribute to maximum compressive residual stress are the following:

1. High hardness with minimal or no tempering.
2. Optimum carbon for given temper: 0.35 to 0.45 percent.
3. Minimum carbon for given hardness.
4. Large sections: 3 to 4-in. diameter.

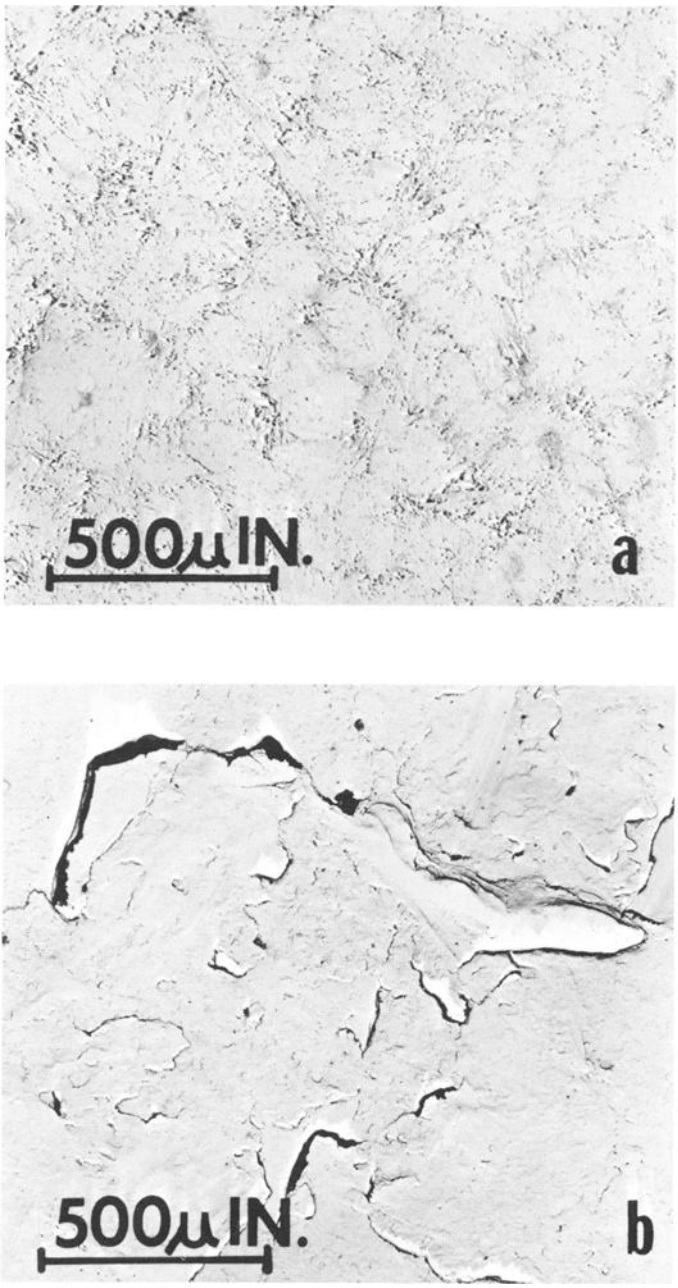

FIG. 19—*Electron micrographs showing surface defects produced by shot peening an SAE 1045 specimen at 63 HRc:* (a) *unpeened, electropolished, and* (b) *shot peened.*

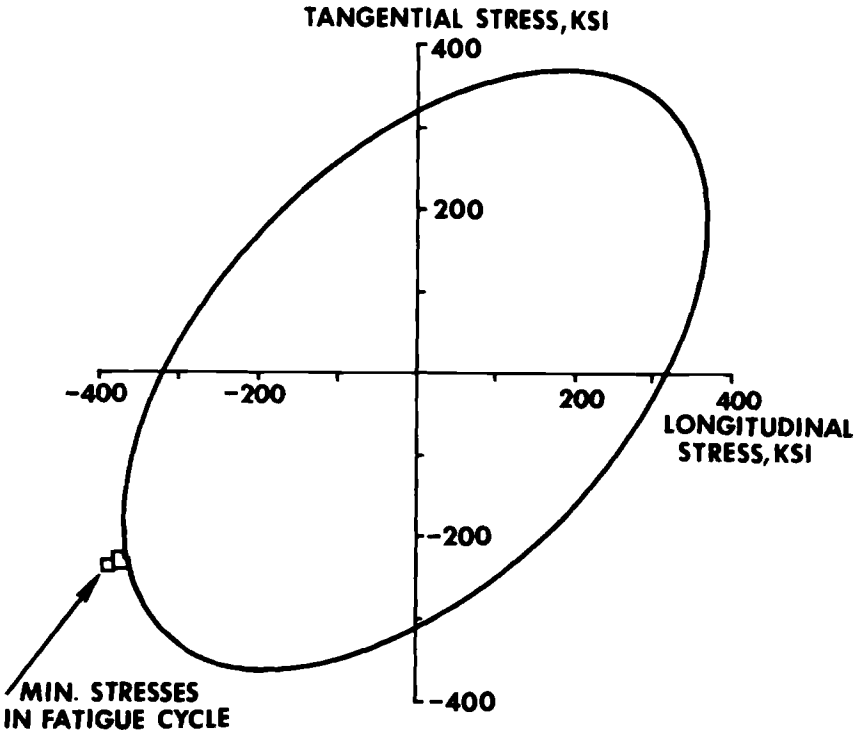

FIG. 20—*Residual stress relaxation data of Fig. 12 compared to the maximum distortional energy ellipse.*

5. Minimal hardenability (as influenced by manganese and boron over the range studied).

6. Water quenching rather than oil quenching.

Very high fatigue strength is obtainable at high hardness if the residual compressive stress is sufficiently high. A maximum compressive residual stress of 250 ksi was produced in the surface of the critical section of 63-HRc specimens, resulting in a maximum fatigue strength of ± 230 ksi at one million cycles.

Shot peening induces surface compressive residual stresses which are independent of the prior-stressed condition. For this reason peening at high hardness may be detrimental because of the possible reduction of the originally high compressive stresses from heat treatment.

Shot peening hard steel can cause crack-like defects on the surface which, in turn, cause the fatigue strength to be governed by a crack propagation criterion.

The effect of residual stress on fatigue limit depends on the governing failure criteria:

1. For crack initiation, an increase in the compressive residual stress causes a small increase in fatigue limit.

2. For crack propagation, an increase in the compressive residual stress can cause a corresponding increase in the fatigue limit.

3. When compressive residual stress is made very high, the crack propagation criterion determines the fatigue limit.

Acknowledgments

The work described in this paper was carried out in the Research Department of Caterpillar Tractor Co., Peoria, Ill. Appreciation is due J. F. Millan, for many discussions and ideas, and R. H. Sailors, who performed the electron microscopy. Appreciation is also due Henry Fuchs, Mechanical Engineering Department, Stanford University, and JoDean Morrow, Theoretical and Applied Mechanics Dept., University of Illinois, for valuable discussions.

References

[1] Landgraf, R. W., "Cyclic Deformation and Fatigue Behavior of Hardened Steels," T&AM Report No. 320, Department of Theoretical and Applied Mechanics, University of Illinois, Urbana, Ill., Nov. 1968.

[2] Garwood, M. F., Zurburg, H. H., and Erickson, M. A. in *Interpretation of Tests and Correlation with Service*. American Society for Metals, Metals Park, Ohio, 1951, pp. 1–77.

[3] Morrow, JoDean, Halford, G. R., and Millan, J. F., "Optimum Hardness for Maximum Fatigue Strength of Steel," International Conference on Fracture, Sendai, Japan, Sept. 1965.

[4] Evans, W. P. and Millan, J. F., "Effect of Microstrains and Particle Size on the Fatigue Properties of Steel," SAE Paper 793B, Society of Automotive Engineers, New York, Jan. 1964.

[5] Fuchs, H. O., *Journal of Basic Engineering*, American Society of Mechanical Engineers, JBAEA, Vol. 87, June 1965, pp. 333–343.

[6] *SAE Handbook, 1969*, Society of Automotive Engineers, New York, 1969, pp. 133–138.

[7] "Measurement of Stress by X-ray," SAE Information Report TR-182, A. L. Christenson, Ed., Society of Automotive Engineers, New York, 1960.

[8] Ricklefs, R. E. and Evans, W. P., *Journal*, Society of Materials Science, Japan, Vol. 17, No. 183, Dec. 1968, pp. 1059–1065.

[9] Moore, M. G. and Evans, W. P., *Transactions*, Society of Automotive Engineers, SAETA, Vol. 66, 1958, pp. 340–345.

[10] Evans, W. P., Ricklefs, R. E., and Millan, J. F. in *Local Atomic Arrangements Studied by X-ray Diffraction*, J. B. Cohen and J. E. Hilliard, Eds., Gordon and Breach Science Publishers, New York, 1966, pp. 351–377.

[11] Almen, J. O. and Black, P. H., *Residual Stresses and Fatigue in Metals*, McGraw-Hill, New York, 1963, pp. 43 and 59.

[12] "Influence of Residual Stress on Fatigue of Steel," SAE Handbook Supplement TR-198, JoDean Morrow and J. F. Millan, Eds., Society of Automotive Engineers, New York, July 1961.

[13] *Fatigue Design Handbook*, J. A. Graham, J. F. Millan, and F. J. Appl, Eds., Society of Automotive Engineers, New York, 1968, pp. 31–37.

[14] Liss, R. B., Massieon, C. G., and McKloskey, A. S., "The Development of Heat-Treat Stresses and Their Effect on Fatigue Strength of Hardened Steels," SAE Paper 650517, Society of Automotive Engineers, New York, May 1965.

DISCUSSION

W. G. Gibbons[1] (*written discussion*)—Subsurface failure initiation sites have frequently been noted in the fatigue of specimens which have experienced a surface residual stress treatment such as shot peening. The authors have not indicated observation of this phenomenon. However, initial results of a rotating beam fatigue study on a steel of comparable hardness do indicate subsurface failure origins for specimens containing surface residual stress. Thus, further discussion of this topic is merited.

The material employed in the aforementioned study was H-11 steel (0.35 C, 5.00 Cr, 0.4 V, 1.5Mo) in a 55 to 56 HRc condition. Discussion of some shot-peening results will indicate similarities and differences with respect to the authors' work. For the H-11 specimens the peak residual stress of −110 ksi, determined by X-ray techniques, occurred at the surface. Since the shot-peening intensity employed was 0.024-in. Almen A-2, comparison with the information of Fig. 8 shows a higher surface residual stress for the H-11. This difference might be partially accounted for in the polishing of the hour-glass gage section of the 0.250-in. minimum diameter specimens subsequent to shot peening. Although the nonpeened H-11 specimens indicated a fatigue limit of 111 ksi at 10^7 cycles (higher than the authors' results of Fig. 13), the peened fatigue limit was 118 ksi, which is essentially identical with the peened results.

Subsurface failure origins were observed to occur in the shot-peened specimens near the location of the maximum net tensile stress. The variation in the results was due to the differences between the specimens of the residual stress gradient and the fatigue strength gradient. The net stress had been considered for only the tension-loading portion of the fatigue cycle. To obtain this for some of the authors' results, the tensile portion of the applied alternating stress would have to be added to the net mean stress curve of Fig. 16. In performing that operation, it appeared that the peak tensile stress would occur at the surface. Thus, failure would initiate at the specimen surface and no subsurface failure origins should be identified.

[1] Materials project engineer, Sunstrand Aviation, Rockford, Ill. 61101. Associate member ASTM.

D. V. Nelson (author's closure)—Mr. Gibbons's interesting results further point out the necessity for analyzing the residual and applied stresses for each particular fatigue problem. A residual stress-inducing process can have widely differing effects in fatigue, depending on the applied stresses. More work is needed to determine how far below the surface the balancing tensile stress has to be before it no longer has a measurable detrimental effect in fatigue. Stress gradients would have an important effect in such an investigation.

The fatigue limit of the H-11 steel in the nonpeened condition ($\sim$111 ksi) is higher than that of our unpeened curve in Fig. 13, because the tougher H-11 steel presumably has more resistance to the tension-governed fatigue failure mode. However, by optimizing hardenability, heat treatment, and section size to obtain high compressive residual stress (in an economical steel) we could obtain a fatigue limit of approximately $\pm$170 ksi at the 55 to 56 HRc level compared to the $\pm$118 ksi for the peened H-11 steel. Our highest fatigue limit of $\pm$215 ksi occurred in SAE 1045 steel at high hardness with a residual compressive stress of 250 ksi. This very high fatigue limit was a direct result of the very high compressive residual stress in the unpeened SAE 1045 steel.

B. I. Sandor[1]

Metal Fatique with Elevated Temperature Rest Periods

REFERENCE: Sandor, B. I., "**Metal Fatique with Elevated Temperature Rest Periods,**" *Achievement of High Fatigue Resistance in Metals and Alloys, ASTM STP 467*, American Society for Testing and Materials, 1970, 254–275.

ABSTRACT: Intermittent annealing of oxygen-free high-conductivity copper is used to investigate the accumulation of low-cycle fatigue damage under total diametral strain control. Cyclic strain-induced cold work can be removed independently of the number of prior strain cycles or annealing periods. Specimens with frequent intermittent annealing have slightly extended fatigue lives instead of reductions in life predicted on the basis of the Manson-Coffin relation.

Frequent rest periods at mildly elevated temperature reduce the cyclic plastic strain and retard the fatigue damage process in mild steel tested under axial stress control. Fatigue life may be increased by a factor of 100 as a result of treatments applied every 1 percent of the estimated life. The Manson-Coffin relation accurately predicts the prolongation of fatigue life in this case.

KEY WORDS: fatigue (materials), annealing, precipitation hardening, axial stress, fatigue life, plastic deformation, metals, cold working, evaluation

Most of the research on metal fatigue has been aimed at prediction of fatigue lives for load-carrying members. Studies of fatigue damage mechanisms have also received considerable attention. In comparison with these areas of interest, little research has been carried out on fatigue damage alleviation, which concerns processes for extending fatigue life that may be applied during fatigue loading. Investigations of such techniques may help in clarifying the mechanisms of fatigue damage accumulation. There is also hope that eventually practical methods will be found to extend the useful fatigue life of structural members.

A number of techniques have been used in previous attempts to reverse or retard fatigue damage. Surface peening [*1*],[2] understressing and coaxing [*2*, *3*], and surface removal [*4*, *5*, *6*] are examples of successful methods. Rest

[1] Assistant professor, College of Engineering, University of Wisconsin, Madison, Wis. 53706. Personal member ASTM.

[2] Italic numbers in brackets refer to the list of references at the end of this paper.

periods and annealing have been tried in a relatively large number of investigations but were found to be generally ineffective. A review [7] of these investigations showed that all of them dealt with the long-life region, that most of them used load control, that cyclic plastic strains were not measured, and that rest periods were applied infrequently during the tests. The reported small improvements in fatigue life were obtained only in ferrous metals.

Intermittent annealing and rest periods remain promising techniques in fatigue research because they affect the bulk properties of the metal and may cause large changes in stress-strain response. Such changes are responsible for the effectiveness of the treatment and provide insight into the damage mechanism. Recent advances in testing facilities and in the understanding of the nature of fatigue damage make it worthwhile to study the effects of intermittent treatments.

The main purpose of the present investigation is to study the feasibility of extending low-cycle fatigue lives under both stress and strain control. Intermittent heat treatments are used to alter the deformation characteristics of copper and steel tested at room temperature. Cyclic stresses and strains are monitored to show the material response between treatments. These measurements are also necessary to judge how frequently the treatments must be repeated to prolong the fatigue life.

Intermittent Annealing of Strain-Cycled Copper

Previous attempts to extend the life of nonferrous metals have been largely unsuccessful. Intermittent annealing of stress-cycled aluminum, brass, copper, and magnesium were virtually ineffective [6, 8, 9]. A recent investigation by Weissman and Park [10] using aluminum single crystals indicates a slight extension of fatigue life, but this work is difficult to interpret because deflection control was used in bending and annealing was done during cycling. The best documented investigation is by Sinclair and Dolan [11], which showed that periodic recrystallization of brass did not affect its finite fatigue life in a constant moment rotating bending test.

Repeated heating of nonferrous metals under load control is not expected to improve the fatigue life, since these metals are generally softened rather than strengthened by heating. After annealing they show considerable cyclic hardening during the early portion of a fatigue test. Reducing the cold work by annealing would therefore permit more cyclic plastic strain just after the treatment, which could increase the fatigue damage as predicted by the Manson-Coffin relation [12].

The behavior under cyclic strain control would be essentially the same except that the cyclic *stress* would be temporarily reduced after each anneal. Even though this is accomplished by an increase in the cyclic plastic strain,

the fatigue life might be increased for nonferrous metals by effectively reducing the role of stress raisers. It is also possible that repeated annealing under this condition may delay the onset of "nonhardening" strain and extend the fatigue life despite the increase in cyclic plastic strain. Alden and Backofen [*13*] applied frequent intermittent annealing in aluminum single crystals that were cycled in pure bending. They found a delay in the clustering of slip that is normally associated with fatigue cracking. Life data were not obtained in these tests.

It appears that only Harries and Smith [*5*] have attempted to obtain fatigue life data using intermittent annealing for a strain-cycled metal. They tested aluminum in the long-life region, annealed once during each test, and reported no effect due to these treatments. Cycle-dependent hardening is rapid in this metal after annealing so that more frequent intermittent treatments are needed to cause a large change in the fatigue behavior.

In the present work annealing was applied frequently during each test to alter the cyclic stress-strain response and thus affect the fatigue life of copper.

Experimental Program

Material and Specimens—Oxygen-free, high-conductivity copper was chosen for its cyclic-hardening characteristics. The chemical composition is shown in Table 1. Hourglass specimens were made with a 1.00-in. radius of curvature and 0.25-in. min diameter. Specimens were annealed in a moderate vacuum of 10^{-3} torr at 630 C for 1 h.

Apparatus—Tests were conducted in an Instron machine. A liquid-solid grip of Wood's metal was used for clamping specimens without distortion. Loads were measured by a cell in series with the specimen, and strains were measured by the diametral clip gage shown in Fig. 1. The clip gage (a strain gage

TABLE 1—*Chemical composition of copper.*

Element	Composition by Volume
Cu	99.99% minimum
Total of As, Sb, Bi, Se, Te, Sn, and Mn	<40 ppm
S	<18
Pb	<10
Se	<10
Te	<10
Bi	<10
O	<10
P	<3
Cd	<1
Zn	<1
Hg	<1

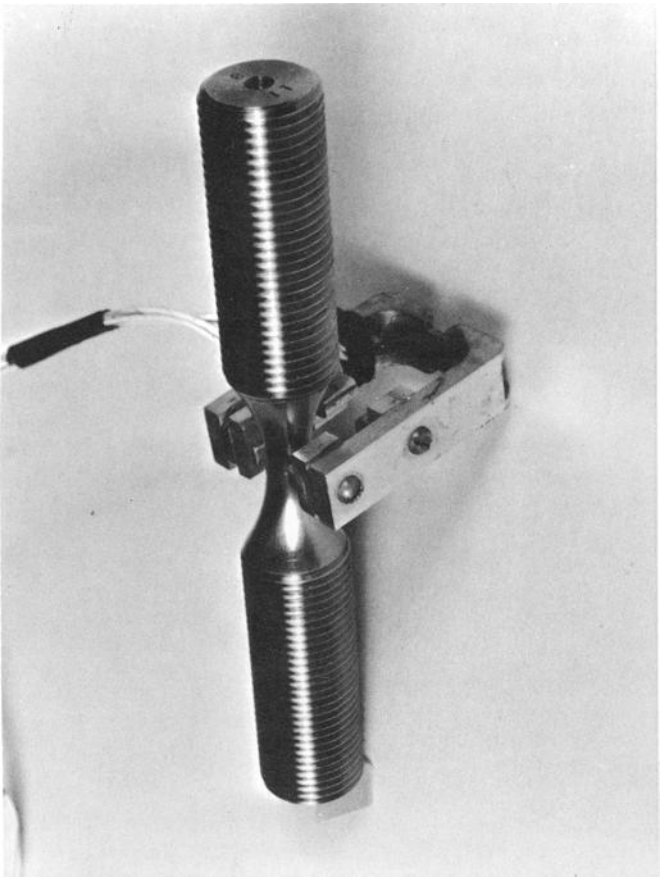

FIG. 1—*Hourglass specimen with diametral clip gage.*

extensometer) exerted a lateral force of 1 lb or less on the specimen. The contact blocks on the gage were contoured to the hourglass shape of the specimen to get low contact pressure. Hysteresis loops were frequently recorded during each test. A vacuum furnace was used for the periodic annealing of the specimens.

Test Conditions—Strain cycling was done at room temperature. Fully reversed, axial push-pull was applied under 0.8 percent total diametral strain control. The resulting total longitudinal strain calculated for the minimum section was 1.75 percent. Tests were performed at the rate of 2 cycles per minute. At the end of each block of cycles, the specimens were returned to zero stress and strain and then removed from the machine for annealing in a 10^{-2}-torr vacuum. Temperature was raised to 575 C in 30 min. Specimens were at the peak temperature for 3 min and were furnace cooled under vacuum in 15 h.

Results and Discussion

The mechanical properties for the copper were determined at 0.02-in./min crosshead speed and are listed in Table 2. The cyclic data show that after each annealing the metal regains its original deformation characteristics. A typical sequence of hysteresis loops in Fig. 2 shows that the increase in plastic strain and the decrease in stress is temporary. Similar loops were obtained throughout the fatigue life, independent of the frequency of annealing, and even in the presence of visible cracks. The variation in plastic strain caused by repeated annealing is shown in Fig. 3. The stresses vary under the constant total strain range, as is demonstrated in Fig. 4.

TABLE 2—*Monotonic mechanical properties of copper.*

Condition	0.2% Offset Yield Strength, ksi	Ultimate Strength, ksi	Reduction of Area, %	Strain Hardening Exponent
Annealed.....	3	30	80	0.40

The distribution of fatigue lives (under 0.8 percent diametral strain control) for various intermittent treatments is given in Table 3. The tests are also shown in the plastic strain range versus fatigue life plot of Fig. 5. Average life increases slightly with the number of annealing periods: specimens annealed every 300 cycles had a 20 percent increase and those annealed every 50 cycles

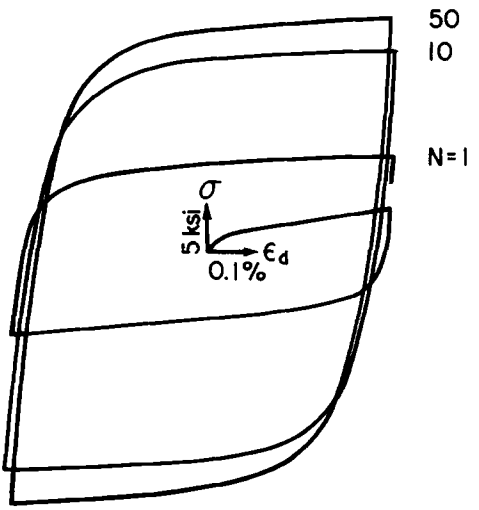

Fig. 2—*Typical hysteresis loops following annealing of strain-cycled copper.*

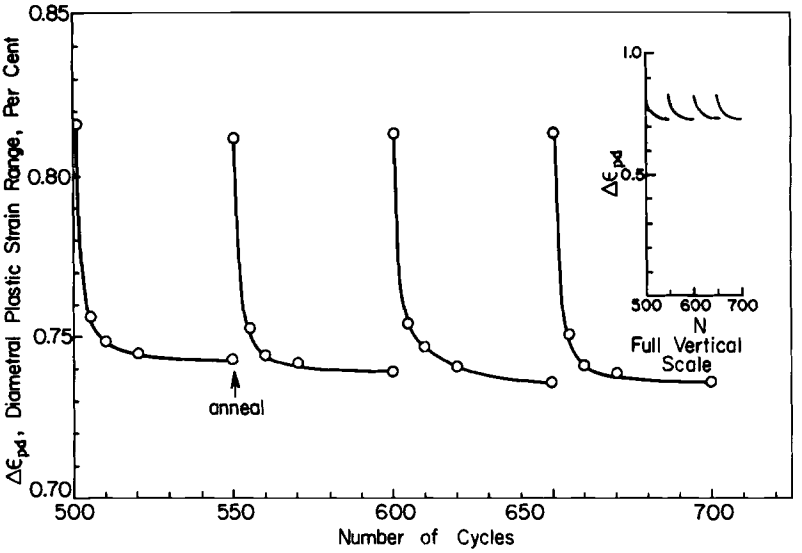

FIG. 3—*Temporary increases of plastic strain range in copper following annealing.*

had a 30 percent increase in life compared with the group not treated during testing. For each group the improvement in mean life is significant at the 99.9 percent level of confidence found from the t-distribution. A comparison of the F ratios with tables of the F-distribution shows that the dispersion was not affected by the treatments.

Damage Analysis—The data show that the cyclic plastic strain increases after intermittent annealing as expected. It was not expected, however, that the fatigue lives would also increase. On the basis of the Manson-Coffin relation [*12*] a shortened fatigue life is predicted for an increase in plastic strain range. Fatigue life depends on cyclic plastic strain according to the following equation:

$$\Delta\epsilon_p/2 = \epsilon_f'(2N_f)^c$$

where:

c = -0.55 for annealed copper [*14*],
$\Delta\epsilon_p$ = plastic strain range,
N_f = fatigue life in cycles, and
ϵ_f' = constant.

This equation may be used to calculate cumulative fatigue damage when the cyclic plastic strains are known. Plastic strain range versus cycles curves, as in Fig. 3, are broken into short segments, and for each segment the representative plastic strain is raised to the $1/c$ power and multiplied by the

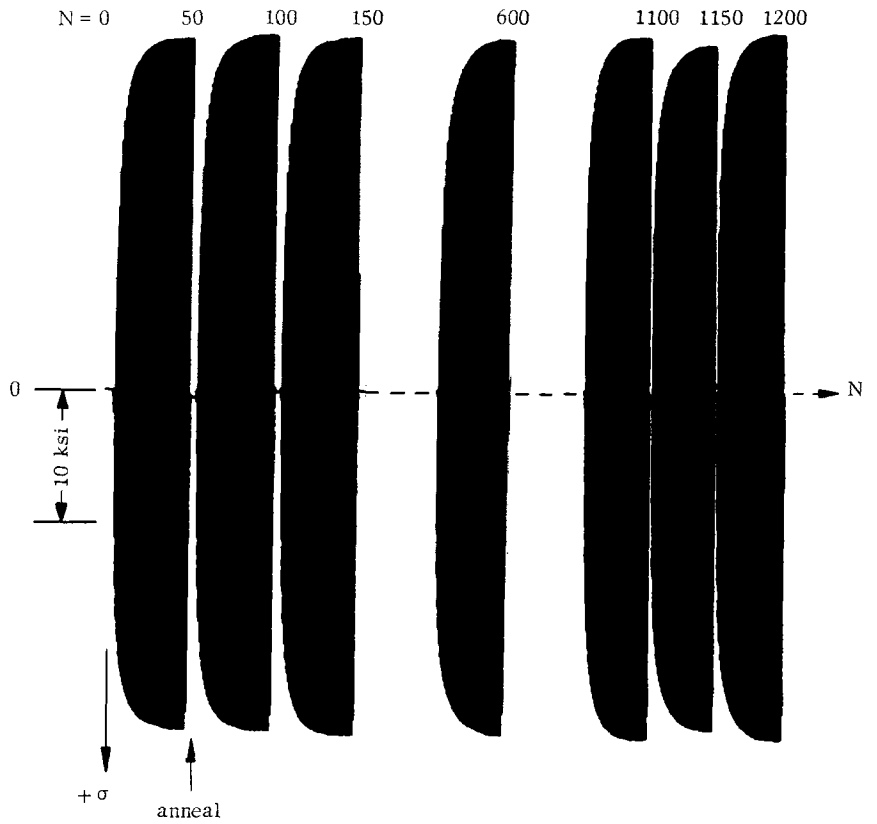

FIG. 4—*Cycle-dependent hardening of copper with intermittent annealing.*

number of cycles in the segment. Summing over the entire test, a number proportional to the total fatigue damage is obtained. Using averages of the measured strain levels for the three groups of specimens in Table 3, the predicted lives for Groups B and C are 1000 and 900 cycles, respectively. Considering the predictions based on plastic strain, the improvement in average life becomes 50 percent for Group B and 80 percent for Group C. It should be emphasized that these theoretical improvements in life are larger than the actual values shown in Table 3.

There are a number of causes for changes in the fatigue life of intermittently annealed specimens: the notch effect of the surface features resulting from enhanced plasticity (to be discussed later), a small degree of oxidation in the high strain region, progressively increasing eccentricity at the test section, and frequent handling of each specimen. All of these are known to be adverse to some extent under any fatigue-loading condition.

TABLE 3—*Fatigue lives of copper.*[a]

A Not Annealed During Test	B Annealed Every 300 Cycles	C Annealed Every 50 Cycles to N = 1200
N_f = 1127	N_f = 1303	N_f = 1508
1129	1346	1510
1141	1456	1594
1166	1464	1619
1210	1465	1716
1298	1472	1791
1329	1560[b]	——
1352	1696	Average 1623
1375	——	Standard deviation 113
——	Average 1470	
Average 1237	Standard deviation 117	
Standard deviation 102		

[a] 0.8 percent total diametral strain range; failure was recorded when a specimen could not support a 20-ksi nominal tensile load.

[b] Specimen was not annealed at N = 1500 because cracks were visible.

The annealing treatments are not expected to heal existing cracks. To achieve solid-phase welding it would be necessary to have the specimens in high vacuum and under compressive load during annealing. Since these conditions were not satisfied, it was only possible to retard, not reverse, the

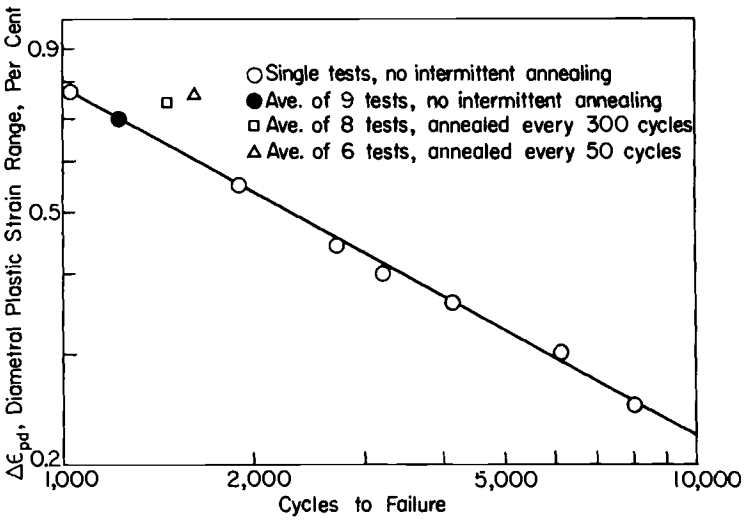

FIG. 5—*Diametral plastic strain range versus fatigue life for copper.*

fatigue damage process. The retardation is believed to be caused by a delay in the clustering of slip. In other words, fatigue cracks propagate slowly when slip is uniform and stresses do not build up at the tips of cracks.

Specimen Surface Features—There is qualitative evidence supporting data which show that intermittent annealing causes increased cyclic plastic strain. Comparison of specimen surfaces shows that enhanced slip took place in the frequently annealed specimens. In Fig. 6 the specimen not annealed during testing shows slip markings that are typical at this life range. The specimen contour is not altered noticeably from that of a virgin specimen, except for a slight bulging at sections away from the minimum diameter. This is caused by plastic flow [*15*] and is typical under diametral strain control. The photograph of the frequently annealed specimen shows unusually severe slip markings but no evidence of cracks. The contour is uneven and the bulging indicates enhanced plasticity. It must be emphasized that there are no surface features that could be attributed to the diametral clip gage.

Grain Size—A consequence of repeated straining and annealing was grain growth from the original size of 3 to 5, determined through ASTM Standard Methods for Estimating the Average Grain Size of Metals (E 112 - 63), to about 1 or less for the specimens of Group C. The change in grain size has to be considered in any discussion of increases in fatigue life. It is well-established that under load control the fatigue life is inversely related to the grain size [*16*]. There are no conclusive reports, however, that are based on strain-controlled tests. Coffin and Read [*17*] reported that at a given strain range fatigue life of stainless steel decreased with increasing prior cold work. Baldwin et al [*18*] showed for the same type of stainless steel that grain size had little or no effect in strain-cycling fatigue. Benham's [*14*] investigation of copper at low endurance revealed identical total strain versus life curves for the annealed and cold-worked specimens of the metal. Results from Feltner and Laird [*19*] and several other investigators discussed by them are also relevant. Flow stresses of annealed and cold-worked copper after high-amplitude fatigue was applied were found to be identically dependent on the temperature of the subsequent annealing. Furthermore, grain size had a negligible effect on the unidirectional flow stress and on the cyclic stress-strain curves of copper.

Thus, definite conclusions cannot be made concerning grain growth. It seems worthwhile, however, to devote future research to the possible effect of grain size in strain-cycling fatigue. Such research may have a practical significance because it is known that the metal at the root of a notch in a member subjected to cyclic loading is under strain control in the steady state [*20*].

Frequency of Annealing—Changes in fatigue life depend on the frequency of annealing, as shown in Fig. 7. Points *a*, *b*, and *d* represent a few tests that

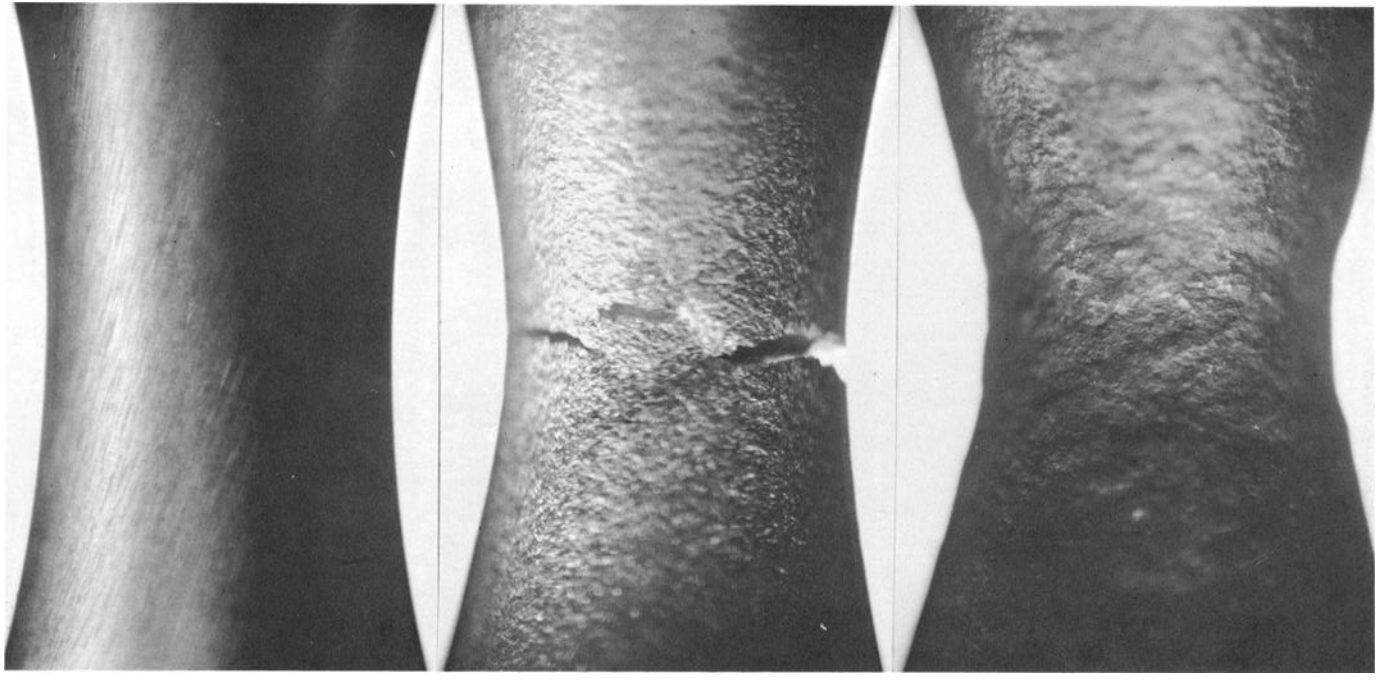

(*left*) Specimen before testing.
(*center*) Specimen not annealed during testing; 0.8 percent diametral strain range; photograph at N = 1170; fatigue life = 1170.
(*right*) Specimen annealed every 50 cycles; 0.8 percent diametral strain range; photograph at N = 1200; fatigue life = 1700.

FIG. 6—*Copper fatigue specimens* ($\times 7$).

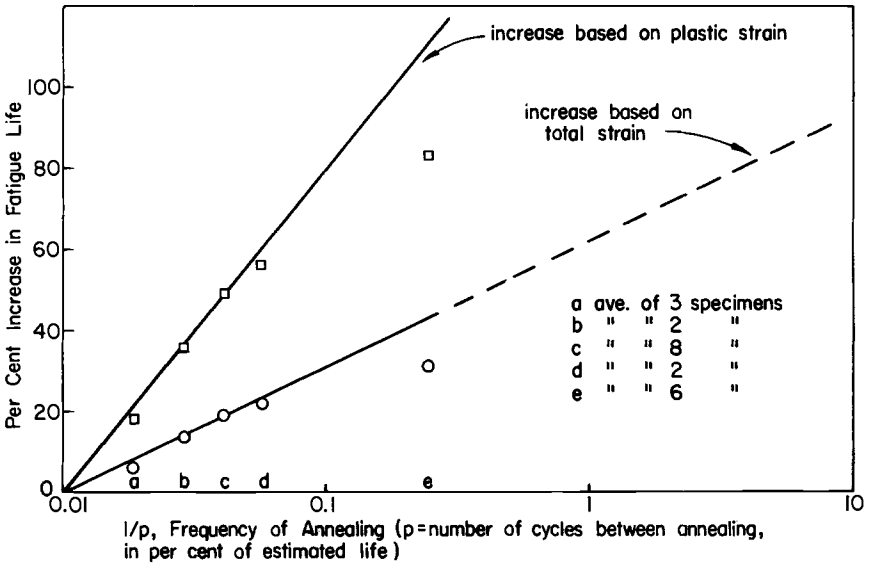

FIG. 7—*Increase in fatigue life versus frequency of annealing for strain-cycled copper.*

were not discussed previously, and points *c* and *e* are the results of tests listed in Table 3. It is possible that the points labeled *e* would have been closer to the respective straight lines had the annealing treatments not been terminated at 1200 cycles for that group. The treatments were discontinued in this case, because the specimen surfaces had become exceedingly rough as a result of enhanced slip. Diametral strain control thus becomes progressively more difficult and eventually meaningless.

The straight lines in Fig. 7 indicate the amount that the fatigue life can be extended under the present conditions. It is seen that infrequent annealing has a negligible effect on life. In the experiments of Harries and Smith [5], for example, annealing was done only once during the life of each specimen. Changes in life due to their treatments could have been obscured by inherent scatter in the results. It will be shown in a later section that infrequent treatments are also ineffective in the case of mild steel.

Increasing the frequency of annealing, on the other hand, does not necessarily result in a large extension of life. Figure 7 shows that the annealing of copper would have to be repeated every 0.1 percent of the estimated life to get an improvement in life by a factor of two based on total strain. But this is not feasible, since more frequent treatment would aggravate the geometrical changes caused by enhanced slip, and also the fatigue tests would become exceedingly long, even for research purposes, as the time of a rest period is large compared to that of a strain cycle. Thus, experimentation is best confined to the range of annealing frequencies used in this investigation.

Conclusions

In strain-cycled copper, intermittent annealing increases the cyclic plastic strain and reduces the stresses caused by cyclic cold work. The original monotonic and cyclic deformation characteristics are restored by annealing. Enhanced slip causes the specimen surfaces to become unusually rough and the geometry to be changed considerably. Strain-cycled copper with intermittent annealing does not obey the Manson-Coffin relation. Average fatigue lives are increased up to 30 percent on the basis of total strain range and up to 80 percent on the basis of cyclic plastic strain. Grain growth due to the treatments may lead to an observed extension of life, but a more probable mechanism is that the fatigue damage process is retarded by a delay in the clustering of slip.

Extension of Fatigue Life in Steel

Attempts to extend the fatigue life have been more successful for ferrous metals than for nonferrous metals. There are two reasons for the difference in results: one is the phenomenon of strain aging in ferrous metals, the other is the use of load control in previous experiments.

Bairstow [*21*] found that in plastically strained steel, elasticity could be recovered by allowing periods of rest after fatigue loading. Later studies of strain aging showed that strengthening is caused by solute carbon and nitrogen atoms that are able to diffuse to dislocation sites during a rest period. Dislocations become anchored and the flow stress is increased, because the solute atoms lower the lattice energy [*22*].

Intermediate strain aging by elevated temperature rest periods may be beneficial in the fatigue of steels under stress control. In this case the cyclic plastic strain is reduced and an increase in life is possible. The same metals subjected to strain control may be expected to show improvement only if the strains are in the elastic range, a condition that is practically the same as stress control. At larger strain ranges the cyclic plastic strain would rapidly wash out the strengthening caused by prior strain aging. Previous investigators did not use similar considerations in planning experiments; they used load control or bending simply because, at the time, these were the only practical techniques of fatigue loading.

A number of different steels have been tested using elevated temperature rest periods during fatigue. Bollenrath and Cornelius [*8*] reported no effect from rest periods in a chromium-molybdenum steel and in an austenitic chromium-nickel steel. They also tested ingot iron and found its life extended by a factor of up to 100. Only a few tests were made, and these are difficult to interpret because the loading was from zero to tension, causing cycle-dependent softening and creep. Freudenthal et al [*9*] observed slight extensions in the fatigue life of SAE 4340 steel. Karius et al [*23*] tested a small

number of low carbon steel specimens with various intermittent heat treatments. Their best result was an improvement in life by a factor of six.

There are reports for steel showing no improvement in fatigue life due to elevated temperature rest periods. Treatments were applied infrequently during a fatigue test [*24*]. The importance of frequent heat treatments to prolong fatigue life has become clear only recently, when cyclic plastic strains were measured and indicated the "temporary" nature of the strengthening achieved by strain aging.

In the present work elevated temperature rest periods were applied in stress-controlled fatigue tests of mild steel. Frequent repetition of the treatments caused a large reduction in cyclic plastic strain; so a significant increase in life could be expected.

Experimental Program

Fifteen SAE 4140 steel specimens were tested to establish procedures and to show that the cyclic deformation characteristics can be changed by intermediate strain aging. Cyclic plastic strains were measured in these tests, and the following results were found most relevant to this investigation of fatigue damage alleviation:

1. Intermittent heating reduces the cyclic plastic strain at any stage during the fatigue life, even when large cracks are present.
2. The plastic strain range rapidly increases with cycles after a rest period. Large increases in fatigue life are possible only if the treatments are repeated frequently in each test.
3. Temperature "spikes" lasting only about a minute and reaching a peak of 600 F are adequate for strengthening by strain aging.
4. Large temperature gradients during the rest period and oxidation due to heating in air do not noticeably affect the life in the low-cycle region.

These preliminary findings were used as guides in planning experiments with low carbon steel.

Material and Specimens—The low carbon steel specimens were taken from the same heat to insure uniform properties. The chemical composition is given in Table 4. Bars of the steel were annealed for 1 h at 1650 F and furnace cooled. The specimen geometry was the same as that described in the section on Intermittent Annealing. Some of the specimens were strained in tension and aged before cycling to raise the original yield strength of 40 ksi to about 85 ksi.

TABLE 4—*Chemical composition of mild steel in weight percent.*

C	Mn	P	S	Si	Al	N
0.17....	0.48	0.007	0.023	0.024	0.010	0.003

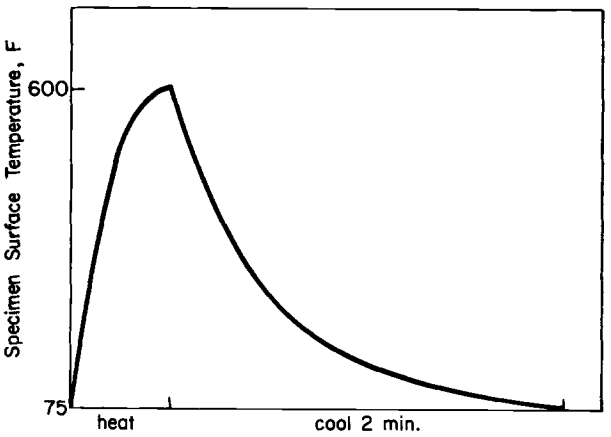

FIG. 8—*Temperature cycle during rest period in mild steel.*

Apparatus—The equipment used in the fatigue tests was described previously. A radiant heater was used for intermittent heating of the specimens *in situ*. The specimen grips were water cooled to protect the load cell and to cool the specimens after heating.

Test Conditions—Load cycling was done at room temperature, at two to four cycles per minute, and under controlled axial stress with zero mean stress. Tests were interrupted periodically at the tensile load limit to apply the temperature cycle shown schematically in Fig. 8. Specimens were constrained during the rest periods so that the loads changed with thermal expansion and contraction, as shown in Fig. 9. Cycling was resumed at the end of the cooling period.

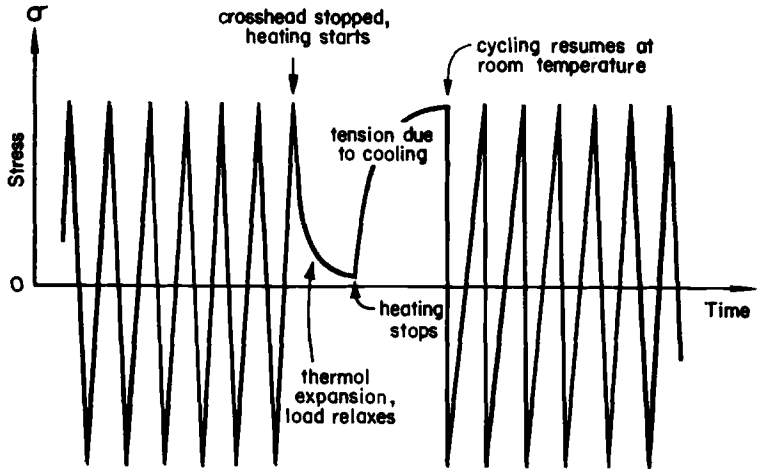

FIG. 9—*Schematic of stresses for load cycling of mild steel with intermittent heating.*

Results and Discussion

The monotonic mechanical properties for the mild steel are listed in Table 5. Results of the cyclic tests are given in the stress range versus fatigue life plot of Fig. 10. The results for specimens that received no intermittent heat treatment conform to data on a similar low carbon steel [*25*]. The specimens without initial strain aging cyclically harden at these high stress levels, as shown by the cyclically decreasing plastic strain for Specimen A8 in Fig. 11. Initially strain-aged specimens rapidly soften at first and then harden (consider Specimen A6 in Fig. 12) and show a slight improvement in fatigue life.

TABLE 5—*Monotonic mechanical properties of mild steel.*

Condition	Yield Strength, ksi	Ultimate Strength, ksi	Fracture Strength,[a] ksi	Reduction of Area, %
Annealed.....	40	65	122	60

[a] Not corrected for triaxial state of stress.

Specimens that were heated after every ten cycles (every 8 percent of the estimated fatigue life) had their lives improved by a factor of about two. This agrees with the results of previous investigations [*9*, *23*]. There were large improvements in life, up to a factor of 100, when heating was done after every 1 percent of the estimated life.

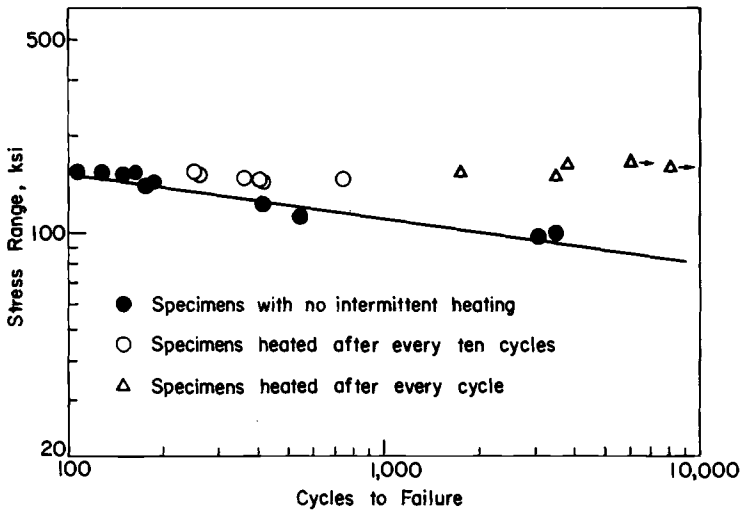

FIG. 10—*Stress range versus fatigue life for mild steel.*

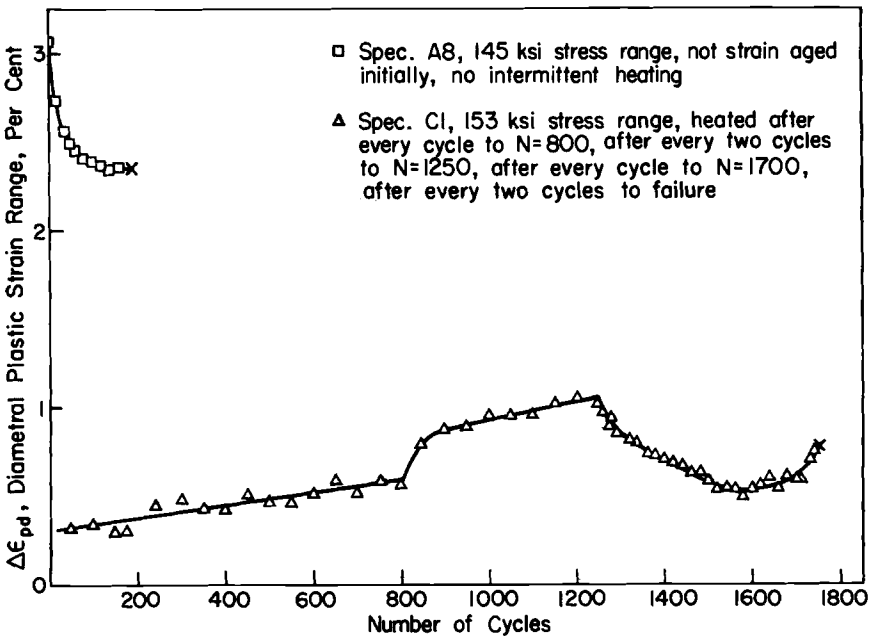

FIG. 11—*Plastic strain versus cycles for mild steel.*

The observed scatter in life of the intermittently heated specimens is only partly inherent in the metal. It is mainly due to variations in the lengths of heating periods from specimen to specimen. The differences in intermittent treatment are also evident in the slopes of the plastic strain versus cycles plots of Figs. 11 and 12.

Damage Analysis—The improvement in fatigue life results from the reduction in cyclic plastic strain range. These two quantities are related by the equation described before; the only difference is in the value of the exponent: for mild steel, $c \sim -0.6$ as found by Topper and Biggs [*25*].

Damage summations for the specimens of Fig. 10 are about equal. Thus, the improvement in fatigue life was due to the artificial reduction in cyclic plastic strain caused by intermittent heating. In other words, strain aging does not alleviate fatigue damage already present in the metal but, rather, retards the damage process by reducing the cyclic plastic strain.

Transients in Plastic Strain—Initially strain-aged specimens cyclically soften at the beginning of the fatigue test and later cyclically harden. The size of the "hump" in plastic strain range versus cycles curves, such as Fig. 12, depends on the extent of strain aging before cycling and on the length and temperature of the rest periods during fatigue. These cycle-dependent changes in plastic strain indicate that the rate of damage accumulation is highest in

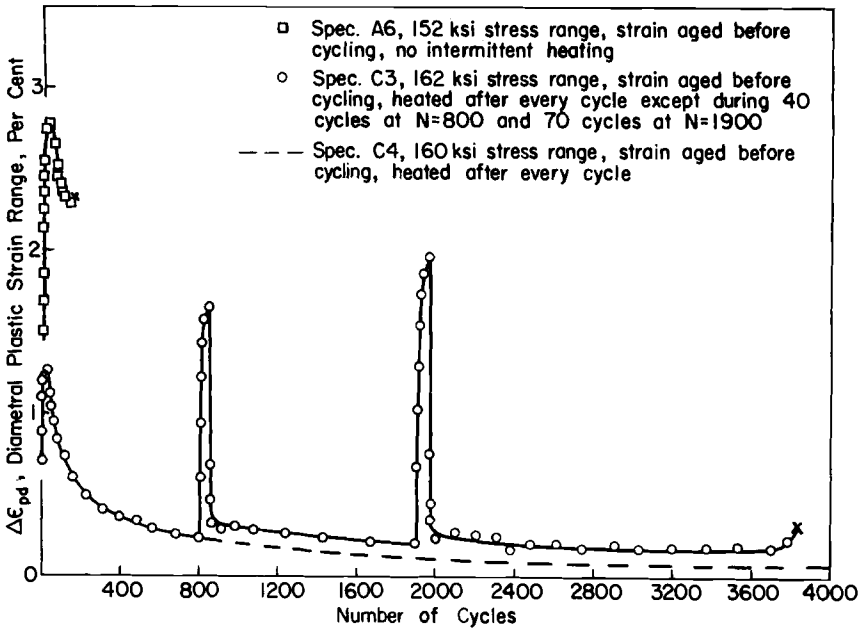

FIG. 12—*Plastic strain versus cycles for mild steel.*

the early part of a fatigue test of mild steel. Further studies of this behavior are encouraged because they could lead to a better understanding of the fatigue damage mechanism.

There are large transients in plastic strain versus cycles behavior when the frequency of application of rest periods is drastically changed during a test, as illustrated in Fig. 12. Specimen C3 was heated after every cycle, except for two separate blocks of cycles during which no rest periods were allowed. There are remarkably rapid changes in cyclic plastic strain at both the beginning of these blocks and immediately following them. These transients show the importance of monitoring the cyclic plastic strain in attempts to alleviate fatigue damage by strain aging. It is worth noting that the two regions of "cyclic overstraining" in Specimen C3 have exhausted one third of the estimated life on the basis of cyclic plastic strain.

Fracture Appearance—Specimens that are not heated intermittently fracture in a ductile manner, as shown by Specimens A8 and A11 in Fig. 13. The only differences between these are in the size of fatigue cracks—the relatively flat and bright areas of Fig. 13 (dark areas show the final shear separations). The intermittently heated Specimen C1 has relatively small fatigue cracks—the dark, oxidized peripheral areas in Fig. 13. The remaining area has a fine, sparkling appearance and only a few secondary cracks. This change

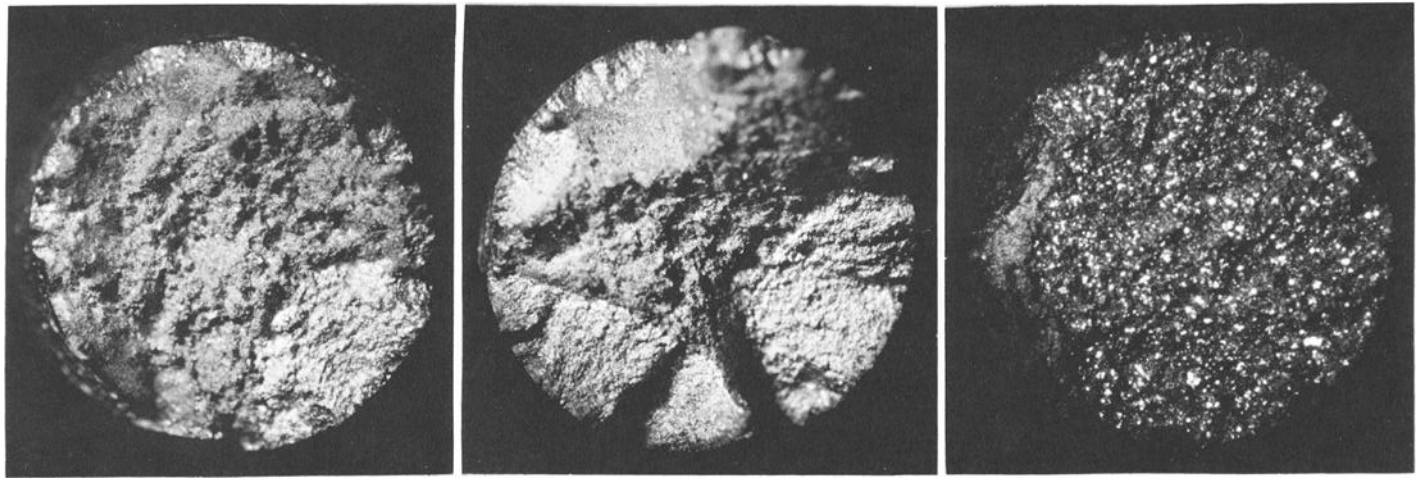

(*left*) Specimen A8: not heated intermittently; 145-ksi stress range; fatigue life = 189.
(*center*) Specimen A11: not heated intermittently; 98-ksi stress range; fatigue life = 3100.
(*right*) Specimen C1: heated 1400 times; 153-ksi stress range; fatigue life = 1750.

FIG. 13—*Fracture surfaces of mild steel* (×*10*).

from the usual ductile failure to a brittle cleavage fracture has not been reported previously.

Microscopic observations at magnifications of up to 1000 were made on a longitudinal section of Specimen C1. Strain aging did not cause noticeable structural changes. Such changes are not expected to be easily detectable, since Coffin [*26*] has found no precipitates at a magnification of 7500 in cyclically strain-aged mild steel.

Cycling at Elevated Temperature—Six mild steel specimens were cycled at 150-ksi stress range and 600 F temperature for comparison with the intermittently heated specimens. Cyclic plastic strains were not measured. Fatigue lives were about a factor of ten longer than in room temperature tests at the same stress range. An increase in life was expected, since Levy and Sinclair [*27*] had found improved fatigue resistance for low carbon steel tested at mildly elevated temperatures in the long-life region.

The fracture appearance of a specimen cycled at elevated temperature is distinctly different from those shown in Fig. 13. The fatigue crack is even smaller than that of Specimen C1, which indicates brittle fracture. However, the final separation is in shear, and the surface does not have the fine and bright features of Specimen C1 in Fig. 13.

Conclusions

Frequent rest periods at mildly elevated temperature prolong the fatigue life of low carbon steel tested under stress control. Improvements in life by a factor of 100 are possible when the rest periods are applied every 1 percent of the estimated fatigue life. Fatigue damage already present in the metal is not eliminated, but the damage process is retarded because the cyclic plastic strain is reduced. It is demonstrated that measurements of plastic strain are important in attempts to extend fatigue life. Frequently repeated strain aging causes the mode of fracture to change from the usual shear failure to a brittle cleavage.

Conclusions

Elevated temperature rest periods were used to change the room temperature stress-strain response of both cyclically hardening and softening metals. The fatigue life was extended under appropriate cyclic control conditions.

Strain-cycled copper was intermittently annealed to reduce the level of stress caused by cyclic cold work. The initial stress-strain response could be restored throughout the fatigue life. Frequently repeated annealing of a specimen resulted in a slight prolongation of fatigue life even though the cyclic plastic strains were increased with treatments. The improvement in life was probably caused by a delay in the clustering of slip.

The fatigue resistance of low carbon steel was improved greatly in stress-controlled tests. Intermittent strain aging treatments retarded the fatigue damage process by reducing the cyclic plastic strain. Fatigue life was increased by a factor of 100 when the treatments were applied every 1 percent of the estimated life. The Manson-Coffin relation accurately predicted the increase in fatigue life in these particular experiments. Frequently repeated cyclic strain aging resulted in a shear-to-tensile transition in the fracture mode.

Acknowledgments

The research was carried out in the H. F. Moore Fracture Research Laboratory of the Department of Theoretical and Applied Mechanics, University of Illinois, Urbana, Ill. T. J. Dolan, head of the department, provided facilities and support for the investigation. Steel specimen material was donated by the United States Steel Corp.

The author acknowledges the variety of stimuli given by his advisor, JoDean Morrow. Helpful discussions were held with G. M. Sinclair and T. H. Topper.

References

[1] Almen, J. O. and Black, P. H., *Residual Stresses and Fatigue in Metals*, McGraw-Hill, New York, 1963, pp. 126 and 154.

[2] Kommers, J. B., *Proceedings*, Society for Experimental Stress Analysis, PSESA, Vol. 3, No. 2, 1946, pp. 137–141.

[3] Sinclair, G. M., *Proceedings*, American Society for Testing and Materials, ASTEA, Vol. 52, 1952, pp. 743–751.

[4] Raymond, M. H. and Coffin, L. F., Jr., *Journal of Basic Engineering*, American Society of Mechanical Engineers, JBAEA, Dec. 1963, pp. 548–554.

[5] Harries, D. R. and Smith, G. C., *Journal of the Institute of Metals*, JIMEA, Vol. 88, 1959, pp. 182–185.

[6] Thompson, N., Wadsworth, N., and Louat, N., *Philosophical Magazine*, PHMAA, Vol. 1, Eighth Series, 1956, pp. 113–126.

[7] Sandor, B. I. and Morrow, JoDean, "Alleviation of Fatigue Damage," T&AM Report No. 311, University of Illinois, Urbana, Ill., March 1968.

[8] Bollenrath, F. and Cornelius, H., *V.D.I. Zeitschrift*, VDIZA, Vol. 84, No. 18, 1940, pp. 295–299; Translation No. 104, The David W. Taylor Model Basin, 1942.

[9] Freudenthal, A. M., Yen, C. S., and Sinclair, G. M., "The Effect of Thermal Activation on the Fatigue Life of Metals," 8th Progress Report, U.S. Navy Contract N6-ori-71, Task Order IV, Engineering Experiment Station, University of Illinois, Urbana, Ill., Aug. 1948.

[10] Weissman, S. and Park, B. K., "Mechanism of Fatigue Failure of Metals," Technical Report AFML-TR-66-123, Part III, Air Force Materials Laboratory, Dayton, Ohio, Nov. 1967.

[11] Sinclair, G. M. and Dolan, T. J., "Use of a Recrystallization Method to Study the Nature of Damage in Fatigue of Metals," *Proceedings*, 1st U.S. National Congress of Applied Mechanics, 1951, pp. 647–651.

[12] Morrow, JoDean in *Internal Friction, Damping, and Cyclic Plasticity, ASTM STP 378*, American Society for Testing and Materials, 1965, p. 72.

[13] Alden, T. H. and Backofen, W. A., *Acta Metallurgiac*, AMETA, Vol. 9, 1961, pp. 352–366.
[14] Benham, P. P., *Journal of the Institute of Metals*, JIMEA, Vol. 89, 1961, pp. 328–339.
[15] Coffin, L. F., Jr., *Transactions*, American Society of Mechanical Engineers, TASMA, Series D, Vol. 82, 1960, pp. 571–682.
[16] Sinclair, G. M. and Craig, W. J., *Transactions*, American Society for Metals, TASEA, Vol. 44, 1952, pp. 929–948.
[17] Coffin, L. F., Jr., and Read, J. M., "A Study of the Strain Cycling and Fatigue Behavior of a Cold-Worked Metal," International Conference on Fatigue of Metals, Institute of Mechanical Engineering, American Society of Mechanical Engineers, London, Sept. 1956.
[18] Baldwin, E. E., Sokol, G. J., and Coffin, L. F., Jr., *Proceedings*, American Society for Testing and Materials, ASTEA, Vol. 57, 1957, pp. 567–586.
[19] Feltner, C. E. and Laird, C., *Acta Metallurgica*, AMETA, Vol. 15, No. 10, 1967, pp. 1621–1653.
[20] Topper, T. H., Sandor, B. I., and Morrow, JoDean, "Cumulative Fatigue Damage Under Cyclic Strain Control," Report No. NAEC-ASL-1115, Aeronautical Structures Laboratory of the Naval Air Engineering Center, June 1967.
[21] Bairstow, L., *Philosophical Transactions of the Royal Society of London, Series A*, PTRMA, Vol. 210, 1911, pp. 35–55.
[22] Cottrell, A. H., *Dislocations and Plastic Flow in Crystals*, Oxford University Press, Oxford, 1953, p. 134.
[23] Karius, A., Gerold, E., and Schulz, E. H., *Archiv für das Eisenhüttenwesen*, AREIA, Vol. 18, No. 1066, Jan./Feb. 1945, pp. 155–159.
[24] Möller, H. and Hempel, M., *Archiv für das Eisenhüttenwesen*, Vol. 25, No. 1415, Jan./Feb. 1954, pp. 39–70.
[25] Topper, T. H. and Biggs, W. D., *Applied Materials Research*, AMRSA, Vol. 5, No. 3, July 1966, pp. 131–137.
[26] Coffin, L. F., Jr., *Journal of Basic Engineering*, American Society of Mechanical Engineers, JBAEA, Vol. 87D, 1965, pp. 269–280.
[27] Levy, J. C. and Sinclair, G. M., *Proceedings*, American Society for Testing and Materials, ASTEA, Vol. 55, 1955, pp. 866–890.

DISCUSSION

C. C. S. Yen[1] *(written discussion)*—Schulz,[2] in a number of papers published between 1922 and 1945, found that rest periods improved the fatigue life of various steels. In 1948 and 1949 Freudenthal et al,[3] in a study of thermal activation, conducted statistical analyses of extensive fatigue test data and concluded that resting at 350 F indeed improved fatigue life of 1045 and 4340 steel. However, it was also found that a resting period slightly reduced the life of fully annealed electrolytic copper and aluminum alloy 7075-T6. In 1963 McEvily et al[4] showed that resting or aging at 150 C (302 F) for 3 h slightly reduced the life of 2024-T4 alloy, but aging at 150 C for 16 h markedly increased the life. All the above results are in the long- or intermediate-life region.

The intriguing complexities of metal behavior under repeated stressing or straining still defy a quantitative prediction of the fatigue life of an actual machine part as influenced by a rest period. In view of the current state of our knowledge, the present paper is an important contribution. I believe that greater effort should now be expended on the study of the effect of a rest period for objectives on both scientific and industrial fronts. Scientifically, the fatigue mechanism as related to dislocation dynamics, thermal activation, alloy reversion, strain aging, etc., can be better understood. Industrially, the results of study may be used beneficially to improve the product life and to prevent failure. I believe that if the effects of resting at ambient temperatures are well known, everybody could use the results of study for better control of the service life of automobile and other machine parts.

[1] Research projects engineer, Hughes Tool Co., Aircraft Division, Culver City, Calif. 90230.

[2] Schulz, E. H., *Stahl und Eisen*, STEIA, Vol. 60, 1940, p. 100; *Archiv fuer das Eisenhuettenwesen*, AREIA, Vol. 12, 1938, p. 141 and Vol. 18, 1945, p. 155.

[3] Freudenthal, A. M. et al, "Materials Behavior Under Repeated Stress," 8th and 12th Progress Report, Engineering Experiment Station, University of Illinois, Urbana, Ill., 1948–1949.

[4] McEvily, A. J., Jr., et al, *Transactions*, American Institute of Mining and Metallurgical Engineers, TAMMA, Vol. 227, 1963, p. 1093.

T. L. Gerber[1] *and H. O. Fuchs*[2]

Improvement in the Fatigue Strength of Notched Bars by Compressive Self-Stresses

REFERENCE: Gerber, T. L. and Fuchs, H. O., **"Improvement in the Fatigue Strength of Notched Bars by Compressive Self-Stresses,"** *Achievement of High Fatigue Resistance in Metals and Alloys, ASTM STP 467*, American Society for Testing and Materilas, 1970, 276–295.

ABSTRACT: In this investigation the long-life fatigue strength of sharply notched steel bars was improved by as much as 300 percent with the introduction of compressive self-stresses. Compressive self-stresses were produced by an axial tensile preload. Quantitative estimates of this improvement were made as a function of preload using suitable failure criteria and an analytical estimate of the stable self-stress distribution. The importance of the distribution in depth is demonstrated. A criterion for predicting crack propagation is improved and clarified.

KEY WORDS: fatigue (materials), residual stress, stresses, notch strength, yield strength, stress concentration, crack initiation, crack propagation, loads (forces)

Since the 1930's the relationship between self-stresses or residual stresses[3] and fatigue resistance has been investigated. Horger [*2*][4] has given a good review of the literature up to 1950. More recently a number of books have been written in whole or in part on the subject [*3–6*].

Two assumptions are usually employed to make quantitative predictions of the effect of self-stress on fatigue resistance: (1) self-stresses are assumed to have the same influence on fatigue strength or fatigue life as a mean stress and (2) the self-stresses that are assumed to be significant to fatigue are those at or near the surface. Rowland [*7*] has reviewed work in which one or both of these assumptions have been substantiated [*8–10*]. Specimens used in these studies were either smooth or midly notched steel specimens of over 25 HRc.

[1] Engineer, Nuclear Energy Div., General Electric Co., San Jose, Calif., 95125. Formerly research assistant, Mechanical Engineering Dept., Stanford University, Stanford, Calif.

[2] Professor, Mechanical Engineering Dept., Stanford University, Stanford, Calif. 94305. Personal member of ASTM.

[3] Self-stress or residual stress in this study implies macroresidual stress as opposed to microresidual stress, although both may affect fatigue performance [*1*].

[4] Italic numbers in brackets refer to the list of references at the end of this paper.

Along with observing that predictions of performance were reasonable when surface self-stresses were treated as a mean stress component, Rowland pointed out that near the fatigue limit the self-stresses were not changed by the fatigue loading.

When stress concentrations are present, or when soft materials (materials for which the ratio of reversed loading fatigue strength to yield strength approaches unity) are used, the distribution of the self-stresses may change during shakedown. It then becomes important to study the influence of fatigue loading on the distribution of self-stresses. Rosenthal and Sines [*11*] studied the effect on fatigue strength of self-stresses produced by preloading notched aluminum plates. Their results showed that the fatigue strength of precipitation-hardened specimens was increased by tensile preloading, while that of specimens annealed before preloading remained unchanged. Taira and Murakami [*12*] show similar results with preloaded, notched, medium carbon steel plates.

For notched plates, quantitative predictions of the effect of self-stress on fatigue strength can be made [*11*, *13*]. For notched bars, the influence of self-stresses is not as well understood. The problem is more difficult because the stress distribution is three-dimensional and the region below the notch root cannot be examined.

Experimental work in which notched bars were preloaded shows that very large improvements in fatigue strength can be produced. Dugdale [*14*] has shown that the fatigue strengths of V-notched specimens are increased 53 percent (mild steel), 114 percent (higher carbon steel), 96 percent (nickel steel), and 266 percent (aluminum). Forest [*15*] produced an improvement of 100 percent and Heller et al [*16*] an improvement of 193 percent by preloading notched aluminum bars. These improvements are larger than could be produced by preloading notched plates [*13*]. (In the tests reported in this paper improvements up to 300 percent were observed.)

Dugdale [*14*] speculated that in notched bars self-stresses have a greater modifying effect on the cyclic stress required to propagate an existing crack than they have on the cyclic stress required to initiate a crack. Heller et al [*16*] pointed out that the strengthening appears to be due to compressive self-stresses that are produced below the notch root. In the experimental work and analysis that are reported in the following sections, both these observations are substantiated.

In the first section of this paper tests and experimental results are reported. Notched steel bars were preloaded in axial tension to produce compressive self-stresses at the notch root. Subsequently, these parts were cycled in rotating bending to determine the fatigue strength. In the next section, design criteria for crack nucleation and propagation are used to predict the influence of self-stresses on fatigue strength. This analysis demonstrates the importance of considering nucleation and propagation separately and emphasizes the

features of the distributions of the load and self-stress that are important to strength. Finally, after estimating the stable self-stress distribution produced by preloading and altered by the cyclic loading, the design criteria are used to predict the strength of the experimentally tested parts.

Experimental Work

Circumferentially notched bars of AISI Type 4340 steel were loaded in axial tension to produce local yielding and, thus, compressive self-stress at the notch root. Following the tensile preload, specimens were cycled in rotating bending to determine the fatigue strength at one million cycles.

The test specimen geometries are shown in Fig. 1 and the stress concentration factors are listed in Table 1. Two sizes of test specimens were employed: "small" specimens, minimum diameter of 0.20 in. (5.1 mm), and "large" specimens, minimum diameter of 0.50 in. (12.7 mm). For the small specimens one smooth and one notch geometry were tested, while for the large specimens one smooth and two notch configurations were used. Note that specimen Types 101 and 202 are geometrically similar and therefore have equal theoretical stress concentration factors.

TABLE 1—*Stress concentration factors for notched test specimens.*

Specimen Geometry Type	Axial Stress Concentration, $K_{T(A)}$	Bending Stress Concentration, $K_{T(B)}$
101	2.65	2.15
201	3.95	3.20
202	2.65	2.15

The test specimens were machined from hot-rolled and annealed AISI E4340 alloy steel, electric furnace produced to U.S. Military Specification MIL-S-5000B-1. This alloy was selected because of good hardenability and because a large change in mechanical properties can be produced by tempering. Also, there is considerable background and experience with the fatigue properties of this material. Following machining the specimens were given one of two heat treatments. The heat treatments consisted of hardening and tempering to produce either 24 or 49 HRc. (In subsequent discussion the subscript S indicates 24 HRc and the subscript H, 49 HRc.) Tension specimens which had been heat-treated were used to determine the 0.2 percent offset yield strength and the ultimate strength:

HRc	Yield Strength (S_Y)	Ultimate Strength (S_U)
24	121 ksi (834 MN/m²)	170 ksi (1170 MN/m²)
49	225 ksi (1550 MN/m²)	265 ksi (1830 MN/m²)

To produce compressive self-stresses in the vicinity of the notch root, specimens were given axial tensile preloads. Notched specimens were given either no preload or one of several different preloads: the lowest 25 percent above the load at which one would predict yielding to begin at the notch root [(Area $\times$ S_Y)/$K_{T(A)}$, where $K_{T(A)}$ is the theoretical stress concentration factor for an axial load], the highest 95 percent of the static tensile fracture load of the notched specimen. Smooth specimens were given no preload or a preload which produced gross yielding at the minimum cross section.

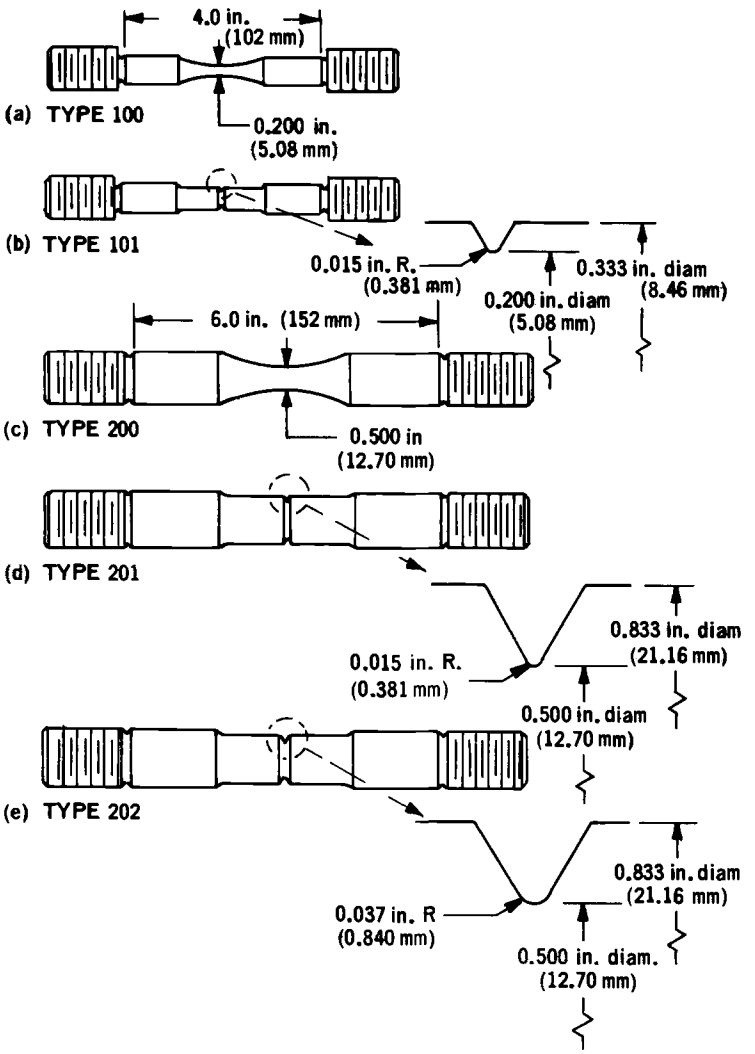

FIG. 1—*Test specimen geometries.*

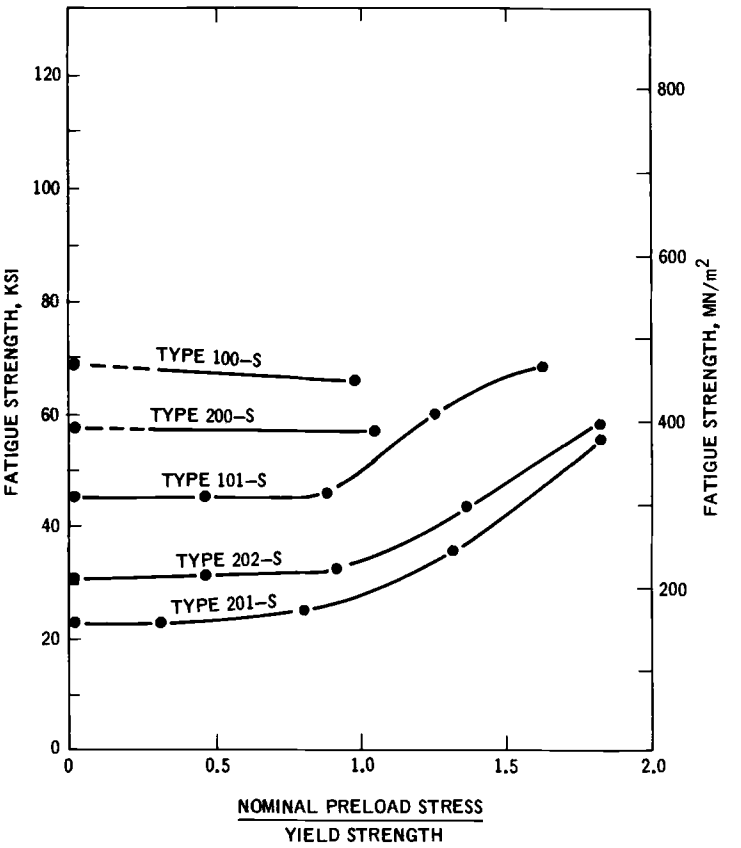

FIG. 2—*The effect of preload on the fatigue strength of soft (24 HRc) specimens.*

All fatigue tests were rotating bending tests. A step test [*17*] was run with one specimen of each type, heat treatment, and preload to estimate the fatigue strength at one million cycles. Based on these preliminary results, staircase tests [*17*] were designed and carried out. For each staircase, 6 to 10 specimens were employed. The staircase test results were analyzed by the methods of Brownlee et al [*18*].

The results of the fatigue tests are summarized in Figs. 2 and 3; detailed test data are reported elsewhere [*19*]. In Figs. 2 and 3 the fatigue strength is given as a function of preload. Two features of the curves should be noted:

1. The largest preload resulted in fatigue strengths of the notched specimens equal to those of the smooth specimens of equal minimum diameter. For specimens of Type 201-H this was an improvement of approximately 300 percent.

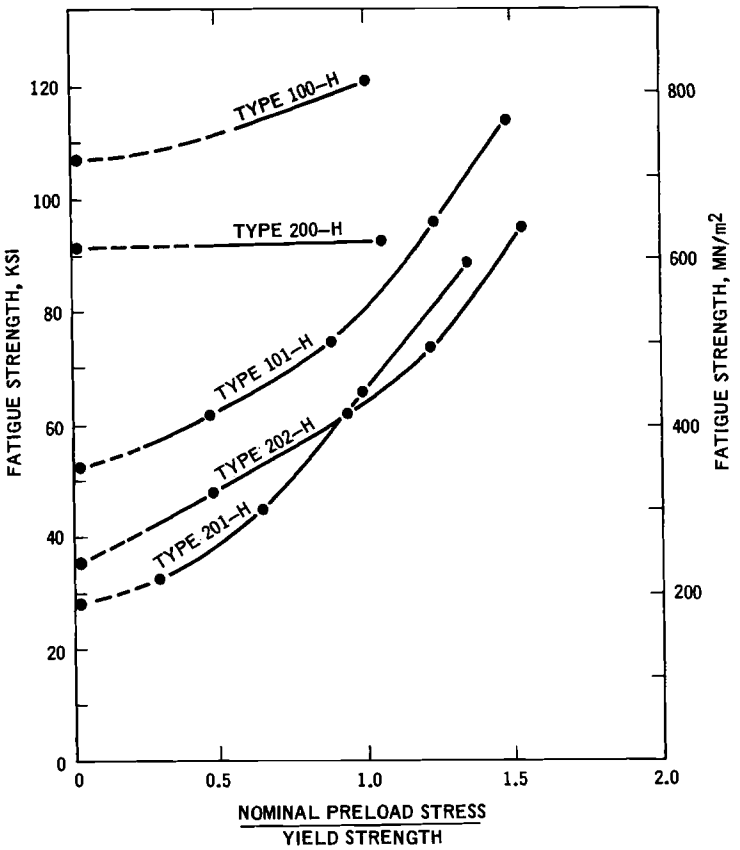

FIG. 3—*The effect of preload on the fatigue strength of hard (49 HRc) specimens.*

2. No appreciable increase in the fatigue strength of soft 24 (HRc) specimens was achieved unless the notched specimens had been given a preload almost three times as large as would be expected to first produce self-stresses. These features are explained in the next section.

Following cyclic loading it was noticed that specimens which had been given one of the larger preloads but had not failed during the fatigue loading had visible circumferential cracks at the notch root (Fig. 4). These cracked specimens were fractured in static tension, the fracture surface photographed (Fig. 5), and the crack depths measured. Cracks were found on both hard and soft specimens. (Figure 13 shows the average crack depths.)

It is justified to call the circumferential cracks "nonpropagating" for the following reason: Not all specimens which survived one million cycles were immediately removed from the fatigue machine. Many of the large specimens

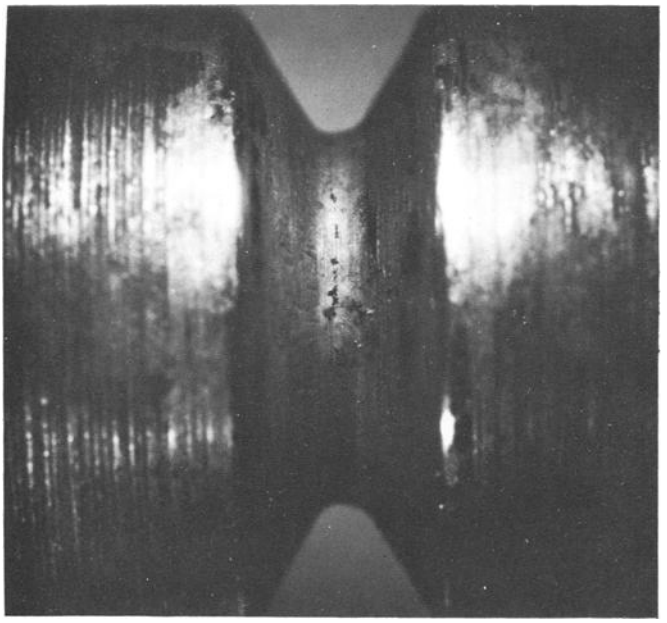

FIG. 4—*Circumferential cracks at the notch root of a preloaded and fatigue-loaded specimen.*

were cycled many more times, a few as much as 16 million cycles. Yet, when these specimens were fractured, the depths of the circumferential cracks were the same as those found in specimens that had been removed from the fatigue machine at one million cycles. An explanation for the existence of these nonpropagating cracks is given in the next section.

Design Criteria for Notched Parts with Self-Stresses

In an earlier paper [*20*] we developed an analytical estimate of the elastic-plastic stress distribution caused by the axial loading of circumferentially notched bars. This estimate employed a slip line field solution for stresses in the plastic zone and a modification of Neuber's elastic equations for stresses in the remaining elastic material. Strain hardening was neglected. Recently, the size of yield zone estimated with this procedure has been compared with that found in loaded, sectioned, and etched iron-silicon specimens [*19*].

When an axial, tensile preload which has caused tensile yielding at the notch root is removed, compressive self-stresses remain near the notch root. If strain hardening can be neglected and stresses due to loading and unloading can be superimposed, this initial self-stress distribution can be estimated with the equations of Ref *20*. Such a self-stress distribution is shown in Fig. 6*b*.

Subsequent compression loading may alter the initial self-stress distribution by causing yielding in compression near the notch root. This will result

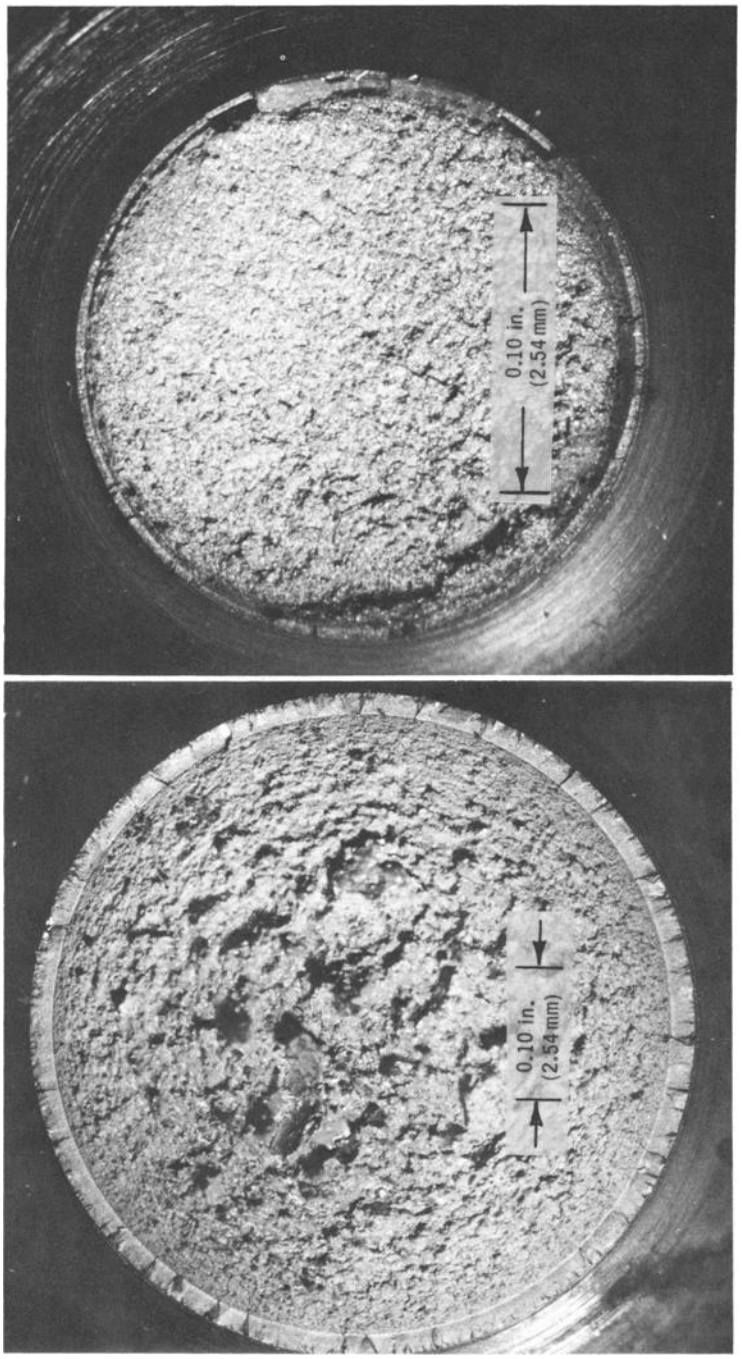

FIG 5—*Fracture surfaces of specimens which were preloaded, fatigue loaded, and fractured in static tension:* (left) *specimen Type 202-S;* (right) *specimen Type 101-H.*

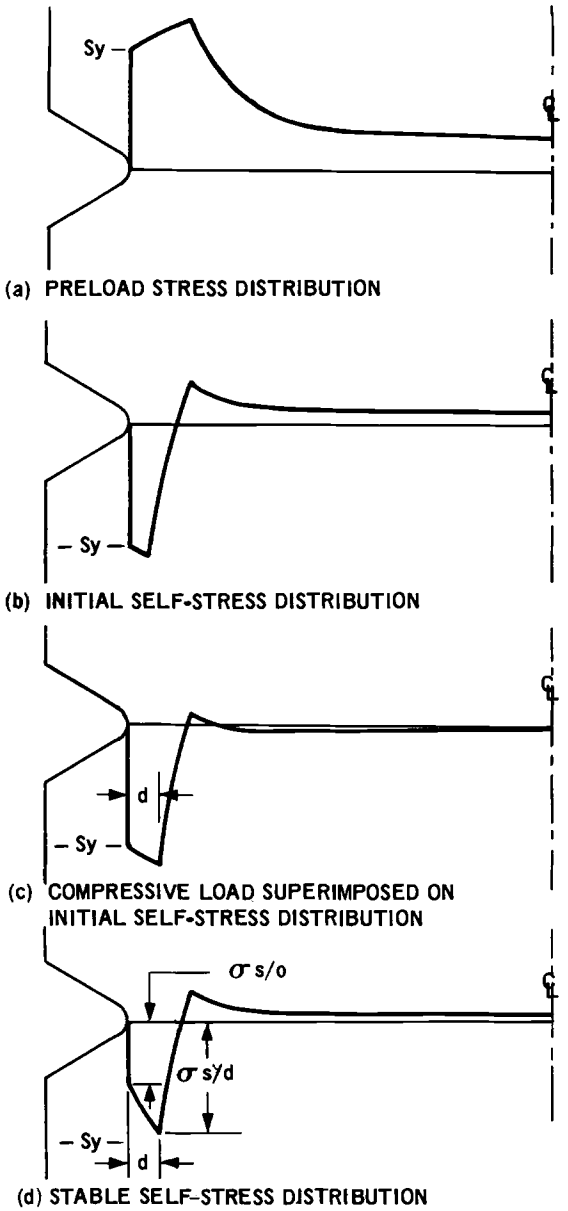

FIG. 6—*Axial stress distributions at the minimum cross section of a notch bar.*

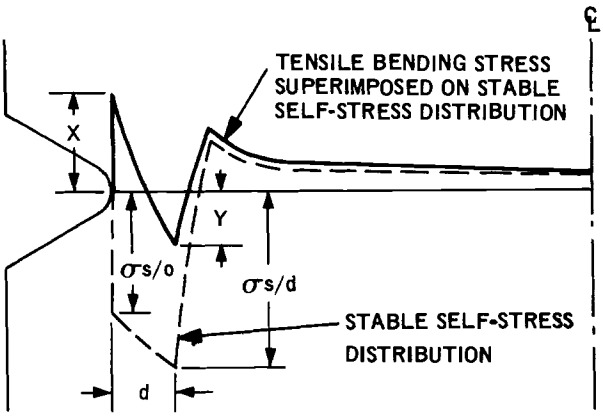

FIG. 7—*Axial tensile stress due to a bending load superimposed on the stable self-stress distribution.*

in relaxation of self-stresses near the notch surface, as shown in Figure 6*d*. Again, this self-stress distribution can be estimated with the equations of Ref *20*, as was done in Ref *19*. Assuming that no fatigue hardening or softening occurs, the resulting self-stress distribution will remain unchanged during subsequent cyclic loading and is called the stable self-stress distribution.[5] In the following paragraphs, stable self-stress distributions with the general shapes shown in Fig. 6*d* or Fig. 7 are used to predict fatigue strengths with the help of failure criteria.

Fuchs, in his paper on forecasting the fatigue life of peened parts [*21*], observed the importance of using separate criteria for crack nucleation and crack propagation. His theory (or engineering approach) is described in detail in other papers [*22*, *23*]. Briefly stated the criteria are

1. Local alternating shear stress (modified by the mean normal stress influence) determines crack initiation.

2. Nominal alternating tensile stress determines crack propagation.

It will be shown that these criteria can be used to predict the influence of self-stresses on the fatigue strength of notched bars if we replace *nominal* by *regional* in the second criterion.

First, crack nucleation occurs when the alternating local shear stress, modified by the mean local normal stress, exceeds a critical value. Fuchs [*22*] presents this criterion in terms of the octahedral shear stress and the mean octahedral normal stress. The maximum alternating shear stress is as serviceable an approximation for the nucleation criterion as the octahedral shear

[5] A possible improvement in the estimate of the stable self-stress distribution would be to determine the yield strength from the cyclic (if available) as well as from the monotonic stress-strain curve.

stress and serves to simplify some calculations. In terms of the alternating component and mean component of the largest principal stress

$$\sigma_{\mathrm{ALT}} < (S_E - m\sigma_M K_N)/K_N$$

where σ_{ALT} is the "safe" alternating stress, σ_M is the nominal mean stress, S_E is the reversed loading fatigue strength of a smooth specimen, K_N is the stress concentration factor effective in fatigue, and m is a material constant (common values of m are between 0.2 and 0.5).

A number of authors have pointed out and used the concept that the self-stress remaining in a part during cyclic loading acts like a mean stress superimposed on an alternating stress [*9, 11, 21*]. For zero applied mean load the local mean stress term at the notch root, $\sigma_M K_N$, can be replaced by the stable self-stress at the notch root, $\sigma_{s/o}$. The expression for the safe alternating stress with respect to crack nucleation then becomes

$$\sigma_{\mathrm{ALT}} < (S_E - m\sigma_{s/o})/K_N$$

The second failure criterion relates the safe alternating stress to the critical tensile stress necessary for crack propagation. Although it is recongized [*22*] that local stress in the vicinity of a crack tip causes growth, this criterion is in terms of nominal stresses. In many cases the criterion predicts results consistent with experience but it does not "explain" the behavior of the test results reported here.

The nucleation criterion was given in terms of local stress, which enabled us to treat the local self-stress as a local mean stress and to utilize the nucleation criterion directly. For the crack propagation criterion one must estimate the alternating tensile stress averaged over a region near the notch root.

Figure 7 shows the tensile portion of a cyclic load superimposed on a stable self-stress distribution. A tensile stress, X, has been produced at the notch root although a compressive peak, Y, remains below the surface. The tension at the surface is equal to the surface self-stress plus the nominal alternating stress times the stress concentration factor for a bending load,

$$X = \sigma_{s/o} + \sigma_{\mathrm{ALT}} K_{T(B)}$$

In a similar manner the compressive peak is given by

$$Y = \sigma_{s/d} + \sigma_{\mathrm{ALT}} K_{T(B)/d}$$

where $\sigma_{s/d}$ is the stable self-stress at depth d and $K_{T(B)/d}$ is the effective stress concentration factor at d.

$$K_{T(B)/d} = \frac{\text{elastic stress (due to load) at depth } d}{\text{nominal elastic stress (due to load) at the surface}}$$

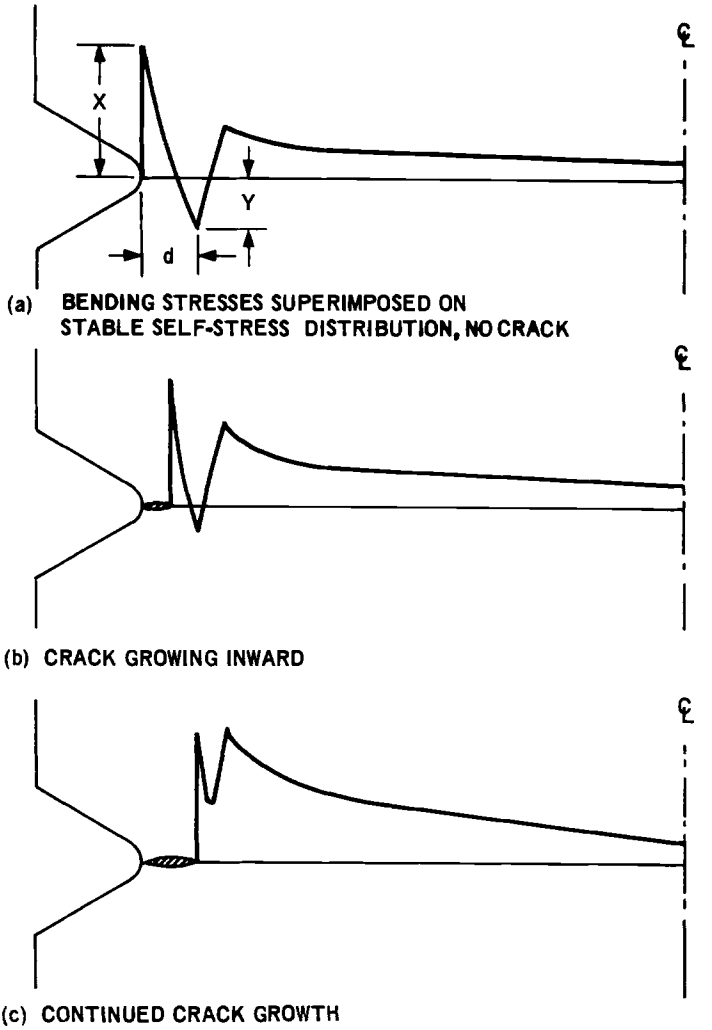

FIG. 8—*Crack growth from the notch root of a specimen which had been given a moderate preload.*

Figure 8 shows crack growth from the surface of a part which has been given a moderate preload. When a crack has been initiated, the tensile stress at the surface causes the crack to grow inward [*24*, *25*]. Since the cracked material cannot support tensile stress normal to the cracked surface, the tensile load previously carried by the cracked material must be assumed by neighboring material; that is, the presence of a crack causes the magnitude of the compressive peak, Y, to be reduced (Fig. 8*b*). After a crack has grown to depth d, it will continue growing and will cause failure (Fig. 8*c*). Figure 9

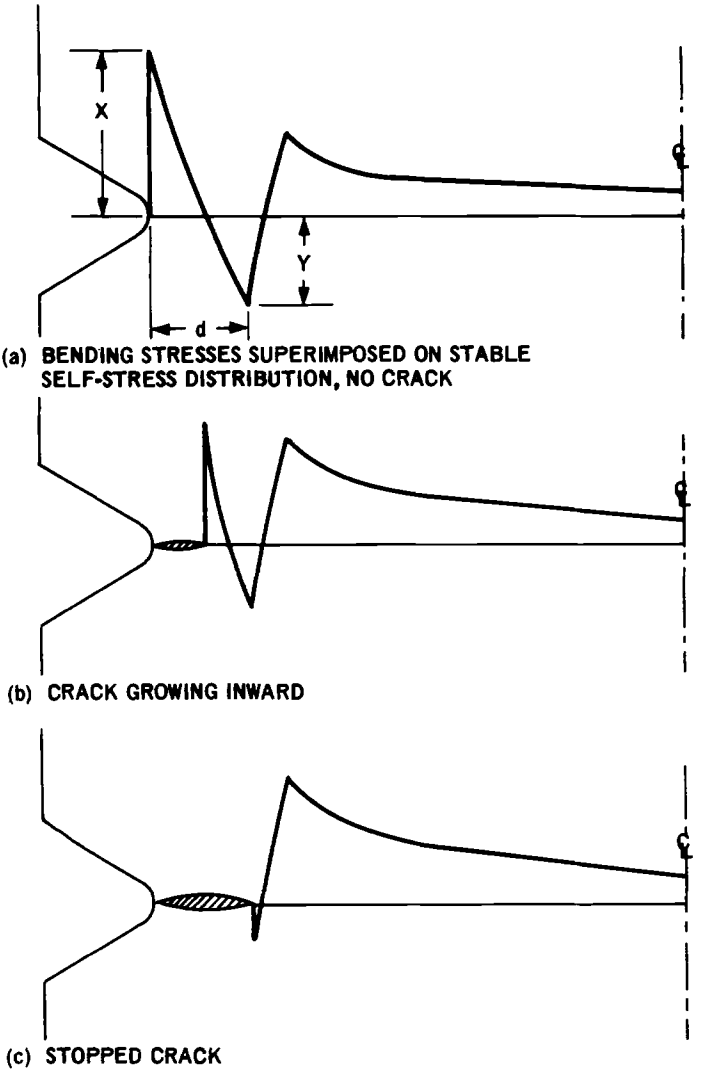

Fig. 9—*Crack growth from the notch root of a specimen which had been given a high preload.*

shows the growth of a crack in a part which has been given a large preload. This specimen is subjected to the same alternating stress as the specimen in Fig. 8, but in this case the crack is stopped by compressive self-stress shortly before it reaches depth *d*.

To describe the safe conditions, that is the conditions under which a crack will be stopped, one must be concerned with the stresses between the notch

root and a depth of the order of the compressive peak. Referring to Fig. 7, where the tensile portion of the cyclic load has been superimposed on the stable self-stress, one can reasonably assume that, if the average stress between the notch root and the compressive peak (at depth d) is tensile, a nucleated crack will propagate. Further, a simple relationship between the stress peaks X and Y can be used to approximate the average stress state over this region. When $X = -2Y$ the net area or average stress between the notch root and depth d is approximately zero, while if $X > -2Y$ the average

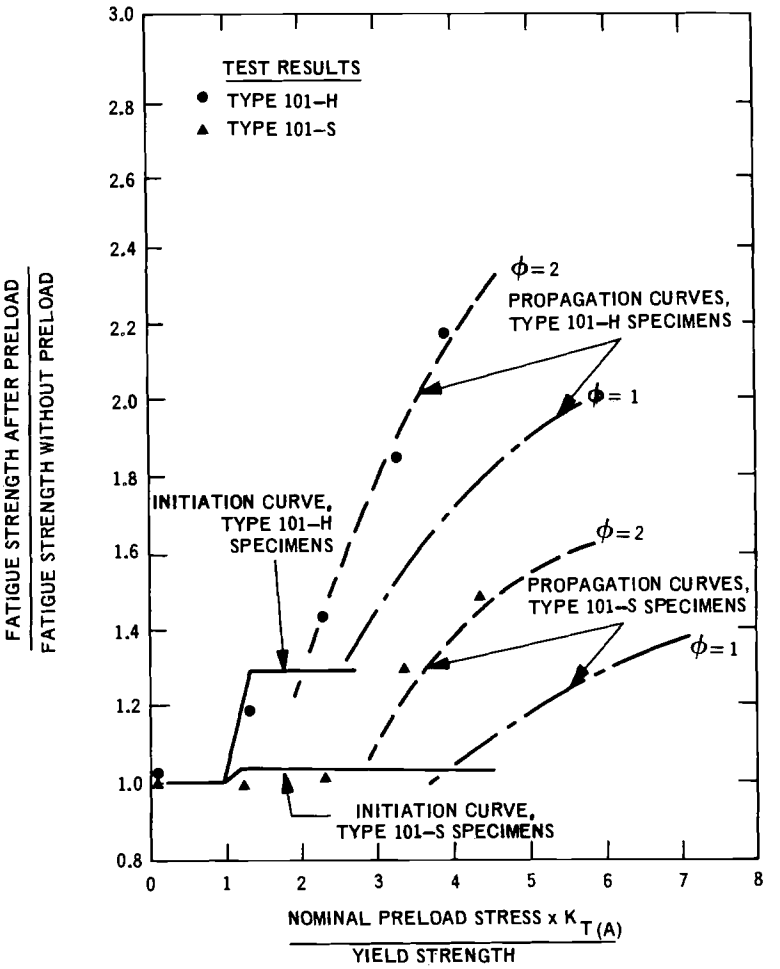

FIG. 10—*Predicted and experimentally measured increases in fatigue strength due to preloading of Type 101 specimens.*

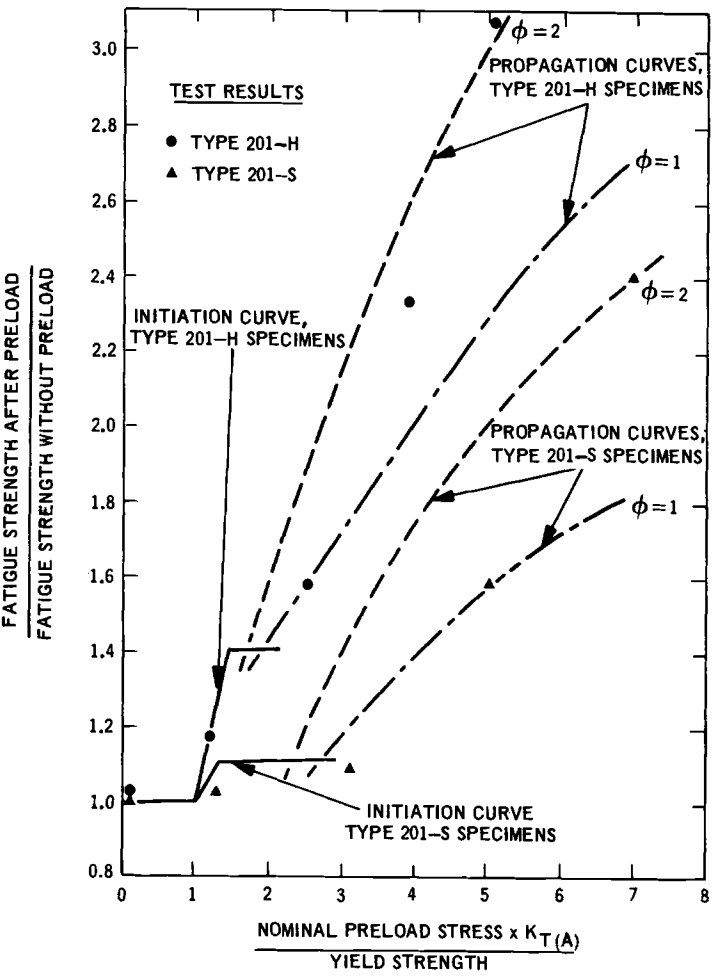

FIG. 11—*Predicted and experimentally measured increases in fatigue strength due to preloading of Type 201 specimens.*

regional stress would be tensile. Let the safe regional stress be described by the expression

$$X < -\Phi Y$$

where Φ is a constant which is assumed to be independent of preload. Substituting into the above experssion the equations for X and Y,

$$\sigma_{ALT} < \frac{-(\sigma_{s/o} + \Phi\sigma_{s/d})}{K_{T(B)} + \Phi K_{T(B)/d}}$$

For a part to fail, a crack must be first nucleated and subsequently propagated to failure. Therefore, the larger of the alternating stresses calculated with either the nucleation or propagation criterion will be the predicted fatigue strength. Figures 10, 11, and 12 compare the experimentally determined fatigue strengths with analytically predicted strengths. The line above which one would predict crack nucleation to occur is shown as a solid line. For propagation, a broken line is employed and predictions with $\Phi = 1$ and $\Phi = 2$ are shown. Note that with $\Phi = 1$ $(X = -Y)$ the predictions are generally conservative, while with $\Phi = 2$ $(X = -2Y)$ they are nonconservative. The equations for estimating the stable seft-stress peaks, $\sigma_{s/o}$ and $\sigma_{s/d}$, which appear in the expressions for σ_{ALT} are reviewed in the Appendix.

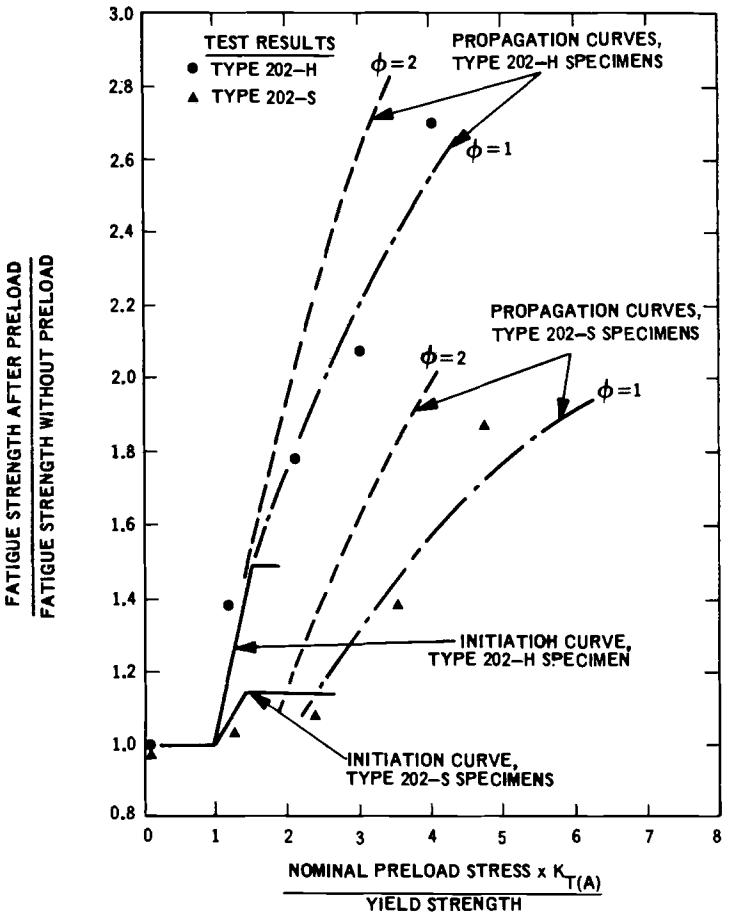

FIG. 12—*Predicted and experimentally measured increases in fatigue strength due to preloading of Type 202 specimens.*

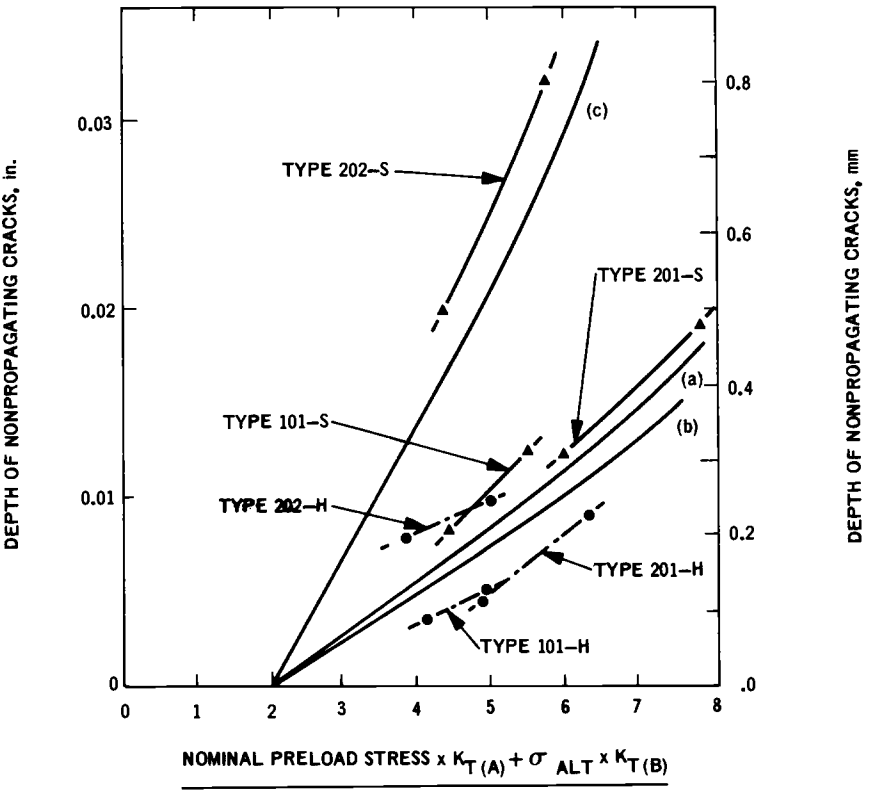

(*a*) Predicted depth *d*, specimen Type 101.
(*b*) Predicted depth *d*, specimen Type 201.
(*c*) Predicted depth *d*, specimen Type 202.

FIG. 13—*The average depth of nonpropagating cracks found in preloaded and fatigue-loaded notched specimens.*

By making a distinction between nucleation and propagation, as has been done, one can explain two outstanding features of the experimental curves. First, the large improvements in fatigue strengths that were observed were due to stopping crack growth. Specimens that had been given a large preload were cycled above the alternating load for which cracks would be initiated, yet the specimens survived and nonpropagating cracks were observed. Second, the reason that soft specimens are not improved unless given a large preload is that surface self-stresses are partially washed out by the first few cycles of alternating load. Therefore, improvement with respect to nucleation is slight and these specimens are not strengthened unless cracks are stopped at a considerable depth below the notch root. This requires a large preload.

If the specimen is to survive, a crack must be stopped before it reaches the depth at which the self-stress peak exists, depth d. In Fig. 13 the estimated depth of the stable self-stress peak is compared with the measured non-propagating crack depths for specimens loaded at their mean fatigue strength. (The calculation of d as a function of preload and alternating load is reviewed in the Appendix.)

Conclusions

1. In designing for long-life fatigue strength one must consider the influence of self-stresses. This is especially true when stress concentrations are present.
2. Compressive self-stresses can increase the fatigue strength of certain parts to more than double that of stress-free parts. This is achieved by the ability of self-stresses in depth to stop cracks.
3. For circumferentially notched round bars the depth to which stable self-stresses must extend to stop crack growth for a given load can be calculated by analytical procedures.
4. The analysis of this one geometry has clarified the concept of a regional stress and its importance to crack propagation.

Acknowledgments

We gratefully acknowledge the financial support of the Advanced Research Projects Agency through the Center for Materials Research at Stanford University and of the Caterpillar Tractor Co., Peoria, Ill. We also wish to express our appreciation to the Homer Research Laboratories, Bethlehem Steel Corp., for the fatigue testing of the large specimens; the testing was carried out under the direction of H. S. Reemsnyder.

APPENDIX

The criteria for crack nucleation and propagation are in terms of the stable self-stresses at the notch root and at a depth d below the notch root. For the special case of preloaded notched bars these stable self-stresses can be estimated as functions of the tensile preload, the cyclic fatigue load, the yield strength, and the specimen geometry [*19*]. Two major assumptions are employed in this analysis: (1) strain hardening is neglected and (2) when reversing the direction of loading, axial stress components are superimposed to find the resulting axial stress.

In terms of the nominal preload stress, σ_p, the initial self-stress at the notch root, $\sigma^*_{s/o}$, following preloading but before cyclic loading, is

$$\text{for } \sigma_p K_{T(A)} < S_Y, \sigma^*_{s/o} = 0;$$

$$\text{for } S_Y < \sigma_p K_{T(A)} < 2S_Y, \sigma^*_{s/o} = S_Y - \sigma_p K_{T(A)};$$

$$\text{for } \sigma_p K_{T(A)} > 2S_Y, \sigma^*_{s/o} = -S_Y$$

where $K_{T(A)}$ is the theoretical stress concentration factor for an axial load.

$\sigma^*_{s/o}$ will be relaxed to the stable self-stress, $\sigma_{s/o}$, by the cyclic loading if

$$|\sigma_{ALT}K_{T(B)}| + |\sigma^*_{s/o}| > S_Y$$

If this expression is satisfied

$$\sigma_{s/o} = \sigma_{ALT}K_{T(B)} - S_Y \quad (1)$$

otherwise $\sigma^*_{s/o}$ is not relaxed and

$$\sigma_{s/o} = \sigma^*_{s/o} \quad (2)$$

The self-stress at depth d below the notch root is found by subtracting $\sigma_{ALT}K_{T(B)/d}$ from the axial stress which satisfies the yield condition at this depth. Due to plastic constraint, yielding at d requires the axial stress component to be larger than the yield strength by a factor of $1 + \ln(1 + d/\rho)$ where ρ is the notch root radius. (This would not be the case if one were considering notched plates rather than notched bars.)

$$\sigma_{s/d} = \sigma_{ALT}K_{T(B)/d} - S_Y[1 + \ln(1 + d/\rho)] \quad (3)$$

Equation 3 gives $\sigma_{s/d}$ in terms of d, the depth to which reversed yielding has occurred. In Ref *19* the relationship between d,σ_p, and σ_{ALT} was calculated with a computer code. This result can be approximated by the equation

$$d/\rho = C\left[\frac{\sigma_p K_{T(A)} + \sigma_{ALT}K_{T(B)}}{S_Y} - 2\right] \quad (4)$$

where C is a constant that depends on notch geometry. For specimen Types 101 and 202, $C = 0.19$, for Type 201, $C = 0.16$.

Neuber's [*26*] equations for elastic stresses in notched bars can be used to calculate $K_{T(A)}$, $K_{T(B)}$, and $K_{T(B)/d}$. With values for the stress concentrations and Eqs 1, 2, 3, and 4, the criteria for crack nucleation and propagation can be used to predict the fatigue strength of preloaded bars cycled in rotating bending.

References

[*1*] Dolan, T. J., "Residual Stress, Strain Hardening and Fatigue," Proceedings of the Symposium on Internal Stress and Fatigue in Metals, Detroit and Warren, Mich., 1958, Elsevier Publishing Co., Amsterdam, 1959.

[*2*] Horger, O. J. in *Handbook of Experimental Stress Analysis*, Wiley, New York, 1950, pp. 459–578.

[*3*] Almen, J. O. and Black, P., *Residual Stress and Fatigue in Metals*, McGraw-Hill, New York, 1963.

[*4*] Rassweiler, G. M. and Grube, W. L., "Internal Stresses and Fatigue in Metals," Proceedings of the Symposium on Internal Stress and Fatigue in Metals, Detroit and Warren, Mich., 1958, Elsevier Publishing Co., Amsterdam, 1959.

[*5*] Sines, G. and Waisman, J., *Metal Fatigue*, University of California Engineering Extension Series, McGraw-Hill, New York, 1959.

[*6*] Osgood, W. R., *Residual Stress in Metals and Metal Construction*, Reinhold Publishing Corp., New York, 1954.

[*7*] Rowland, E. S., "Effect of Residual Stress on Fatigue," Proceedings, Tenth Sagamore Conference, Syracuse University Press, 1964, pp. 229–244.

[*8*] Morrow, JoDean and Millan, J. F., "Influence of Residual Stress on Fatigue of Steel," SAE J783, Division 4 of the SAE Iron and Steel Technical Committee, Society of Automotive Engineers, July, 1961.

[*9*] Morrow, JoDean and Sinclair, G. M., "An Analysis of Cyclic Stress Behavior for Conditions of Controlled Strain," Report No. 543, Department of Theoretical and Applied Mechanics, University of Illinois, Urbana, Ill., Aug. 1957.

[10] Mattson, R. L. and Roberts, J. G., "The Effect of Residual Stresses Induced by Strain Peening upon Fatigue Strength," Proceedings of the Symposium on Internal Stress and Fatigue in Metals, Detroit and Warren, Mich., 1958, Elsevier Publishing Co., Amsterdam, 1959, pp. 337–360.
[11] Rosenthal, D. and Sines, G., *Proceedings*, American Society for Testing and Materials, ASTEA, Vol. 51, 1951, pp. 593–610.
[12] Taira, S. and Murakami, Y., *Bulletin of Japan Society of Mechanical Engineers*, BJSEA, Vol. 4, No. 15, 1961, pp. 453–460.
[13] Rosenthal, D. in *Metal Fatigue*, University of California Engineering Extension Series, McGraw-Hill, New York, 1959, pp. 168–196.
[14] Dugdale, D. S., *Welding Journal*, WEJUA, Vol. 38, 1959, pp. 45S–48S.
[15] Forrest, G., *Journal of the Institute of Metals*, London, JIMEA, Vol. 72, 1946, pp. 1–7.
[16] Heller, R. A., Seki, M., and Freudenthal, A. M., *Proceedings*, American Society for Testing and Materials, ASTEA, Vol. 64, 1964, pp. 516–535.
[17] *A Guide for Fatigue Testing and the Statistical Analysis of Fatigue Data, ASTM STP 91-A (Second Edition)*, 1963.
[18] Brownlee, K. A., Hodges, J. L., and Rosenblatt, M., *Journal of the American Statistical Association*, JSTNA, Vol. 48, 1953, pp. 262-277.
[19] Gerber, T. L., "The Effect of Tensile Preload on the Fatigue Strength of Notched Steel Bars," PhD thesis, Stanford University, Stanford, Calif., 1969.
[20] Gerber, T. L. and Fuchs, H. O., *Journal of Materials*, JMLSA, Vol. 3, No. 2, June 1968, pp. 359–374.
[21] Fuchs, H. O., *Metal Progress*, MEPOA, May 1963, pp. 75–78, 116–120.
[22] Fuchs, H. O., *Journal of Basic Engineering, ASME Transactions, Series D*, American Society of Mechanical Engineers, June 1965, pp. 333–343.
[23] *Fatigue Design Handbook—Advances in Engineering*, Society of Automotive Engineers, Vol. 4, 1968.
[24] Almen, J. O., *Product Engineering*, PRENA, Vol. 22, March 1951, pp. 101–124.
[25] Allen, N. F., "Discussion of Papers," Proceedings of the International Conference on Fatigue of Metals, London-New York, 1956, pp. 779–780.
[26] Neuber, H., *Theory of Notch Stresses: Principles for Exact Calculation of Strength with Reference to Structural Form and Material*, AEC-TR-4547, Clearinghouse for Federal and Scientific Information, U.S. Department of Commerce, Springfield, Va., 1958; translated from a publication of Springer-Verlag, Berlin, Goettingen, Heidelberg.

DISCUSSION*

R. N. Wright[1] *(written discussion)*—The authors have used the terms Stage I and Stage II to categorize fatigue crack propagation phenomena and have implied that the former has a crystallographic nature and that the latter is noncrystallographic. I think it is important to point out that the terms as used by Forsyth[2] were defined in a significantly different manner. Forsyth referred to Stage I growth as growth along a slip plane by some unslipping or reverse slip process, and described Stage II as being characterized by the appearance of striations and by growth roughly perpendicular to the axis of maximum tensile stress.

While Forsyth's Stage I is clearly crystallographic in nature, it is not fair to say that Stage II is free from substantial crystallographic influence. In particular, the "brittle striations" observed by Forsyth in Stage II growth in strong aluminum alloys involved local crack growth along {100} planes even though the overall macroscopic growth plane was roughly perpendicular to the axis of maximum tensile stress. Similar observations have been reported by Pelloux recently at the Brighton conference. Furthermore, crack propagation planes in coarse-grained materials can be observed by the naked eye to change from one grain to another even while the "average" plane of growth corresponds closely to the plane of maximum tensile stress. Examples of this have recently been observed in silicon-iron by A. S. Argon and me in work now in press.

Thus, while it may be useful to categorize fatigue crack propagation as crystallographic and noncrystallographic, these categories are not, strictly speaking, the conventional definitions of Stage I and Stage II crack propagation. Though continuum mechanical considerations may dictate the overall growth plane of Forsyth's Stage II, local growth planes and local growth rates can be highly dependent on crystallography.

M. Gell (author's closure)—A precise and unique definition for the two stages of fatigue crack propagation is difficult to obtain. If one looks care-

* The discussion and closure which follow concern the paper, "The Fatigue Strength of Nickel-Base Superalloys," by M. Gell, G. R. Leverant, and C. H. Wells on pp. 113–153.

[1] Research metallurgist, Allegheny Ludlum Steel Corp. Research Center, Brackenridge, Pa.

[2] Forsyth, P. J. E., *Acta Metallurgica*, AMETA, Vol. 11, 1963, pp. 703–715.

fully at the definitions of Stage I and Stage II as originally given by Forsyth and then repeated by him and his co-workers in a number of papers,[3,4,5] differences can be found. In addition, by observing characteristics of fatigue crack propagation in a wide range of materials, it can be seen that no single definition covers all cases. For example: (1) Stage II fracture surfaces may or may not exhibit striations, (2) Stage I fractures may or may not show striations, (3) Stage II fractures may be microscopically crystallographic or they may not, (4) Stage I fractures may be macroscopically crystallographic or they may not, and (5) Stage II usually follows Stage I, but there are instances where it does not. Despite this variation in behavior, fatigue crack propagation in most materials does occur in two stages, and it is worthwhile to retain the Forsyth terminology. In the case of the nickel-base superalloys, we have described Stage I as occurring on crystallographic slip planes and Stage II as occurring noncrystallographically and normal to the stress axis. These descriptions are appropriate for crack propagation in these materials.

It appears worthwhile to attempt a more general characterization of Stage I and Stage II at this time. Stage I cracking occurs on slip planes on a microscopic scale. Macroscopically, the Stage I fracture area may or may not correspond to a surface of maximum resolved shear stress. For example, it is possible in polycrystalline materials for a crack to propagate in each grain on a slip plane approximately 45 deg to the stress axis and for the macroscopic path to be approximately normal to the stress axis. The same is true in single crystals when slip plane cracking occurs on a number of slip planes of the same family. The important aspect of Stage I cracking is that on a microscopic scale cracking is occurring on only one slip plane in a given region. It is not appropriate to define Stage I in terms of a specific mechanism because more than one mechanism can produce the same results.

Stage II fractures, on the other hand, are always approximately normal to the stress axis on a macroscopic scale and often on a microscopic scale as well. If the latter is true, cracking is noncrystallographic and there is then a clear distinction between Stage I and Stage II.

A number of cases may arise that require somewhat more interpretation. For example, microscopic or submicroscopic cracking may occur in planar slip materials such that cracking in each cycle occurs first on one slip system and then on another, while the macroscopic fracture is normal to the stress axis. We would classify this as Stage II cracking because of the operation of more than one slip plane at the crack tip and the realization that, under conditions of wavy slip, microscopic, noncrystallographic cracking would

[3] Forsyth, P. J. E., "A Two Stage Process of Fatigue Crack Growth," Proceedings, Cranfield Crack Propagation Symposium, Cranfield, Beds., England, Sept. 1961, p. 1.

[4] Stubbington, C. A., *Metallurgia*, METLA, Vol. 68, 1963, pp. 109–121.

[5] Stubbington, C. A. and Forsyth, P. J. E., *Metallurgia*, METLA, Vol. 74, 1966, pp. 15–21.

result. On the other hand, if cracking occurs for a number of cycles on the same slip plane and then deviates onto another slip plane, then this would be considered Stage I cracking. A third example is the microscopic crystallographic cracking observed on {100} planes in Al alloys.[6] The cube planes are not slip planes in these materials, and failure on them is evidence for normal stress mode cracking and should therefore be classified as Stage II.

At present, the number of instances that require special interpretation is small. If this situation changes with the increased study of fatigue crack propagation, especially in body centered cubic and intermetallic materials, then more explicit descriptions of the different stages of cracking in each material will be required.

[6] Forsyth, P. J. E., Stubbington, C. A., and Clark, D., *Journal*, Institute of Metals, JIMEA, Vol. 90, 1961-62, pp. 238–239.